



Durham E-Theses

Two loop vertices and tree level multicollinear limits in QCD

Birthwright, Thomas G.

How to cite:

Birthwright, Thomas G. (2005) *Two loop vertices and tree level multicollinear limits in QCD*, Durham theses, Durham University. Available at Durham E-Theses Online: <http://etheses.dur.ac.uk/2794/>

Use policy

The full-text may be used and/or reproduced, and given to third parties in any format or medium, without prior permission or charge, for personal research or study, educational, or not-for-profit purposes provided that:

- a full bibliographic reference is made to the original source
- a [link](#) is made to the metadata record in Durham E-Theses
- the full-text is not changed in any way

The full-text must not be sold in any format or medium without the formal permission of the copyright holders.

Please consult the [full Durham E-Theses policy](#) for further details.

Two loop vertices and Tree level multicollinear limits in QCD

A thesis presented for the degree of

Doctor of Philosophy

by

Thomas G. Birthwright

The copyright of this thesis rests with the author or the university to which it was submitted. No quotation from it, or information derived from it may be published without the prior written consent of the author or university, and any information derived from it should be acknowledged.

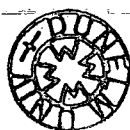
Institute for Particle Physics Phenomenology

University of Durham

2005



Durham
University



31 MAY 2006

Abstract

We present a summary of the methods required to solve loop-integrals and their reduction to Master Integrals. We then present the expansion in $d = 4 - 2\epsilon$ of the Master Integrals required for the two loop massless vertex diagrams with three off-shell legs. The results are analytic and contain a new class of two-dimensional harmonic polylogarithms, which match onto the allowed phase-space boundary for the $1 \rightarrow 2$ process. These Master Integrals are relevant for the QCD corrections to $H \rightarrow V^*V^*$ (where $V = W, Z$) and for two-loop studies of the triple gluon (and quark-gluon) vertex.

We consider multi-parton collinear limits of QCD amplitudes at tree level. Using the MHV formalism we specify the underlying analytic structure of the resulting multi-collinear splitting functions. We adapt the MHV-rules to enable us to derive splitting functions without the need to evaluate the full amplitude. We derive general results for these splitting functions that are valid for specific numbers of negative helicity partons and an arbitrary number of positive helicity partons (or vice versa). Our method can be used to find splitting amplitudes with higher numbers of negative helicity partons. We present new results describing the collinear limits of up to six gluons and up to four partons. These results will have applications in the evaluation of higher order corrections to QCD cross-sections and jet evolution.

Acknowledgements

First and foremost I need to thank my supervisor, Nigel Glover, for all his help and guidance during my studies. Pointing out where I needed to go with my work, and helping me see the obvious answer when I couldn't.

I owe great thanks to Peter Marquard for his seemingly endless patience with me, always ready to answer any stupid questions with kind words, and for always being happy to chat through the work when we were stuck. Without this I wouldn't have understood half of what I do, or had as much fun in the IPPP.

Special thanks must go to my office mates, firstly Paul Brooks, for office cricket and our always amusing 'jamming' sessions on the guitar, and to Julie, our honorary office-mate. Marcus Aurelius Morley-Fletcher, for knowing everything but the order of the planets, and dragging me to hockey. Angelique Talbot, for always being there to help, and for being a great desk-buddy. Richard Whisker for football fun, and not gloating too much about Chelsea. The latecomer to office life, James Haestier, for introducing me to the painful world of 24-hour mountain bike racing at SITS, you have my endless respect for doing it solo.

I would also like to thank Ben Schofield for giving us arXiv reformatted, Simon Badger, John Levell, Pete Williams, Kemal, Karina, Gareth, Martyn, and all the members of the IPPP.

Many thanks to Mum and Dad, Jack and Caroline for their support and encouragement over the years, and the relaxing times they have given me away from Durham. Ian, the most generous brother in the world, what would I do without you?

My (many) house-mates deserve thanks for creating a nice atmosphere to go home to. Honourable mentions must be given to Dan, Laura, Phil, Uli, Johns, G, K, Susanne, and Nick WC for getting me "Lost." Andy H, you get a special mention for the laughs we had climbing, and for always catching me from my comedy dives.

off the wall. Lastly, Mike and Emily have my undying gratitude for letting me stay with them in times of need.

This work was supported by a PPARC studentship which I gratefully acknowledge.

Declaration

I declare that no material presented in this thesis has previously been submitted for a degree at this or any other university.

The research described in this thesis has been carried out in collaboration with Professor E. W. N Glover, Dr. P. Marquard and Professor V. V. Khoze, and has been published as follows:

- Master integrals for massless two-loop vertex diagrams with three offshell legs. T.G.Birthwright, E.W.N.Glover and P. Marquard, *JHEP* **09** (2004) 042 (hep-ph/0407343).
- Multi-Gluon collinear limits from MHV diagrams. T.G.Birthwright, E.W.N.Glover, V.V.Khoze and P. Marquard, *JHEP* **05** (2005) 013 (hep-ph/0503063).
P. Marquard and T. G. Birthwright, hep-ph/0505264 - Talk given by P. Marquard at XXXXth Rencontres de Moriond, QCD and Hadronic interactions at high energy, March 2005.
- Collinear limits in QCD from MHV rules. T.G.Birthwright, E.W.N.Glover, V.V.Khoze and P. Marquard, *JHEP* **07** (2005) 068 (hep-ph/0505219).

©The copyright of this thesis rests with the author.

“Singularity is almost invariably a clue.”

Sir Arthur Conan Doyle, “The Adventures of Sherlock Holmes, The Boscombe Valley Mystery. ”

“Only two things are infinite, the universe and human stupidity, and I’m not sure about the former.”

Albert Einstein.

Contents

Preface	1
1 Field theory basics	8
1.1 Fundamentals	8
1.2 Feynman rules	12
1.3 Ultra-Violet Divergences	16
1.4 Infra-Red Divergences	17
1.5 Regularisation	21
1.6 Feynman Parameters	23
1.7 1-loop Minkowski space integration	24
1.8 Summary	27
2 Loop integral methods	29
2.1 One-loop integration	31
2.2 Sunsets and glasses	35
2.3 IBP identities	38
2.3.1 Triangle IBP's	40
2.4 Lorentz Invariance Identities	42
2.5 The Laporta Algorithm	44
2.6 Differential equations	46

2.6.1	Deriving differential equations	47
2.6.2	Solving differential equations	49
2.6.3	The boundary conditions	51
2.7	Harmonic polylogarithms	52
2.7.1	1-d HPL's	53
2.7.2	2-d HPL's	55
2.7.3	Properties of the HPL's	55
2.8	Summary	57
3	Master Integrals for the offshell vertex	58
3.1	Kinematics	62
3.1.1	Extended Harmonic Polylogarithms	64
3.2	One Loop	68
3.2.1	Two point integrals	68
3.2.2	Three point integrals	69
3.3	Two Loop	73
3.3.1	Two point integrals	73
3.3.2	Three point integrals	74
3.4	Application	96
3.5	Summary	99
4	The MHV Construction	100
4.1	Introduction	100
4.2	Colour-ordered amplitudes	104
4.3	Spinor helicity formalism	107
4.4	MHV amplitudes	108

4.5	MHV rules	111
4.6	BCF recursion relations	118
4.6.1	An example: $A(1^-, 2^+, 3^+, 4^+, 5^-, 6^-)$	120
4.7	Summary	122
5	Collinear limits	124
5.1	Introduction	124
5.2	Collinear limits	128
5.3	Analytic structure	132
5.4	General results	137
5.4.1	Purely gluonic limits – no quarks in the collinear set: $ng \rightarrow g$	139
5.4.2	One quark in the collinear set: $q(ng) \rightarrow q$	146
5.4.3	Two quarks in the collinear set: $(ng)\bar{q}q \rightarrow g$	148
5.4.4	Two quarks in the collinear set: $q(ng)\bar{q} \rightarrow \gamma$	149
5.4.5	Three quarks in the collinear set: $q(ng)\bar{Q}Q \rightarrow q$	151
5.4.6	Three quarks in the collinear set: $q(ng)\bar{q}Q \rightarrow Q$	152
5.4.7	Four quarks in the collinear set: $\bar{Q}Q(ng)\bar{q}q \rightarrow g$	154
5.4.8	Four quarks in the collinear set: $\bar{Q}q(ng)\bar{q}Q \rightarrow g$	156
5.5	Specific results	159
5.5.1	Purely gluonic $n \leq 6$	159
5.5.2	Selected specific results for triple collinear limits involving quarks	175
5.6	Summary	179
6	Conclusion	180
A	Properties of extended HPL's	186

B	F_4 at $\mathcal{O}(\epsilon)$	188
C	Spinor product identities	198
	Bibliography	199

List of Figures

1.1	The only non-zero one-loop QCD correction to the massless quark QED form factor.	18
1.2	The tree-level QCD corrections to the quark QED form factor.	19
2.1	The massless scalar bubble diagram	32
2.2	The sunset integral.	35
2.3	The glasses integral.	37
2.4	Glasses integral as the product of one-loop integrals.	37
2.5	The massless scalar triangle diagram with two on-shell legs.	40
2.6	Figure showing the massless scalar triangle decomposed as a “dotted” scalar bubble diagram.	41
3.1	A two-loop vertex diagram for the $H \rightarrow V^*V^*$ decay.	59
3.2	Example two-loop diagrams for the triple gluon and quark-gluon vertices.	59
3.3	The phase space for the vertex graph with three off-shell legs.	63
3.4	The one-loop Master Integral, $BB(q^2)$	68
3.5	The one-loop Master Integral, $F_0(m_1^2, m_2^2, m_3^2)$	69
3.6	The two-loop Master Integral, $SS(q^2)$	74
3.7	The two-loop Master Integral, $GL(q^2)$	74
3.8	The two-loop Master Integral, $TGL(p_1^2, p_2^2)$	74

3.9	The two-loop Master Integrals, $F_1(m_1^2, m_2^2, m_3^2), F_2(m_1^2, m_2^2, m_3^2)$	75
3.10	The two-loop Master Integral, $TB(m_1^2, m_2^2, m_3^3)$	86
3.11	The two-loop Master Integral, $F_3(m_1^2, m_2^2, m_3^3)$	87
3.12	The two-loop Master Integral, $F_4(m_1^2, m_2^2, m_3^3)$	94
3.13	An example of a two-loop master integral with four external legs. . .	97
4.1	The two colour flows in a four quark amplitude.	106
4.2	The pattern of available \pm states for helicity amplitudes.	109
4.3	NMHV Diagrams contributing to $A(1^+, 2^-, 3^-, 4^-)$	113
4.4	NMHV Diagrams contributing to $A_n(1^+, 2^-, 3^-, 4^-, 5^+, \dots, n^+)$	115
4.5	Skeleton diagrams for $A_n(1^+, \dots, m_1^-, \dots, m_2^-, \dots, m_3^-, \dots, n^+)$	116
4.6	The BCF configurations contributing to $A(1^-, 2^+, 3^+, 4^+, 5^-, 6^-)$	121
5.1	Collinear factorisation of amplitudes into a splitting function multiplied by an amplitude with fewer legs.	129
5.2	The pattern of multi-collinear splitting functions accessible using the MHV amplitudes.	134
5.3	The pattern of multi-collinear splitting functions accessible using the NMHV amplitudes.	135
5.4	The pattern of multi-collinear splitting functions accessible using the NNMHV amplitudes.	136
5.5	MHV topologies contributing to $\text{Split}_+^{(n)}(m_1)$ & $\text{Split}_-^{(n)}(m_1, m_2)$	138
5.6	MHV diagrams contributing to $\text{Split}_+^{(n)}(m_1)$	140
5.7	MHV diagrams contributing to $\text{Split}_-^{(n)}(m_1, m_2)$	141
5.8	MHV diagrams contributing to $\text{Split}_+^{(n)}(m_1, m_2)$	142
5.9	MHV topologies contributing to $\text{Split}_-^{(n)}(m_1, m_2, m_3)$	144
5.10	MHV topologies contributing to the two quark collinear limit of the type $\text{Split}_{\gamma^-}^{(n)}(1_{\bar{q}}, m^-, n_{\bar{q}}^+)$	150

5.11 MHV topologies contributing to the four quark collinear limit of the type $\text{Split}_-^{(n)}(s_{\hat{Q}}^\lambda, (s+1)_{\hat{Q}}^{-\lambda}, t_{\hat{q}}^{\lambda'}, (t+1)_{\hat{q}}^{-\lambda'})$	154
5.12 MHV topologies contributing to the four quark collinear limit of the type $\text{Split}_-^{(n)}(s_{\hat{Q}}^\lambda, (s+1)_{\hat{q}}^{-\lambda'}, t_{\hat{q}}^{\lambda'}, (t+1)_{\hat{Q}}^{-\lambda})$	157

Preface

At the beginning of the last century our understanding of the laws of physics was shaken by the emergence of two new fields of physics. Firstly, the field of quantum mechanics, the physics which applies at very small distances, and secondly special relativity, the physics that governs at very high energies. As the century progressed came the birth of relativistic quantum field theory, the unification of these two theories, to begin to explain the properties and behaviour of the Universe's fundamental particles. With this new theory came many new and interesting problems to be solved, for example the role played by infinities and how to interpret them. However, through the ensuing developments we have seen some of the beauty that nature has to share with us, the hidden symmetries obeyed by the fundamental particles, and the strange properties that they produce, such as asymptotic freedom.

In nature we know of four fundamental forces, the electromagnetic force, the weak force, the strong force, and gravity. The gravitational interaction is described by general relativity (developed by Einstein) and is by far the weakest of the four fundamental forces. As such, the role it plays in high-energy particle physics can be considered negligible. The Standard Model (SM) is the currently accepted description of the fundamental constituents of matter and their interactions through the remaining three forces. It is described by the symmetries which are associated with the three forces and obeyed by the fundamental particles, the quarks, leptons and



gauge bosons.

The quark model was introduced by Gell-Mann [1] in order to explain the proliferation of mesons and baryons discovered at experiments in the 1950's and 1960's. Using quarks as the building blocks, we can reproduce the observed hadrons and their properties by assuming that baryons consist of three quarks qqq , and that mesons consist of a quark and an anti-quark $q\bar{q}$. In this way the spectrum of hadrons could be explained in a similar way to how the periodic table of Mendeleev explains the patterns in the properties of the elements. Although the quark construction could be used to explain (and even predict) the observed hadrons, there was no explanation as to why only certain combinations of quarks, $q\bar{q}$ and qqq , were seen in nature. In addition, the quark model meant that some fermionic states, such as the Δ^{++} (which consists of uuu), appeared to possess symmetric wave-functions under the interchange of two quarks. However as fermions obey Fermi-Dirac statistics¹ they are required to have anti-symmetric wavefunctions under the exchange of two fermions quantum numbers. To explain this apparent contradiction, the colour degree of freedom was introduced by Han and Nambu [2]. This postulates that each quark also carries one of three colours, commonly denoted red(r), green(g) and blue(b), in addition to their flavour. In addition all hadrons are postulated to be singlets under the colour gauge transformation, i.e. they are colourless, to satisfy the spin statistics. Thus baryons will be composed of one red, one green and one blue quark, making an overall colourless object, and mesons will be composed of a coloured quark, and an anti-quark with the corresponding anti-colour.

The quark model could have proved to be simply a useful way of explaining the observed hadrons, with no physical basis. Quarks had never been observed at collider

¹The particles of nature are classified as either Fermions or Bosons according to the statistics which they obey, Fermi-Dirac statistics for fermions which have half-integer spin (quantised in units of \hbar), and Bose-Einstein statistics for Bosons which have integer spin.

experiments, and so they could be just a useful mathematical formalism. However in the late 1960's deep-inelastic scattering (DIS) experiments provided the first evidence for sub-structure within protons. High-energy incident electrons colliding with protons appeared to be scattering off point particles within the protons, quarks. In DIS these quarks act as though they are free states within the proton, and yet we cannot observe them outside of hadrons! This can be explained by the theory of Quantum Chromodynamics (QCD) [3,4], and the strange feature of asymptotic freedom [5]. QCD proposes that the colour symmetry is a result of invariance under the local $SU(3)$ gauge transformation. To satisfy this gauge invariance, 8 gauge bosons, called *gluons*, are required. As QCD is a non-abelian theory, these gluons will also carry the colour charge, which means that gluon self interactions are possible. This leads to a positive β coefficient for QCD, which means that the QCD coupling constant decreases as the momentum scale is increased. This is the basic statement of asymptotic freedom, that as we go to shorter distance scales the coupling between quarks will become weaker. Thus in DIS as we increase the incident electron's energy we will be able to resolve more of the partonic structure of the proton. Conversely the interaction energy between quarks will increase as they are pulled apart. This indicates that we can never observe a free quark (or gluon), which is termed quark confinement, and so we never observe free quarks as final states at collider experiments. This leads to the phenomenon of jets at colliders, as quark pairs fly apart the energy between them is able to create new quark pairs, and so we end up with showers of hadrons carrying the parent partons properties into the detectors.

Asymptotic freedom means that QCD has two different energy regions. The “soft” physics region at low energy scales, where the coupling constant is relatively large, and the “hard” physics region at high energies where the coupling constant is rel-

atively small. We are unable to solve QCD exactly, but for the hard physics we can use a technique known as perturbation theory. This relies on the ability to perform a perturbative expansion of amplitudes in orders of the coupling constant. For abelian theories such as Quantum Electrodynamics (QED), the coupling constant is very small and so this technique is very useful. In non-abelian QCD, although the coupling constant is relatively large (in comparison to QED), asymptotic freedom allows us to examine high energy QCD using the techniques of perturbation theory.

Perturbation theory is the means by which we can test the SM at current particle physics experiments. We use it to produce testable predictions for reaction cross-sections which can be measured at the current generation of colliders. To be able to do so we need to understand the theory more thoroughly. To test theory against experiment, we need to evaluate higher order terms in the perturbative expansion to ensure that the theoretical prediction is of the same level of accuracy, or more accurate, than the available experimental results, and those that will be produced at the Large Hadron Collider (LHC). To do this we need to understand the source of the divergences that arise in perturbative QCD, and be able to calculate them.

The SM provides the best method we have of explaining the behaviour of fundamental particles through field theories. Although it is a supremely accurate model, with many beautiful aspects, it still has its problems. Some properties of the Standard Model are deemed unsatisfactory by physicists; the hierarchy problem, the lack of a fundamental reason why the masses of the leptons and quarks should be as they are with such a large discrepancy between the lightest and heaviest quarks, and the explanation for nature providing us with three “generations” of particles. At this current time, the main problem with the concept of mass in the SM is that the Higgs particle, which generates particles mass through its coupling to them, is so far undiscovered up to energies of 114 GeV, though the high energy physics community is

holding its breath until the LHC is switched on to see whether it will be discovered. To completely understand nature, the SM will need to be combined with the force of gravity, and the theory of General Relativity that describes it. Many theories abound as to how this should be accomplished, string theory being the most prominent, but we must completely understand the physics of the SM to be able to see the effects of these new theories. To find out what lies beyond the Standard Model, we first have to find the limits of the model itself. The aim of this thesis is to provide a small step along the path to testing the Standard Model at colliders, by examining some of the properties of the SM using perturbation theory. In particular we examine the singularities that arise in the calculation of particle reactions at colliders. In this respect we first look at the evaluation of two-loop integrals by evaluating the master integrals required for the massless two-loop vertex with three offshell legs. We give their expansion in $\epsilon = 2 - \frac{d}{2}$ to elucidate their singular structure. Secondly we evaluate the collinear limits of tree-level processes. These are the singularities of tree level amplitudes when two or more particles become collinear.

The outline of this thesis is as follows:

In Chapter 1 we introduce the fundamentals underlying field theories in the SM, such as the Lagrangian of QCD and the associated Feynman rules. We then examine the Ultra-Violet and Infra-Red singularities which occur in Feynman diagrams, discussing their origin and treatment. To treat the singularities in a mathematically consistent way we introduce the concept of regularisation, in particular Dimensional Regularisation which is used in the rest of this thesis. We then discuss the solution of 1-loop integrals in Minkowski space using Feynman parameters.

In Chapter 2 we discuss methods for solving more general loop-integrals. We begin by deriving the one-loop scalar bubble with arbitrary powers of propagators, which we use to derive the two-loop Sunset integral and the two-loop Glasses integral.

We then discuss the linear identities which loop integrals obey, the IBP and LI identities, and their use in reducing large sets of integrals to a smaller basis set known as Master Integrals. We then discuss the method of Differential Equations to solve these Master Integrals, and the Harmonic Polylogarithms which form a natural set of functions in which to express the solutions.

In Chapter 3 we use the method of differential equations to provide series expansions in ϵ for all two-loop Master Integrals with three external off-shell legs and all internal lines being massless. We present the results in terms of an extended basis of 2-dimensional harmonic polylogarithms which we introduce here. For each Master Integral, we present the differential equations which they satisfy, and sufficient terms in their ϵ -expansion to describe two-loop vertex corrections for physical processes. We conclude this section with a discussion of the application of these Master Integrals in the calculation of the Master Integrals for the two-loop massless box with two adjacent off-shell legs.

In Chapter 4 we introduce the MHV construction for the calculation of tree-level helicity amplitudes. This method uses colour ordered amplitudes and the spinor helicity formalism which we outline. We then give the MHV amplitudes and discuss the MHV-rules method, giving some simple examples of their use in amplitude calculations. For completeness we discuss a second formalism for the calculation of helicity amplitudes, the BCF recursion relations.

In Chapter 5 we consider the collinear limit of multi-parton QCD amplitudes at tree level. We adapt the MHV-rules to enable us to calculate collinear limits and discuss their analytic structure. We then provide general results for splitting functions containing up to three negative helicity gluons, and for up to four partons (including massless quarks). Using these general results we provide explicit results for splitting functions with up to 5 collinear gluons and up to 3 collinear partons.

Finally, in Chapter 6 we present our conclusions. We summarise our findings, and discuss their salient features and future applications.

Chapter 1

Field theory basics

In this section we will introduce the fundamental ideas behind the Standard Model (SM) of particle physics, with emphasis on Quantum Chromodynamics (QCD) and the ideas pertinent to the research in this thesis. A fuller introduction to these ideas, and field theories in general, can be found in many introductory texts, including references [6–11].

1.1 Fundamentals

The Standard Model is a quantum field theory describing the interactions of the fundamental particles invariant under the group of local gauge transformations

$$U(1)_Y \otimes SU(2)_L \otimes SU(3)_C$$

This corresponds to the combination of the Electroweak (Salam, Glashow, Weinberg) [12–14] and colour [1–4] sectors.

The Electroweak sector is invariant under the gauge group

$$U(1)_Y \otimes SU(2)_L$$

This symmetry is spontaneously broken via the Higgs mechanism to the gauge group $U(1)_Q$ of QED. The gauge particle required for invariance under this group is the photon. As QED is an abelian theory, the photon carries no electromagnetic charge. QED describes the interactions of electromagnetically charged particles with photons and thus the electromagnetic force.

The Weak force obeys the gauge group $SU(2)_L$, with three gauge fields W_μ^a , where $a = 1, 2, 3$. Through the spontaneous symmetry breaking of the Higgs mechanism, these three gauge fields mix with the $U(1)_Y$ gauge field, B_μ , to create three mass eigenstates, the W^\pm and Z^0 bosons. The fourth superposition, between the neutral W_μ^3 and B_μ , remains massless and is identified as the photon of the group $U(1)_Q$ of QED. The Higgs particle produced via the Higgs mechanism is responsible for giving all other massive particles their mass through Yukawa couplings to the Higgs particle.

QCD is invariant under gauge transformations corresponding to the non-Abelian $SU(3)_C$ group, with $N_c = 3$ colour degrees of freedom. The gauge quanta required to maintain gauge invariance under this group are the 8 coloured gluons. QCD is a non-Abelian theory, and so these gluons can have self interactions, unlike the photons of QED. This is an important fact as it results in the asymptotic freedom of the theory, which enables us to study high energy QCD using perturbation theory.

The QCD Lagrangian describes the dynamics of fermionic particles (quarks) carrying a colour charge, invariant under the $SU(3)$ gauge transformations. This gauge

invariance requires¹ there to be 8 spin-1 gluon fields, A_μ^a , where $a = 1 \dots 8$. The QCD Lagrangian is given by

$$\mathcal{L}_{\text{QCD}} = -\frac{1}{4}F_{\mu\nu}^a F^{a\mu\nu} + \sum_{\text{flavours}} \bar{\psi}_\alpha (i\not{D} - m)_{\alpha\beta} \psi_\beta + \mathcal{L}_{\text{gaugefixing}} + \mathcal{L}_{\text{ghost}} \quad (1.1)$$

where the index a runs over the 8 colour degrees of freedom, and the (anti-) quark fields $\psi, (\bar{\psi})$ carry a flavour index which we have left implicit, and are in the triplet or fundamental representation of $SU(3)$.

The field strength tensor is defined as

$$F_{\mu\nu}^a = \partial_\mu A_\nu^a - \partial_\nu A_\mu^a - g_s f_{abc} A_\mu^b A_\nu^c. \quad (1.2)$$

It is the last term in this expression that makes QCD non-Abelian, resulting in the self-interaction of gluons through the term $-\frac{1}{4}F_{\mu\nu}^a F^{a\mu\nu}$ in the Lagrangian. This leads to cubic and quartic self-couplings of the gluons, which ultimately leads to asymptotic freedom in QCD.

The covariant derivative is denoted by D , with

$$\not{D} = \gamma^\mu D_\mu \quad (1.3)$$

$$(D_\mu)_{\alpha\beta} = \partial_\mu \delta_{\alpha\beta} + ig_s (t^a A_\mu^a)_{\alpha\beta} \quad (1.4)$$

where the t^a are matrices called the generators of the group $SU(3)$ in the fundamental representation. These generators obey the commutation relations

$$[t^a, t^b] = if_{abc} t^c \quad (1.5)$$

¹In general for an $SU(N)$ gauge group $N^2 - 1$ gauge fields are required for gauge invariance.

where f_{abc} are the totally antisymmetric structure constants of the group. The t^a matrices are hermitian, traceless and normalised such that

$$\text{Tr}(t^a t^b) = \frac{\delta^{ab}}{2} \quad (1.6)$$

In the fundamental representation of $SU(3)$, the t^a can be given in terms of the eight Gell-Mann matrices λ^a , via the relation² $t^a = \frac{\lambda^a}{2}$.

Due to gauge invariance we cannot define the gluon propagator without first fixing the gauge. We do this by adding the following term to the Lagrangian,

$$\mathcal{L}_{gauge\ fixing} = -\frac{1}{2\xi}(\partial^\mu A_\mu^a)^2 \quad (1.7)$$

which defines the covariant gauge with arbitrary ξ . The choice $\xi = 1$ corresponds to the Feynman gauge, which is the most common choice due to its simplification of both the gluon and the photon propagators. The gauge-fixing term is not invariant under gauge transformations. In covariant gauges, gauge invariance is ensured through the introduction of ‘Faddeev-Popov ghosts’. The ghost contribution to the Lagrangian is required to reduce the number of degrees of freedom of the gluon to 2, as physical states of massless vector bosons can only have two polarisations [15]. The ghost fields act as scalar particles within loops, with an additional minus sign to cancel out the contribution of two of the gluon’s polarisations.

$$\begin{aligned} \mathcal{L}_{ghost} &= (\partial_\mu \eta^{a*})(D_{ab}^\mu \eta^b) \\ &= (\partial_\mu \eta^{a*})(\partial^\mu \delta_{ab} - g f_{abc} A_c^\mu) \eta^b \end{aligned} \quad (1.8)$$

BRST symmetry [16] then ensures the unitarity of the S-matrix. With gauge invari-

²In $SU(2)$ the t^a can be given in terms of the Pauli matrices via the same relation.

ance ensured, any physical prediction based on this Lagrangian will be independent of the gauge parameter ξ .

1.2 Feynman rules

In practice we cannot find exact solutions for amplitudes of particle processes. Instead we find approximate solutions through the use of perturbation theory. In QCD the expansion parameter is the strong coupling constant

$$\alpha_s = \frac{g_s^2}{4\pi} \quad (1.9)$$

and is a measure of the strength of the interaction between quarks and gluons. Due to asymptotic freedom, perturbation in this parameter can potentially provide accurate values for observables at the energy scales of modern collider experiments. To find the analytic expressions for amplitudes in perturbation theory there is a pictorial method known as the Feynman diagram method. To use this method we must draw all possible diagrams representing a given process up to the required order in the perturbative expansion. Then for each diagram we can assign analytic factors to each line and vertex, to enable us to compute each diagram in turn. These associated factors are given by the Feynman rules of the theory in question, and are given below for QED and QCD. Finally the amplitude itself can be found by summing all of the Feynman diagrams.

The following momentum-space Feynman rules can be derived from the Lagrangian for the theory in question. They can be found in many references, for example Peskin and Schroeder, appendix A.1 [6], or Aitchison and Hey, appendix F [11]. We represent photons by wavy lines, gluons with curly lines, fermions with solid straight lines and ghost particles with dotted straight lines. Lorentz indices are denoted by

the greek letters μ, ν, λ, ρ , while colour indices are denoted here by $\alpha, \beta, \gamma, \delta$. All propagators carry a momentum p in the direction indicated by the arrow alongside the propagator.

- Photon propagator in general (covariant) gauge.

$$\begin{array}{c} \longrightarrow \\ \mu \text{ ~~~~~ } \nu \end{array} \quad = \frac{i}{p^2} \left\{ -g^{\mu\nu} + (1 - \xi) \frac{p^\mu p^\nu}{p^2} \right\}$$

where $g^{\mu\nu}$ is the Minkowski metric. For simplicity we always take the Feynman gauge $\xi = 1$, in which case the photon propagator reduces to

$$\begin{array}{c} \longrightarrow \\ \mu \text{ ~~~~~ } \nu \end{array} \quad = \frac{i}{p^2} \{ -g^{\mu\nu} \}$$

- Spin- $\frac{1}{2}$ propagator, i.e. quark propagator.

$$\begin{array}{c} \longrightarrow \\ \longrightarrow \end{array} \quad = \frac{i}{\not{p} - m} = i \frac{\not{p} + m}{p^2 - m^2}$$

where m is the mass of the particle propagated by the line. For fermions the arrow on the propagator line indicates the direction of the momentum. Here \not{p} denotes the contraction of the momentum vector with the Dirac matrices, $\not{p} = \gamma^\mu p_\mu$.

- Gluon propagator in general gauge.

$$\begin{array}{c} \longrightarrow \\ \alpha, \mu \text{ ~~~~~ } \beta, \nu \end{array} \quad = \frac{i}{p^2} \left\{ -g^{\mu\nu} + (1 - \xi) \frac{p^\mu p^\nu}{p^2} \right\} \delta^{\alpha\beta}$$

Which in the Feynman gauge, $\xi = 1$, reduces to

$$\begin{array}{c} \longrightarrow \\ \alpha, \mu \text{ ~~~~~ } \beta, \nu \end{array} \quad = \frac{i}{p^2} \{ -g^{\mu\nu} \} \delta^{\alpha\beta}$$

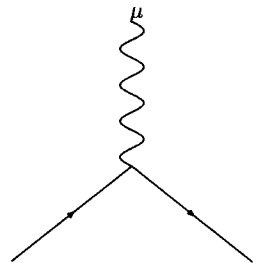
- External quarks and antiquarks. Spinors with 3 colour components (left implicit) and four Dirac components

$$\begin{array}{l} \text{Initial} \quad u(p, s) \quad \text{or} \quad \bar{v}(p, s) \\ \text{Outgoing} \quad \bar{u}(p', s') \quad \text{or} \quad v(p', s') \end{array}$$

- External gluons. As well as the spin-1 polarisation vector ε_μ , external gluons also have a “Colour polarisation” vector a^α ($\alpha = 1 \dots 8$) which specifies the colour state of the gluon.

$$\begin{array}{l} \text{Initial} \quad \varepsilon_\mu(p, \lambda) a^\alpha \\ \text{Final} \quad \varepsilon_\mu^*(p', \lambda') a^{*\alpha} \end{array}$$

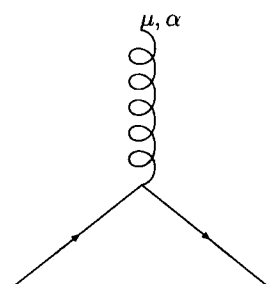
- QED vertex



$$= -iQe\gamma_\mu$$

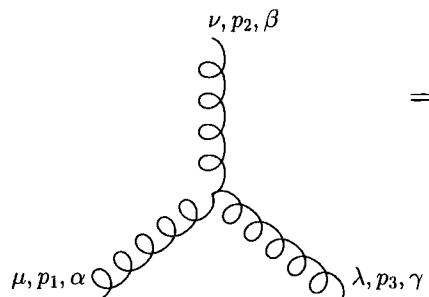
where $Q = -1$ for the electron.

- Quark-Gluon vertex



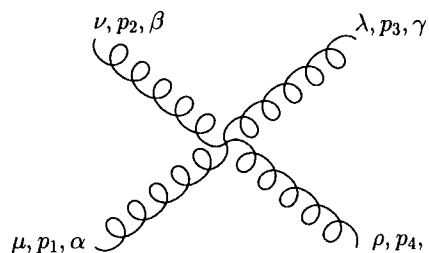
$$= -ig_s \frac{\lambda^\alpha}{2} \gamma_\mu = -ig_s t^\alpha \gamma_\mu$$

- Three gluon vertex. All momenta p_i are taken flowing into the diagram.



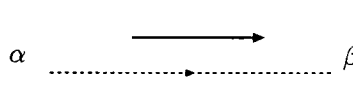
$$= -g_s f_{\alpha\beta\gamma} \left\{ \begin{aligned} &+g_{\mu\nu}(p_1 - p_2)_\lambda \\ &+g_{\nu\lambda}(p_2 - p_3)_\mu \\ &+g_{\lambda\mu}(p_3 - p_1)_\nu \end{aligned} \right\}$$

- Four gluon vertex. All momenta p_i are taken flowing into the diagram.



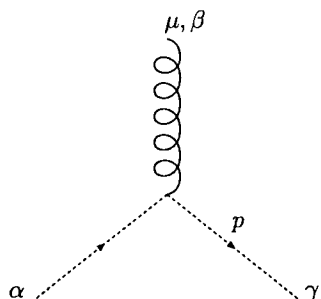
$$= -ig_s^2 \left\{ \begin{aligned} &f_{\alpha\beta\eta} f_{\gamma\delta\eta} (g_{\mu\lambda} g_{\nu\rho} - g_{\mu\rho} g_{\nu\lambda}) \\ &f_{\alpha\delta\eta} f_{\beta\gamma\eta} (g_{\mu\nu} g_{\lambda\rho} - g_{\mu\lambda} g_{\nu\rho}) \\ &f_{\alpha\gamma\eta} f_{\delta\beta\eta} (g_{\mu\rho} g_{\nu\lambda} - g_{\mu\nu} g_{\lambda\rho}) \end{aligned} \right\}$$

- Ghost propagator



$$= \frac{i\delta^{\alpha\beta}}{p^2}$$

- Ghost vertex



$$= -g_s f^{\alpha\beta\gamma} p^\mu$$

We also have the additional rules that:

and parameters contained in the Lagrangian are not the real physical fields and parameters. We will call these quantities the bare parameters. In a renormalisable theory, such as QCD, these will contain UV divergences that can be renormalised order by order in a consistent way. This is achieved through the rescaling of the quantum fields, masses and coupling constants involved in the theory, such that they are all UV finite, as follows:

$$\psi_B = Z_2^{\frac{1}{2}} \psi_R \quad (1.11)$$

$$A_B^\mu = Z_3^{\frac{1}{2}} A_R^\mu \quad (1.12)$$

$$g_B = Z_g g_R \quad (1.13)$$

where B indicates the bare quantities and R indicates the renormalised quantities. In a renormalisable theory, there will be a finite number of such rescalings needed at each order in perturbation theory. The renormalisation parameters Z contain a fixed divergent part such that they cancel the UV divergences of the bare quantities leaving the renormalised fields and parameters finite. The finite parts of the renormalisation parameters are not fixed, and are thus open to choice. This choice is known as the “renormalisation scheme,” typically chosen to reduce the complexity of the final result. A standard choice is the so-called \overline{MS} -scheme, but other schemes exist, for example the “on-shell” scheme.

1.4 Infra-Red Divergences

Loop integrals can also be divergent when propagators diverge for specific values of the loop momentum k . As an example the only non-zero one-loop QCD correction to the quark QED form factor is the one-loop massless triangle diagram as shown

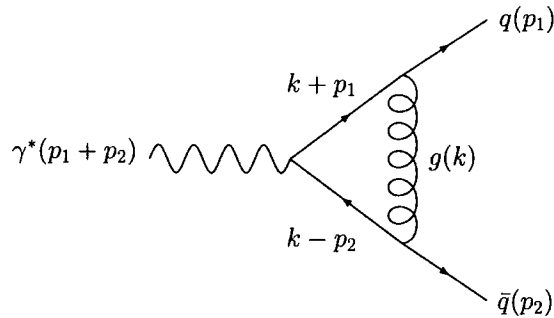


Figure 1.1: The only non-zero one-loop QCD correction to the massless quark QED form factor.

in Fig. 1.1. This integral has the following form

$$\begin{aligned}
 I &= \int \frac{d^4k}{(2\pi)^4} \frac{f(k^2)}{k^2 (k+p_1)^2 (k-p_2)^2} \\
 &= \int \frac{d^4k}{(2\pi)^4} \frac{f(k^2)}{k^2 (k^2 + 2k \cdot p_1) (k^2 - 2k \cdot p_2)}
 \end{aligned} \tag{1.14}$$

with $p_1^2 = 0$, $p_2^2 = 0$. Expanding the integrand in powers of k around $k = 0$, the integrand is $\propto k^{-4} + \mathcal{O}(k^{-3})$, and so at the lower limit of integration this integral will behave as

$$I|_{k \rightarrow 0} = \int \frac{d^4k}{k^4} \propto \int \frac{k^3 dk}{k^4} = \int \frac{dk}{k} = \ln(0) = -\infty \tag{1.15}$$

giving a logarithmic singularity. This is because all the propagators tend to zero in the limit $k \rightarrow 0$. Divergences also arise when $k \rightarrow -p_1$, or when $k \rightarrow p_2$, such that the corresponding propagators diverge. As these divergences are associated with low loop momentum they are known as Infra-Red (IR) divergences. These divergences occur as a result of the use of massless particles in our theory. The IR divergences would remain if we used massive quarks, however, if all of the particles propagating in the loop had a mass, then the mass would act as a regulator to ensure that the integral was IR finite.

Unlike UV singularities, the IR singularities of loop integrals cannot be renormalised away through the rescaling of parameters. Instead, the IR singularities at loop level can be cancelled by considering tree-level processes with additional final state particles at the same order in perturbation theory.

At tree level singularities arise from the emission of massless particles by particles which remain on-shell. When the emitted particles become “soft” (their momentum goes to zero) or collinear to the particle which emitted it, singularities can arise. An example of this can be seen by looking at the propagators involved in the emission of a gluon from a $q\bar{q}$ pair as depicted in figure 1.2. These are the tree-level QCD corrections to the quark QED form factor.

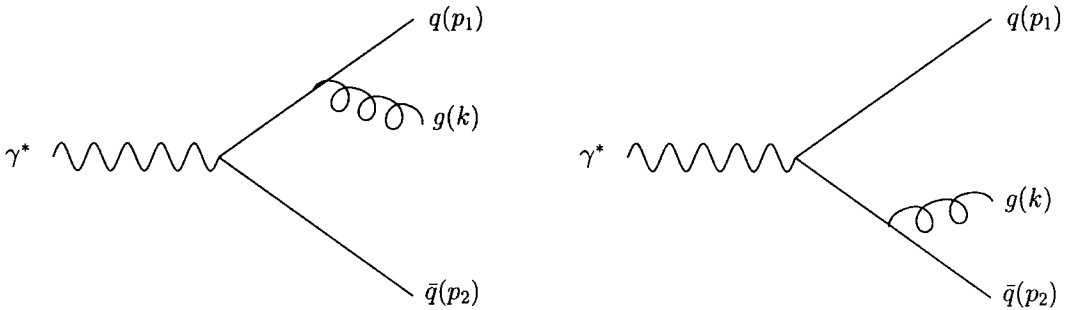


Figure 1.2: The tree-level QCD corrections to the quark QED form factor.

In these diagrams the internal propagators are

$$\begin{aligned} \propto \frac{1}{2k \cdot p_1} &= \frac{1}{2|E_k| (E_1 - p_1 \cos \theta_{p_1 k})} \\ \propto \frac{1}{2k \cdot p_2} &= \frac{1}{2|E_k| (E_2 - p_2 \cos \theta_{p_2 k})} \end{aligned} \quad (1.16)$$

for the first and second diagrams respectively. These propagators apply for both massive and massless quarks, and are obviously divergent when the emitted gluon is soft, $E_k \rightarrow 0$. Hence the phase space integral for this process will also be divergent in this soft region, regardless of whether the quarks have a mass.

With massless quarks, $E = p$, and hence these propagators are also divergent when the angle between the parent particle and the emitted particle $\theta \rightarrow 0$, i.e. the emitted gluon becomes collinear to its massless parent. An alternative way to see this, is to write $k = z_k P$, with $P^2 = 0$, where P is the overall collinear momentum, and z_k is the fraction of that momentum carried by the collinear gluon. Similarly we have that $p = z_p P$, and so $z_p + z_k = 1$ to satisfy momentum conservation. This means that the denominator of the propagator will become $2k \cdot p \propto P^2 = 0$ and so, the integral over the available phase space will have IR singularities in these collinear regions. However with massive quarks $E \neq p$, and so the mass lifts the collinear divergence.

These tree-level soft and collinear singularities will cancel those from the one-loop processes at the same order in perturbation theory, for example here they will cancel against the one-loop vertex. This is because in practice we cannot distinguish between final states with extra particles which are soft or collinear (for example due to detector resolution), and so we must include these extra particle processes in our calculations. The cancellation of divergences is assured by the Kinoshita-Lee-Nauenberg theorem [17, 18], as long as we sum over all possible initial and final states (at a given order in perturbation theory) that are degenerate in the soft or collinear limits. This cancellation works to higher orders in perturbation theory beyond the one loop level as follows: to compute a cross section at N^n LO, we must include processes with n -final state particles at tree-level, $(n - 1)$ -particles at one-loop, $(n - 2)$ -particles at two-loop etc. The initial state divergences are absorbed into the parton distribution functions (pdf's) as in practice it is impossible to create a “clean” initial state of free quarks or gluons from hadrons.

Collinear singularities are discussed in more detail in chapter 5 where we will examine multiparticle collinear singularities.

1.5 Regularisation

A method is required to be able to deal with the divergences that we have discussed in a consistent way. Regularisation is an intermediate step to make divergent integrals mathematically well-defined. There are a number of different methods to regularise a loop integral, these include:

- Introduce a high momentum cut-off on the integral. This breaks gauge invariance and so it is not suitable for gauge theories. Divergences arise, for example, as logarithms of the cut-off scale.
- Give the photon or gluon mass. Giving the massless particles a small mass regulates the IR divergences, however it explicitly breaks gauge invariance. At the end of the calculation the mass can then be taken to zero.
- Pauli Villars. This method modifies the propagator to regulate the divergence, but does not maintain gauge invariance.
- Lattice regularisation. This requires that we discretise space-time at short distance scales, therefore any short distance contribution to the space-time integral is removed. In the momentum picture this is like a high momentum cut-off.
- Dimensional Regularisation (DR). We take loop integrals to be analytic in the space-time dimension d . As the loop integrals are divergent when the dimension $d = 4$, we analytically continue d away from 4 by a small amount to $d = 4 - 2\epsilon$. The advantages of this approach are that it is technically relatively simple, it maintains Lorentz and gauge invariance, and it regularises the IR singularities at the same time as the UV divergences. The UV and IR poles manifest themselves as poles in the analytic continuation parameter ϵ .

For a more detailed discussion of regularisation methods see Muta [7]. Here we will concentrate on Dimensional Regularisation as it is the most commonly used procedure, and is the procedure used in the rest of this thesis.

In dimensional regularisation, with the spacetime dimension d , the space-time index runs from $0 \dots d - 1$. We have

$$g_{\mu\nu}g^{\mu\nu} = d \quad (1.17)$$

For dimensional consistency this alters the mass dimensions of the terms contained within the Lagrangian. The action

$$S = \int d^d x \mathcal{L} \quad (1.18)$$

is dimensionless. This results in the coupling constant having dimension

$$[g_s] = 2 - \frac{d}{2} = \epsilon \quad (1.19)$$

such that it is dimensionless when $d = 4$. To maintain a dimensionless coupling constant we therefore introduce a scale μ such that

$$g \rightarrow \mu^\epsilon g \quad (1.20)$$

Therefore DR introduces an extra scale into our theory. One of the most important reasons for continuing to higher order corrections in perturbation theory is to reduce the dependence of our theoretical predictions on this scale.

DR also alters the Clifford algebra satisfied by the Dirac matrices. We have that

$$\{\gamma^\mu, \gamma^\nu\} = 2g^{\mu\nu} \quad (1.21)$$

which modifies the contraction identities such that

$$\gamma_\mu \gamma^\mu = d \quad (1.22)$$

$$\gamma_\mu \gamma^\nu \gamma^\mu = (2 - d) \gamma^\nu \quad (1.23)$$

$$\gamma_\mu \gamma^\nu \gamma^\rho \gamma^\mu = 4g^{\rho\nu} + (d - 4) \gamma^\nu \gamma^\rho \quad (1.24)$$

$$\gamma_\mu \gamma^\nu \gamma^\rho \gamma^\sigma \gamma^\mu = -2\gamma^\sigma \gamma^\rho \gamma^\nu - (d - 4) \gamma^\nu \gamma^\rho \gamma^\sigma \quad (1.25)$$

These identities are then used in the evaluation of the dimensionally regularised (sub-)amplitudes.

1.6 Feynman Parameters

The method of Feynman parameters enables us to phrase loop integrals in such a way that we can use spherical integration to evaluate the four-momentum integral, see e.g. [6, 7]. We use the method of Feynman parameters to collect all denominator terms into a single quadratic polynomial in the integration momentum, raised to some power n . We can then complete the square and perform the integral over the loop-momentum with relative ease. Following this the only remaining hurdle is to calculate the integrals over the introduced Feynman parameters.

As an example, with A and B propagators in a loop integral, we can use

$$\frac{1}{AB} = \int_0^1 dx \frac{1}{[xA + (1-x)B]^2} = \int_0^1 dx dy \delta(x+y-1) \frac{1}{[xA + yB]^2} \quad (1.26)$$

which combines AB into a single term in the denominator $[xA + yB]^2$. In general

for any number of terms in the denominator we can use

$$\frac{1}{A_1^{m_1} A_2^{m_2} \dots A_n^{m_n}} = \int_0^1 dx_1 \dots dx_n \delta\left(\sum x_i - 1\right) \frac{\prod x_i^{m_i-1}}{[\sum x_i A_i]^{\sum m_i}} \cdot \frac{\Gamma(m_1 + \dots + m_n)}{\Gamma(m_1) \dots \Gamma(m_n)} \quad (1.27)$$

This formula also applies for non-integer m_i .

It is then possible to complete the square in the loop momentum. DR preserves translational invariance, and so we can shift the momentum variable k by a linear amount e.g. $k \rightarrow k - xp$ so that the integral only depends on k^2 and not k .

Using this method we can transform loop integrals into the form

$$I_1 = \int \frac{d^d k}{(2\pi)^d} \frac{1}{(k^2 - M^2 + i\varepsilon)^n} \quad (1.28)$$

where M will be some function of the Feynman parameters and the scales of the loop integral. The $+i\varepsilon$ term is due to the Feynman prescription for propagators, and keeps the integral convergent for all values of M^2 (see also section 1.2).

1.7 1-loop Minkowski space integration

We are now in a position to evaluate the loop momentum integral. To do this we could evaluate the integrations over the time and space components separately, instead we make use of the so-called Wick rotation to enable us to use four dimensional spherical coordinates to evaluate the integral. We cannot do this before the Wick rotation because of the relative minus sign between the time and spatial components of the Minkowski metric. To overcome this, the Wick rotation changes variables such that we have a Euclidean four-momentum by rotating the contour of the k^0 integration by $+\pi/2$ in the complex k^0 plane. In this way we avoid rotation

through the poles in $i\varepsilon$. The Wick rotation is defined by the change of variables

$$k^0 \equiv ik_E^0 \quad \mathbf{k} \equiv \mathbf{k}_E \quad (1.29)$$

where the subscript E denotes the Euclidean variables.

Our integral is then

$$I_1 = \int \frac{d^d k_E}{(2\pi)^d} \frac{i(-1)^n}{(k_E^2 + M^2)^n} \quad (1.30)$$

To evaluate the integral over the loop momentum we proceed as follows. Using

$$d^d k_E = k_E^{d-1} dk_E d\Omega_d \quad (1.31)$$

our basic integral takes the form

$$I_1 = i(-1)^n \int d\Omega_d \cdot \int_0^\infty \frac{dk_E}{(2\pi)^d} \frac{k_E^{d-1}}{(k_E^2 + M^2)^n} \quad (1.32)$$

where $\int d\Omega_d$ is the solid angle of a d -dimensional sphere.

We can then use the definition of the gamma function

$$\begin{aligned} \Gamma(z) &= \int_0^\infty dy y^{z-1} e^{-y} = \int_0^\infty d(ay) (ay)^{z-1} e^{-ay} \\ &= a^z \int_0^\infty dy y^{z-1} e^{-ay} \\ \Rightarrow a^{-z} &= \frac{1}{\Gamma(z)} \int_0^\infty dy y^{z-1} e^{-ay} \end{aligned} \quad (1.33)$$

where we take a to be the denominator of the second factor of eq. (1.33), giving

$$I_1 = \frac{i(-1)^n}{(2\pi)^d \Gamma(n)} \int d\Omega_d \int_0^\infty dy y^{n-1} e^{-M^2 y} \cdot \int_0^\infty dk_E k_E^{d-1} e^{-k_E^2 y} \quad (1.34)$$

Following this we can then use the change of variable $x^2 = k_E^2 y$ to give

$$I_1 = \frac{i(-1)^n}{(2\pi)^d \Gamma(n)} \int d\Omega_d \cdot \int_0^\infty dy y^{n-1-\frac{d}{2}} e^{-M^2 y} \cdot \int_0^\infty dx x^{d-1} e^{-x^2} \quad (1.35)$$

The following identity³

$$\begin{aligned} \pi^{\frac{d}{2}} &= \left(\int_{-\infty}^{+\infty} dx e^{-x^2} \right)^d = \int d^d x \exp \left(- \sum_{i=1}^d x_i^2 \right) \\ &= \int d\Omega_d \int_0^\infty dx x^{d-1} e^{-x^2} \end{aligned} \quad (1.36)$$

reduces our integral to

$$I_1 = \frac{i(-1)^n \pi^{(d/2)}}{(2\pi)^d \Gamma(n)} \cdot \int_0^\infty dy y^{n-1-\frac{d}{2}} e^{-M^2 y} \quad (1.37)$$

Using the substitution $t = M^2 y$ we have

$$I_1 = \frac{i(-1)^n}{(4\pi)^{\frac{d}{2}} \Gamma(n)} (M^2)^{\frac{d}{2}-n} \cdot \int_0^\infty dt t^{n-\frac{d}{2}-1} e^{-t} \quad (1.38)$$

which, from the definition of the Gamma function, eq. 1.33, gives us the overall formula for one loop integration

$$\int \frac{d^d k}{(2\pi)^d} \frac{1}{(k^2 - M^2)^n} = \frac{i(-1)^n}{(4\pi)^{\frac{d}{2}}} \frac{\Gamma(n - \frac{d}{2})}{\Gamma(n)} (M^2)^{\frac{d}{2}-n}. \quad (1.39)$$

This completes the integration over the loop momentum, leaving only the integrals over the Feynman parameters to be carried out to complete the loop integral. We

³This identity tells us that the d -dimensional solid angle is given by

$$\int d\Omega_d = \frac{2\pi^{\frac{d}{2}}}{\Gamma(\frac{d}{2})}.$$

now present some basic formulas for one loop integration;

$$\int \frac{d^d k}{(2\pi)^d} \frac{1}{(k^2 + 2k \cdot q - M^2)^n} = \frac{i(-1)^n \Gamma(n - \frac{d}{2})}{(4\pi)^{\frac{d}{2}} \Gamma(n)} (q^2 + M^2)^{\frac{d}{2} - n}, \quad (1.40)$$

$$\int \frac{d^d k}{(2\pi)^d} \frac{1}{(k^2)^n} = 0. \quad (1.41)$$

And by anti-symmetry:

$$\int \frac{d^d k}{(2\pi)^d} \frac{k^\mu}{(k^2 - M^2)^n} = 0 \quad (1.42)$$

and for example

$$\int \frac{d^d k}{(2\pi)^d} \frac{k^\mu k^\nu}{(k^2 - M^2)^n} = \frac{g^{\mu\nu}}{2(n-1)} \int \frac{d^d k}{(2\pi)^d} \frac{1}{(k^2 - M^2)^{n-1}} \quad (1.43)$$

which can be derived from the general result by differentiating twice with respect to q^α .

1.8 Summary

In this chapter we have introduced the basics of quantum field theory, beginning with the fundamentals of the SM and the Lagrangian of QCD. We have then given the Feynman rules derived from this Lagrangian to enable us to examine the mathematical structure of Feynman diagrams. In doing so we have seen that Feynman diagrams have divergences in both the UV and IR regions, and that the UV singularities can be removed by the process of renormalisation. We have then examined the IR singularities of Feynman diagrams, which cancel between loop diagrams and the soft and collinear limits of tree-level processes. These tree-level collinear singularities will be investigated further in chapter 5. Regularisation has been introduced to enable us to deal with the divergences of Feynman diagrams in a mathemati-

cally consistent way. Using the method of Feynman parameters, we were then able to evaluate the loop momentum integral for the basic structure of a loop integral in Minkowski space, leaving only the integration over the Feynman parameters remaining. This enables us to calculate one-loop diagrams in the following chapter, beginning with the one-loop bubble integral, which will then lead us on to the techniques required for the evaluation of more complicated integrals.

Chapter 2

Loop integral methods

In this chapter we introduce the methods required to solve loop integrals, specifically with respect to the methods used in chapter 3 to find the ϵ -expansion of the integrals required for the massless two-loop vertex with three offshell legs. In this respect we shall introduce repeated one-loop integration via bubble insertions and products of one-loop solutions to find two of the integrals required in chapter 3. This is followed by the introduction of the linear identities obeyed by loop integrals, the Integration by Parts and Lorentz Invariance identities. We then outline how these can be used to reduce the hundreds of integrals required for the calculation of an amplitude to a small basis set of so called “Master Integrals”, and how these can be evaluated through the use of differential equations.

A generic loop integral with L -loops, m propagators and n legs, is given by the integral:

$$I(\nu_1, \nu_2, \dots, \nu_m; \{s_{ij}\}) = \int \prod_{l=1}^L \frac{d^d k_l}{(2\pi)^d} \frac{1}{A_1^{\nu_1} A_2^{\nu_2} \dots A_m^{\nu_m}} \quad (2.1)$$

where $\{s_{ij}\}$ are the set of Lorentz invariant external momentum scales that are involved in the integral. The set of propagators $A_1 \dots A_m$ specifies the “topology”

of the diagram, and integrals sharing this set of common propagators are then said to belong to the same topology. Integrals within each topology are specified by the powers of the propagators $\{\nu_i\}$ and the scales involved, $\{s_{ij}\}$. If an integral shares a subset of these propagators, it is said to belong to a simpler topology.

The denominator terms A_i take the general form

$$A_i = \left(\sum_{j=1}^L \varepsilon_{ij} k_j + q_i \right)^2 - m^2 \quad (2.2)$$

with q_i some linear combination of the external momenta involved in the diagram and m the mass of the internal line. The factor $\varepsilon_{ij} = 0, \pm 1$ takes into account whether a given internal line depends on a given loop momenta, and the direction that each loop momenta is taken to flow along that line. If all the internal lines of a given integral have $m = 0$, then the integral is called massless.

The denominator terms $A_i^{\nu_i}$ in the integral can have either positive or negative powers ν_i . Negative powers correspond to terms in the numerator, which will consist of scalar products of either loop momenta with external momenta or with other loop momenta, or of the scales of the integral $\{s_{ij}\}$. If the numerator depends on loop-momenta then the integral is called a tensor integral, otherwise it is called a scalar integral. Positive powers of denominator terms $\nu > 1$ correspond to extra powers of propagators. These are “dotted” propagators, as in the pictorial representation of these integrals the extra powers are represented by dots on the propagator line. Denominators with zero powers correspond to terms that have been cancelled from the integral, and so belong to a simpler topology. These terms are called “pinched” propagators, as pictorially it is as though the two ends of the propagator have been pinched together. Due to these cancellations the diagrams that represent integrals do not necessarily obey the Feynman rules of section. 1.2.

A loop integral is termed planar if it can be represented by a 2-dimensional diagram without any lines crossing each other. If this is not possible, then the diagram is termed non-planar. Non-planar diagrams have proved to be more complicated to solve than planar diagrams [19, 20]. Most integrals we investigate here are planar, but for an example of a non-planar diagram see the two-loop crossed triangle F_4 , which we solve in section. 3.3.2.

In general loop integrals become more complicated to evaluate for increasing numbers of loops, increasing numbers of denominators (both in the denominator and the numerator) and with increasing numbers of external legs and scales. For this reason we begin our evaluation of loop integrals with the simplest massless one-loop bubble and its further applications.

2.1 One-loop integration

One-loop integration relies on the 1-loop Minkowski space integration formulae developed in section. 1.7. Using these formulae we will now derive the expression for the massless scalar bubble integral with arbitrary powers of legs. Using this formula we will then be able to solve two-loop integrals through the use of repeated one-loop integration, or through the factorisation of multi-loop integrals into one-loop integrals.

The massless scalar bubble integral with arbitrary powers of legs is shown in figure 2.1, and is given by the following integral:

$$B(\nu_1, \nu_2, p^2) = \int \frac{d^d k}{(2\pi)^d} \frac{1}{(k^2)^{\nu_1} ((p-k)^2)^{\nu_2}} \quad (2.3)$$

In Dimensional Regularisation (section 1.5), and using the method of Feynman

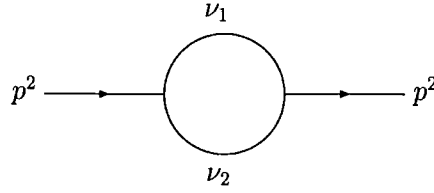


Figure 2.1: The massless scalar bubble diagram with arbitrary powers of propagators represented by ν_1 and ν_2 .

parameters (section 1.6), this can be written as

$$\begin{aligned}
 B(\nu_1, \nu_2, p^2) &= \frac{\Gamma(\nu_1 + \nu_2)}{\Gamma(\nu_1)\Gamma(\nu_2)} \int_0^1 dx \int \frac{d^d k}{(2\pi)^d} \frac{(1-x)^{\nu_1-1} x^{\nu_2-1}}{[x(p-k)^2 + (1-x)k^2]^{\nu_1+\nu_2}} \\
 &= \frac{\Gamma(\nu_{12})}{\Gamma(\nu_1)\Gamma(\nu_2)} \int_0^1 dx \int \frac{d^d k}{(2\pi)^d} \frac{(1-x)^{\nu_1-1} x^{\nu_2-1}}{[k^2 + x(1-x)p^2]^{\nu_{12}}} \quad (2.4)
 \end{aligned}$$

where we have completed the square, performed the shift $k \rightarrow k + px$ and used Eq. 1.42. For simplicity, we have introduced the following notation.

$$\nu_{ijk\dots} = \nu_i + \nu_j + \nu_k + \dots \quad (2.5)$$

Comparing with Eq. 1.39, we now have $M^2 = -x(1-x)p^2$ and $n = \nu_1 + \nu_2 = \nu_{12}$, and so

$$\begin{aligned}
 B(\nu_1, \nu_2, p^2) &= \frac{i(-1)^{\nu_{12}}}{(4\pi)^{\frac{d}{2}}} \frac{\Gamma(\nu_{12} - \frac{d}{2})}{\Gamma(\nu_1)\Gamma(\nu_2)} \int_0^1 dx (M^2)^{\frac{d}{2} - \nu_{12}} (1-x)^{\nu_1-1} x^{\nu_2-1} \\
 &= \frac{i(-1)^{\nu_{12}}}{(4\pi)^{\frac{d}{2}}} \frac{\Gamma(\nu_{12} - \frac{d}{2})}{\Gamma(\nu_1)\Gamma(\nu_2)} (-p^2)^{\frac{d}{2} - \nu_{12}} \int_0^1 dx (x)^{\frac{d}{2} - \nu_1 - 1} (1-x)^{\frac{d}{2} - \nu_2 - 1} \quad (2.6)
 \end{aligned}$$

The remaining integral is easily solved using the definition of the β function.

$$\beta(r, s) = \int_0^1 dx x^{r-1} (1-x)^{s-1} = \frac{\Gamma(r)\Gamma(s)}{\Gamma(r+s)} \quad (2.7)$$

This gives us the general formula for the massless scalar bubble integral with arbitrary powers of legs:

$$B(\nu_1, \nu_2, p^2) = \frac{i(-1)^{\frac{d}{2}} \Gamma(\nu_{12} - \frac{d}{2}) \Gamma(\frac{d}{2} - \nu_1) \Gamma(\frac{d}{2} - \nu_2)}{(4\pi)^{\frac{d}{2}} \Gamma(\nu_1) \Gamma(\nu_2) \Gamma(d - \nu_{12})} (p^2)^{\frac{d}{2} - \nu_{12}} \quad (2.8)$$

The bubble $B(\nu_1, \nu_2, p^2)$ is symmetric under the interchange $\nu_1 \leftrightarrow \nu_2$ as we would expect from the diagram 2.1, as we could have labelled either internal leg as ν_1 .

The gamma function is undefined for zero argument, and so we can see that there are singularities when

$$\begin{aligned} \nu_{12} &= \frac{d}{2} \\ \nu_1 &= \frac{d}{2} \\ \nu_2 &= \frac{d}{2} \end{aligned} \quad (2.9)$$

The first singularity occurs in the factor $\Gamma(\nu_{12} - \frac{d}{2}) = \Gamma(\nu_{12} - 2 + \epsilon)$. This singularity is associated with UV divergences, as at $\nu_{12} = \frac{d}{2}$ a positive value of ϵ is required to keep the argument of gamma positive. A power counting argument shows us that $\epsilon > 0$ protects against this UV divergence. For example with $d = 4 - 2\epsilon$ and $\nu_{12} = 4$ our integral behaves in the UV region as

$$\int \frac{d^d k}{k^4} \sim \int k^{-1-2\epsilon} dk \quad (2.10)$$

which is well behaved for large k when $\epsilon > 0$. The remaining singularities are associated with the factor $\Gamma(\frac{d}{2} - \nu_i) = \Gamma(2 - \epsilon - \nu_i)$ where $i = 1, 2$. These singularities are associated with IR singularities, as $\epsilon < 0$ is required to keep the arguments of the gamma function positive.

We can see that for integer ν_1, ν_2 this is reducible to $B(1, 1, p^2)$ using the property

of the gamma function

$$z \Gamma(z) = \Gamma(z + 1) \quad (2.11)$$

and

$$(p^2)^{\frac{d}{2}-\nu_{12}} = (p^2)^{\frac{d}{2}-2}(p^2)^{2-\nu_{12}}. \quad (2.12)$$

Due to the large number of integrals required to evaluate matrix elements beyond the Leading Order in perturbation theory, and the increasing difficulty of solving the integrals involved, we find it useful to express all integrals in terms of a small set of integrals, which are called Master Integrals (MIs). For the simple scalar bubble case in consideration here it makes little difference to perform the reduction to $B(1, 1, p^2)$, but it simplifies the calculation immensely when there are more loops and scales involved in the process. Hence the Master Integral of this topology is the one-loop massless scalar bubble, which we denote by $BB(p^2) = B(1, 1, p^2)$, and so

$$BB(p^2) = \frac{i}{(4\pi)^{2-\epsilon}} \frac{\Gamma(\epsilon)\Gamma^2(1-\epsilon)}{\Gamma(2-2\epsilon)} (-p^2)^{-\epsilon}. \quad (2.13)$$

There is a common overall factor amongst Master Integrals which we denote S_D , given by

$$S_D = \frac{(4\pi)^\epsilon \Gamma(1+\epsilon)\Gamma^2(1-\epsilon)}{16\pi^2 \Gamma(1-2\epsilon)}. \quad (2.14)$$

To perform general ϵ expansions we need the following expansions of the gamma function about $\epsilon = 0$,

$$\Gamma(1+a\epsilon) = 1 - a\gamma\epsilon + \frac{a^2}{2} (\zeta(2) + \gamma^2) \epsilon^2 - \frac{a^3}{12} (3\zeta(3) + 6\zeta(2)\gamma + 2\gamma^3) \epsilon^3 + \mathcal{O}(\epsilon^4) \quad (2.15)$$

where a is some constant. In this expansion, γ is the Euler-Mascheroni constant which has the numerical value $\gamma = 0.57721566\dots$, and $\zeta(x)$ is the Riemann zeta function, where $\zeta(2) = \frac{\pi^2}{6}$, $\zeta(3) = 1.2020569$ and $\zeta(4) = \frac{\pi^4}{90}$. Expansions of the gamma function with different arguments can then be found using the properties of the gamma function, for example we can shift the argument by ± 1 using Eq. 2.11. We now find the ϵ expansion of S_D ,

$$S_D = \frac{(4\pi)^\epsilon}{16\pi^2} e^{-\gamma\epsilon} \left(1 - \frac{1}{2}\zeta(2)\epsilon^2 - \frac{7}{3}\zeta(3)\epsilon^3 - \frac{47}{16}\zeta(4)\epsilon^4 + \mathcal{O}(\epsilon^5) \right). \quad (2.16)$$

As S_D is finite as $\epsilon \rightarrow 0$ we can safely factor it out when performing ϵ expansions. Factoring out S_D , the one-loop Master Integral BB with its epsilon expansion is given by

$$\begin{aligned} \text{BB}(q^2) &= iS_D(-q^2)^{-\epsilon} \frac{1}{\epsilon(1-2\epsilon)}, \\ &= iS_D(-q^2)^{-\epsilon} \frac{1}{\epsilon} (1 + 2\epsilon + 4\epsilon^2 + 8\epsilon^3 + 16\epsilon^4 + \mathcal{O}(\epsilon^5)). \end{aligned} \quad (2.17)$$

2.2 Sunsets and glasses

We are now in a position to see the usefulness of the one-loop bubble with arbitrary powers of propagators. Repeated one-loop integration can be used to solve multi-loop integrals which have bubble insertions. As an example of this method, the simplest of these is the two-loop massless scalar sunset graph, $\text{SS}(p^2)$, as shown in Fig. 2.2.

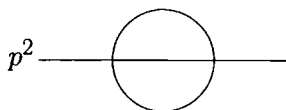


Figure 2.2: The sunset integral.

The three-propagator sunset graph is given by the scalar integral

$$\text{SS}(p^2) = \iint \frac{d^d l}{(2\pi)^d} \frac{d^d k}{(2\pi)^d} \frac{1}{k^2 (k+l+p)^2 l^2} \quad (2.18)$$

We can see from both the integral, and the momentum flow through the diagram, that this can be written as a bubble insertion into another bubble integral. If we take the k integration loop as the inserted bubble, we can see that it corresponds to a bubble with unit powers of propagators “carrying” the scale $(l+p)^2$.

$$\begin{aligned} \text{SS}(p^2) &= \int \frac{d^d l}{(2\pi)^d} \frac{1}{l^2} B(1, 1, (l+p)^2) \\ &= \frac{i(-1)^{\frac{d}{2}} \Gamma(2 - \frac{d}{2}) \Gamma^2(\frac{d}{2} - 1)}{(4\pi)^{\frac{d}{2}} \Gamma(d-2)} \int \frac{d^d l}{(2\pi)^d} \frac{1}{l^2 ((l+p)^2)^{2-\frac{d}{2}}} \end{aligned} \quad (2.19)$$

Now that we have inserted the k momentum bubble, we are left with a one-loop bubble with scale p^2 , and the power of the second propagator is now $2 - \frac{d}{2}$ due to the evaluation of the first integral.

$$\begin{aligned} \text{SS}(p^2) &= \frac{i(-1)^{\frac{d}{2}} \Gamma(2 - \frac{d}{2}) \Gamma^2(\frac{d}{2} - 1)}{(4\pi)^{\frac{d}{2}} \Gamma(d-2)} B(1, 2 - \frac{d}{2}, p^2) \\ &= \left(\frac{i(-1)^{\frac{d}{2}}}{(4\pi)^{\frac{d}{2}}} \right)^2 \frac{\Gamma^3(\frac{d}{2} - 1) \Gamma(3-d)}{\Gamma(3\frac{d}{2} - 3)} (p^2)^{d-3} \end{aligned} \quad (2.20)$$

Note that we could have evaluated this topology with arbitrary powers of propagators, ν_1, ν_2, ν_3 , via the same method. However we have used unit powers of propagators as this provides us with the Sunset Master Integral which is required in chapter 3 as one of the basis set of integrals required for the two-loop vertex.

The method of Bubble insertions works because the Bubble integral is proportional to the square of the momentum entering it, p^2 , and hence is proportional to a propagator with that momentum, and so a bubble is equivalent to a propagator

raised to some power. Hence in a diagram a Bubble can be replaced by a propagator with additional powers. In this way Bubble insertions can be used to solve all L -loop integrals that have the “sunset” configuration.

Factoring out S_D^2 we find the sunset integral and its ϵ expansion is given by

$$\begin{aligned} \text{SS}(p^2) &= S_D^2 (-p^2)^{1-2\epsilon} \frac{\Gamma(2\epsilon-1)\Gamma(1-2\epsilon)^2}{\Gamma(3-3\epsilon)\Gamma(1-\epsilon)\Gamma(1+\epsilon)^2} \\ &= S_D^2 (-p^2)^{1-2\epsilon} \left[-\frac{1}{4\epsilon} - \frac{13}{8} - \frac{115}{16}\epsilon - \left(\frac{865}{32} - \frac{3}{2}\zeta(3) \right) \epsilon^2 + \mathcal{O}(\epsilon^3) \right]. \end{aligned} \quad (2.21)$$

When a two-loop diagram consists of two loop integrals which do not share a

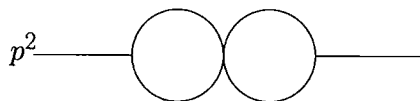


Figure 2.3: The glasses integral.

common propagator, the two-loop integral factorises into the product of two one-loop integrals. A simple example of this is the four-propagator “glasses” integral shown in Fig. 3.3.1, which we denote by $\text{GL}(p^2)$. In this case the two-loop integrals factorises into the product of two one-loop scalar bubbles, as shown in Fig. 2.4. They are both dependent on the same scale as there is only one scale present in the process.

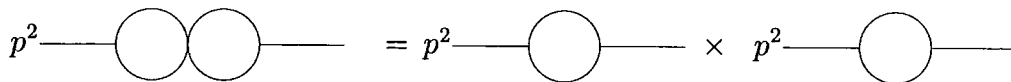


Figure 2.4: A diagram showing the factorisation of the two-loop Glasses integral into the product of two one-loop bubble integrals.

The integral is therefore given by,

$$\begin{aligned} \text{GL}(p^2) = \text{BB}(p^2)^2 &= -(-p^2)^{-2\epsilon} S_D^2 \frac{1}{\epsilon^2(1-2\epsilon)^2} \\ &= -(-p^2)^{-2\epsilon} S_D^2 \frac{1}{\epsilon^2} (1 + 4\epsilon + 12\epsilon^2 + 32\epsilon^3 + 80\epsilon^4 + \mathcal{O}(\epsilon^5)). \end{aligned} \quad (2.22)$$

We will use this factorisation property of integrals which have no common denominators to solve for the master integral which we call TB , in section 3.3.2.

2.3 Integration by Parts Identities (IBP's)

The Integration by Parts identities rely on the fact that the integral over the total derivative with respect to the loop momentum vanishes in dimensional regularisation [21].

Integrals of the same topology will be related linearly via these identities. These identities can then be used to express unknown complicated integrals as a combination of simpler and hopefully known integrals. This process is known as reduction.

The IBP identities are given by

$$0 = \int \prod_{j=1}^L \frac{d^d k_j}{(2\pi)^d} \frac{\partial}{\partial K^\mu} \frac{v^\mu}{A_1^{\nu_1} \dots A_n^{\nu_m}} \quad (2.23)$$

where j runs from 1 to the number of loops L , v^μ is any of the loop or external momenta, and K is any of the loop momenta. With n external momenta, there will be $n - 1$ independent momenta due to momentum conservation, and therefore $L + n - 1$ possible independent v^μ . Each of these v^μ can be differentiated by any of

the L loop momenta, and so the total number of independent IBP identities will be

$$N_{IBP} = L(L + n - 1) \quad (2.24)$$

In this thesis we look to solve integrals with no internal masses, and so we can set $m = 0$ in our general form for the propagator Eq. 2.2.

$$A_i = \left(\sum_j \varepsilon_{ij} k_j + q_i \right)^2 \quad (2.25)$$

Using the chain-rule, the differentials involved in the IBP identities are either of the numerator terms,

$$\frac{\partial}{\partial K^\mu} v^\mu, \quad (2.26)$$

or propagator terms

$$\frac{\partial}{\partial K^\mu} \frac{1}{A_i^{\nu_i}}. \quad (2.27)$$

Unless v^μ contains K^μ the differential of the numerators will be zero. However if $v^\mu = K^\mu$ then

$$\frac{\partial}{\partial K^\mu} K^\mu = \delta_\mu^\mu = d \quad (2.28)$$

The differential of the propagator terms is zero if the propagator does not contain K^μ , however if it does the differential will be

$$v^\mu \frac{\partial}{\partial K^\mu} \frac{1}{A_i^{\nu_i}} = \frac{-2\nu_i \varepsilon_{iK} \left(\sum_j \varepsilon_{ij} k_j \cdot v + q_i \cdot v \right)}{A_i^{\nu_i+1}}. \quad (2.29)$$

We can see that the term $A_i \cdot v$ will produce terms with scalar products $p_i \cdot p_j$ which correspond to external scales, and $p_i \cdot k_j$ and $k_i \cdot k_j$. These last two types can sometimes be cancelled against propagators, in which case they are classed as

reducible numerator terms. However if they can not be cancelled they are classed as irreducible, which means that combinations of IBP identities are required to eliminate them so that we can end up with only scalar integrals.

The cancellation of scalar products with denominator terms, and the action of the differential on the propagators, means that we have integrals with either raised or lowered powers of their numerators. For convenience we define raising and lowering operators that have the action of increasing or decreasing the powers of propagators by 1.

$$i^\pm I(\nu_1, \dots, \nu_i \dots, \nu_n; \{s_{ij}\}) = I(\nu_1, \dots, \nu_i \pm 1, \dots, \nu_n; \{s_{ij}\}) \quad (2.30)$$

We shall now use a simple example to demonstrate the use of IBP identities to reduce a simple integral.

2.3.1 Triangle IBP's

The one-loop massless scalar triangle with one massive leg is given in figure 2.5.

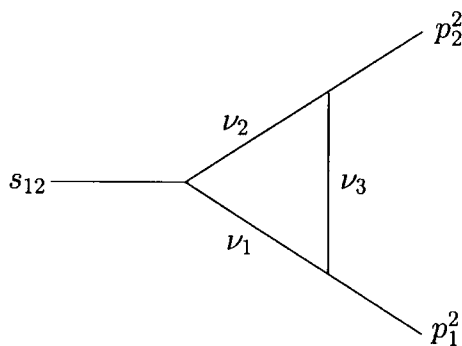


Figure 2.5: The massless scalar triangle diagram with arbitrary powers of propagators represented by ν_1 , ν_2 and ν_3 , and two on-shell legs, $p_1^2 = 0$, $p_2^2 = 0$.

This integral can be solved using the one-loop Minkowski space integration rules of section 1.7 followed by a relatively straightforward integration over the Feynman parameters. However, a simpler method is to use the IBP identities. For the triangle

topology these are given by

$$\begin{aligned}
 0 &= -(d - \nu_{1233})I_0 + (\nu_1\mathbf{1}^+ + \nu_2\mathbf{2}^+)\mathbf{3}^- I_0 \\
 0 &= -(d - \nu_{1123})I_0 + (\nu_2\mathbf{2}^+ + \nu_3\mathbf{3}^+)\mathbf{1}^- I_0 \\
 0 &= -(d - \nu_{1223})I_0 + (\nu_1\mathbf{1}^+ + \nu_3\mathbf{3}^+)\mathbf{2}^- I_0
 \end{aligned} \tag{2.31}$$

Hence the massless scalar triangle $I_0(1, 1, 1)$ can be reduced to bubble integrals ($\mathbf{i}^- I_0$) via the IBP identities. Using the first identity we have

$$\begin{aligned}
 0 &= -(d - 4)I_0(1, 1, 1; \{s_{ij}\}) + (1 \cdot \mathbf{1}^+ + 1 \cdot \mathbf{2}^+)\mathbf{3}^- I_0(1, 1, 1; \{s_{ij}\}) \\
 \Rightarrow I_0(1, 1, 1) &= \frac{1}{d - 4} \{I_0(2, 1, 0; s_{12}) + I_0(1, 2, 0; s_{12})\} \\
 &= \frac{1}{d - 4} \{B(2, 1, s_{12}) + B(1, 2, s_{12})\} \\
 &= \frac{2}{d - 4} \{B(1, 2, s_{12})\}
 \end{aligned} \tag{2.32}$$

where $B(1, 2, s_{12})$ can be easily found using equation 2.8. This reduction is represented schematically in Fig. 2.6, where the dotted propagator represents the extra power on the propagator.

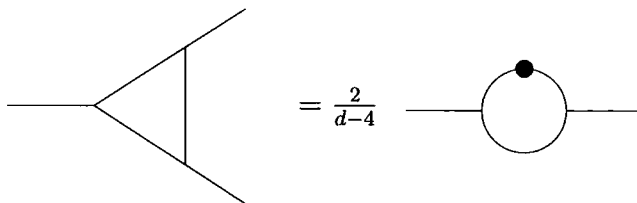


Figure 2.6: Figure showing the massless scalar triangle decomposed as a “dotted” scalar bubble diagram.

This demonstrates that linear identities such as the IBP relations can be used to express more complicated integrals as combinations of simpler integrals. The example

used here is particularly simple, in that the bubble integrals which the triangle is reduced to are already known. However, if the integrals from the simpler topology are not already known, in general we can reduce them further through the use of their own linear identities. Therefore the reduction via linear identities can be repeated iteratively until we are left with a set of integrals that can no-longer be reduced, and therefore have to be solved by other methods. These irreducible integrals are called Master Integrals (MI's) and the iterative process is known as the reduction to Master Integrals. This process has been fully automated in computer programs such as AIR [22] using the Laporta Algorithm of sect. 2.5.

2.4 Lorentz Invariance Identities

The Lorentz Invariance (LI) identities were introduced by Gehrmann and Remiddi [21] to provide an extra set of identities for the reduction of loop integrals. Although they are not always required for complete reduction, they can be necessary, for example in the evaluation of the non-planar massless double box with light-like legs [20]. Following [21] we present the derivation of the LI identities.

The LI exploit the fact that the loop integrals are Lorentz scalars, as they are a function of only scalar products of the external momenta. This means that they are invariant under Lorentz transforms of the external momenta, which in DR can be considered a d -dimensional rotation. The infinitesimal Lorentz transformation on the external momentum

$$p^\mu \rightarrow p^\mu + \delta p^\mu = p^\mu + \delta \epsilon_\nu^\mu p^\nu \quad \text{where} \quad \delta \epsilon_\nu^\mu = -\delta \epsilon_\mu^\nu \quad (2.33)$$

will leave the integral I unchanged, and so using a Taylor expansion we can write

$$\begin{aligned} I(p_1, \dots, p_n) &= I(p_1 + \delta p_1, \dots, p_n + \delta p_n) \\ &= I(p_1, \dots, p_n) + \delta p_1^\mu \frac{\partial}{\partial p_1^\mu} I(p_1, \dots, p_n) + \dots + \delta p_n^\mu \frac{\partial}{\partial p_n^\mu} I(p_1, \dots, p_n) \end{aligned} \quad (2.34)$$

which gives us the identity

$$0 = \delta \epsilon_\nu^\mu \left(p_1^\nu \frac{\partial}{\partial p_1^\mu} + \dots + p_n^\nu \frac{\partial}{\partial p_n^\mu} \right) I(p_1, \dots, p_n) \quad (2.35)$$

Due to its antisymmetry, $\delta \epsilon_\nu^\mu$ has six independent components, giving us a maximum of six LI identities. However these are not always independent, and so using the antisymmetric property of $\delta \epsilon_\nu^\mu$ we can rewrite Eq. 2.35 as

$$0 = \sum_{i=1}^n \left(p_i^\nu \frac{\partial}{\partial p_i^\mu} - p_i^\mu \frac{\partial}{\partial p_i^\nu} \right) I(p_1, \dots, p_n) \quad (2.36)$$

This can then be Lorentz contracted with all possible antisymmetric combinations of independent momenta $p_{i\mu} p_{j\nu}$ to give all of the possible independent identities. In DR we can then exchange the derivatives in Eq. 2.36 with the loop integrations involved in I , such that the derivatives act on the integrand, which will then give the full LI identities. These identities will relate integrals with differing powers of propagators, because they contain differentials of the propagators, in a similar manner to the IBP identities of section 2.3, and so they can be used in the reduction to Master Integrals. For three external particles there is only one antisymmetric combination e.g. $p_{1\mu} p_{2\nu}$ and so there is only one LI. The maximum of six LI is only achievable for integrals with 5 or more external legs.

2.5 The Laporta Algorithm

The reduction via IBP (& LI) identities to MIs has been fully automated via the Laporta algorithm [23] for the reduction of generic loop integrals. This algorithm has been encoded in programs such as the Automatic Integral Reduction package AIR [22]. This algorithm orders the identities according to the complexity of the equation, and then through Gauss elimination uses these identities to reduce each integral in turn. For a more detailed explanation of the Laporta algorithm, please see the original paper, Ref. [23], and for an example of its operation see Ref. [22].

If we wish to solve the class of integrals $I(\nu_1, \nu_2, \dots, \nu_m)$ then the algorithm proceeds as follows. Firstly we generate the IBP and LI identities for I with generic ν . Secondly a *seed* integral is generated. This is the integral with the simplest set of $\{\nu_1, \nu_2, \dots, \nu_m\}$ that give a non-zero value¹ for I . We then input this set of ν_i into the set of IBP and LI identities to give us the full set of identities applicable to the seed integral. To use these identities for the process of reduction, we need to know which of the integrals involved in each identity are the most complicated, so that we can solve for them first. To do this the following criteria are applied:

- The most complicated integral is assumed to have the largest number of propagators:

$$\mathcal{N}_{prop} = \sum_i \Theta(\nu_i). \quad (2.37)$$

where we define

$$\Theta(x) = \begin{cases} 1 & \text{if } x > 0 \\ 0 & \text{if } x \leq 0 \end{cases}. \quad (2.38)$$

¹For this, it is computationally easier to provide the program with the criteria for which the integral is zero for a given a set of ν_i . The algorithm will eventually find that the applicable integrals are zero through elimination, however this is a less efficient use of the algorithm.

- If there is more than one integral with the same maximum \mathcal{N}_{prop} then the integral with the largest sum of positive indices is selected (i.e. the one with the most dotted propagators):

$$\mathcal{N}_+ = \sum_i \Theta(\nu_i)(\nu_i - 1). \quad (2.39)$$

- If there is still more than one integral with the maximum values of both \mathcal{N}_{prop} and \mathcal{N}_+ then the integral with the largest magnitude of the sum of negative indices is selected (i.e. the one with the most terms in the numerator):

$$\mathcal{N}_- = - \sum_i \Theta(-\nu_i)\nu_i. \quad (2.40)$$

- If there are still integrals with the same values for all three of these \mathcal{N} , then one of the remaining integrals is chosen at random to be the most complicated integral.

The identities are then rearranged to give the most complicated integral as a combination of simpler integrals. This process is then repeated for all the generated identities for the given seed integral. Having exhausted the linear identities from the first seed integral, the whole process is then repeated by generating a new seed, finding its identities, and carrying out the re-arrangement to give the more complicated integrals in terms of simpler ones. A new seed integral can be generated by applying the opposite selection procedure to that used to find the most complicated integral. The identities for the new seed will be more complicated than those for the previous seed, and if they contain any of the integrals already solved for via the previous seeds identities, then the reduced forms can be substituted into these new identities. The process of seed generation and reduction is repeated until the most

complicated integrals involved in the process under investigation have been reduced, and can be expressed in terms of simpler Master Integrals.

There is a small degree of freedom as to the choice of Master Integrals used due to the relations between integrals, as long as the Master Integrals themselves cannot be related via these identities. The programs we have used choose the Master integrals to be scalar integrals with all powers of denominators $\nu = 1$. Where this is not possible, for example where a topology has two Master Integrals, we choose the second Master Integral to be a scalar integral with one denominator with power $\nu = 2$, i.e. a dotted propagator.

2.6 Using differential equations to calculate Master Integrals

The differential equation (DE) method was first suggested as a means to solve loop integrals in [24], and was subsequently expanded in detail in [25]. The method has been used to calculate many two-loop MI, including those with multiple off-shell legs or internal masses [26–32]. Here we present an outline of this method, which we shall use to solve the MI required for the two-loop off-shell vertex in chapter 3. For further details in the use of this method to find the ϵ -expansion of Master Integrals we refer the reader to Refs. [26, 29].

The main idea of this method is to derive differential equations in external invariants for the Master Integrals. These equations are then solved using suitable boundary conditions to fix the constants of integration.

2.6.1 Deriving differential equations

The differential equations are obtained by differentiating the MI with respect to the external momenta. Via the chain rule, linear combinations of these differentials are used to find the first order differential equations in the external invariants. To relate the differentials in external momenta to the differentials in external invariants we use the following chain rule:

$$p_j^\mu \frac{\partial}{\partial p_k^\mu} \mathcal{I}(s_i) = p_j^\mu \sum_\xi \frac{\partial s_\xi}{\partial p_k^\mu} \frac{\partial}{\partial s_\xi} \mathcal{I}(s_i) \quad (2.41)$$

where $p_j^\mu \frac{\partial s_\xi}{\partial p_k^\mu}$ will be a linear combination of invariants. This will lead to a series of linear equations which we can then solve for the differentials in the invariant scales.

As an example of this method, we examine an integral \mathcal{I} with three off-shell legs, which is necessary for the derivation of the differential equations used in chapter 3.

We assign to each external leg a momentum scale

$$s_i = p_i^2 = m_i^2 \quad i \in \{1, 2, 3\}$$

Due to momentum conservation we can write $p_3 = -(p_1 + p_2)$, and so we have that

$$s_3 = m_3^2 = m_1^2 + m_2^2 + 2p_1 \cdot p_2 \quad (2.42)$$

Therefore to give independent relations between differentials, the indices j and k in Eq. 2.41 can be either 1 or 2.

The non-zero $\frac{\partial s_\xi}{\partial p_k^\mu}$ are then

$$\begin{aligned} \frac{\partial s_1}{\partial p_1^\mu} &= 2p_1^\mu & \frac{\partial s_3}{\partial p_1^\mu} &= 2(p_1^\mu + p_2^\mu) \\ \frac{\partial s_2}{\partial p_2^\mu} &= 2p_2^\mu & \frac{\partial s_3}{\partial p_2^\mu} &= 2(p_1^\mu + p_2^\mu) \end{aligned} \quad (2.43)$$

Using these in Eq. 2.41 leads to the chain rule relations

$$\begin{aligned} p_1^\mu \frac{\partial \mathcal{I}}{\partial p_1^\mu} &= 2m_1^2 \frac{\partial \mathcal{I}}{\partial m_1^2} + (m_1^2 - m_2^2 + m_3^2) \frac{\partial \mathcal{I}}{\partial m_3^2} \\ p_1^\mu \frac{\partial \mathcal{I}}{\partial p_2^\mu} &= (m_3^2 - m_1^2 - m_2^2) \frac{\partial \mathcal{I}}{\partial m_2^2} + (m_1^2 - m_2^2 + m_3^2) \frac{\partial \mathcal{I}}{\partial m_3^2} \\ p_2^\mu \frac{\partial \mathcal{I}}{\partial p_1^\mu} &= (m_3^2 - m_1^2 - m_2^2) \frac{\partial \mathcal{I}}{\partial m_1^2} + (m_2^2 + m_3^2 - m_1^2) \frac{\partial \mathcal{I}}{\partial m_3^2} \\ p_2^\mu \frac{\partial \mathcal{I}}{\partial p_2^\mu} &= 2m_2^2 \frac{\partial \mathcal{I}}{\partial m_2^2} + (m_2^2 + m_3^2 - m_1^2) \frac{\partial \mathcal{I}}{\partial m_3^2} \end{aligned} \quad (2.44)$$

We can then solve this system of relations for the differentials in the invariants. We find

$$\begin{aligned} \frac{\partial \mathcal{I}}{\partial m_1^2} &= \frac{1}{\Lambda^2} \left\{ (m_1^2 - m_2^2 - m_3^2) p_1^\mu \frac{\partial \mathcal{I}}{\partial p_1^\mu} + (m_1^2 - m_2^2 + m_3^2) p_2^\mu \frac{\partial \mathcal{I}}{\partial p_1^\mu} \right\} \\ \frac{\partial \mathcal{I}}{\partial m_2^2} &= \frac{1}{\Lambda^2} \left\{ (m_1^2 - m_2^2 - m_3^2) p_1^\mu \frac{\partial \mathcal{I}}{\partial p_2^\mu} + (m_1^2 - m_2^2 + m_3^2) p_2^\mu \frac{\partial \mathcal{I}}{\partial p_2^\mu} \right\} \\ \frac{\partial \mathcal{I}}{\partial m_3^2} &= \frac{1}{\Lambda^2} \left\{ 2m_2^2 p_1^\mu \frac{\partial \mathcal{I}}{\partial p_2^\mu} + (m_1^2 + m_2^2 - m_3^2) p_2^\mu \frac{\partial \mathcal{I}}{\partial p_2^\mu} \right\} \end{aligned} \quad (2.45)$$

where,

$$\Lambda^2 = m_1^4 + m_2^4 + m_3^4 - 2m_1^2 m_2^2 - 2m_1^2 m_3^2 - 2m_2^2 m_3^2. \quad (2.46)$$

This Λ factor will play an important part in our investigation into the Master Integrals for the two-loop vertex with three off-shell legs, which we shall see in chapter 3.

These differential equations will involve loop integrals with additional powers of propagators, belonging to the same topology as the differentiated integral. This can

be seen via the same argument as that for the IBP and LI identities, due to the presence of differentials of propagators. However, as all the integrals belong to the same topology, the reduction via the IBP and LI identities of sections 2.3 and 2.4 using the Laporta algorithm of section 2.5, can be used to simplify the equations² so that the differential equation is expressed only in terms of the MI itself and combinations of simpler topologies (i.e. integrals with less denominators). In order to solve the differential equation we need to know the analytic form of these simpler integrals (or at least the relevant terms in the ϵ -expansion should be known), and so it is sensible to apply a 'bottom-up' approach to the evaluation of MI's via this method, working from simpler to more complicated topologies, so that the MI is the only unknown in the differential equation. For some topologies there is more than one MI leading to coupled differential equations. However as there is some freedom in the choice of which two-loop graphs to use as the Master Integrals, it simplifies the calculation to choose the Master Integrals such that they have different leading powers of ϵ . In this case, the system of differential equations decouples on expansion in ϵ (see, for example, [29]).

2.6.2 Solving differential equations

The differential equations are exact in the space-time dimension d , and can be solved as follows. Consider the inhomogeneous differential equation for the MI F with respect to the external scale x ,

$$\frac{d}{dx}F(x) = A(x)F(x) + B(x). \quad (2.47)$$

²To achieve this we have made extensive use of the Laporta algorithm [23]. We have a version encoded using FORM [33] which we have checked against the Automatic Integral Reduction package AIR [22].

We use an integrating factor

$$H(x) = \exp \left\{ \int A(x) dx \right\} \quad (2.48)$$

such that $H(x)$ is a solution of the homogeneous equation

$$\frac{d}{dx} H(x) = A(x)H(x). \quad (2.49)$$

Then the full solution is given by

$$F(x) = H(x) \left(\int^x H^{-1}(x') B(x') dx' + C \right) \quad (2.50)$$

where the constant C has to be fixed from the boundary conditions. These solutions are generally combinations of hypergeometric functions which are difficult to expand in powers of ϵ . Thus to find the ϵ -expansion of the MI we must systematically expand each master integral F , and all d -dependent terms of the differential equation in powers of ϵ

$$F = \sum_{i=-m}^n f^i \epsilon^i, \quad A = \sum_{i=0}^{n+m} a^i \epsilon^i, \quad B = \sum_{i=-m}^n b^i \epsilon^i \quad (2.51)$$

where $-m$ is the lowest power of ϵ in the expansion and n is the highest power of ϵ needed. It is assumed that the a^i and b^i are already known. Each coefficient f^i satisfies the differential equation given by,

$$\frac{d}{dx} f^i(x) = \sum_{j=0}^{m-i} a^j(x) f^{i-j}(x) + b^i(x). \quad (2.52)$$

It can be seen that the homogeneous part of all the equations generated by the ϵ -expansion is simply the homogeneous solution H evaluated at $d = 4$,

$$h(x) = H(x)|_{d=4} \quad (2.53)$$

and so the solution is given by

$$f^i(x) = h(x) \left(\int^x h^{-1}(x') \left(\sum_{j=1}^{m-i} a^j(x') f^{i-j}(x') + b^i(x') \right) dx' + c^i \right) \quad (2.54)$$

where the constants c^i have to be fixed from the boundary conditions at each order in ϵ . Note that in general each coefficient f^i will depend on f^{i-1} so we solve the system of equations order by order, using repeated integration of the lower order results. It is for this reason that we require that $A(x)$ has no poles in ϵ as then f^i would depend on f^{i+1} and the bottom-up approach would not be valid.

2.6.3 The boundary conditions

In general, the lowest order coefficient in ϵ is determined solely by the boundary conditions. The boundary conditions are either obtained from the differential equation or from the master integral itself. To obtain limits from the differential equation it is necessary to examine the singular points in the coefficients of the differential equation. For example, if eq. (2.47) were to take the form

$$\frac{d}{dx} F(x) = \frac{1}{x-a} F(x) + \frac{1}{x-a} B(x) \quad (2.55)$$

then we could multiply the whole equation by $(x-a)$ and let $x \rightarrow a$, then we have

$$0 = F(x)|_{x=a} + B(x)|_{x=a} \quad (2.56)$$

giving the boundary condition on $F(x)$. To obtain boundary conditions from the integral itself, we can use limits where the ϵ expansion is known, for example where an offshell leg becomes massless. In both methods care has to be taken that the integral has a smooth limit at the chosen point so as not to miss or introduce hidden singularities.

If $H(x)$ is divergent at the boundary then the constant C is already determined by the necessary condition,

$$\int^x H^{-1}(x')B(x')dx' + C = 0 \Big|_{x=a}, \quad (2.57)$$

which can be fulfilled by choosing the boundary point as the lower integration limit.

The solution of the differential equation is then given by

$$F(x) = H(x)\tilde{F}(x) = H(x) \left(\int_a^x H^{-1}(x')B(x')dx' \right). \quad (2.58)$$

It can be easily shown that this function satisfies the boundary condition.

2.7 Harmonic polylogarithms

Solving the differential equations by repeated integration immediately suggests that the results be given in terms of Harmonic Polylogarithms (HPL's), whose properties are defined by repeated integration. As such HPL's are a useful tool in the solution of loop integrals via the DE method.

The HPL's were first introduced in [34] as extensions of Nielsens polylogarithms, and later extended to 2-dimensions by [35]. In this section we briefly review the properties of one-dimensional HPL's (1-d HPL) and introduce the concept of two-dimensional HPL's which we shall use in chapter3.

2.7.1 1-d HPL's

The weight, w , of a one-dimensional HPL, $H(\vec{b}; x)$, is the number of dimensions of the vector of parameters \vec{b} . This vector, along with the argument x , fully describes the HPL.

1-d HPL's with $w = 1$

The weight-1 HPL's are defined as follows,

$$H(a; x) = \begin{cases} \int_0^x f(a, x') dx', & a \in \{1, -1\} \\ \int_1^x f(a, x') dx', & a = 0 \end{cases} \quad (2.59)$$

where,

$$f(1; x) \equiv \frac{1}{1-x}, \quad (2.60)$$

$$f(0; x) \equiv \frac{1}{x}, \quad (2.61)$$

$$f(-1; x) \equiv \frac{1}{1+x}. \quad (2.62)$$

Note that $H(0; x)$ is defined differently to avoid the logarithmic singularity at $x = 0$.

Thus we have

$$H(1; x) \equiv -\ln(1-x), \quad (2.63)$$

$$H(0; x) \equiv \ln x, \quad (2.64)$$

$$H(-1; x) \equiv \ln(1+x), \quad (2.65)$$

and

$$\frac{\partial}{\partial x} H(a; x) = f(a; x) \quad \text{with} \quad a \in \{+1, 0, -1\}. \quad (2.66)$$

1-d HPL's with $w > 1$

The higher weight HPL's are recursively defined by,

$$H(a, \vec{b}; x) \equiv \int_0^x dx' f(a; x') H(\vec{b}; x'), \quad (2.67)$$

$$H(0, \dots, 0; x) \equiv \frac{1}{w!} \ln^w x. \quad (2.68)$$

Note that only the HPL's with weight vectors comprising only 0's are defined differently, and are integrated between 1 and x to avoid logarithmic singularities. All others involve integration from 0 to x . Under differentiation, the weight is reduced by unity,

$$\frac{\partial}{\partial x} H(a, \vec{b}; x) = f(a; x) H(\vec{b}; x). \quad (2.69)$$

As an example we provide the 1-d HPL's with weight 2.

$$H(0, 0; x) \equiv \frac{1}{2!} \ln^2 x, \quad (2.70)$$

$$H(0, 1; x) \equiv \text{Li}_2(x), \quad (2.71)$$

$$H(0, -1; x) \equiv -\text{Li}_2(-x), \quad (2.72)$$

$$H(1, 0; x) \equiv -\ln x \ln(1-x) - \text{Li}_2(x), \quad (2.73)$$

$$H(1, 1; x) \equiv \frac{1}{2!} \ln^2(1-x), \quad (2.74)$$

$$H(1, -1; x) \equiv \text{Li}_2\left(\frac{1-x}{2}\right) - \ln 2 \ln(1-x) - \text{Li}_2\left(\frac{1}{2}\right), \quad (2.75)$$

$$H(-1, 0; x) \equiv \ln x \ln(1+x) + \text{Li}_2(-x), \quad (2.76)$$

$$H(-1, 1; x) \equiv \text{Li}_2\left(\frac{1+x}{2}\right) - \ln 2 \ln(1+x) - \text{Li}_2\left(\frac{1}{2}\right), \quad (2.77)$$

$$H(-1, -1; x) \equiv \frac{1}{2!} \ln^2(1+x), \quad (2.78)$$

where Li_2 is the dilogarithm

$$\text{Li}_2(x) = - \int_0^x \frac{\ln(1-t)}{t} dt. \quad (2.79)$$

2.7.2 2-d HPL's

The 2-d HPL's were introduced in [35] as the logical extension of the 1-d HPL's. The common extension is the linear basis

$$f(a, x) = \frac{1}{a-x}, \quad (2.80)$$

$$f(-a, x) = \frac{1}{a+x}, \quad (2.81)$$

which gives the first order 2-d HPL's as

$$H(a; x) = -\ln(a-x), \quad (2.82)$$

$$H(-a; x) = \ln(a+x). \quad (2.83)$$

These HPL's were introduced in order to solve differential equations with two scales, and with homogeneous terms containing the factors $f(a, x)$ and $f(-a, x)$, so that upon integration the 2-d HPL's provide a basis set for the analytic form of the integral. The 2-d HPL's are defined to have the same properties under differentiation and integration as the 1-d HPL's.

2.7.3 Properties of the HPL's

HPL's obey a number of useful identities. The most useful identity is the shuffle identity which allows us to write products of two HPL's as a sum of HPL's with

higher weight.

$$H(\vec{p}; x)H(\vec{q}; x) = \sum_{\vec{r}=\vec{p} \uplus \vec{q}} H(\vec{r}; x) \quad (2.84)$$

where $\vec{p} \uplus \vec{q}$ represents the mergers of \vec{p} and \vec{q} in which the relative orders of the elements of \vec{p} and \vec{q} are preserved.

For example, with $\vec{p} = (a, b)$ and $\vec{q} = (c, d)$, we have

$$\begin{aligned} H(a, b; x)H(c, d; x) &= H(a, b, c, d; x) + H(a, c, b, d; x) + H(a, c, d, b; x) \\ &\quad + H(a, c, b, d; x) + H(c, a, b, d; x) + H(c, d, a, b; x). \end{aligned}$$

This shuffle identity gives us the following useful relation:

$$H^n(0; x) = n!H(\underbrace{0 \dots 0}_n; x). \quad (2.85)$$

HPL's also obey integration by parts identities, given as follows.

$$\begin{aligned} H(m_1 \cdots m_q; x) &= \int_0^x dx' f(m_1; x')H(m_2 \cdots m_q; x') \\ &= H(m_1; x)H(m_2 \cdots m_q; x) \\ &\quad - \int_0^x dx' H(m_1; x')f(m_2; x')H(m_3 \cdots m_q; x') \\ &= H(m_1; x)H(m_2 \cdots m_q; x) - H(m_2 m_1; x)H(m_3 \cdots m_q; x) \\ &\quad + H(m_3 m_2 m_1; x)H(m_4 \cdots m_q; x) - \cdots - (-1)^p H(m_q \cdots m_1; x). \end{aligned} \quad (2.86)$$

2.8 Summary

In this chapter we have introduced the tools necessary to solve loop integrals, focussing on the methods that will be used in the following chapter. We have introduced the terminology associated with loop integrals and their general representation. Using the one-loop Minkowski space integration rules from the previous chapter, we have solved the one-loop scalar bubble diagram with arbitrary powers of propagators. We have then used this result to solve the two-loop Master Integrals which we call Sunset and Glasses, via the methods of bubble insertions and factorisation of integrals. We have then introduced the linear identities satisfied by loop integrals, the Integration by Parts and Lorentz Invariance identities, and demonstrated their use to express an integral in terms of simpler integrals. This reduction has been fully automated, and so we have described the Laporta Algorithm which has been used to find the Master Integrals presented in the following chapter. We have then described the Differential Equations method for solving loop integrals, looking at the derivation of the differential equations and the method of their solution. We have concluded by examining the Harmonic Polylogarithms which are the natural set of functions in which to express the solutions of the differential equations. In the next chapter we will use the differential equation method to solve two-loop integrals, and in doing so we will reuse the expressions for the Sunset and Glasses Master Integrals derived in this chapter.

Chapter 3

Master Integrals For Massless Two-Loop Vertex Diagrams With Three Offshell Legs

In this chapter we compute the Master Integrals (MI) for massless two-loop vertex graphs with three off-shell legs. These results are published in Ref. [36]. These Master Integrals are ingredients for several interesting two-loop processes, as well as having applications in the calculation of two-loop integrals with more than three external legs.

In Higgs physics, the $H \rightarrow V^*V^*$ decay receives QCD corrections when the Higgs couples to gluons (via a heavy top quark loop) which then couple to the weak bosons via a massless quark loop, as shown in Fig. 3.1. This may be relevant for Higgs searches in the mass regions where the Higgs decays into two off-shell W bosons. In pure QCD, one can evaluate the two-loop triple gluon and quark-gluon two-loop vertices with massless quarks in a covariant gauge (as well as the gluon-ghost

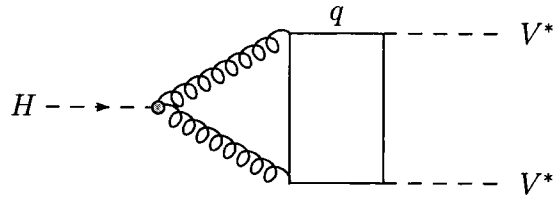


Figure 3.1: A two-loop vertex diagram for the $H \rightarrow V^*V^*$ decay. The Higgs couples to the gluons via a heavy top quark loop, depicted here by a grey shaded dot. q denotes the second loop as a massless quark loop.

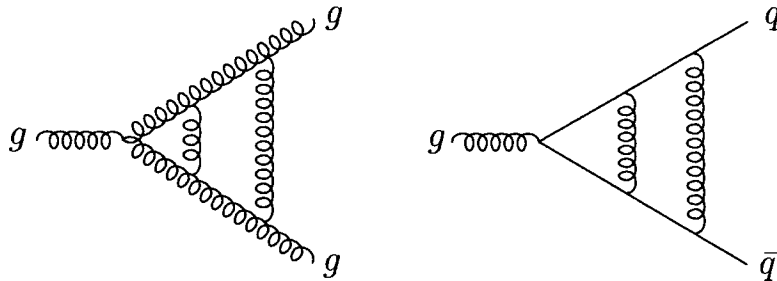


Figure 3.2: Example two-loop diagrams for the triple gluon and quark-gluon vertices.

vertex), of which example diagrams are shown in Fig. 3.2.¹ This is a useful input for Schwinger-Dyson studies of confinement as well as exploring how the Ward-Slavnov-Taylor identities generalise to the off-shell case. These vertices will also contribute to the QCD background for processes at the LHC, for example through gluon fusion and multi-jet production.

The Master Integrals presented here also form a first step towards the calculation of massless two-loop $2 \rightarrow 2$ scattering amplitudes with two off-shell legs. These processes include the NNLO QCD corrections to $q\bar{q} \rightarrow V^*V^*$ (where $V = W, Z$) and the NLO corrections to $gg \rightarrow V^*V^*$. Here we indicate that the gauge bosons are off-shell to account for resonance effects in the decay of the gauge boson. As in the on-shell and single off-shell cases, the MI include planar and non-planar box graphs as well as vertex and self energies. Altogether there are 11 planar box and 3 non-planar box master topologies, some of which require 2 or more MI to be computed.

¹Note that Davydychev and Osland have studied the two-loop case where only one of the legs is off-shell [37]

The Master Integrals we present here belong to a subset of the necessary MI for these processes.

It is well known that many of the loop integrals that appear in Feynman diagram calculations can be expressed in terms of hypergeometric functions with parameters that depend on the number of space time dimensions d and a number of kinematic scales. However, expressing these hypergeometric functions as expansions in $\epsilon = (4 - d)/2$ is rather non-trivial. In general the coefficients involve polylogarithms, both of the Nielsen [38] and harmonic [34,35] varieties, and often new polylogarithms need to be introduced.

We have seen in chapter 2 that the Integration by parts [39,40] (IBP) and Lorentz invariance [21](LI) identities are crucial in reducing [23] the number of Master Integrals that actually need to be evaluated. Several powerful tools have been established to deal with their solution. Often, these methods rely on the link between the hypergeometric functions that yield (nested) sums and their integral representations that yield polylogarithms. Two of the most powerful analytic methods are the Mellin-Barnes technique [41] and the differential equations approach [24] which we have introduced in section 2.6. Both methods have been used extensively to provide expansions in ϵ for two-loop box graphs with massless internal propagators when all the external legs are on-shell [19,20,42–44] and when one of the external legs is off-shell [26,27]. All of these expansions have been checked by Binoth and Heinrich’s numerical program [45] for evaluating loop integrals. Once analytic expansions for the two-loop Master Integrals were known, they were rapidly exploited in the calculation of the amplitudes for physical scattering processes.

The two-loop helicity amplitudes have been evaluated for the gluon-gluon [46,47], quark-gluon [48,49] and quark-quark [50] processes and have confirmed the earlier “squared” matrix elements [51–54]. Similarly, amplitudes for the phenomenologi-

cally important $gg \rightarrow \gamma\gamma$ [55] and $q\bar{q} \rightarrow \gamma\gamma$ [56] processes as well as $\gamma\gamma \rightarrow \gamma\gamma$ [57, 58] and (massless) Bhabha scattering [59] have also been computed. The processes with one off-shell leg include $e^+e^- \rightarrow 3$ jets [60–62] which is crucial in making a precise determination of the strong coupling constant at the NLC. Progress is also being made in calculating the two-loop QED corrections to Bhabha scattering which is of crucial importance in determining the luminosity at the NLC (see the nice review of the current status in Ref. [28]). Here there are 33 double box graphs to evaluate of which seven have been studied [28, 63–65]. Analytic expressions for the associated vertex graphs are also known [28, 29] and have been employed to calculate the QED [66] and QCD [67] corrections to the massive fermion form factor.

As in Refs. [26–32], we employ the differential equation technique, as introduced in chapter 2, to evaluate the MI systematically order by order in ϵ . At each order we encounter one-dimensional integrals over the terms in the result for one order lower. These integrals yield polylogarithms and, because of the specific kinematics of the vertex graph with three off-shell legs, we find it necessary to extend the set of two-dimensional harmonic polylogarithms (2-d HPL) to include quadratic factors in the denominator (see also Ref. [32]). Our results are therefore presented in terms of the extended set of 2-d HPL's.

To apply these integrals in the evaluation of the two-loop Master Integrals with two off-shell and two on-shell legs, we present the ϵ expansions of our Master Integrals up to $\mathcal{O}(\epsilon^2)$. In this way it will be possible to obtain the necessary finite pieces of the Master Integrals for the $2 \rightarrow 2$ processes.

3.1 Kinematics

We consider the vertex graph with three off-shell legs such that,

$$0 = p_1 + p_2 + p_3. \quad (3.1)$$

The three kinematic scales are p_i^2 . It is convenient to use the dimensionless variables

$$x = \frac{p_1^2}{p_3^2}, \quad y = \frac{p_2^2}{p_3^2} \quad (3.2)$$

together with the determinant of the 2×2 Gram matrix,

$$\lambda \equiv \lambda(x, y) = \frac{\Lambda^2}{p_3^4} = \sqrt{(1-x-y)^2 - 4xy} = \sqrt{(x-x_0)(x-x_1)} \quad (3.3)$$

where Λ is defined in eq. (2.46) and

$$x_0 = (1 - \sqrt{y})^2, \quad x_1 = (1 + \sqrt{y})^2.$$

We also have the following simple relations:

$$\begin{aligned} \sqrt{x_0 x_1} &= 1 - y, \\ x_0 + x_1 &= 2(1 + y). \end{aligned}$$

In the following the dependence of λ , x_0 and x_1 on x and y will be implicitly understood.

Here we choose the kinematical configuration to suit the case of a heavy/offshell particle with momentum p_3 decaying into two lighter particles with momenta p_1, p_2 .

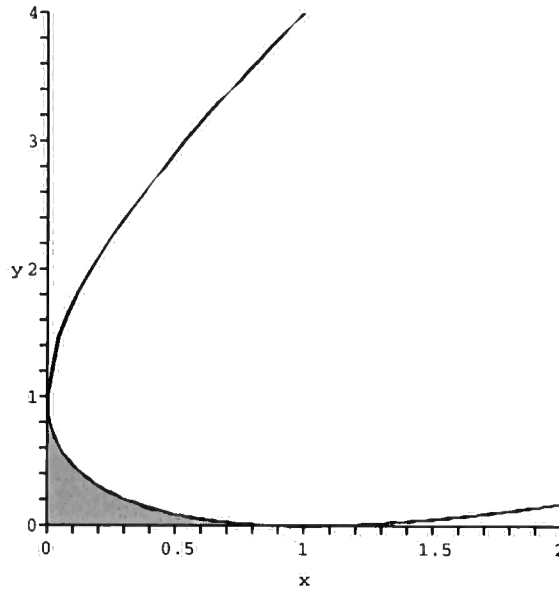


Figure 3.3: The phase space for the vertex graph with three off-shell legs. The shaded region corresponds to the case where $p_3^2 > p_1^2, p_2^2$. The solid line marks the boundary where $\lambda = 0$.

In this case the kinematically accessible region is given by the inequality,

$$\sqrt{p_1^2} + \sqrt{p_2^2} \leq \sqrt{p_3^2}, \quad (3.4)$$

or after introduction of the dimensionless parameters x and y

$$\sqrt{x} + \sqrt{y} \leq 1. \quad (3.5)$$

The allowed parameter space is depicted by the shaded region in figure 3.3. Other regions are simply obtained by relabelling.

3.1.1 Extended Harmonic Polylogarithms

The 2-d HPL's were introduced in [35] as the logical extension of the 1-d HPL's.

The common extension is the linear basis

$$f(a, x) = \frac{1}{a - x}, \quad (3.6)$$

$$f(-a, x) = \frac{1}{a + x}. \quad (3.7)$$

which we have briefly discussed in section 2.7.2. However, while it is possible to use this basis to evaluate the integrals under investigation here, a more natural extension involves the square roots that are generated by Eq. 3.3. This factor, λ , originates from the derivation of the differential equations for integrals with three off-shell legs, as shown in section 2.6.1. As such, this factor is common amongst all of our differential equations, and so it is natural that it should provide us with the basis set of HPL's in which to phrase our solutions. To this end, we extend the 2-d basis by the (quadratic) functions,

$$f(\lambda, x) = \frac{1}{\lambda}, \quad (3.8)$$

$$f(x\lambda, x) = \frac{1}{x\lambda}, \quad (3.9)$$

$$f(x_0, x) = -\frac{1}{x - x_0}, \quad (3.10)$$

$$f(x_1, x) = -\frac{1}{x - x_1}. \quad (3.11)$$

These functions are two dimensional, with explicit dependence on x and the dependence on y coming from $x_0(y)$ and $x_1(y)$. The functions are chosen to be positive in the region,

$$0 < x < 1, \quad 0 < y < 1, \quad 0 < \lambda^2,$$

which immediately implies

$$0 < x < x_0 = (1 - \sqrt{y})^2 < 1, \quad 0 < y < y_0 = (1 - \sqrt{x})^2 < 1, \quad \sqrt{x} + \sqrt{y} < 1, \quad (3.12)$$

and which corresponds to the kinematically allowed shaded region depicted in fig 3.3.²

We define the extended harmonic polylogarithms in the following way,

$$G(a, \vec{w}; x, y) = \int_{x_0}^x f(a, x') G(\vec{w}; x', y) dx', \quad (3.13)$$

and where the dependence on y is made explicit. This follows the definition of the standard HPL's, with the exception of the lower limit on the integration, which in our case is chosen to be x_0 . This definition is chosen due to the boundary conditions on the differential equations which we wish to solve. If the homogeneous part of the differential equation is divergent at the boundary then the boundary conditions are automatically satisfied by choosing the boundary point as the lower integration limit when integrating the differential equation, for example see Eq. 2.58. In the differential equations we wish to solve we often find that we can use x_0 as the boundary point, and hence it is useful to define our basis functions with this point as the lower limit of integration. The only exception from this definition is

$$G(x_0, \dots, x_0; x, y) = \int_0^x f(x_0, x') G(x_0, \dots, x_0; x', y) dx'. \quad (3.14)$$

This is chosen to have a different lower limit of integration to avoid the logarithmic singularity of this function at $x = x_0$, in a similar fashion to the choice of a different lower limit for $H(0, \dots, 0; x)$. However, 2-d HPL's of this form do not appear in the

²It is also possible to define a linear basis by making the Euler transformation, $\lambda = 2t + x$. The connection between the quadratic basis and a linear basis is detailed in Appendix A.

results presented in this thesis.

The choice of the integration limits is governed by the kinematic boundaries. To be able to evaluate the extended HPL's for $x \rightarrow x_0$, the condition $\lim_{x \rightarrow x_0} G(\vec{w}; x, y) = 0$ has to be fulfilled. This ensures that

$$\int^x f(x_0, x') G(\vec{w}; x', y) dx' \quad (3.15)$$

is finite in the limit $x \rightarrow x_0$.

Note that HPL's of the form $G(0, \vec{w}; x, y)$ and $G(x\lambda, \vec{w}; x, y)$ are divergent in the limit that $x \rightarrow 0$. This reflects the fact that taking the massless limit and making the ϵ -expansion does not necessarily commute. In the cases where the $x \rightarrow 0$ limit is smooth, we find that the HPL's appear in the combination,

$$\Delta G(0, \vec{w}; x, y) \equiv G(0, \vec{w}; x, y) - (1 - y)G(x\lambda, \vec{w}; x, y) \quad (3.16)$$

which is finite as $x \rightarrow 0$.

For the generalised HPL's of weight 1 we find,

$$G(0; x, y) = \log\left(\frac{x}{x_0}\right), \quad (3.17)$$

$$G(\lambda; x, y) = \log\left(\frac{1 - x + y - \lambda}{2\sqrt{y}}\right), \quad (3.18)$$

$$G(x\lambda; x, y) = \frac{1}{1 - y} \log\left(\frac{(1 - y)(1 + x - y - \lambda) - 2x}{2x\sqrt{y}}\right), \quad (3.19)$$

$$G(x_0; x, y) = -\log\left(\frac{x_0 - x}{x_0}\right), \quad (3.20)$$

$$G(x_1; x, y) = -\log\left(\frac{x_1 - x}{x_1 - x_0}\right). \quad (3.21)$$

In the course of solving the differential equations for the MI, we also find integrands

of the form,

$$\frac{1}{\lambda^2}, \frac{1}{(x-x_{0,1})\lambda} \approx (x-x_0)^\alpha (x-x_1)^\beta.$$

These are not independent and can be reduced to the set of quadratic basis functions.

To do this we use relations obtained via integration by parts. Denoting

$$\tilde{I}(\alpha, \beta) = \int (x-x_0)^\alpha (x-x_1)^\beta dx \quad (3.22)$$

we have the following relation

$$\tilde{I}(\alpha, \beta) = \frac{(x-x_0)^{\alpha+1}(x-x_1)^{\beta+1}}{(\beta+1)(x_1-x_0)} - \frac{(\alpha+\beta+2)}{(\beta+1)(x_1-x_0)} \tilde{I}(\alpha, \beta+1) \quad (3.23)$$

This equation allows us to raise or lower the powers α, β , until we are left with solely weight one HPL's. This allows us to see that, for example,

$$\int_{x_0}^x \frac{1}{x_0 \lambda} = \tilde{I}\left(-\frac{3}{2}, -\frac{1}{2}\right) = \frac{2(x-x_1)^{\frac{1}{2}}}{(x_1-x_0)(x-x_0)^{\frac{1}{2}}} \quad (3.24)$$

For integrals with a higher weight we use the following relation, again obtained via integration by parts,

$$\begin{aligned} I(\alpha, \beta) &= \int (x-x_0)^\alpha (x-x_1)^\beta G(v, \vec{w}; x, y) dx = \\ &= \frac{\alpha+\beta+2}{(\beta+1)(x_0-x_1)} \int (x-x_0)^\alpha (x-x_1)^{\beta+1} G(v, \vec{w}; x, y) dx \\ &+ \frac{1}{(\beta+1)(x_0-x_1)} \int (x-x_0)^{\alpha+1} (x-x_1)^{\beta+1} f(v) G(\vec{w}; x, y) dx \\ &- \frac{(x-x_0)^{\alpha+1} (x-x_1)^{\beta+1}}{(\beta+1)(x_0-x_1)} G(v, \vec{w}; x, y). \end{aligned} \quad (3.25)$$

These equations can be used to raise or lower the powers α, β until we are left with a sum of terms that can be given in terms of the basis set of higher weight HPL's.

For example,

$$\int_{x_0}^x \frac{1}{x_1 \lambda} G(a; x) = -\frac{2}{(x_1 - x_0)} \left(-\frac{(x - x_0)^{1/2}}{(x - x_1)^{1/2}} f(a; x) + \frac{(x - x_0)^{1/2}}{(x - x_1)^{1/2}} G(a; x) \right) \quad (3.26)$$

All other integrands that are not of this quadratic form are reduced to the set of basis HPL's by the use of partial fractions.

3.2 One Loop

At one-loop there are only two Master Integrals required. These are the one-loop Bubble and the one-loop Triangle.

3.2.1 Two point integrals

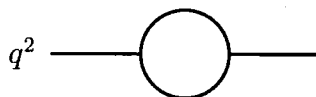


Figure 3.4: The one-loop Master Integral, $BB(q^2)$

The only two point integral at one-loop level is the bubble graph shown in figure 3.4 which has been calculated using Feynman parameters in section 2.1 and is given here for the sake of completeness,

$$BB(q^2) = iS_D(-q^2)^{-\epsilon} \frac{1}{\epsilon(1-2\epsilon)}. \quad (3.27)$$

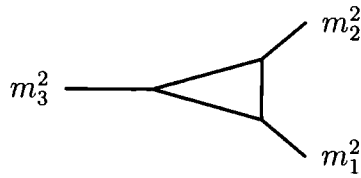


Figure 3.5: The one-loop Master Integral, $F_0(m_1^2, m_2^2, m_3^2)$.

3.2.2 Three point integrals

The three point integrals with less than three massive legs are reducible to bubble integrals. The only master integral is the triangle with three massive legs, as shown in figure 3.5. The finite part of this diagram has been calculated in [68]. The d -dimensional result for this integral can be found in [41, 69, 70], where it is given in terms of Appell functions. Davydychev calculated this integral to all orders in terms of log-sine functions [71]. The generalised log-sine functions can be directly related to Nielsen polylogarithms [72, 73] and the all-order epsilon-expansion of one-loop massless vertex diagrams with three off-shell legs is given in terms of Nielsen polylogarithms in Ref. [73]. However, here we will convert these results into 2-d HPL so that they can simply be combined with the other two-loop MI.

This integral is finite in $d = 4$. In terms of dilogarithms, the finite result is given by

$$F_0(m_1^2, m_2^2, m_3^2) = \frac{i\pi^2}{m_3^2} \Phi\left(\frac{m_1^2}{m_3^2}, \frac{m_2^2}{m_3^2}\right) \quad (3.28)$$

with

$$\Phi(x, y) = \frac{1}{\lambda(x, y)} \left\{ 2(\text{Li}_2(-\rho x) + \text{Li}_2(-\rho y)) + \ln \frac{y}{x} \ln \frac{1 + \rho y}{1 + \rho x} + \ln(\rho x) \ln(\rho y) + \frac{\pi^2}{3} \right\} \quad (3.29)$$

$$\rho(x, y) = \frac{2}{1 - x - y + \lambda} \quad (3.30)$$

and λ is as defined in Eq. 3.3.

Φ can also be written in terms of Harmonic Polylogarithms,

$$\begin{aligned} \Phi(x, y) = \frac{1}{\lambda} \left\{ 2(H(0, 1; -\rho x) + H(0, 1; -\rho y)) + H\left(0; \frac{y}{x}\right) H\left(0; \frac{1 + \rho y}{1 + \rho x}\right) \right. \\ \left. + H(0; \rho x) H(0; \rho y) + \frac{\pi^2}{3} \right\}. \end{aligned} \quad (3.31)$$

In two-loop calculations this integral appears in products with other one-loop integrals, and so to obtain the proper ϵ expansions we need the one-loop triangle expressed as an ϵ expansion itself. To be able to combine the one-loop integrals with the genuine two loop integrals, it is necessary to express all of the integrals in terms of the same set of functions. To achieve this we apply the differential equation method to the one loop triangle.

The DE for $F_0(m_1^2, m_2^2, m_3^2)$ is given by

$$\begin{aligned} m_1^2 \Lambda^2 \frac{\partial F_0}{\partial m_1^2} = & \left(\left(\frac{d-4}{2} \right) \Lambda^2 + (3-d)m_1^2(m_1^2 - m_2^2 - m_3^2) \right) F_0 \\ & + (d-3)(m_3^2 + m_1^2 - m_2^2) \text{BB}(m_3^2) \\ & + (d-3)(m_1^2 + m_2^2 - m_3^2) \text{BB}(m_2^2) \\ & - 2(d-3)m_1^2 \text{BB}(m_1^2), \end{aligned} \quad (3.32)$$

where,

$$\Lambda^2 = m_1^4 + m_2^4 + m_3^4 - 2m_1^2 m_2^2 - 2m_1^2 m_3^2 - 2m_2^2 m_3^2. \quad (3.33)$$

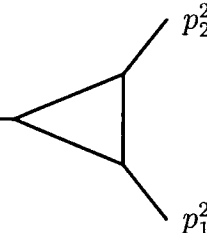
has been introduced in section 2.6, and we have seen that this factor arises from the transformation from differentials in momenta to differentials in external invariants.

The scalar triangle is completely symmetric under the interchange of the external scales. We choose to solve it in the configuration $m_i^2 = p_i^2$ with $p_3^2 > p_1^2, p_2^2$. In this case, $\Lambda^2 = p_3^4 \lambda^2$ (with λ given by Eq. 3.3) and $m_1^2 = p_3^2 x, m_2^2 = p_3^2 y$. By performing

a transformation of variable $m_1^2 \equiv x \rightarrow \lambda$ it can easily be seen that the homogeneous solution at $d = 4$ is $F_0^{hom} = \frac{1}{\lambda}$. To fix the constant of integration it is necessary to look for suitable boundary points. Note that the limit $x \rightarrow 0$ is not allowed because the one-loop triangle with only two external masses is divergent at $d = 4$. The only remaining possibility is to choose a point on the parabola given by $\lambda = 0$, as shown in fig 3.3, i.e. $x \rightarrow x_{0,1} = (1 \pm \sqrt{y})^2$. In this case the homogeneous solution is divergent at the boundary and so we apply the treatment discussed in section 2.6.3. The boundary condition for $x \rightarrow x_0$, corresponding to $m_1^2 \rightarrow (m_2 - m_3)^2$ is given by,

$$F_0(m_1^2, m_2^2, m_3^2)|_{m_1^2=(m_2-m_3)^2} = -\frac{\text{BB}(m_2^2)}{(m_2 - m_3) m_3} + \frac{\text{BB}((m_2 - m_3)^2)}{m_2 m_3} + \frac{\text{BB}(m_3^2)}{m_2 (m_2 - m_3)}. \quad (3.34)$$

Solving the differential equation order by order in ϵ , we find the following expansion in ϵ ,

$$F_0(p_1^2, p_2^2, p_3^2) = \frac{p_3^2}{\lambda} \left(\sum_{i=0, \dots, 2} f_0^i \left(\frac{p_1^2}{p_3^2}, \frac{p_2^2}{p_3^2} \right) \epsilon^i + \mathcal{O}(\epsilon^3) \right), \quad (3.35)$$


where,

$$f_0^0(x, y) = -2 G(\lambda, 0; x, y) - 2 G(\lambda; x, y) H(0; x_0) + G(\lambda; x, y) H(0; y) + (-1 + y) G(x\lambda; x, y) H(0; y),$$

$$\begin{aligned}
f_0^1(x, y) = & + 2 G(0, \lambda, 0; x, y) + 2 G(\lambda, 0, 0; x, y) + 2 G(x_0, \lambda, 0; x, y) \\
& + 2 G(x_1, \lambda, 0; x, y) + 2 G(\lambda; x, y) H(0, 0; x_0) - (G(\lambda; x, y) H(0, 0; y)) \\
& + (1 - y) G(x\lambda; x, y) H(0, 0; y) + 2 G(0, \lambda; x, y) H(0; x_0) \\
& - (G(0, \lambda; x, y) H(0; y)) + (1 - y) G(0, x\lambda; x, y) H(0; y) \\
& + 2 G(\lambda, 0; x, y) H(0; x_0) + 2 G(x_0, \lambda; x, y) H(0; x_0) \\
& - (G(x_0, \lambda; x, y) H(0; y)) + (1 - y) G(x_0, x\lambda; x, y) H(0; y) \\
& + 2 G(x_1, \lambda; x, y) H(0; x_0) - (G(x_1, \lambda; x, y) H(0; y)) \\
& + (1 - y) G(x_1, x\lambda; x, y) H(0; y),
\end{aligned}$$

$$\begin{aligned}
f_0^2(x, y) = & - 2 G(0, 0, \lambda, 0; x, y) - 2 G(0, \lambda, 0, 0; x, y) - 2 G(0, x_0, \lambda, 0; x, y) \\
& - 2 G(0, x_1, \lambda, 0; x, y) - 2 G(\lambda, 0, 0, 0; x, y) - 2 G(x_0, 0, \lambda, 0; x, y) \\
& - 2 G(x_0, \lambda, 0, 0; x, y) - 2 G(x_0, x_0, \lambda, 0; x, y) - 2 G(x_0, x_1, \lambda, 0; x, y) \\
& - 2 G(x_1, 0, \lambda, 0; x, y) - 2 G(x_1, \lambda, 0, 0; x, y) - 2 G(x_1, x_0, \lambda, 0; x, y) \\
& - 2 G(x_1, x_1, \lambda, 0; x, y) - 2 G(\lambda; x, y) H(0, 0, 0; x_0) + G(\lambda; x, y) H(0, 0, 0; y) \\
& + (-1 + y) G(x\lambda; x, y) H(0, 0, 0; y) - 2 G(0, \lambda; x, y) H(0, 0; x_0) \\
& + G(0, \lambda; x, y) H(0, 0; y) + (-1 + y) G(0, x\lambda; x, y) H(0, 0; y) \\
& - 2 G(\lambda, 0; x, y) H(0, 0; x_0) - 2 G(x_0, \lambda; x, y) H(0, 0; x_0) \\
& + G(x_0, \lambda; x, y) H(0, 0; y) + (-1 + y) G(x_0, x\lambda; x, y) H(0, 0; y) \\
& - 2 G(x_1, \lambda; x, y) H(0, 0; x_0) + G(x_1, \lambda; x, y) H(0, 0; y) \\
& + (-1 + y) G(x_1, x\lambda; x, y) H(0, 0; y) - 2 G(0, 0, \lambda; x, y) H(0; x_0) \\
& + G(0, 0, \lambda; x, y) H(0; y) + (-1 + y) G(0, 0, x\lambda; x, y) H(0; y) \\
& - 2 G(0, \lambda, 0; x, y) H(0; x_0) - 2 G(0, x_0, \lambda; x, y) H(0; x_0) +
\end{aligned}$$

$$\begin{aligned}
& + G(0, x_0, \lambda; x, y) H(0; y) + (-1 + y) G(0, x_0, x\lambda; x, y) H(0; y) \\
& - 2 G(0, x_1, \lambda; x, y) H(0; x_0) + G(0, x_1, \lambda; x, y) H(0; y) \\
& + (-1 + y) G(0, x_1, x\lambda; x, y) H(0; y) - 2 G(\lambda, 0, 0; x, y) H(0; x_0) \\
& - 2 G(x_0, 0, \lambda; x, y) H(0; x_0) + G(x_0, 0, \lambda; x, y) H(0; y) \\
& + (-1 + y) G(x_0, 0, x\lambda; x, y) H(0; y) - 2 G(x_0, \lambda, 0; x, y) H(0; x_0) \\
& - 2 G(x_0, x_0, \lambda; x, y) H(0; x_0) + G(x_0, x_0, \lambda; x, y) H(0; y) \\
& + (-1 + y) G(x_0, x_0, x\lambda; x, y) H(0; y) - 2 G(x_0, x_1, \lambda; x, y) H(0; x_0) \\
& + G(x_0, x_1, \lambda; x, y) H(0; y) + (-1 + y) G(x_0, x_1, x\lambda; x, y) H(0; y) \\
& - 2 G(x_1, 0, \lambda; x, y) H(0; x_0) + G(x_1, 0, \lambda; x, y) H(0; y) \\
& + (-1 + y) G(x_1, 0, x\lambda; x, y) H(0; y) - 2 G(x_1, \lambda, 0; x, y) H(0; x_0) \\
& - 2 G(x_1, x_0, \lambda; x, y) H(0; x_0) + G(x_1, x_0, \lambda; x, y) H(0; y) \\
& + (-1 + y) G(x_1, x_0, x\lambda; x, y) H(0; y) - 2 G(x_1, x_1, \lambda; x, y) H(0; x_0) \\
& + G(x_1, x_1, \lambda; x, y) H(0; y) + (-1 + y) G(x_1, x_1, x\lambda; x, y) H(0; y)
\end{aligned}$$

We have checked that the ϵ^0 term agrees with the results of Ref. [68] while the $\mathcal{O}(\epsilon)$ term numerically agrees with that given in Ref. [71].

3.3 Two Loop

3.3.1 Two point integrals

There are only two two-point Master Integrals, both of which can be obtained by repeated one-loop integration. These are the three propagator sunset graph and the four propagator glasses graph. Both of these integrals have been evaluated using one-loop method in section 2.2 and their ϵ expansions can be found in equations

2.21 and 2.22. Here we provide their diagrams for the sake of completeness.

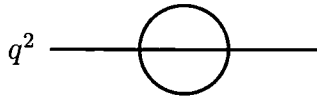


Figure 3.6: The two-loop Master Integral, $SS(q^2)$.



Figure 3.7: The two-loop Master Integral, $GL(q^2)$.

3.3.2 Three point integrals

Master Integrals with four propagators

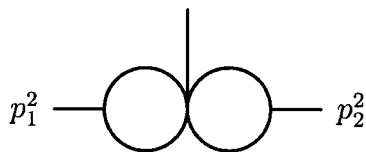


Figure 3.8: The two-loop Master Integral, $TGL(p_1^2, p_2^2)$

The simplest graph with four propagators is denoted by TGL and is shown in figure 3.3.2. This integral factorises into the product of two bubbles, much like the Glasses integral of section 2.2, but in this case each bubble is dependent on a different scale.

$$TGL(p_1^2, p_2^2) = BB(p_1^2)BB(p_2^2) = -(-p_1^2)^{-\epsilon}(-p_2^2)^{-\epsilon}S_D^2 \frac{1}{\epsilon^2(1-2\epsilon)^2}. \quad (3.36)$$

There are two genuine two loop integrals with four propagators. These are denoted by F_1 and F_2 and shown in figure 3.3.2. The ϵ expansion of these integrals is given

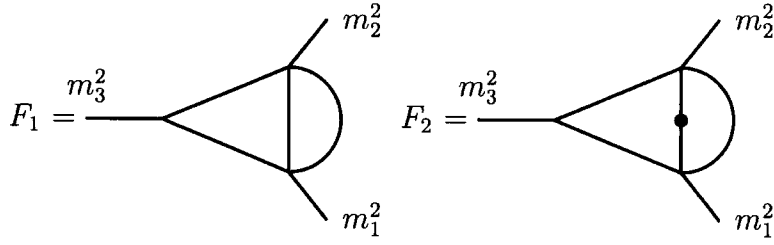


Figure 3.9: The two-loop Master Integrals, $F_1(m_1^2, m_2^2, m_3^2)$, $F_2(m_1^2, m_2^2, m_3^2)$

to order ϵ^0 in [74]. The corresponding two scale diagrams, when one of the legs becomes massless, are given in [26] to order ϵ^2 in terms of HPL's.

We obtain two coupled differential equations for F_1 and F_2 ,

$$\begin{aligned} \frac{\partial}{\partial m_1^2} F_1(m_1^2, m_2^2, m_3^2) &= \frac{(d-4) m_2^2 (m_1^2 - m_2^2 + m_3^2)}{2 (d-3) \Lambda^2} F_2 \\ &\quad - \frac{(d-4) (-m_1^2 + m_2^2 + m_3^2)}{2 \Lambda^2} F_1 \\ &\quad + \frac{(3d-8) (-m_1^2 - m_2^2 + m_3^2)}{2 \Lambda^2 m_1^2} \text{SS}(m_1^2) + \frac{(3d-8)}{\Lambda^2} \text{SS}(m_2^2), \end{aligned} \quad (3.37)$$

$$\begin{aligned} \frac{\partial}{\partial m_1^2} F_2(m_1^2, m_2^2, m_3^2) &= \frac{-((d-3) (3d-10) (m_1^2 - m_2^2 + m_3^2))}{2 \Lambda^2 m_1^2} F_1 \\ &\quad - \frac{1}{2 \Lambda^2 m_1^2} \left((3d-10) m_1^2 (m_1^2 - m_2^2 - m_3^2) - 2(d-4) \Lambda^2 \right) F_2 \\ &\quad + \frac{(d-3) (3d-8) (3d-10)}{(d-4) \Lambda^2 m_1^2} \text{SS}(m_1^2) \\ &\quad - \frac{(d-3) (3d-8) (3d-10) (m_1^2 + m_2^2 - m_3^2)}{2 (d-4) \Lambda^2 m_1^2 m_2^2} \text{SS}(m_2^2). \end{aligned} \quad (3.38)$$

These two integrals have different leading powers of ϵ , and so the differential equations decouple on expansion in ϵ , enabling us to use the differential equations method in their solution. In practice, the decoupling of the equations means that we solve for the lowest order of F_1 , then the next lowest order of F_1 followed by lowest order of F_2 , which both have the same order in ϵ . So we proceed by evaluating the F_1

term followed by the F_2 term for each order in ϵ until we have the required order of the expansion in both integrals.

The homogeneous solutions at $d = 4$ are found to be

$$F_1^{hom} = 1, \quad F_2^{hom} = \frac{1}{\lambda}.$$

Finding suitable boundary conditions for these coupled equations is more difficult than for the one loop triangle. Only F_1 has a smooth limit for $x \rightarrow 0$ (F_2 develops additional poles in ϵ in that limit). On the other hand, taking the limit $\lambda \rightarrow 0$ in either differential equation only provides a single relation between the two integrals. Therefore we combine both approaches. Firstly we use the limit $x \rightarrow 0$ to fix the integration constant of F_1 , matching the integral in this limit to the two-scale result given in [26]. Secondly we take the limit $\lambda \rightarrow 0$ (i.e. $x \rightarrow x_0$) of F_1 and use the limiting relation obtained from the differential equation to find F_2 in the limit $\lambda \rightarrow 0$, thereby fixing the integration constant of F_2 .

The limiting relation in the limit $x \rightarrow x_0$ is,

$$\begin{aligned} F_2(m_1^2, m_2^2, m_3^2)|_{m_1^2=(m_2-m_3)^2} = & - \left(\frac{(d-3) F_1(m_1^2, m_2^2, m_3^2)|_{m_1^2=(m_2-m_3)^2}}{m_2 m_3} \right) \\ & + \frac{(d-3)(3d-8) \text{SS}(m_2^2)}{(d-4) m_2^2 (m_2 - m_3) m_3} \\ & - \frac{(d-3)(3d-8) \text{SS}(m_3^2)}{(d-4) m_2 m_3^2 (m_2 - m_3)}. \end{aligned} \quad (3.39)$$

Without the second boundary constraint on F_1 as $x \rightarrow 0$, this would only be sufficient to yield an independent determination of f_1^{-2} .

The expansions in ϵ are needed for two separate configurations. First, when the largest scale p_3^2 is situated opposite the bubble (corresponding to $m_1^2 = p_3^2$) and second, when it lies adjacent to the bubble ($m_2^2 = p_3^2$). For the first momentum

configuration, we find that the expansions are as follows,

$$F_1^\alpha(p_1^2, p_2^2, p_3^2) = \text{Diagram}$$

$$F_1^\alpha(p_1^2, p_2^2, p_3^2) = S_D^2(-p_3^2)^{-2\epsilon} \left(\sum_{i=-2, \dots, 1} f_1^i \left(\frac{p_1^2}{p_3^2}, \frac{p_2^2}{p_3^2} \right) \epsilon^i + \mathcal{O}(\epsilon^2) \right), \quad (3.40)$$

where,

$$f_1^{-2}(x, y) = -\frac{1}{2},$$

$$f_1^{-1}(x, y) = -\frac{5}{2},$$

$$\begin{aligned} f_1^0(x, y) = & \frac{-57 - \pi^2}{6} - H(1, 0; y) + \frac{-1 + x + y}{\lambda} G(\lambda, 0; x, y) + G(\lambda, 0; 0, y) \\ & - \frac{1}{2} \Delta G(0; 0, y) H(0; y) + \frac{1}{2} G(0; x, y) H(0; y) \\ & + \frac{-((-1 + y)(-1 + x + y))}{2\lambda} G(x\lambda; x, y) H(0; y) \\ & + G(\lambda; 0, y) H(0; x_0) - \frac{1}{2} G(\lambda; 0, y) H(0; y) \\ & + \frac{-(-1 + x + y)}{2\lambda} G(\lambda; x, y) H(0; y) + \frac{-1 + x + y}{\lambda} G(\lambda; x, y) H(0; x_0), \end{aligned}$$

$$\begin{aligned} f_1^1(x, y) = & -\left(\frac{65}{2}\right) - \frac{5\pi^2}{6} + 2\zeta_3 + \frac{-\pi^2}{12} \Delta G(0; 0, y) - \Delta G(0, \lambda, 0; 0, y) \\ & + \frac{\pi^2}{12} G(0; x, y) + \frac{\pi^2}{12} G(\lambda; 0, y) + \frac{\pi^2(x + y - 1)}{12\lambda} G(\lambda; x, y) \\ & + \frac{-\pi^2(y - 1)(x + y - 1)}{12\lambda} G(x\lambda; x, y) + 5G(\lambda, 0; 0, y) + \end{aligned}$$

$$\begin{aligned}
& + \frac{5(x+y-1)}{\lambda} G(\lambda, 0; x, y) + \frac{-3(x+y-1)}{2\lambda} G(0, \lambda, 0; x, y) \\
& - G(\lambda, 0, 0; 0, y) + \frac{-2(x+y-1)}{\lambda} G(\lambda, 0, 0; x, y) \\
& - \frac{1}{2} G(\lambda, 0, \lambda; 0, y) + \frac{y-1}{2} G(\lambda, 0, x\lambda; 0, y) + \frac{1}{2} G(\lambda, \lambda, 0; 0, y) \\
& - \frac{3}{2} G(\lambda, \lambda, 0; x, y) + \frac{y-1}{2} G(\lambda, x\lambda, 0; 0, y) - G(x_0, \lambda, 0; 0, y) \\
& - \left(\frac{x+y-1}{\lambda} \right) G(x_0, \lambda, 0; x, y) - G(x_1, \lambda, 0; 0, y) \\
& - \left(\frac{x+y-1}{\lambda} \right) G(x_1, \lambda, 0; x, y) + \frac{3(y-1)}{2} G(x\lambda, \lambda, 0; x, y) \\
& + \frac{-\pi^2}{6} H(1; y) - 5 H(1, 0; y) + 2 H(1, 0, 0; y) - H(1, 1, 0; y) \\
& - \frac{5}{2} \Delta G(0; 0, y) H(0; y) + \Delta G(0; 0, y) H(0, 0; y) \\
& - \frac{1}{2} \Delta G(0; 0, y) H(1, 0; y) - \frac{1}{4} \Delta G(0, 0; 0, y) H(0; y) \\
& - \Delta G(0, \lambda; 0, y) H(0; x_0) + \frac{3}{4} \Delta G(0, \lambda; 0, y) H(0; y) \\
& + \frac{y-1}{4} \Delta G(0, x\lambda; 0, y) H(0; y) - \frac{1}{2} G(0; x, y) G(\lambda, 0; 0, y) \\
& + \frac{5}{2} G(0; x, y) H(0; y) - G(0; x, y) H(0, 0; y) + \frac{1}{2} G(0; x, y) H(1, 0; y) \\
& + 5 G(\lambda; 0, y) H(0; x_0) - \frac{5}{2} G(\lambda; 0, y) H(0; y) - 2 G(\lambda; 0, y) H(0, 0; x_0) \\
& + G(\lambda; 0, y) H(0, 0; y) + \frac{1}{2} G(\lambda; 0, y) H(1, 0; y) \\
& - \frac{(x+y-1)}{2\lambda} G(\lambda; x, y) G(\lambda, 0; 0, y) + \frac{5(x+y-1)}{\lambda} G(\lambda; x, y) H(0; x_0) \\
& - \frac{5(x+y-1)}{2\lambda} G(\lambda; x, y) H(0; y) + \frac{-2(x+y-1)}{\lambda} G(\lambda; x, y) H(0, 0; x_0) \\
& + \frac{x+y-1}{\lambda} G(\lambda; x, y) H(0, 0; y) + \frac{x+y-1}{2\lambda} G(\lambda; x, y) H(1, 0; y) \\
& + \frac{(y-1)(x+y-1)}{2\lambda} G(x\lambda; x, y) G(\lambda, 0; 0, y) \\
& + \frac{-5(y-1)(x+y-1)}{2\lambda} G(x\lambda; x, y) H(0; y) \\
& + \frac{(y-1)(x+y-1)}{\lambda} G(x\lambda; x, y) H(0, 0; y) \\
& + \frac{-((y-1)(x+y-1))}{2\lambda} G(x\lambda; x, y) H(1, 0; y) \\
& - \frac{1}{4} G(0, 0; x, y) H(0; y) + \frac{-3(x+y-1)}{2\lambda} G(0, \lambda; x, y) H(0; x_0) +
\end{aligned}$$

$$\begin{aligned}
& + \frac{3(x+y-1)}{4\lambda} G(0, \lambda; x, y) H(0; y) \\
& + \frac{3(y-1)(x+y-1)}{4\lambda} G(0, x\lambda; x, y) H(0; y) \\
& - \frac{3}{2} G(\lambda, 0; 0, y) H(0; x_0) - \frac{1}{4} G(\lambda, 0; 0, y) H(0; y) \\
& + \frac{-2(x+y-1)}{\lambda} G(\lambda, 0; x, y) H(0; x_0) \\
& + \frac{-(x+y-1)}{4\lambda} G(\lambda, 0; x, y) H(0; y) \\
& + \frac{1}{2} G(\lambda, \lambda; 0, y) H(0; x_0) - \frac{1}{4} G(\lambda, \lambda; 0, y) H(0; y) \\
& - \frac{3}{2} G(\lambda, \lambda; x, y) H(0; x_0) + \frac{3}{4} G(\lambda, \lambda; x, y) H(0; y) \\
& + \frac{y-1}{2} G(\lambda, x\lambda; 0, y) H(0; x_0) + \frac{-3(y-1)}{4} G(\lambda, x\lambda; 0, y) H(0; y) \\
& + \frac{3(y-1)}{4} G(\lambda, x\lambda; x, y) H(0; y) - (G(x_0, \lambda; 0, y) H(0; x_0)) \\
& + \frac{1}{2} G(x_0, \lambda; 0, y) H(0; y) - \left(\frac{x+y-1}{\lambda} \right) G(x_0, \lambda; x, y) H(0; x_0) \\
& + \frac{x+y-1}{2\lambda} G(x_0, \lambda; x, y) H(0; y) + \frac{y-1}{2} G(x_0, x\lambda; 0, y) H(0; y) \\
& + \frac{(y-1)(x+y-1)}{2\lambda} G(x_0, x\lambda; x, y) H(0; y) - (G(x_1, \lambda; 0, y) H(0; x_0)) \\
& + \frac{1}{2} G(x_1, \lambda; 0, y) H(0; y) - \left(\frac{x+y-1}{\lambda} \right) G(x_1, \lambda; x, y) H(0; x_0) \\
& + \frac{x+y-1}{2\lambda} G(x_1, \lambda; x, y) H(0; y) + \frac{y-1}{2} G(x_1, x\lambda; 0, y) H(0; y) \\
& + \frac{(y-1)(x+y-1)}{2\lambda} G(x_1, x\lambda; x, y) H(0; y) \\
& + \frac{(y-1)(x+y-1)}{4\lambda} G(x\lambda, 0; x, y) H(0; y) \\
& + \frac{3(y-1)}{2} G(x\lambda, \lambda; x, y) H(0; x_0) \\
& + \frac{-3(y-1)}{4} G(x\lambda, \lambda; x, y) H(0; y) + \frac{-3(y-1)^2}{4} G(x\lambda, x\lambda; x, y) H(0; y) \\
& + \frac{1}{4} \Delta G(0; 0, y) G(0; x, y) H(0; y) + \frac{x+y-1}{4\lambda} \Delta G(0; 0, y) G(\lambda; x, y) H(0; y) \\
& + \frac{-((y-1)(x+y-1))}{4\lambda} \Delta G(0; 0, y) G(x\lambda; x, y) H(0; y) \\
& - \frac{1}{2} G(0; x, y) G(\lambda; 0, y) H(0; x_0) + \frac{1}{4} G(0; x, y) G(\lambda; 0, y) H(0; y) +
\end{aligned}$$

$$\begin{aligned}
& + \frac{-(x+y-1)}{2\lambda} G(\lambda; 0, y) G(\lambda; x, y) H(0; x_0) \\
& + \frac{x+y-1}{4\lambda} G(\lambda; 0, y) G(\lambda; x, y) H(0; y) \\
& + \frac{(y-1)(x+y-1)}{2\lambda} G(\lambda; 0, y) G(x\lambda; x, y) H(0; x_0) \\
& + \frac{-((y-1)(x+y-1))}{4\lambda} G(\lambda; 0, y) G(x\lambda; x, y) H(0; y),
\end{aligned}$$

and,

$$F_2^a(p_1^2, p_2^2, p_3^2) = \text{Diagram}$$

$$F_2^a(p_1^2, p_2^2, p_3^2) = S_D^2 (-p_3^2)^{-1-2\epsilon} \frac{1}{\lambda} \left(\sum_{i=-1, \dots, 1} f_2^i \left(\frac{p_1^2}{p_3^2}, \frac{p_2^2}{p_3^2} \right) \epsilon^i + \mathcal{O}(\epsilon^2) \right), \quad (3.41)$$

where,

$$\begin{aligned}
f_2^{-1}(x, y) &= -2G(\lambda, 0; x, y) - 2G(\lambda; x, y) H(0; x_0) \\
&+ G(\lambda; x, y) H(0; y) + (-1 + y) G(x\lambda; x, y) H(0; y),
\end{aligned}$$

$$\begin{aligned}
f_2^0(x, y) &= + \frac{-\pi^2}{6} G(\lambda; x, y) + \frac{\pi^2 (y-1)}{6} G(x\lambda; x, y) + 3G(0, \lambda, 0; x, y) \\
&+ 4G(\lambda, 0, 0; x, y) + 2G(x_0, \lambda, 0; x, y) + 2G(x_1, \lambda, 0; x, y) \\
&+ G(\lambda; x, y) G(\lambda, 0; 0, y) + 4G(\lambda; x, y) H(0, 0; x_0) - 2G(\lambda; x, y) H(0, 0; y) \\
&- (G(\lambda; x, y) H(1, 0; y)) + (1 - y) G(x\lambda; x, y) G(\lambda, 0; 0, y) \\
&+ (2 - 2y) G(x\lambda; x, y) H(0, 0; y) + (y - 1) G(x\lambda; x, y) H(1, 0; y) \\
&+ 3G(0, \lambda; x, y) H(0; x_0) - \frac{3}{2} G(0, \lambda; x, y) H(0; y) \\
&+ \frac{-3(y-1)}{2} G(0, x\lambda; x, y) H(0; y) + 4G(\lambda, 0; x, y) H(0; x_0) \\
&+ \frac{1}{2} G(\lambda, 0; x, y) H(0; y) + 2G(x_0, \lambda; x, y) H(0; x_0) +
\end{aligned}$$

$$\begin{aligned}
& - (G(x_0, \lambda; x, y) H(0; y)) + (1 - y) G(x_0, x\lambda; x, y) H(0; y) \\
& + 2 G(x_1, \lambda; x, y) H(0; x_0) - (G(x_1, \lambda; x, y) H(0; y)) \\
& + (1 - y) G(x_1, x\lambda; x, y) H(0; y) + \frac{1 - y}{2} G(x\lambda, 0; x, y) H(0; y) \\
& - \frac{1}{2} \Delta G(0; 0, y) G(\lambda; x, y) H(0; y) + \frac{y - 1}{2} \Delta G(0; 0, y) G(x\lambda; x, y) H(0; y) \\
& + G(\lambda; 0, y) G(\lambda; x, y) H(0; x_0) - \frac{1}{2} G(\lambda; 0, y) G(\lambda; x, y) H(0; y) \\
& + (1 - y) G(\lambda; 0, y) G(x\lambda; x, y) H(0; x_0) \\
& + \frac{y - 1}{2} G(\lambda; 0, y) G(x\lambda; x, y) H(0; y),
\end{aligned}$$

$$\begin{aligned}
f_2^1(x, y) = & - \zeta_3 G(\lambda; x, y) + (y - 1) \zeta_3 G(x\lambda; x, y) + \frac{\pi^2}{4} G(0, \lambda; x, y) \\
& + \frac{-(\pi^2 (y - 1))}{4} G(0, x\lambda; x, y) + \frac{\pi^2}{12} G(\lambda, 0; x, y) + \frac{\pi^2}{6} G(x_0, \lambda; x, y) \\
& + \frac{-(\pi^2 (y - 1))}{6} G(x_0, x\lambda; x, y) + \frac{\pi^2}{6} G(x_1, \lambda; x, y) \\
& + \frac{-(\pi^2 (y - 1))}{6} G(x_1, x\lambda; x, y) + \frac{-(\pi^2 (y - 1))}{12} G(x\lambda, 0; x, y) \\
& - \frac{9}{2} G(0, 0, \lambda, 0; x, y) - 6 G(0, \lambda, 0, 0; x, y) - 3 G(0, x_0, \lambda, 0; x, y) \\
& - 3 G(0, x_1, \lambda, 0; x, y) - 8 G(\lambda, 0, 0, 0; x, y) - \frac{3}{2} G(\lambda, \lambda, \lambda, 0; x, y) \\
& + \frac{3 (y - 1)}{2} G(\lambda, x\lambda, \lambda, 0; x, y) - 3 G(x_0, 0, \lambda, 0; x, y) - 4 G(x_0, \lambda, 0, 0; x, y) \\
& - 2 G(x_0, x_0, \lambda, 0; x, y) - 2 G(x_0, x_1, \lambda, 0; x, y) - 3 G(x_1, 0, \lambda, 0; x, y) \\
& - 4 G(x_1, \lambda, 0, 0; x, y) - 2 G(x_1, x_0, \lambda, 0; x, y) - 2 G(x_1, x_1, \lambda, 0; x, y) \\
& + \frac{3 (y - 1)}{2} G(x\lambda, \lambda, \lambda, 0; x, y) + \frac{-3 (y - 1)^2}{2} G(x\lambda, x\lambda, \lambda, 0; x, y) \\
& + \frac{-\pi^2}{12} \Delta G(0; 0, y) G(\lambda; x, y) + \frac{\pi^2 (y - 1)}{12} \Delta G(0; 0, y) G(x\lambda; x, y) \\
& - (\Delta G(0, \lambda, 0; 0, y) G(\lambda; x, y)) + (y - 1) \Delta G(0, \lambda, 0; 0, y) G(x\lambda; x, y) \\
& + \frac{\pi^2}{12} G(\lambda; 0, y) G(\lambda; x, y) + \frac{-(\pi^2 (y - 1))}{12} G(\lambda; 0, y) G(x\lambda; x, y) \\
& - (G(\lambda; x, y) G(\lambda, 0, 0; 0, y)) - \frac{1}{2} G(\lambda; x, y) G(\lambda, 0, \lambda, 0; y) +
\end{aligned}$$

$$\begin{aligned}
& + \frac{y-1}{2} G(\lambda; x, y) G(\lambda, 0, x\lambda; 0, y) + \frac{1}{2} G(\lambda; x, y) G(\lambda, \lambda, 0; 0, y) \\
& + \frac{y-1}{2} G(\lambda; x, y) G(\lambda, x\lambda, 0; 0, y) - (G(\lambda; x, y) G(x_0, \lambda, 0; 0, y)) \\
& - (G(\lambda; x, y) G(x_1, \lambda, 0; 0, y)) + \frac{-\pi^2}{6} G(\lambda; x, y) H(1; y) \\
& - 8 G(\lambda; x, y) H(0, 0, 0; x_0) + 4 G(\lambda; x, y) H(0, 0, 0; y) \\
& + 2 G(\lambda; x, y) H(1, 0, 0; y) - (G(\lambda; x, y) H(1, 1, 0; y)) \\
& + (y-1) G(x\lambda; x, y) G(\lambda, 0, 0; 0, y) + \frac{y-1}{2} G(x\lambda; x, y) G(\lambda, 0, \lambda; 0, y) \\
& + \frac{-(y-1)^2}{2} G(x\lambda; x, y) G(\lambda, 0, x\lambda; 0, y) + \frac{1-y}{2} G(x\lambda; x, y) G(\lambda, \lambda, 0; 0, y) \\
& + \frac{-(y-1)^2}{2} G(x\lambda; x, y) G(\lambda, x\lambda, 0; 0, y) + (y-1) G(x\lambda; x, y) G(x_0, \lambda, 0; 0, y) \\
& + (y-1) G(x\lambda; x, y) G(x_1, \lambda, 0; 0, y) + \frac{\pi^2 (y-1)}{6} G(x\lambda; x, y) H(1; y) \\
& + 4 (y-1) G(x\lambda; x, y) H(0, 0, 0; y) + (2-2y) G(x\lambda; x, y) H(1, 0, 0; y) \\
& + (y-1) G(x\lambda; x, y) H(1, 1, 0; y) - \frac{3}{2} G(0, \lambda; x, y) G(\lambda, 0; 0, y) \\
& - 6 G(0, \lambda; x, y) H(0, 0; x_0) + 3 G(0, \lambda; x, y) H(0, 0; y) \\
& + \frac{3}{2} G(0, \lambda; x, y) H(1, 0; y) + \frac{3 (y-1)}{2} G(0, x\lambda; x, y) G(\lambda, 0; 0, y) \\
& + 3 (y-1) G(0, x\lambda; x, y) H(0, 0; y) + \frac{-3 (y-1)}{2} G(0, x\lambda; x, y) H(1, 0; y) \\
& - \frac{1}{2} G(\lambda, 0; 0, y) G(\lambda, 0; x, y) - (G(\lambda, 0; 0, y) G(x_0, \lambda; x, y)) \\
& + (y-1) G(\lambda, 0; 0, y) G(x_0, x\lambda; x, y) - (G(\lambda, 0; 0, y) G(x_1, \lambda; x, y)) \\
& + (y-1) G(\lambda, 0; 0, y) G(x_1, x\lambda; x, y) + \frac{y-1}{2} G(\lambda, 0; 0, y) G(x\lambda, 0; x, y) \\
& - 8 G(\lambda, 0; x, y) H(0, 0; x_0) - (G(\lambda, 0; x, y) H(0, 0; y)) \\
& + \frac{1}{2} G(\lambda, 0; x, y) H(1, 0; y) - 4 G(x_0, \lambda; x, y) H(0, 0; x_0) \\
& + 2 G(x_0, \lambda; x, y) H(0, 0; y) + G(x_0, \lambda; x, y) H(1, 0; y) \\
& + 2 (y-1) G(x_0, x\lambda; x, y) H(0, 0; y) + (1-y) G(x_0, x\lambda; x, y) H(1, 0; y) \\
& - 4 G(x_1, \lambda; x, y) H(0, 0; x_0) + 2 G(x_1, \lambda; x, y) H(0, 0; y) + G(x_1, \lambda; x, y) H(1, 0; y) \\
& + 2 (y-1) G(x_1, x\lambda; x, y) H(0, 0; y) + (1-y) G(x_1, x\lambda; x, y) H(1, 0; y) +
\end{aligned}$$

$$\begin{aligned}
& + (y-1) G(x\lambda, 0; x, y) H(0, 0; y) + \frac{1-y}{2} G(x\lambda, 0; x, y) H(1, 0; y) \\
& - \frac{9}{2} G(0, 0, \lambda; x, y) H(0; x_0) + \frac{9}{4} G(0, 0, \lambda; x, y) H(0; y) \\
& + \frac{9(y-1)}{4} G(0, 0, x\lambda; x, y) H(0; y) - 6 G(0, \lambda, 0; x, y) H(0; x_0) \\
& - \frac{3}{4} G(0, \lambda, 0; x, y) H(0; y) - 3 G(0, x_0, \lambda; x, y) H(0; x_0) \\
& + \frac{3}{2} G(0, x_0, \lambda; x, y) H(0; y) + \frac{3(y-1)}{2} G(0, x_0, x\lambda; x, y) H(0; y) \\
& - 3 G(0, x_1, \lambda; x, y) H(0; x_0) + \frac{3}{2} G(0, x_1, \lambda; x, y) H(0; y) \\
& + \frac{3(y-1)}{2} G(0, x_1, x\lambda; x, y) H(0; y) + \frac{3(y-1)}{4} G(0, x\lambda, 0; x, y) H(0; y) \\
& - 8 G(\lambda, 0, 0; x, y) H(0; x_0) - \frac{1}{4} G(\lambda, 0, 0; x, y) H(0; y) \\
& - \frac{3}{2} G(\lambda, \lambda, \lambda; x, y) H(0; x_0) + \frac{3}{4} G(\lambda, \lambda, \lambda; x, y) H(0; y) \\
& + \frac{3(y-1)}{4} G(\lambda, \lambda, x\lambda; x, y) H(0; y) + \frac{3(y-1)}{2} G(\lambda, x\lambda, \lambda; x, y) H(0; x_0) \\
& + \frac{-3(y-1)}{4} G(\lambda, x\lambda, \lambda; x, y) H(0; y) + \frac{-3(y-1)^2}{4} G(\lambda, x\lambda, x\lambda; x, y) H(0; y) \\
& - 3 G(x_0, 0, \lambda; x, y) H(0; x_0) + \frac{3}{2} G(x_0, 0, \lambda; x, y) H(0; y) \\
& + \frac{3(y-1)}{2} G(x_0, 0, x\lambda; x, y) H(0; y) - 4 G(x_0, \lambda, 0; x, y) H(0; x_0) \\
& - \frac{1}{2} G(x_0, \lambda, 0; x, y) H(0; y) - 2 G(x_0, x_0, \lambda; x, y) H(0; x_0) \\
& + G(x_0, x_0, \lambda; x, y) H(0; y) + (y-1) G(x_0, x_0, x\lambda; x, y) H(0; y) \\
& - 2 G(x_0, x_1, \lambda; x, y) H(0; x_0) + G(x_0, x_1, \lambda; x, y) H(0; y) \\
& + (y-1) G(x_0, x_1, x\lambda; x, y) H(0; y) + \frac{y-1}{2} G(x_0, x\lambda, 0; x, y) H(0; y) \\
& - 3 G(x_1, 0, \lambda; x, y) H(0; x_0) + \frac{3}{2} G(x_1, 0, \lambda; x, y) H(0; y) \\
& + \frac{3(y-1)}{2} G(x_1, 0, x\lambda; x, y) H(0; y) - 4 G(x_1, \lambda, 0; x, y) H(0; x_0) \\
& - \frac{1}{2} G(x_1, \lambda, 0; x, y) H(0; y) - 2 G(x_1, x_0, \lambda; x, y) H(0; x_0) \\
& + G(x_1, x_0, \lambda; x, y) H(0; y) + (y-1) G(x_1, x_0, x\lambda; x, y) H(0; y) \\
& - 2 G(x_1, x_1, \lambda; x, y) H(0; x_0) \\
& + G(x_1, x_1, \lambda; x, y) H(0; y) + (y-1) G(x_1, x_1, x\lambda; x, y) H(0; y) +
\end{aligned}$$

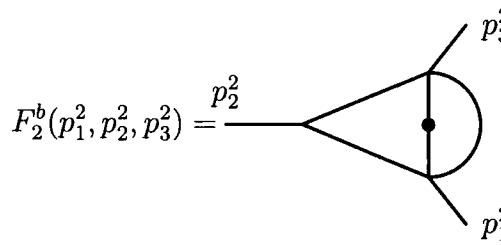
$$\begin{aligned}
& + \frac{y-1}{2} G(x_1, x\lambda, 0; x, y) H(0; y) + \frac{y-1}{4} G(x\lambda, 0, 0; x, y) H(0; y) \\
& + \frac{3(y-1)}{2} G(x\lambda, \lambda, \lambda; x, y) H(0; x_0) + \frac{-3(y-1)}{4} G(x\lambda, \lambda, \lambda; x, y) H(0; y) \\
& + \frac{-3(y-1)^2}{4} G(x\lambda, \lambda, x\lambda; x, y) H(0; y) + \frac{-3(y-1)^2}{2} G(x\lambda, x\lambda, \lambda; x, y) H(0; x_0) \\
& + \frac{3(y-1)^2}{4} G(x\lambda, x\lambda, \lambda; x, y) H(0; y) + \frac{3(y-1)^3}{4} G(x\lambda, x\lambda, x\lambda; x, y) H(0; y) \\
& + \Delta G(0; 0, y) G(\lambda; x, y) H(0, 0; y) - \frac{1}{2} \Delta G(0; 0, y) G(\lambda; x, y) H(1, 0; y) \\
& + (1-y) \Delta G(0; 0, y) G(x\lambda; x, y) H(0, 0; y) + \frac{y-1}{2} \Delta G(0; 0, y) G(x\lambda; x, y) H(1, 0; y) \\
& + \frac{3}{4} \Delta G(0; 0, y) G(0, \lambda; x, y) H(0; y) + \frac{-3(y-1)}{4} \Delta G(0; 0, y) G(0, x\lambda; x, y) H(0; y) \\
& + \frac{1}{4} \Delta G(0; 0, y) G(\lambda, 0; x, y) H(0; y) + \frac{1}{2} \Delta G(0; 0, y) G(x_0, \lambda; x, y) H(0; y) \\
& + \frac{1-y}{2} \Delta G(0; 0, y) G(x_0, x\lambda; x, y) H(0; y) + \frac{1}{2} \Delta G(0; 0, y) G(x_1, \lambda; x, y) H(0; y) \\
& + \frac{1-y}{2} \Delta G(0; 0, y) G(x_1, x\lambda; x, y) H(0; y) + \frac{1-y}{4} \Delta G(0; 0, y) G(x\lambda, 0; x, y) H(0; y) \\
& - \frac{1}{4} \Delta G(0, 0, 0, y) G(\lambda; x, y) H(0; y) + \frac{y-1}{4} \Delta G(0, 0, 0, y) G(x\lambda; x, y) H(0; y) \\
& - (\Delta G(0, \lambda; 0, y) G(\lambda; x, y) H(0; x_0)) + \frac{3}{4} \Delta G(0, \lambda; 0, y) G(\lambda; x, y) H(0; y) \\
& + (y-1) \Delta G(0, \lambda; 0, y) G(x\lambda; x, y) H(0; x_0) + \frac{-3(y-1)}{4} \Delta G(0, \lambda; 0, y) G(x\lambda; x, y) H(0; y) \\
& + \frac{y-1}{4} \Delta G(0, x\lambda; 0, y) G(\lambda; x, y) H(0; y) + \frac{-(y-1)^2}{4} \Delta G(0, x\lambda; 0, y) G(x\lambda; x, y) H(0; y) \\
& - 2 G(\lambda; 0, y) G(\lambda; x, y) H(0, 0; x_0) + G(\lambda; 0, y) G(\lambda; x, y) H(0, 0; y) \\
& + \frac{1}{2} G(\lambda; 0, y) G(\lambda; x, y) H(1, 0; y) + 2(y-1) G(\lambda; 0, y) G(x\lambda; x, y) H(0, 0; x_0) \\
& + (1-y) G(\lambda; 0, y) G(x\lambda; x, y) H(0, 0; y) + \frac{1-y}{2} G(\lambda; 0, y) G(x\lambda; x, y) H(1, 0; y) \\
& - \frac{3}{2} G(\lambda; 0, y) G(0, \lambda; x, y) H(0; x_0) + \frac{3}{4} G(\lambda; 0, y) G(0, \lambda; x, y) H(0; y) \\
& + \frac{3(y-1)}{2} G(\lambda; 0, y) G(0, x\lambda; x, y) H(0; x_0) + \frac{-3(y-1)}{4} G(\lambda; 0, y) G(0, x\lambda; x, y) H(0; y) \\
& - \frac{1}{2} G(\lambda; 0, y) G(\lambda, 0; x, y) H(0; x_0) + \frac{1}{4} G(\lambda; 0, y) G(\lambda, 0; x, y) H(0; y) \\
& - (G(\lambda; 0, y) G(x_0, \lambda; x, y) H(0; x_0)) + \frac{1}{2} G(\lambda; 0, y) G(x_0, \lambda; x, y) H(0; y) \\
& + (y-1) G(\lambda; 0, y) G(x_0, x\lambda; x, y) H(0; x_0) + \frac{1-y}{2} G(\lambda; 0, y) G(x_0, x\lambda; x, y) H(0; y) +
\end{aligned}$$

$$\begin{aligned}
& - (G(\lambda; 0, y) G(x_1, \lambda; x, y) H(0; x_0)) + \frac{1}{2} G(\lambda; 0, y) G(x_1, \lambda; x, y) H(0; y) \\
& + (y-1) G(\lambda; 0, y) G(x_1, x\lambda; x, y) H(0; x_0) + \frac{1-y}{2} G(\lambda; 0, y) G(x_1, x\lambda; x, y) H(0; y) \\
& + \frac{y-1}{2} G(\lambda; 0, y) G(x\lambda, 0; x, y) H(0; x_0) + \frac{1-y}{4} G(\lambda; 0, y) G(x\lambda, 0; x, y) H(0; y) \\
& - \frac{3}{2} G(\lambda; x, y) G(\lambda, 0; 0, y) H(0; x_0) - \frac{1}{4} G(\lambda; x, y) G(\lambda, 0; 0, y) H(0; y) \\
& + \frac{1}{2} G(\lambda; x, y) G(\lambda, \lambda; 0, y) H(0; x_0) - \frac{1}{4} G(\lambda; x, y) G(\lambda, \lambda; 0, y) H(0; y) \\
& + \frac{y-1}{2} G(\lambda; x, y) G(\lambda, x\lambda; 0, y) H(0; x_0) + \frac{-3(y-1)}{4} G(\lambda; x, y) G(\lambda, x\lambda; 0, y) H(0; y) \\
& - (G(\lambda; x, y) G(x_0, \lambda; 0, y) H(0; x_0)) + \frac{1}{2} G(\lambda; x, y) G(x_0, \lambda; 0, y) H(0; y) \\
& + \frac{y-1}{2} G(\lambda; x, y) G(x_0, x\lambda; 0, y) H(0; y) - (G(\lambda; x, y) G(x_1, \lambda; 0, y) H(0; x_0)) \\
& + \frac{1}{2} G(\lambda; x, y) G(x_1, \lambda; 0, y) H(0; y) + \frac{y-1}{2} G(\lambda; x, y) G(x_1, x\lambda; 0, y) H(0; y) \\
& + \frac{3(y-1)}{2} G(x\lambda; x, y) G(\lambda, 0; 0, y) H(0; x_0) + \frac{y-1}{4} G(x\lambda; x, y) G(\lambda, 0; 0, y) H(0; y) \\
& + \frac{1-y}{2} G(x\lambda; x, y) G(\lambda, \lambda; 0, y) H(0; x_0) + \frac{y-1}{4} G(x\lambda; x, y) G(\lambda, \lambda; 0, y) H(0; y) \\
& + \frac{-(y-1)^2}{2} G(x\lambda; x, y) G(\lambda, x\lambda; 0, y) H(0; x_0) + \frac{3(y-1)^2}{4} G(x\lambda; x, y) G(\lambda, x\lambda; 0, y) H(0; y) \\
& + (y-1) G(x\lambda; x, y) G(x_0, \lambda; 0, y) H(0; x_0) + \frac{1-y}{2} G(x\lambda; x, y) G(x_0, \lambda; 0, y) H(0; y) \\
& + \frac{-(y-1)^2}{2} G(x\lambda; x, y) G(x_0, x\lambda; 0, y) H(0; y) + (y-1) G(x\lambda; x, y) G(x_1, \lambda; 0, y) H(0; x_0) \\
& + \frac{1-y}{2} G(x\lambda; x, y) G(x_1, \lambda; 0, y) H(0; y) + \frac{-(y-1)^2}{2} G(x\lambda; x, y) G(x_1, x\lambda; 0, y) H(0; y)
\end{aligned}$$

The second momentum configuration is defined by,

$$F_1^b(p_1^2, p_2^2, p_3^2) = \text{Diagram}$$

$$= S_D^2 (-p_3^2)^{-2\epsilon} \left(\sum_{i=-2, \dots, 1} f_1^i \left(\frac{p_1^2}{p_3^2}, \frac{p_2^2}{p_3^2} \right) \epsilon^i + \mathcal{O}(\epsilon^2) \right), \quad (3.42)$$



$$F_2^b(p_1^2, p_2^2, p_3^2) = S_D^2 (-p_3^2)^{-1-2\epsilon} \frac{1}{\lambda} \left(\sum_{i=-1, \dots, 1} f_2^i \left(\frac{p_1^2}{p_3^2}, \frac{p_2^2}{p_3^2} \right) \epsilon^i + \mathcal{O}(\epsilon^2) \right). \quad (3.43)$$

Expressions for $f_{1,2}^i$ in this momentum configuration are similarly lengthy to those for $F_{1,2}^a$ and can be obtained in computer readable form from the authors. In each case, we have checked that the leading contribution agrees with the results of Ref. [74].

Note that solving the differential equation for the crossed triangle requires the functions $F_{1,2}^a(x, y)$ which are symmetric in x and y and in addition the functions $F_{1,2}^b(x, y)$ and $F_{1,2}^b(y, x)$. The functions $F_{1,2}^b(y, x)$ are, of course, in principle known. However, exchanging x and y puts them in a form that is not suited for further integration over x . To get them into a suitable form we therefore recalculate them directly from the differential equations.

Master Integrals with five propagators

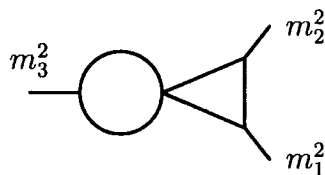


Figure 3.10: The two-loop Master Integral, $TB(m_1^2, m_2^2, m_3^2)$

There are two Master Integrals with five propagators. The first is solved by factorisation into the product of one loop integrals as demonstrated in section 2.2, and the second is a genuine two-loop integral. The first integral, denoted by TB, is shown in figure 3.10. This integral obviously factorises into the product of a one-loop bubble

diagram with a one-loop triangle. As such the graph TB is given by,

$$\text{TB}(p_1^2, p_2^2, p_3^2) = \text{BB}(p_3^2)F_0(p_1^2, p_2^2, p_3^2). \quad (3.44)$$

The ϵ expansion for this integral is straightforwardly obtained from eq. 3.35 and we do not show it here.

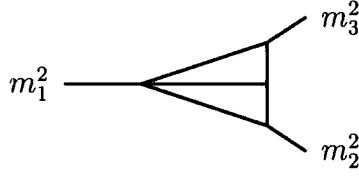


Figure 3.11: The two-loop Master Integral, $F_3(m_1^2, m_2^2, m_3^2)$

The second irreducible two-loop diagram is denoted by F_3 , and is shown in figure 3.11. This integral is finite in 4-dimensions and the leading contribution has been calculated in Ref. [74].

The differential equation for F_3 is given by,

$$\begin{aligned} \frac{\partial}{\partial m_1^2} F_3(m_1^2, m_2^2, m_3^2) &= \frac{(d-3)(-m_1^2 + m_2^2 + m_3^2)}{\Lambda^2} F_3 \\ &- \frac{2(3d-10)(d-3)}{(d-4)\Lambda^2} F_1(m_1^2, m_2^2, m_3^2) - \frac{2(3d-10)(d-3)}{(d-4)\Lambda^2} F_1(m_3^2, m_1^2, m_2^2) \\ &+ \frac{(-m_1^2 - m_2^2 + m_3^2)}{\Lambda^2} F_2(m_1^2, m_2^2, m_3^2) - \frac{(m_1^2 - m_2^2 + m_3^2)}{\Lambda^2} F_2(m_3^2, m_1^2, m_2^2) \\ &+ \frac{4(d-3)^2}{(d-4)\Lambda^2} \text{TGL}(m_3^2, m_2^2). \end{aligned} \quad (3.45)$$

The solution of the homogeneous equation at $d = 4$ is given by $F_3^{\text{hom}} = \frac{1}{\lambda}$ and we

therefore take the boundary condition at $\lambda = 0$ corresponding to $x \rightarrow x_0$, so that

$$\begin{aligned}
F_3(m_1^2, m_2^2, m_3^2)|_{m_1^2=(m_2-m_3)^2} = & -\frac{(3d-10)}{(d-4)(m_2-m_3)m_3} F_1(m_2^2, m_3^2, (m_2-m_3)^2) \\
& -\frac{(3d-10)}{(d-4)(m_2-m_3)m_3} F_1((m_2-m_3)^2, m_2^2, m_3^2) \\
& -\frac{m_2}{(d-3)(m_2-m_3)} F_2(m_2^2, m_3^2, (m_2-m_3)^2) \\
& -\frac{m_2}{(d-3)m_3} F_2((m_2-m_3)^2, m_2^2, m_3^2) \\
& +\frac{2(d-3)}{(d-4)(m_2-m_3)m_3} \text{TGL}((m_2-m_3)^2, m_3^2).
\end{aligned} \tag{3.46}$$

Once again, there are two distinct kinematic configurations depending on the position of the large scale p_3^2 . For the first momentum configuration, the first two terms in the ϵ expansion are given by,

$$F_3^a(p_1^2, p_2^2, p_3^2) = \text{Diagram}$$

$$F_3^a(p_1^2, p_2^2, p_3^2) = S_D^2(-p_3^2)^{-1-2\epsilon} \frac{1}{\lambda} \left(\sum_{i=0, \dots, 1} f_3^i \left(\frac{p_1^2}{p_3^2}, \frac{p_2^2}{p_3^2} \right) \epsilon^i + \mathcal{O}(\epsilon^2) \right), \tag{3.47}$$

where,

$$\begin{aligned}
f_3^0 = & -6\zeta_3 G(\lambda; x, y) + 6G(\lambda, \lambda, \lambda, 0; x, y) \\
& + \frac{-\pi^2}{3} G(\lambda; 0, y) G(\lambda; x, y) + 2G(\lambda; x, y) G(\lambda, 0, \lambda; 0, y) \\
& - 2G(\lambda; x, y) G(\lambda, \lambda, 0; 0, y) + \frac{\pi^2}{3} G(\lambda; x, y) H(0; y) \\
& + 2G(\lambda; x, y) H(0, 1, 0; y) - 2G(\lambda; x, y) H(1, 0, 0; y) +
\end{aligned}$$

$$\begin{aligned}
& + G(\lambda, 0; x, y) H(0, 0; y) + 6 G(\lambda, \lambda, \lambda; x, y) H(0; x_0) \\
& - 3 G(\lambda, \lambda, \lambda; x, y) H(0; y) + (3 - 3y) G(\lambda, \lambda, x\lambda; x, y) H(0; y) \\
& - \Delta G(0; 0, y) G(\lambda; x, y) H(0, 0; y) - \Delta G(0, \lambda; 0, y) G(\lambda; x, y) H(0; y) \\
& - G(\lambda; 0, y) G(\lambda; x, y) H(0, 0; y) - 2 G(\lambda; 0, y) G(\lambda; x, y) H(1, 0; y) \\
& - 2 G(\lambda; x, y) G(\lambda, \lambda; 0, y) H(0; x_0) + G(\lambda; x, y) G(\lambda, \lambda; 0, y) H(0; y) \\
& + 2 (-1 + y) G(\lambda; x, y) G(\lambda, x\lambda; 0, y) H(0; y) \\
f_3^1 = & + \frac{-3\pi^4}{20} G(\lambda; x, y) - 3 \zeta_3 G(\lambda, 0; x, y) + 6 \zeta_3 G(x_0, \lambda; x, y) + 6 \zeta_3 G(x_1, \lambda; x, y) \\
& + \frac{-(\pi^2 (y-1))}{2} G(\lambda, \lambda, x\lambda; x, y) + \frac{-(\pi^2 (y-1))}{2} G(\lambda, x\lambda, \lambda; x, y) \\
& - 3 G(\lambda, 0, \lambda, \lambda, 0; x, y) - 9 G(\lambda, \lambda, 0, \lambda, 0; x, y) - 12 G(\lambda, \lambda, \lambda, 0, 0; x, y) \\
& - 6 G(\lambda, \lambda, x_0, \lambda, 0; x, y) - 6 G(\lambda, \lambda, x_1, \lambda, 0; x, y) - 6 G(x_0, \lambda, \lambda, \lambda, 0; x, y) \\
& - 6 G(x_1, \lambda, \lambda, \lambda, 0; x, y) + 3 \zeta_3 \Delta G(0; 0, y) G(\lambda; x, y) \\
& + \frac{\pi^2}{6} \Delta G(0, \lambda; 0, y) G(\lambda; x, y) - 3 \Delta G(0, \lambda, 0, \lambda; 0, y) G(\lambda; x, y) \\
& - 6 \Delta G(0, \lambda, \lambda, 0; 0, y) G(\lambda; x, y) + \zeta_3 G(\lambda; 0, y) G(\lambda; x, y) \\
& + \frac{\pi^2}{6} G(\lambda; 0, y) G(\lambda, 0; x, y) + \frac{\pi^2}{3} G(\lambda; 0, y) G(x_0, \lambda; x, y) \\
& + \frac{\pi^2}{3} G(\lambda; 0, y) G(x_1, \lambda; x, y) + \frac{-\pi^2}{6} G(\lambda; x, y) G(\lambda, 0; 0, y) \\
& + \frac{\pi^2 (y-1)}{6} G(\lambda; x, y) G(\lambda, x\lambda; 0, y) + \frac{\pi^2}{3} G(\lambda; x, y) G(x_0, \lambda; 0, y) \\
& + \frac{\pi^2}{3} G(\lambda; x, y) G(x_1, \lambda; 0, y) - 4 G(\lambda; x, y) G(\lambda, 0, 0, \lambda; 0, y) \\
& - (G(\lambda; x, y) G(\lambda, 0, \lambda, 0; 0, y)) - 2 G(\lambda; x, y) G(\lambda, \lambda, 0, 0; 0, y) \\
& + (3 - 3y) G(\lambda; x, y) G(\lambda, \lambda, 0, x\lambda; 0, y) + (3 - 3y) G(\lambda; x, y) G(\lambda, \lambda, x\lambda, 0; 0, y) \\
& + 4 G(\lambda; x, y) G(\lambda, x_0, \lambda, 0; 0, y) + 4 G(\lambda; x, y) G(\lambda, x_1, \lambda, 0; 0, y) \\
& + (3 - 3y) G(\lambda; x, y) G(\lambda, x\lambda, \lambda, 0; 0, y) - 2 G(\lambda; x, y) G(x_0, \lambda, 0, \lambda; 0, y) +
\end{aligned}$$

$$\begin{aligned}
& -4G(\lambda; x, y)G(x_0, \lambda, \lambda, 0; 0, y) - 2G(\lambda; x, y)G(x_1, \lambda, 0, \lambda; 0, y) \\
& -4G(\lambda; x, y)G(x_1, \lambda, \lambda, 0; 0, y) + 8\zeta_3 G(\lambda; x, y)H(0; y) \\
& + 6\zeta_3 G(\lambda; x, y)H(1; y) + \frac{-\pi^2}{3}G(\lambda; x, y)H(0, 0; y) \\
& + \frac{\pi^2}{3}G(\lambda; x, y)H(0, 1; y) + \frac{\pi^2}{3}G(\lambda; x, y)H(1, 0; y) \\
& + 2G(\lambda; x, y)H(0, 0, 0, 0; y) - 2G(\lambda; x, y)H(0, 0, 1, 0; y) \\
& - 2G(\lambda; x, y)H(0, 1, 0, 0; y) + 2G(\lambda; x, y)H(0, 1, 1, 0; y) \\
& + 6G(\lambda; x, y)H(1, 0, 0, 0; y) + 2G(\lambda; x, y)H(1, 0, 1, 0; y) \\
& - 2G(\lambda; x, y)H(1, 1, 0, 0; y) + 3(y-1)G(\lambda, 0; 0, y)G(\lambda, \lambda, x\lambda; x, y) \\
& + 3(y-1)G(\lambda, 0; 0, y)G(\lambda, x\lambda, \lambda; x, y) - (G(\lambda, 0; x, y)G(\lambda, 0, \lambda; 0, y)) \\
& + G(\lambda, 0; x, y)G(\lambda, \lambda, 0; 0, y) + \frac{-\pi^2}{6}G(\lambda, 0; x, y)H(0; y) \\
& - 3G(\lambda, 0; x, y)H(0, 0, 0; y) - (G(\lambda, 0; x, y)H(0, 1, 0; y)) \\
& + G(\lambda, 0; x, y)H(1, 0, 0; y) - 2G(x_0, \lambda; x, y)G(\lambda, 0, \lambda; 0, y) \\
& + 2G(x_0, \lambda; x, y)G(\lambda, \lambda, 0; 0, y) + \frac{-\pi^2}{3}G(x_0, \lambda; x, y)H(0; y) \\
& - 2G(x_0, \lambda; x, y)H(0, 1, 0; y) + 2G(x_0, \lambda; x, y)H(1, 0, 0; y) \\
& - 2G(x_1, \lambda; x, y)G(\lambda, 0, \lambda; 0, y) + 2G(x_1, \lambda; x, y)G(\lambda, \lambda, 0; 0, y) \\
& + \frac{-\pi^2}{3}G(x_1, \lambda; x, y)H(0; y) - 2G(x_1, \lambda; x, y)H(0, 1, 0; y) \\
& + 2G(x_1, \lambda; x, y)H(1, 0, 0; y) - \frac{1}{2}G(\lambda, 0, 0; x, y)H(0, 0; y) \\
& - 12G(\lambda, \lambda, \lambda; x, y)H(0, 0; x_0) + \frac{9}{2}G(\lambda, \lambda, \lambda; x, y)H(0, 0; y) \\
& + \frac{9(y-1)}{2}G(\lambda, \lambda, x\lambda; x, y)H(0, 0; y) + (3-3y)G(\lambda, \lambda, x\lambda; x, y)H(1, 0; y) \\
& + \frac{-3(y-1)}{2}G(\lambda, x\lambda, \lambda; x, y)H(0, 0; y) + (3-3y)G(\lambda, x\lambda, \lambda; x, y)H(1, 0; y) \\
& + \frac{-3(y-1)^2}{2}G(\lambda, x\lambda, x\lambda; x, y)H(0, 0; y) - (G(x_0, \lambda, 0; x, y)H(0, 0; y)) \\
& - (G(x_1, \lambda, 0; x, y)H(0, 0; y)) - 3G(\lambda, 0, \lambda, \lambda; x, y)H(0; x_0) +
\end{aligned}$$

$$\begin{aligned}
& + \frac{3}{2} G(\lambda, 0, \lambda, \lambda; x, y) H(0; y) + \frac{3(y-1)}{2} G(\lambda, 0, \lambda, x\lambda; x, y) H(0; y) \\
& - 9 G(\lambda, \lambda, 0, \lambda; x, y) H(0; x_0) + \frac{9}{2} G(\lambda, \lambda, 0, \lambda; x, y) H(0; y) \\
& + \frac{9(y-1)}{2} G(\lambda, \lambda, 0, x\lambda; x, y) H(0; y) - 12 G(\lambda, \lambda, \lambda, 0; x, y) H(0; x_0) \\
& - 6 G(\lambda, \lambda, x_0, \lambda; x, y) H(0; x_0) + 3 G(\lambda, \lambda, x_0, \lambda; x, y) H(0; y) \\
& + 3(y-1) G(\lambda, \lambda, x_0, x\lambda; x, y) H(0; y) - 6 G(\lambda, \lambda, x_1, \lambda; x, y) H(0; x_0) \\
& + 3 G(\lambda, \lambda, x_1, \lambda; x, y) H(0; y) + 3(y-1) G(\lambda, \lambda, x_1, x\lambda; x, y) H(0; y) \\
& + \frac{3(y-1)}{2} G(\lambda, \lambda, x\lambda, 0; x, y) H(0; y) + \frac{3(y-1)}{2} G(\lambda, x\lambda, \lambda, 0; x, y) H(0; y) \\
& - 6 G(x_0, \lambda, \lambda, \lambda; x, y) H(0; x_0) + 3 G(x_0, \lambda, \lambda, \lambda; x, y) H(0; y) \\
& + 3(y-1) G(x_0, \lambda, \lambda, x\lambda; x, y) H(0; y) - 6 G(x_1, \lambda, \lambda, \lambda; x, y) H(0; x_0) \\
& + 3 G(x_1, \lambda, \lambda, \lambda; x, y) H(0; y) + 3(y-1) G(x_1, \lambda, \lambda, x\lambda; x, y) H(0; y) \\
& + \frac{\pi^2}{6} \Delta G(0; 0, y) G(\lambda; x, y) H(0; y) + 3 \Delta G(0; 0, y) G(\lambda; x, y) H(0, 0, 0; y) \\
& + \Delta G(0; 0, y) G(\lambda; x, y) H(0, 1, 0; y) - (\Delta G(0; 0, y) G(\lambda; x, y) H(1, 0, 0; y)) \\
& + \frac{1}{2} \Delta G(0; 0, y) G(\lambda, 0; x, y) H(0, 0; y) + \Delta G(0; 0, y) G(x_0, \lambda; x, y) H(0, 0; y) \\
& + \Delta G(0; 0, y) G(x_1, \lambda; x, y) H(0, 0; y) + \frac{-3(y-1)}{2} \Delta G(0; 0, y) G(\lambda, \lambda, x\lambda; x, y) H(0; y) \\
& + \frac{-3(y-1)}{2} \Delta G(0; 0, y) G(\lambda, x\lambda, \lambda; x, y) H(0; y) - \frac{1}{2} \Delta G(0, 0, 0, y) G(\lambda; x, y) H(0, 0; y) \\
& - (\Delta G(0, \lambda; 0, y) G(\lambda; x, y) G(\lambda, 0; 0, y)) + \frac{5}{2} \Delta G(0, \lambda; 0, y) G(\lambda; x, y) H(0, 0; y) \\
& + \Delta G(0, \lambda; 0, y) G(\lambda; x, y) H(1, 0; y) + \frac{1}{2} \Delta G(0, \lambda; 0, y) G(\lambda, 0; x, y) H(0; y) \\
& + \Delta G(0, \lambda; 0, y) G(x_0, \lambda; x, y) H(0; y) + \Delta G(0, \lambda; 0, y) G(x_1, \lambda; x, y) H(0; y) \\
& + \frac{y-1}{2} \Delta G(0, x\lambda; 0, y) G(\lambda; x, y) H(0, 0; y) + \frac{3}{2} \Delta G(0, 0, \lambda; 0, y) G(\lambda; x, y) H(0; y) \\
& - \frac{1}{2} \Delta G(0, \lambda, 0; 0, y) G(\lambda; x, y) H(0; y) - 8 \Delta G(0, \lambda, \lambda; 0, y) G(\lambda; x, y) H(0; x_0) \\
& + 4 \Delta G(0, \lambda, \lambda; 0, y) G(\lambda; x, y) H(0; y) + \frac{5(y-1)}{2} \Delta G(0, \lambda, x\lambda; 0, y) G(\lambda; x, y) H(0; y) \\
& + \Delta G(0, x_0, \lambda; 0, y) G(\lambda; x, y) H(0; y) + \Delta G(0, x_1, \lambda; 0, y) G(\lambda; x, y) H(0; y) \\
& + \frac{5(y-1)}{2} \Delta G(0, x\lambda, \lambda; 0, y) G(\lambda; x, y) H(0; y) + \frac{\pi^2}{6} G(\lambda; 0, y) G(\lambda; x, y) H(0; y) +
\end{aligned}$$

$$\begin{aligned}
& + \frac{-\pi^2}{3} G(\lambda; 0, y) G(\lambda; x, y) H(1; y) + 3 G(\lambda; 0, y) G(\lambda; x, y) H(0, 0, 0; y) \\
& + G(\lambda; 0, y) G(\lambda; x, y) H(0, 1, 0; y) + 3 G(\lambda; 0, y) G(\lambda; x, y) H(1, 0, 0; y) \\
& - 2 G(\lambda; 0, y) G(\lambda; x, y) H(1, 1, 0; y) + \frac{1}{2} G(\lambda; 0, y) G(\lambda, 0; x, y) H(0, 0; y) \\
& + G(\lambda; 0, y) G(\lambda, 0; x, y) H(1, 0; y) + G(\lambda; 0, y) G(x_0, \lambda; x, y) H(0, 0; y) \\
& + 2 G(\lambda; 0, y) G(x_0, \lambda; x, y) H(1, 0; y) + G(\lambda; 0, y) G(x_1, \lambda; x, y) H(0, 0; y) \\
& + 2 G(\lambda; 0, y) G(x_1, \lambda; x, y) H(1, 0; y) + 3 (y - 1) G(\lambda; 0, y) G(\lambda, \lambda, x\lambda; x, y) H(0; x_0) \\
& - \frac{3 (y - 1)}{2} G(\lambda; 0, y) G(\lambda, \lambda, x\lambda; x, y) H(0; y) \\
& + 3 (y - 1) G(\lambda; 0, y) G(\lambda, x\lambda, \lambda; x, y) H(0; x_0) \\
& - \frac{3 (y - 1)}{2} G(\lambda; 0, y) G(\lambda, x\lambda, \lambda; x, y) H(0; y) \\
& + G(\lambda; x, y) G(\lambda, 0; 0, y)^2 \\
& + (1 - y) G(\lambda; x, y) G(\lambda, 0; 0, y) G(\lambda, x\lambda; 0, y) - 2 G(\lambda; x, y) G(\lambda, 0; 0, y) G(x_0, \lambda; 0, y) \\
& - 2 G(\lambda; x, y) G(\lambda, 0; 0, y) G(x_1, \lambda; 0, y) - \frac{1}{2} G(\lambda; x, y) G(\lambda, 0; 0, y) H(0, 0; y) \\
& - (G(\lambda; x, y) G(\lambda, 0; 0, y) H(1, 0; y)) + 4 G(\lambda; x, y) G(\lambda, \lambda; 0, y) H(0, 0; x_0) \\
& - \frac{3}{2} G(\lambda; x, y) G(\lambda, \lambda; 0, y) H(0, 0; y) + \frac{-7 (y - 1)}{2} G(\lambda; x, y) G(\lambda, x\lambda; 0, y) H(0, 0; y) \\
& + (y - 1) G(\lambda; x, y) G(\lambda, x\lambda; 0, y) H(1, 0; y) + G(\lambda; x, y) G(x_0, \lambda; 0, y) H(0, 0; y) \\
& + 2 G(\lambda; x, y) G(x_0, \lambda; 0, y) H(1, 0; y) + (y - 1) G(\lambda; x, y) G(x_0, x\lambda; 0, y) H(0, 0; y) \\
& + G(\lambda; x, y) G(x_1, \lambda; 0, y) H(0, 0; y) + 2 G(\lambda; x, y) G(x_1, \lambda; 0, y) H(1, 0; y) \\
& + (y - 1) G(\lambda; x, y) G(x_1, x\lambda; 0, y) H(0, 0; y) - (G(\lambda; x, y) G(\lambda, 0, \lambda; 0, y) H(0; x_0)) \\
& - \frac{3}{2} G(\lambda; x, y) G(\lambda, 0, \lambda; 0, y) H(0; y) + (1 - y) G(\lambda; x, y) G(\lambda, 0, x\lambda; 0, y) H(0; y) \\
& + 3 G(\lambda; x, y) G(\lambda, \lambda, 0; 0, y) H(0; x_0) + \frac{1}{2} G(\lambda; x, y) G(\lambda, \lambda, 0; 0, y) H(0; y) \\
& + (5 - 5y) G(\lambda; x, y) G(\lambda, \lambda, x\lambda; 0, y) H(0; x_0) \\
& + \frac{5 (y - 1)}{2} G(\lambda; x, y) G(\lambda, \lambda, x\lambda; 0, y) H(0; y) \\
& + 2 G(\lambda; x, y) G(\lambda, x_0, \lambda; 0, y) H(0; x_0) - (G(\lambda; x, y) G(\lambda, x_0, \lambda; 0, y) H(0; y)) +
\end{aligned}$$

$$\begin{aligned}
& + (2 - 2y) G(\lambda; x, y) G(\lambda, x_0, x\lambda; 0, y) H(0; y) + 2 G(\lambda; x, y) G(\lambda, x_1, \lambda; 0, y) H(0; x_0) \\
& - (G(\lambda; x, y) G(\lambda, x_1, \lambda; 0, y) H(0; y)) + (2 - 2y) G(\lambda; x, y) G(\lambda, x_1, x\lambda; 0, y) H(0; y) \\
& + (y - 1) G(\lambda; x, y) G(\lambda, x\lambda, 0; 0, y) H(0; y) \\
& + (5 - 5y) G(\lambda; x, y) G(\lambda, x\lambda, \lambda; 0, y) H(0; x_0) \\
& + \frac{5(y - 1)}{2} G(\lambda; x, y) G(\lambda, x\lambda, \lambda; 0, y) H(0; y) \\
& + 4(y - 1)^2 G(\lambda; x, y) G(\lambda, x\lambda, x\lambda; 0, y) H(0; y) \\
& + G(\lambda; x, y) G(x_0, 0, \lambda; 0, y) H(0; y) - 8 G(\lambda; x, y) G(x_0, \lambda, \lambda; 0, y) H(0; x_0) \\
& + 4 G(\lambda; x, y) G(x_0, \lambda, \lambda; 0, y) H(0; y) + 2(y - 1) G(\lambda; x, y) G(x_0, \lambda, x\lambda; 0, y) H(0; y) \\
& + 2(y - 1) G(\lambda; x, y) G(x_0, x\lambda, \lambda; 0, y) H(0; y) + G(\lambda; x, y) G(x_1, 0, \lambda; 0, y) H(0; y) \\
& - 8 G(\lambda; x, y) G(x_1, \lambda, \lambda; 0, y) H(0; x_0) + 4 G(\lambda; x, y) G(x_1, \lambda, \lambda; 0, y) H(0; y) \\
& + 2(y - 1) G(\lambda; x, y) G(x_1, \lambda, x\lambda; 0, y) H(0; y) \\
& + 2(y - 1) G(\lambda; x, y) G(x_1, x\lambda, \lambda; 0, y) H(0; y) \\
& + G(\lambda, 0; x, y) G(\lambda, \lambda; 0, y) H(0; x_0) - \frac{1}{2} G(\lambda, 0; x, y) G(\lambda, \lambda; 0, y) H(0; y) \\
& + (1 - y) G(\lambda, 0; x, y) G(\lambda, x\lambda; 0, y) H(0; y) + 2 G(\lambda, \lambda; 0, y) G(x_0, \lambda; x, y) H(0; x_0) \\
& - (G(\lambda, \lambda; 0, y) G(x_0, \lambda; x, y) H(0; y)) + 2 G(\lambda, \lambda; 0, y) G(x_1, \lambda; x, y) H(0; x_0) \\
& - (G(\lambda, \lambda; 0, y) G(x_1, \lambda; x, y) H(0; y)) + (2 - 2y) G(\lambda, x\lambda; 0, y) G(x_0, \lambda; x, y) H(0; y) \\
& + (2 - 2y) G(\lambda, x\lambda; 0, y) G(x_1, \lambda; x, y) H(0; y)
\end{aligned}$$

The other momentum configuration required is defined by,

$$F_3^b(p_1^2, p_2^2, p_3^2) = \text{Diagram}$$

$$F_3^b(p_1^2, p_2^2, p_3^2) = S_D^2 (-p_3^2)^{-1-2\epsilon} \frac{1}{\lambda} \left(\sum_{i=0, \dots, 1} f_3^i \left(\frac{p_1^2}{p_3^2}, \frac{p_2^2}{p_3^2} \right) \epsilon^i + \mathcal{O}(\epsilon^2) \right). \quad (3.48)$$

Expressions for f_3^i in this momentum configuration are similarly lengthy to those for F_3^a and can be obtained in computer readable form upon request. In each case, we have checked that the finite contribution agrees with the results of Ref. [74].

Master Integrals with six propagators

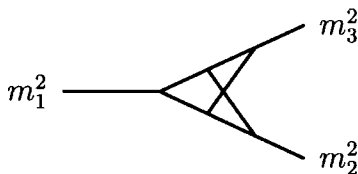


Figure 3.12: The two-loop Master Integral, $F_4(m_1^2, m_2^2, m_3^2)$

The only MI with 6 propagators is the crossed triangle which is denoted by F_4 and is shown in figure 3.12. This integral is the only non-planar Master Integral required and is finite in 4-dimensions. Considering the diagram in 3-dimensions, we can see that this integral is fully symmetric in all three legs, and so we only need to evaluate a single momentum configuration for this integral.

This MI satisfies the differential equation,

$$\begin{aligned} \frac{\partial}{\partial m_1^2} F_4 &= \frac{(6-d)(-m_1^2 + m_2^2 + m_3^2)}{\Lambda^2} F_4 - \frac{8}{\Lambda^2} F_2(m_1^2, m_2^2, m_3^2) \\ &+ \frac{4(m_1^2 + m_2^2 - m_3^2)}{\Lambda^2 m_1^2} F_2(m_2^2, m_3^2, m_1^2) \\ &- \frac{4(-m_1^2 + m_2^2 - m_3^2)}{\Lambda^2 m_1^2} F_2(m_3^2, m_2^2, m_1^2) \\ &- \frac{4(d-4)F_3(m_1^2, m_2^2, m_3^2)}{\Lambda^2} \\ &+ \frac{2(d-4)(m_1^2 + m_2^2 - m_3^2)}{\Lambda^2 m_1^2} F_3(m_2^2, m_3^2, m_1^2) \\ &- \frac{2(d-4)(-m_1^2 + m_2^2 - m_3^2)}{\Lambda^2 m_1^2} F_3(m_3^2, m_2^2, m_1^2). \end{aligned} \quad (3.49)$$

The homogeneous solution at $d = 4$ is $F_4^{hom} = \lambda^{-2}$ while the boundary condition at $\lambda = 0$ corresponding to $x \rightarrow x_0$ is given by,

$$\begin{aligned}
F_4(m_1^2, m_2^2, m_3^2)|_{m_1^2=(m_2-m_3)^2} &= \frac{4(m_2-m_3)}{(d-6)m_1^2 m_3} F_2(m_2^2, m_3^2, (m_2-m_3)^2) \\
&\quad - \frac{4}{(d-6)m_2 m_3} F_2((m_2-m_3)^2, m_2^2, m_3^2) \\
&\quad - \frac{4(m_2-m_3)}{(d-6)m_1^2 m_2} F_2(m_3^2, m_2^2, (m_2-m_3)^2) \\
&\quad + \frac{2(d-4)(m_2-m_3)}{(d-6)m_1^2 m_3} F_3(m_2^2, m_3^2, (m_2-m_3)^2) \\
&\quad - \frac{2(d-4)}{(d-6)m_2 m_3} F_3((m_2-m_3)^2, m_2^2, m_3^2) \\
&\quad - \frac{2(d-4)(m_2-m_3)}{(d-6)m_1^2 m_2} F_3(m_3^2, m_2^2, (m_2-m_3)^2).
\end{aligned} \tag{3.50}$$

We find that the first two terms of the ϵ -expansion are given by,

$$F_4(p_1^2, p_2^2, p_3^2) = \text{Diagram}$$

$$F_4(p_1^2, p_2^2, p_3^2) = S_D^2(-p_3^2)^{-2\epsilon} \left(\sum_{i=0, \dots, 1} f_1^i \left(\frac{p_1^2}{p_3^2}, \frac{p_2^2}{p_3^2} \right) \epsilon^i + \mathcal{O}(\epsilon^2) \right), \tag{3.51}$$

where,

$$\begin{aligned}
f_4^0(x, y) &= + \frac{-8\pi^2}{3} G(\lambda, \lambda; x, y) + \frac{-4\pi^2(y-1)}{3} G(\lambda, x\lambda; x, y) \\
&\quad + \frac{-4\pi^2(y-1)}{3} G(x\lambda, \lambda; x, y) - 8G(\lambda, 0, \lambda, 0; x, y) - 16G(\lambda, \lambda, 0, 0; x, y) \\
&\quad + 16G(\lambda, 0; 0, x_0) G(\lambda, \lambda; x, y) + 8(y-1) G(\lambda, 0; 0, y) G(\lambda, x\lambda; x, y) \\
&\quad + 8(y-1) G(\lambda, 0; 0, y) G(x\lambda, \lambda; x, y) - 16G(\lambda, \lambda; x, y) H(0, 0; x_0) \\
&\quad - 4G(\lambda, \lambda; x, y) H(0, 0; y) - 16G(\lambda, \lambda; x, y) H(1, 0; x_0) +
\end{aligned}$$

$$\begin{aligned}
& + (4 - 4y) G(\lambda, x\lambda; x, y) H(0, 0; y) + (8 - 8y) G(\lambda, x\lambda; x, y) H(1, 0; y) \\
& + (4 - 4y) G(x\lambda, \lambda; x, y) H(0, 0; y) + (8 - 8y) G(x\lambda, \lambda; x, y) H(1, 0; y) \\
& - 4(y - 1)^2 G(x\lambda, x\lambda; x, y) H(0, 0; y) - 8 G(\lambda, 0, \lambda; x, y) H(0; x_0) \\
& + 4 G(\lambda, 0, \lambda; x, y) H(0; y) + 4(y - 1) G(\lambda, 0, x\lambda; x, y) H(0; y) \\
& - 16 G(\lambda, \lambda, 0; x, y) H(0; x_0) + 8 G(\lambda, \lambda, 0; x, y) H(0; y) \\
& + 4(y - 1) G(\lambda, x\lambda, 0; x, y) H(0; y) + 4(y - 1) G(x\lambda, \lambda, 0; x, y) H(0; y) \\
& - 8 \Delta G(0; 0, x_0) G(\lambda, \lambda; x, y) H(0; x_0) \\
& + (4 - 4y) \Delta G(0; 0, y) G(\lambda, x\lambda; x, y) H(0; y) \\
& + (4 - 4y) \Delta G(0; 0, y) G(x\lambda, \lambda; x, y) H(0; y) \\
& - 8 G(\lambda; 0, x_0) G(\lambda, \lambda; x, y) H(0; x_0) \\
& + 16 G(\lambda; 0, x_0) G(\lambda, \lambda; x, y) H(0; y) \\
& + 8(y - 1) G(\lambda; 0, y) G(\lambda, x\lambda; x, y) H(0; x_0) \\
& + (4 - 4y) G(\lambda; 0, y) G(\lambda, x\lambda; x, y) H(0; y) \\
& + 8(y - 1) G(\lambda; 0, y) G(x\lambda, \lambda; x, y) H(0; x_0) \\
& + (4 - 4y) G(\lambda; 0, y) G(x\lambda, \lambda; x, y) H(0; y)
\end{aligned}$$

$f_4^1(x, y)$ is given in appendix B. As with the other MI, we have checked that the leading (finite) contribution agrees with the results of Ref. [74].

3.4 Application

To illustrate the application of these Master Integrals in the evaluation of the two-loop box Master Integrals with two off-shell legs, we present the differential equation for the Master Integral illustrated in figure 3.13. This Master Integral has two adjacent off-shell legs, and requires the Master Integrals SS , F_1 , and F_2 which we have

evaluated in this section. Double-box Master Integrals with more denominators will also require the Master Integrals F_3, F_4 , which can be seen by performing pinchings on a general two-loop box diagram.

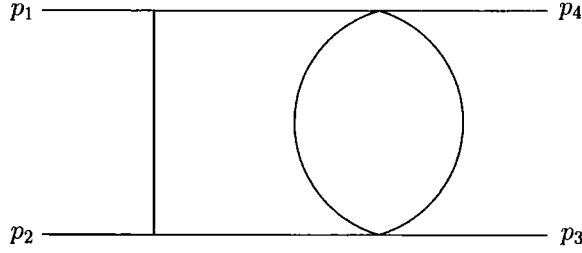


Figure 3.13: An example of a two-loop master integral with four external legs, of which two are off-shell.

For this integral we have two external legs off-shell and two on-shell. We take

$$\begin{aligned} p_1^2 &= 0 & p_3^2 &= m_a^2 \\ p_2^2 &= 0 & p_4^2 &= m_b^2. \end{aligned}$$

With these scales the box integral obeys the following differential equation in m_a^2 .

$$\begin{aligned} \frac{\partial I(s_{12}, s_{23}, m_a^2, m_b^2)}{\partial m_a^2} &= - \frac{(3d-10)(3d-8)SS(m_a^2)}{2(d-4)m_a^2 s_{12}(m_a^2 - s_{23})} \\ &\quad - \frac{(3d-10)(-8+3d)SS(s_{23})}{2(d-4)(m_a^2 - s_{23})\Phi} \\ &\quad - \frac{(3d-10)(-m_b^2 + s_{23})F_1(m_a^2, m_b^2, s_{12})}{2s_{12}\Phi} \\ &\quad + \frac{(d-4)m_b^2(m_b^2 - s_{12} - s_{23})F_2(m_a^2, m_b^2, s_{12})}{2(d-3)s_{12}\Phi} \\ &\quad + \frac{(d-4)(m_b^2 - s_{23})I(s_{12}, s_{23}, m_a^2, m_b^2)}{2\Phi}, \end{aligned} \quad (3.52)$$

and in s_{12} ,

$$\begin{aligned} \frac{\partial I(s_{12}, s_{23}, m_a^2, m_b^2)}{\partial s_{12}} = & + \frac{(3d-10)(3d-8)SS(s_{23})}{2(d-4)s_{12}\Phi} \\ & + \frac{(3d-10)s_{23}F_1(m_a^2, m_b^2, s_{12})}{2s_{12}\Phi} \\ & + \frac{(d-4)m_a^2m_b^2F_2(m_a^2, m_b^2, s_{12})}{2(d-3)s_{12}\Phi} \\ & + \frac{((d-6)\Phi + (d-4)s_{12}s_{23})I(s_{12}, s_{23}, m_a^2, m_b^2)}{2s_{12}\Phi}, \end{aligned} \quad (3.53)$$

where

$$\begin{aligned} \Phi &= m_a^2s_{23} + m_b^2s_{23} - s_{12}s_{23} - s_{23}^2 - m_a^2 - m_b^2 \\ &= s_{13}s_{23} - m_a^2m_b^2 \end{aligned} \quad (3.54)$$

and

$$\begin{aligned} s_{12} &= (p_1 + p_2)^2 = 2p_1 \cdot p_2 \\ s_{23} &= (p_2 + p_3)^2 = m_a^2 + 2p_2 \cdot p_3. \end{aligned} \quad (3.55)$$

The denominator term Φ is the typical mass scale for the adjacent mass box, analogous to Λ for the three off-shell leg vertex in Eq. (2.46). As a four-scale integral, thus three ratios of scales, it is likely that to solve this integral it will be necessary to introduce three dimensional Harmonic Polylogarithms. In this case however, the differential equations contain Φ as opposed to Φ^2 , so we expect the three-dimensional polylogarithms will be linear in the scale ratios, and not quadratic. The solutions will then be given in terms of three-, two- and one-dimensional Harmonic Polylogarithms. Had we used a linear basis in solving the vertex integrals, it is unclear how the integrations involved in the box-integral differential equations would pro-

ceed, due to the transformation of variables $x \rightarrow \lambda - 2t$. The differential equations here remain unsolved due to the lack of a definition for the three-dimensional Harmonic Polylogarithms, and the difficulty of finding the boundary conditions for each integral required.

3.5 Summary

In this section, we have provided series expansions in the dimensional regularisation parameter ϵ for all two-loop Master Integrals with three external off-shell legs and all internal lines being massless. The results are presented in terms of an extended basis of 2-dimensional harmonic polylogarithms. The novel feature is that this basis includes quadratic forms. These match on to the allowed phase space boundary for the $1 \rightarrow 2$ decay. For each Master Integral, we have given sufficient terms in the ϵ -expansion to describe two-loop vertex corrections for physical processes.

The MI presented here are ingredients for a variety of interesting two-loop processes such as the QCD corrections to $H \rightarrow V^*V^*$ decay in the heavy top quark limit and the QCD corrections to the fully off-shell triple gluon (and quark-gluon) vertices.

The MI also form a staging post for the study of massless two-loop $2 \rightarrow 2$ scattering amplitudes with two off-shell legs. These processes include the NNLO QCD corrections to $q\bar{q} \rightarrow V^*V^*$ (where $V = W, Z$) and the NLO corrections to $gg \rightarrow V^*V^*$. Altogether there are 11 planar box and 3 non-planar box master topologies which remain to be studied.

Chapter 4

The MHV Construction

In this section we introduce the ‘MHV rules’ approach as proposed in Ref. [75]. This approach establishes a powerful framework for the calculation of tree-level and one-loop scattering amplitudes in gauge theories, in a compact form, and without appealing to Feynman diagrams. Here we shall concentrate on the method for calculating tree-level amplitudes, which we will then adapt in the next chapter to calculate tree-level multi-parton collinear limits.

4.1 Introduction

Witten’s proposal [76] of a weak-weak coupling duality between a perturbative $\mathcal{N} = 4$ gauge theory and a topological string theory in twistor space has inspired the ‘MHV-rules’ approach of Cachazo, Svrcek and Witten [75]. For a long time [77] it has been noted that the structure of helicity amplitudes is much simpler than would be expected from their Feynman-rule construction. In particular, tree-level gluon amplitudes with just two negative helicity gluons (known as maximal helicity violating or MHV amplitudes) have a particularly simple form, as noted by Parke

and Taylor ¹ [78, 79]. Written in terms of spinor inner products [80], they are composed entirely of the holomorphic products $\langle ij \rangle$, rather than their anti-holomorphic partners $[ij]$,

$$A_n(1^+, \dots, p^-, \dots, q^-, \dots, n^+) = \frac{\langle pq \rangle^4}{\langle 12 \rangle \langle 23 \rangle \dots \langle n-1, n \rangle \langle n1 \rangle}, \quad (4.1)$$

where we introduce the common notation $\langle p_i p_j \rangle = \langle ij \rangle$ and $[p_i p_j] = [ij]$. Helicity amplitudes with less than two negative (or positive) helicity legs are zero, and again this is not obvious from their Feynman diagram construction. The simple structure of helicity amplitudes in terms of spinor products is indicative that the Feynman rules are not the best description for helicity processes. Instead we look for a corresponding set of rules to build up amplitudes from vertices and propagators using spinor products. These are the MHV-rules.

The MHV rules can be motivated by considering MHV amplitudes in a twistor space. Performing a Fourier transformation of the MHV amplitude into twistor space, the external gluons are each associated with a point P_i in the projective twistor space [81], and all of these points lie on a (straight) line in (real) complex twistor space. It is known [82] that a point in Minkowski space, and therefore an interaction vertex, also corresponds to a line in twistor space, and so we can see that there is a correspondence between MHV amplitudes and interaction vertices in the twistor space picture.

Due to this correspondence, the basic building blocks of the MHV rules approach are the colour-ordered n -point vertices which are the off-shell continuations of the MHV scattering amplitudes. By connecting these vertices with scalar propagators, amplitudes involving more negative helicity gluons can be constructed. The scalar propagators must connect an off-shell positive helicity leg from one vertex, with an

¹The MHV amplitudes are thus sometimes referred to as ‘PT’ or ‘Parke-Taylor’ amplitudes.



off-shell negative helicity leg from another vertex, and so the number of vertices required scales with only the number of negative helicity legs for the amplitude. This is in stark contrast to the Feynman rules of section 1.2, where the vertices can only be three or four point vertices, and so the number of vertices required scales as the total number of particles in the amplitude. The use of the MHV-rules to construct helicity amplitudes has been proved through the use of recursion relations by Risager [83].

It is possible to perform a parity transformation on the MHV amplitudes, such that they have only 2 positive helicity legs and $n - 2$ negative helicity legs. These amplitudes are known as $\overline{\text{MHV}}$ amplitudes, and the MHV rules approach allows us to connect $\overline{\text{MHV}}$ vertices by scalar propagators.

The MHV rules are postulated for $\mathcal{N} = 4$ supersymmetric theories, so the question arises as to how we can use them in non-supersymmetric QCD calculations? At tree-level, QCD gluonic amplitudes will be identical to the $\mathcal{N} = 4$ amplitudes, due to the absence of propagating fermions at tree-level. The fermions in the theory may as well be gluinos and it would make no difference to the final amplitude. Therefore tree-level gluonic amplitudes are the same in both QCD and supersymmetric Yang-Mills theories, and so we can use the MHV approach for purely gluonic QCD processes. Tree-level QCD amplitudes with quarks are not supersymmetric, however the MHV-rules approach uses colour stripped amplitudes, and with no colour information massless quarks and gluinos are indistinguishable. This means that the colour stripped amplitudes are effectively supersymmetric, and so again we can use the MHV approach to calculate the QCD partial amplitudes involving massless quarks at tree-level.

The MHV rules for gluons [75] have been extended to amplitudes with fermions [84] using MHV - like basic vertices involving two negative helicity particles but allowing

for up to two fermion pairs in the vertex. Vertices with more than two fermion pairs are not allowed as MHV amplitudes must have precisely two particles with negative helicity, and fermions always come in pairs with opposite helicity. New compact results for tree-level gauge-theory results for non-MHV amplitudes involving arbitrary numbers of gluons [85–87], and fermions [84, 88–90] have been derived. The MHV rules have been applied to processes involving external Higgs bosons [91, 92], electroweak bosons [93], and more recently to QED processes [94]. The MHV rules for tree amplitudes have further been recast in the form of recursive relations [87, 92, 93] which facilitate calculations of higher order non-MHV amplitudes in terms of the known lower-order results. In many cases new classes of tree amplitudes were derived, and in all cases, numerical agreement with previously known amplitudes has been found.

MHV rules have also been shown to work at one-loop level for supersymmetric theories [95]. Building on the earlier work of Bern, Dixon, Dunbar and Kosower [96, 97], there has been a remarkable progress in computing cut-constructible multi-leg loop amplitudes in $\mathcal{N} = 4$ [95, 98–106] and $\mathcal{N} = 1$ [107–111] supersymmetric gauge theories. Encouraging progress has also been made using MHV rules for non-supersymmetric loop amplitudes [112, 113], and recently [114] the one-loop amplitude with 5 positive helicity particles in non-supersymmetric pure yang mills has been calculated in $d = 4 - 2\epsilon$.

A second formalism has been developed to evaluate helicity amplitudes, the BCF recursion relations [115, 116] of Britto, Cachazo, Feng and Witten. This method arose from the observation that the expressions obtained for the infrared singular parts of $\mathcal{N} = 4$ one-loop amplitudes (which are known to be proportional to tree-level results) were found to produce even more compact expressions for gluonic tree amplitudes [106, 117], as well as extremely compact six-parton amplitudes [115, 118,

119]. The BCF method has recently been proved based on the analytic structure and asymptotic behaviour of the known MHV amplitudes [120]. These tree-level BCF recursion relations for massless particles have recently been generalised in three ways. In Refs. [121, 122] a new version of recursion relations was adopted to calculate all finite one-loop amplitudes in non-supersymmetric QCD. At the same time, Ref. [123] generalised BCF recursion relations to include massive particles at tree level, and Ref. [124] provides recursion relations for d -dimensional scalars and fermions. The use of recursion relations has also been applied to the calculation of tree-level amplitudes for the scattering of gravitons [125, 126].

A comprehensive list of references and a more detailed discussion of recent developments can be found in the recent review [81].

4.2 Colour-ordered amplitudes

Tree-level multi-particle amplitudes can be decomposed into colour-ordered partial amplitudes. This reduces the number of diagrams that we need to calculate for a particular process.

For gluons only, the colour decomposition is given by

$$\mathcal{A}_n(\{p_i, \lambda_i, a_i\}) = ig^{n-2} \sum_{\sigma \in S_n/Z_n} \text{Tr}(T^{a_{\sigma(1)}} \dots T^{a_{\sigma(n)}}) A_n(\sigma(1^{\lambda_1}, \dots, n^{\lambda_n})). \quad (4.2)$$

Here S_n/Z_n is the group of non-cyclic permutations on n symbols, and j^{λ_j} labels the momentum p_j and helicity λ_j of the j^{th} gluon, which carries the adjoint representation index a_i . The T^{a_i} are fundamental representation $SU(N_c)$ colour matrices, normalized so that $\text{Tr}(T^a T^b) = \delta^{ab}$. The strong coupling constant is $\alpha_s = g^2/(4\pi)$. Note that the MHV rules method of Ref. [75] is used to evaluate only the purely

kinematic amplitudes A_n . Full amplitudes are then determined uniquely from the kinematic part A_n , and the known expressions for the colour traces.

For processes involving a quark-antiquark pair and an arbitrary number of gluons, the colour decomposition is given by

$$\begin{aligned} \mathcal{A}_n(\{p_i, \lambda_i, a_i\}, \{p_j, \lambda_j, i_j\}) & \quad (4.3) \\ &= ig^{n-2} \sum_{\sigma \in S_{n-2}} (T^{a_{\sigma(2)}} \dots T^{a_{\sigma(n-1)}})_{i_1 i_n} A_n(1_q^{\lambda_1}, \sigma(2^{\lambda_2}, \dots, (n-1)^{\lambda_{n-1}}), n_{\bar{q}}^{\lambda_n}), \end{aligned}$$

where S_{n-2} is the set of permutations of $(n-2)$ gluons and the fermions carry the fundamental colour labels i_1 and i_n . By current conservation, the quark and antiquark helicities are related such that $\lambda_1 = -\lambda_n \equiv \lambda$ where $\lambda = \pm \frac{1}{2}$.

When an additional photon with momentum P_γ is emitted, the amplitudes have the following form,

$$\begin{aligned} \mathcal{A}_n(\{p_i, \lambda_i, a_i\}, \{p_j, \lambda_j, i_j\}, P_\gamma) & \quad (4.4) \\ &= ieg^{n-2} \sum_{\sigma \in S_{n-2}} (T^{a_{\sigma(2)}} \dots T^{a_{\sigma(n-1)}})_{i_1 i_n} \tilde{A}_n(1_q^{\lambda_1}, \sigma(2^{\lambda_2}, \dots, (n-1)^{\lambda_{n-1}}), n_{\bar{q}}^{\lambda_n}; P_\gamma), \end{aligned}$$

where e is the electric charge of the quark.

When there are two quark-antiquark pairs the tree-level amplitude can be decom-

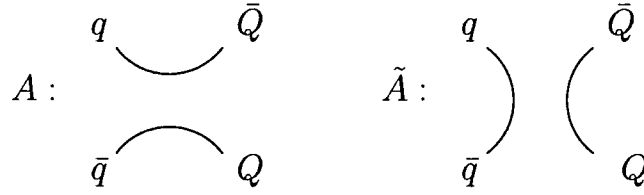


Figure 4.1: A figure showing the two different colour connections corresponding to the two amplitudes A_n and \tilde{A}_n in a four quark amplitude.

posed into colour ordered amplitudes as,

$$\begin{aligned}
\mathcal{A}_n(\{p_i, \lambda_i, a_i\}, \{p_j, \lambda_j, i_j\}) &= ig^{n-2} \sum_k^{n-4} \sum_{\sigma \in S_k} \sum_{\rho \in S_l} \left\{ \right. \\
&(T^{a_{\sigma(1)}} \dots T^{a_{\sigma(k)}})_{i_1 i_n} (T^{a_{\rho(1)}} \dots T^{a_{\rho(l)}})_{i_{s+1} i_s} \\
&\times A_n(1_q^\lambda, \sigma(1), \dots, \sigma(k), s_{\bar{Q}}^{-\lambda'}; (s+1)_{\bar{Q}}^{\lambda'}, \rho(1), \dots, \rho(l), n_{\bar{q}}^{-\lambda}) \\
- \frac{1}{N} &(T^{a_{\sigma(1)}} \dots T^{a_{\sigma(k)}})_{i_1 i_s} (T^{a_{\rho(1)}} \dots T^{a_{\rho(l)}})_{i_{s+1} i_n} \\
&\times \tilde{A}_n(1_q^\lambda, \sigma(1), \dots, \sigma(k), s_{\bar{q}}^{-\lambda}; (s+1)_{\bar{Q}}^{\lambda'}, \rho(1), \dots, \rho(l), n_{\bar{Q}}^{-\lambda'}) \left. \right\} \quad (4.5)
\end{aligned}$$

where S_k and S_l are permutation groups such that $k + l = n - 4$ and represent the possible ways of distributing the gluons in a colour ordered way between the quarks. For $i = j = 0$, $(T^{a_i} \dots T^{a_j})_{kl}$ reduces to δ_{kl} . We see that the two amplitudes A_n and \tilde{A}_n correspond to different ways of connecting the fundamental colour charges, as shown in Fig. 4.1. For the A amplitudes, there is a colour line connecting q and \bar{Q} and a second line connecting Q and \bar{q} , while for the QED-like \tilde{A} amplitudes the colour lines connect q to \bar{q} and Q to \bar{Q} . Any number of gluons may be radiated from each colour line. As before, by current conservation, the quark and antiquark helicities are related such that $\lambda_q = -\lambda_{\bar{q}} \equiv \lambda$ and $\lambda_Q = -\lambda_{\bar{Q}} \equiv \lambda'$ where $\lambda, \lambda' = \pm \frac{1}{2}$.

4.3 Spinor helicity formalism

In the spinor helicity formalism [78–80] an on-shell momentum of a massless particle, $p_\mu p^\mu = 0$, is represented as

$$p_{a\dot{a}} \equiv p_\mu \sigma_{a\dot{a}}^\mu = \lambda_a \tilde{\lambda}_{\dot{a}} , \quad (4.6)$$

where λ_a and $\tilde{\lambda}_{\dot{a}}$ are two commuting spinors of positive and negative chirality. Spinor inner products are defined by²

$$\langle \lambda, \lambda' \rangle = \epsilon_{ab} \lambda^a \lambda'^b , \quad [\tilde{\lambda}, \tilde{\lambda}'] = -\epsilon_{\dot{a}\dot{b}} \tilde{\lambda}^{\dot{a}} \tilde{\lambda}'^{\dot{b}} , \quad (4.7)$$

and a scalar product of two null vectors, $p_{a\dot{a}} = \lambda_a \tilde{\lambda}_{\dot{a}}$ and $q_{a\dot{a}} = \lambda'_a \tilde{\lambda}'_{\dot{a}}$, becomes

$$p_\mu q^\mu = -\frac{1}{2} \langle \lambda, \lambda' \rangle [\tilde{\lambda}, \tilde{\lambda}'] . \quad (4.8)$$

A list of spinor product identities is given in Appendix C.

The spinor representation is particularly useful because it accurately captures the collinear behaviour of QCD amplitudes, which involve square-roots of Lorentz invariants. Up to a phase factor, the spinor products themselves are square-roots of Lorentz invariants and so are an ideal means of expressing collinear limits in QCD, as we shall see in chapter 5.

The MHV rules of Ref. [75] were developed for calculating purely gluonic amplitudes at tree level. In this approach all non-MHV n -gluon amplitudes (including $\overline{\text{MHV}}$) are expressed as sums of tree diagrams in an effective scalar perturbation theory. The vertices in this theory are the MHV amplitudes of Eq. (4.1) continued off-shell as described below, and connected by scalar propagators $1/q^2$. The full amplitude

²Our conventions for spinor helicities follow [75, 76], except that $[ij] = -[ij]_{CSW}$ as in ref. [136].

is obtained by the sum of all possible combinations MHV vertices which have the required helicity structure for the process.

When one positive helicity leg of an MHV vertex is connected by a propagator to a negative helicity leg from another MHV vertex, both legs become internal to the diagram and have to be continued off-shell. Off-shell continuation is defined as follows [75]: we pick an arbitrary reference spinor $\eta^{\dot{a}}$ and define λ_a for any internal line carrying momentum $q_{a\dot{a}}$ by

$$\lambda_a = q_{a\dot{a}}\eta^{\dot{a}}. \quad (4.9)$$

External lines in a diagram remain on-shell, and for them λ is defined in the usual way. For the off-shell lines, the same reference spinor η is used in all diagrams contributing to a given amplitude.

4.4 MHV amplitudes

The colour ordered n -gluon MHV amplitude is given by

$$A_n(1^+, \dots, m_1^-, \dots, m_2^-, \dots, n^+) = \frac{\langle m_1 m_2 \rangle^4}{\prod_{i=1}^n \langle i i+1 \rangle}, \quad (4.10)$$

with all indices taken mod n . It can be shown that any amplitudes with less than two negative (or positive) helicity legs are zero.

$$A_n(1^\pm, 2^+, 3^+, \dots, n^+) = 0. \quad (4.11)$$

This is depicted in Fig. 4.2 where these states are shown as crossed circles to indicate their null value.

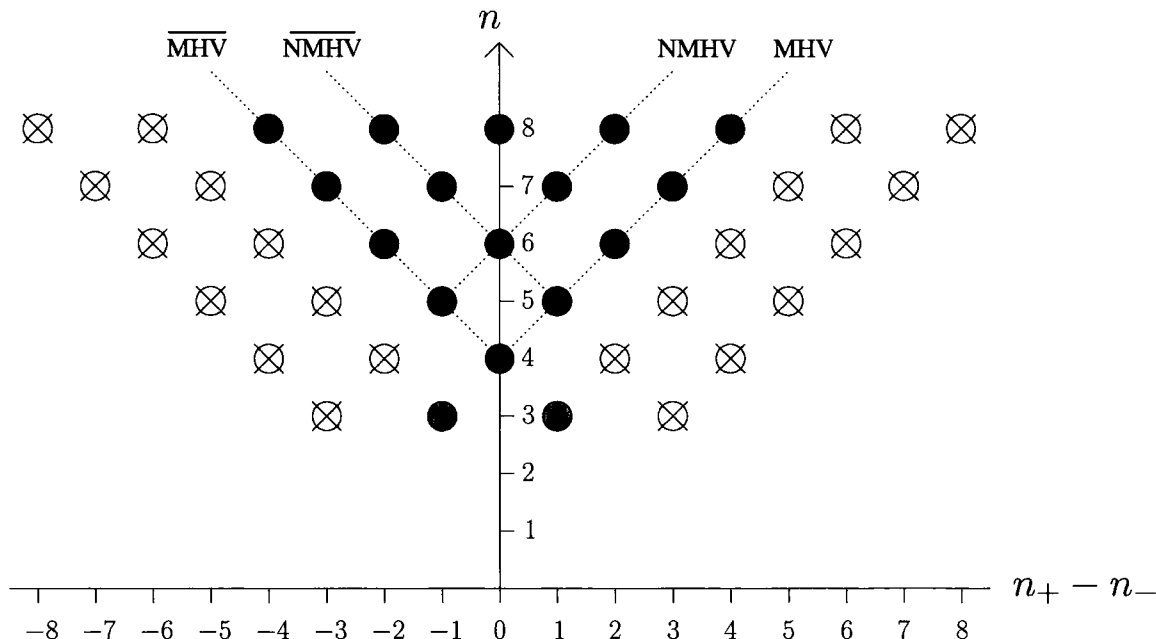


Figure 4.2: Pattern of available states (black dots) for helicity amplitudes showing the dependence on the difference between the number of positive and negative helicity particles involved. The crossed out states show the amplitudes that are zero. The red circles show the three point vertices.

MHV amplitudes involving fermions and gluons in $\mathcal{N} < 1$ theories exist only for one or two pairs of fermions [88]. This is because MHV amplitudes can have only two negative helicity particles, and fermions always come in pairs with opposite helicities, so we have at most two negative quarks and therefore at most four quarks overall. This means that we have the following vertices involving massless quarks:

The two-quark multi-gluon MHV amplitudes are,

$$A_n(1_q^\lambda, \dots, m^-, \dots, n_{\bar{q}}^{-\lambda}) = \frac{\langle m 1 \rangle^{2-2\lambda} \langle m n \rangle^{2+2\lambda}}{\prod_{l=1}^n \langle l l+1 \rangle}. \quad (4.12)$$

Here the helicity of the quark is denoted by $\lambda = \pm \frac{1}{2}$ while \dots denotes an arbitrary number of positive helicity gluons. Amplitudes for a quark-antiquark pair, many

gluons and a photon are given by,

$$\tilde{A}(1_q^\lambda, \dots, n_{\bar{q}}^{-\lambda}; P_\gamma^-) = \frac{\langle P 1 \rangle^{2-2\lambda} \langle P n \rangle^{2+2\lambda}}{\langle P 1 \rangle \langle 1 2 \rangle \cdots \langle n P \rangle}, \quad (4.13)$$

$$\tilde{A}(1_q^\lambda, \dots, m^-, \dots, n_{\bar{q}}^{-\lambda}; P_\gamma^+) = \frac{\langle m 1 \rangle^{2-2\lambda} \langle m n \rangle^{2+2\lambda}}{\langle P 1 \rangle \langle 1 2 \rangle \cdots \langle n P \rangle}. \quad (4.14)$$

In the four-quark case, there are four MHV amplitudes where two of the fermions have negative helicity and two have positive helicity for each colour structure. For each helicity configuration we can write,

$$A_n(1_q^+, \dots, s_{\bar{Q}}^-, (s+1)_Q^+, \dots, n_{\bar{q}}^-) = \frac{\langle 1 s \rangle \langle s n \rangle^2 \langle n s+1 \rangle}{\prod_{l=1}^n \langle ll+1 \rangle}, \quad (4.15)$$

$$A_n(1_q^+, \dots, s_{\bar{Q}}^+, (s+1)_{\bar{Q}}^-, \dots, n_{\bar{q}}^-) = \frac{\langle 1 s \rangle \langle n s+1 \rangle^3}{\prod_{l=1}^n \langle ll+1 \rangle}, \quad (4.16)$$

$$A_n(1_q^-, \dots, s_{\bar{Q}}^+, (s+1)_{\bar{Q}}^-, \dots, n_{\bar{q}}^+) = \frac{\langle 1 s \rangle \langle 1 s+1 \rangle^2 \langle n s+1 \rangle}{\prod_{l=1}^n \langle ll+1 \rangle}, \quad (4.17)$$

$$A_n(1_q^-, \dots, s_{\bar{Q}}^-, (s+1)_Q^+, \dots, n_{\bar{q}}^+) = \frac{\langle 1 s \rangle^3 \langle n s+1 \rangle}{\prod_{l=1}^n \langle ll+1 \rangle}, \quad (4.18)$$

with the other colour ordering given by,

$$\tilde{A}_n(1_q^+, \dots, s_{\bar{q}}^-, (s+1)_Q^+, \dots, n_{\bar{Q}}^-) = \frac{\langle 1 n \rangle \langle n s \rangle^2 \langle s s+1 \rangle}{\prod_{l=1}^n \langle ll+1 \rangle}, \quad (4.19)$$

$$\tilde{A}_n(1_q^+, \dots, s_{\bar{q}}^-, (s+1)_{\bar{Q}}^-, \dots, n_{\bar{Q}}^+) = \frac{\langle 1 n \rangle \langle s s+1 \rangle^3}{\prod_{l=1}^n \langle ll+1 \rangle}, \quad (4.20)$$

$$\tilde{A}_n(1_q^-, \dots, s_{\bar{q}}^+, (s+1)_{\bar{Q}}^-, \dots, n_{\bar{Q}}^+) = \frac{\langle 1 n \rangle \langle 1 s+1 \rangle^2 \langle s s+1 \rangle}{\prod_{l=1}^n \langle ll+1 \rangle}, \quad (4.21)$$

$$\tilde{A}_n(1_q^-, \dots, s_{\bar{q}}^+, (s+1)_Q^+, \dots, n_{\bar{Q}}^-) = \frac{\langle 1 n \rangle^3 \langle s s+1 \rangle}{\prod_{l=1}^n \langle ll+1 \rangle}. \quad (4.22)$$

The $\overline{\text{MHV}}$ amplitudes are related by parity and can be obtained by conjugating the MHV expressions,

$$A_n(1^{\lambda_1}, \dots, n^{\lambda_n}) = (-1)^n (A_n(1^{-\lambda_1}, \dots, n^{-\lambda_n}))^*, \quad (4.23)$$

and similarly for the \tilde{A} amplitudes.

4.5 The MHV-rules

The MHV-rules use the MHV amplitudes as given in section 4.4 as scalar vertices. Connecting these vertices via scalar propagators we can construct amplitudes involving more than two negative helicity particles. In the twistor space picture the connection of two MHV vertices can be pictured as the intersection of the two-lines which represent those vertices in twistor space.

An amplitude constructed by the connection of two MHV amplitudes is denoted a next-to-MHV amplitude, or NMHV amplitude. Similarly an amplitude which connects three MHV vertices is known as NNMHV, and so on. These higher order MHV diagrams are formed from the connection of v vertices by $v - 1$ propagators. Each propagator must join a negative helicity leg to a positive helicity leg, and so from our initial $2v$ negative legs we are left with $v + 1$ negative helicity external particles. Therefore to construct an amplitude we must sum all graphs with v connected vertices such that $v + 1$ is the required number of external negative helicity particles. In doing so we must only consider diagrams with the required colour ordering. The number of negative helicity particles is fixed at each vertex, but the positive helicity particles can be distributed over all of the available vertices, as long as they maintain the correct colour ordering.

The dependence of a given amplitude on the order of MHV diagram required is pictured in Fig. 4.2. All of the amplitudes with an identical number of negative helicity particles lie along the same diagonal line in this state-space. Each of these lines represents a different order in the MHV hierarchy, as the number of vertices required to evaluate them increases as we move towards the top-left of the diagram.

If we work in the $\overline{\text{MHV}}$ scheme the amplitudes get more complicated towards the top right of this diagram, and so for amplitudes with more negative particles it is easier to use the $\overline{\text{MHV}}$ scheme than the MHV scheme. However, we can see that the state space is symmetric under the parity transformation, and thus a time saving method to evaluate the mostly-negative amplitudes from the left hand side of the diagram, is to perform the parity operation $\langle ij \rangle \leftrightarrow -[ij]$ on the equivalent amplitude from the right hand side of the diagram, i.e the amplitude with opposite helicities. Thus to find all of the amplitudes for a given number of particles (i.e. across a horizontal line in figure 4.2, we need only evaluate the amplitudes with mostly positive helicities, or equal numbers of positive and negative helicities.

To construct amplitudes we will need to use the 3-point vertices given by

$$A_3(1^-, 2^-, 3^+) = \frac{\langle 12 \rangle^4}{\langle 12 \rangle \langle 23 \rangle \langle 31 \rangle} \quad (4.24)$$

These vertices are zero if all of the legs are on-shell. However when one of the legs is continued off-shell the vertex exists and we can use it to construct NMHV amplitudes. This is shown in figure 4.2 where the vertices are given by red dots.

As an example we consider the first example of Witten [75], the construction of the purely gluonic amplitude $A(1^+, 2^-, 3^-, 4^-)$, which vanishes in Yang-Mills theory. The two diagrams which contribute are shown in figure 4.3. To connect the vertices by propagators we use the off-shell continuation given by equation 4.9. In this way the first diagram gives

$$\frac{\langle 2\lambda \rangle^4}{\langle 12 \rangle \langle 2\lambda \rangle \langle \lambda 1 \rangle} \frac{1}{p^2} \frac{\langle 34 \rangle^4}{\langle 34 \rangle \langle 4\lambda \rangle \langle \lambda 3 \rangle} \quad (4.25)$$

where the internal momentum $p = p_1 + p_2 = -p_3 - p_4$ and λ is defined via the off-shell continuation to be $\lambda_a = p_{a\dot{a}}\eta^{\dot{a}}$, where η is a reference momentum.

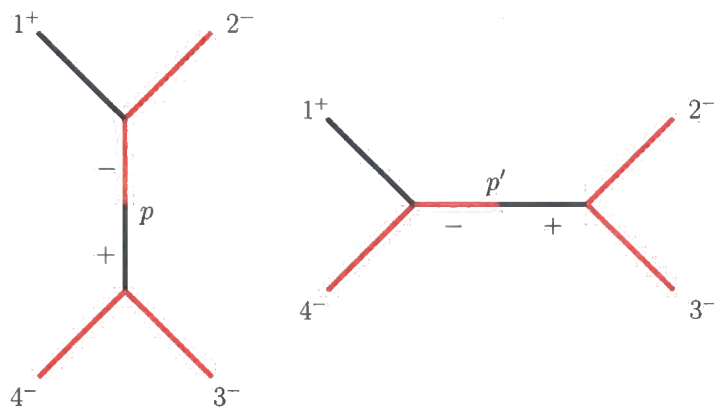


Figure 4.3: The two NMHV diagrams necessary for the construction of the $A(1^+, 2^-, 3^-, 4^-)$ amplitude. For clarity the negative helicity legs are shown in red, and positive helicity legs are shown in black.

The second diagram is given by

$$\frac{\langle \lambda' 4 \rangle^4}{\langle 1 \lambda' \rangle \langle \lambda' 4 \rangle \langle 4 1 \rangle} \frac{1}{p'^2} \frac{\langle 2 3 \rangle^4}{\langle 2 3 \rangle \langle 3 \lambda' \rangle \langle \lambda' 2 \rangle} \quad (4.26)$$

where the internal momentum $p' = p_1 + p_4 = -p_2 - p_3$ and $\lambda'_a = p'_{a\dot{a}} \eta^{\dot{a}}$, where η is a reference momentum.

Utilising the properties of the spinors as given in appendix C, we have for example,

$$\begin{aligned} \langle 2 \lambda \rangle &= \langle 2 (1 + 2) \eta \rangle = \langle 2 1 \rangle [1 \eta] \\ \langle 1 \lambda' \rangle &= \langle 1 (1 + 4) \eta \rangle = \langle 1 4 \rangle [4 \eta] \end{aligned}$$

We also have the useful relation

$$(p_i + p_j)^2 = 2p_i \cdot p_j = \langle i j \rangle [j i] \quad (4.27)$$

which we can use to express the scalar propagators in terms of spinor products. Utilising these identities for all spinor products involving the off-shell continued

legs, the sum of these two diagrams gives

$$\frac{[1\eta]^3}{[2\eta][3\eta][4\eta]} \left(\frac{\langle 34 \rangle}{[21]} + \frac{\langle 32 \rangle}{[41]} \right) = 0. \quad (4.28)$$

This is zero as required due to momentum conservation, see Eq. C.1, since $\langle 32 \rangle [21] + \langle 34 \rangle [41] = \sum_{i=1}^4 \langle 3i \rangle [i1] = 0$.

In the same way we can draw all the diagrams necessary for more complicated diagrams and perform their sum. However the beauty of the MHV method is that it allows us to find amplitudes for an arbitrary number of positive helicity particles given a set number of negative helicity particles (or vice versa in the $\overline{\text{MHV}}$ approach). To see this we use the above example but consider the amplitude with an arbitrary number of additional positive helicity particles, to give us the amplitude $A_n(1^+, 2^-, 3^-, 4^-, 5^+, \dots, n^+)$. The colour ordering must be maintained so the extra positive helicity gluons have to come after the 4^- gluon. However in the first diagram in figure 4.3 we could add them onto either vertex. This will give us diagrams of the form given in figure 4.4, where we have to sum the first diagram over all distributions of the positive helicity particles across the two vertices. We choose the lower limit of this sum to be the negative leg $i = 4$ as this enables us to easily identify the lower limit of the sum, and to recover the previous example when $i = n = 4$. Therefore the contribution to the amplitude from the first diagram is given by

$$\sum_{i=4}^n \frac{\langle 2\lambda \rangle^4}{\langle 12 \rangle \langle 2\lambda \rangle \langle \lambda i + 1 \rangle \langle i + 1 i + 2 \rangle \dots \langle n1 \rangle} \frac{1}{p^2} \frac{\langle 34 \rangle^4}{\langle 34 \rangle \langle 45 \rangle \dots \langle i - 1 i \rangle \langle i \lambda \rangle \langle \lambda 3 \rangle} \quad (4.29)$$

and the contribution from the second diagram is

$$\frac{\langle \lambda' 4 \rangle^4}{\langle 1 \lambda' \rangle \langle \lambda' 4 \rangle \langle 45 \rangle \dots \langle n - 1 n \rangle \langle n1 \rangle} \frac{1}{p'^2} \frac{\langle 23 \rangle^4}{\langle 23 \rangle \langle 3 \lambda' \rangle \langle \lambda' 2 \rangle} \quad (4.30)$$

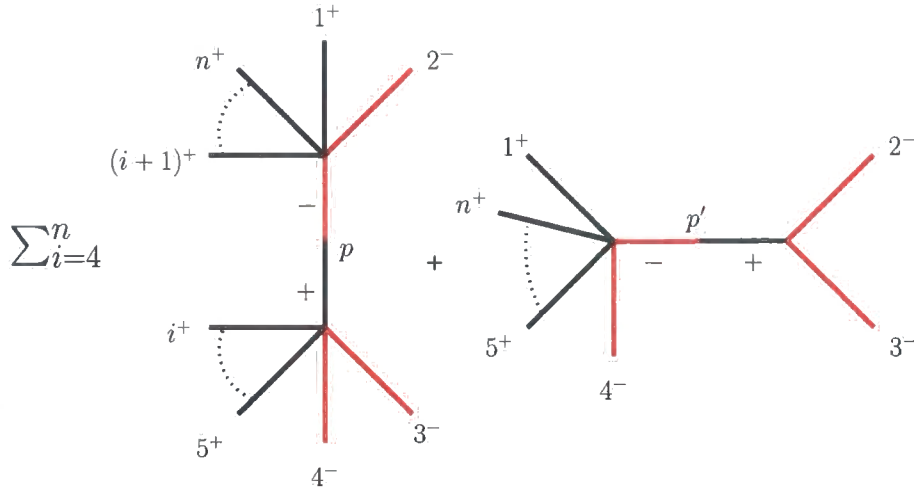


Figure 4.4: The NMHV diagrams necessary for the construction of the $A_n(1^+, 2^-, 3^-, 4^-, 5^+, \dots, n^+)$ amplitude. The negative helicity legs are shown in red, and positive helicity legs are shown in black. The dotted lines between legs indicate a number of positive helicity. The first diagram is summed over the possible distributions of the positive helicity legs between the two vertices.

This method of distributing positive helicity particles across vertices and taking the sum can be applied to more complicated diagrams, to give us general expressions for n point amplitudes with a given number of negative helicity particles. To find the set of amplitudes A_n , all we have to do is draw the basic “skeleton” diagrams consisting only of the propagators and the negative helicity legs which can contribute to the process. We then sum over all the distributions of positive helicity legs across the vertices which maintain the colour ordering.

So to find all of the amplitudes with three negative helicity legs in any given position,³ $A_n(1^+, \dots, m_1^-, \dots, m_2^-, \dots, m_3^-, \dots, n^+)$, we use the skeleton diagrams as given in figure 4.5 and sum over the positive legs distributions. These skeleton diagrams are also called topologies. We can express our results in a simple form if we

³Here the negative helicity particles m_j could take the positions 1^- and / or n^- . We express the amplitude as containing 1^+ and n^+ only to indicate that all other particles in the amplitude have positive helicity.

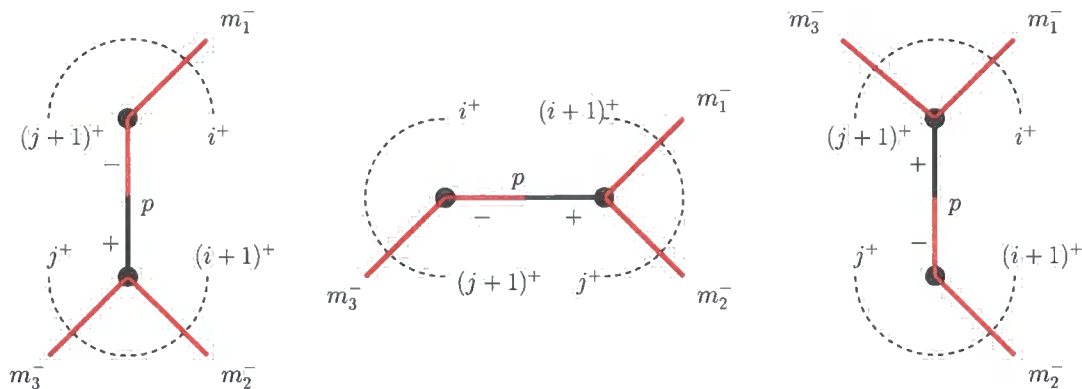


Figure 4.5: The NMHV skeleton diagrams necessary for the construction of the $A_n(1^+, \dots, m_1^-, \dots, m_2^-, \dots, m_3^-, \dots, n^+)$ amplitude. Black dots indicate vertices. The dotted semicircles indicate positive helicity particles emitted at each vertex, with the labels indicating the bounding positive lines at each vertex.

factor out the cyclic product

$$\frac{1}{\prod_{l=1}^n \langle ll+1 \rangle} = \frac{1}{\langle 12 \rangle \langle 23 \rangle \dots \langle n-1 n \rangle \langle n1 \rangle} \quad (4.31)$$

This factor accounts for the spinor products of all adjacent legs in the denominator of MHV diagrams. However the spinor products of adjacent legs separated by a propagator are not present, and so we must multiply our expression by these factors, which for the diagrams in figure 4.5 will be the factor $\langle ii+1 \rangle \langle jj+1 \rangle$. The contribution of the first diagram in figure 4.5 is then

$$\frac{1}{\prod_{l=1}^n \langle ll+1 \rangle} \left(\sum_{i=m_1}^{m_2-1} \sum_{j=m_3}^{m_1-1} \frac{\langle m_1^- | q_{i+1,j} | \eta^- \rangle^4}{\langle i^- | \not{q} | \eta^- \rangle \langle j+1^- | \not{q} | \eta^- \rangle} \cdot \frac{\langle i, i+1 \rangle \langle j, j+1 \rangle}{q_{i+1,j}^2} \times \frac{\langle m_2 m_3 \rangle^4}{\langle i+1^- | \not{q} | \eta^- \rangle \langle j^- | \not{q} | \eta^- \rangle} \right). \quad (4.32)$$

We can see from this that another common factor in the denominator of each diagram will be the spinor products between the off-shell continued legs and the legs adjacent to the propagator, along with the scalar propagator itself. With this in mind we

define the effective propagator

$$D(i, j, q_{i+1, j}) = q^2 \frac{\langle i^- | \not{q} | \eta^- \rangle \langle i+1^- | \not{q} | \eta^- \rangle \langle j^- | \not{q} | \eta^- \rangle \langle j+1^- | \not{q} | \eta^- \rangle}{\langle i, i+1 \rangle \langle j, j+1 \rangle} \quad (4.33)$$

where we have introduced the standard Lorentz invariant matrix element

$$\langle i^- | \not{p}_j | k^- \rangle = \langle i j \rangle [j k] \quad (4.34)$$

and $q_{i+1, j} = (p_{i+1} + \dots + p_j)$ is the propagators momentum. This effective propagator accounts for all the spinor products associated with the propagator. Having factored out the product given by Equation 4.31, the only spinor products remaining to give the expression for the diagram are those numerator terms involving the negative helicity particles (including the propagator when it is a continued negative helicity leg). These are simple to write down, and so the final amplitude is given as the sum of skeleton diagrams, where each skeleton is given by the simple negative helicity numerator terms, over the effective propagator and summed over the distributions of positive helicity particles, all multiplied by the overall factor as given in equation 4.31. In this way we can quickly give the expressions for the skeleton diagrams as given in Figure 4.5.

$$\begin{aligned} A_n(m_1^-, m_2^-, m_3^-) = \frac{1}{\prod_{l=1}^n \langle l l+1 \rangle} & \left(\sum_{i=m_1}^{m_2-1} \sum_{j=m_3}^{m_1-1} \frac{\langle m_1^- | q_{i+1, j} | \eta^- \rangle^4 \langle m_2 m_3 \rangle^4}{D(i, j, q_{i+1, j})} \right. \\ & + \sum_{i=m_3}^{m_1-1} \sum_{j=m_2}^{m_3-1} \frac{\langle m_1 m_2 \rangle^4 \langle m_3^- | q_{i+1, j} | \eta^- \rangle^4}{D(i, j, q_{i+1, j})} \\ & \left. + \sum_{i=m_1}^{m_2-1} \sum_{j=m_2}^{m_3-1} \frac{\langle m_1 m_3 \rangle^4 \langle m_2^- | q_{i+1, j} | \eta^- \rangle^4}{D(i, j, q_{i+1, j})} \right) \end{aligned} \quad (4.35)$$

where $A_n(m_1^-, m_2^-, m_3^-) = A_n(1^+, \dots, m_1^-, \dots, m_2^-, \dots, m_3^-, \dots, n^+)$, and all sum-

mations are taken to be cyclic.

Amplitudes involving quarks are constructed in a similar way to those for gluons. The two- and four-quark MHV amplitudes, as given in section 4.4, are used as vertices alongside the purely gluonic MHV amplitude. Quark or anti-quark lines can form connecting propagators as long as they connect opposite helicity quark or anti-quark states. Quark lines cannot connect to gluonic lines due to colour and spin conservation. In constructing the quark amplitudes we also have to evaluate both colour orderings from the decomposition into colour ordered amplitudes (sect. 4.2), and in doing so we must use the correct vertices corresponding to each colour ordering.

4.6 BCF recursion relations

The second formalism for the evaluation of helicity amplitudes is the use of recursion relations [115, 116] developed by Britto, Cachazo, Feng and Witten. This method constructs tree amplitudes as the connection of two completely on-shell amplitudes by a scalar propagator. This is in contrast to the MHV-rules method which relies on the connected amplitudes having off-shell continued legs. The use of recursion relations then enables amplitudes with higher numbers of legs to be built from amplitudes with lower numbers of legs, so that previous results can be used to find more complicated amplitudes. Ultimately, all amplitudes can be constructed from three gluon vertices. The resulting amplitudes tend to have a simpler form than those derived from the recursion relations of Berends and Giele [79]. The BCF method has recently been proved based on the analytic structure and asymptotic behaviour of the known MHV amplitudes [120]. Here we introduce the BCF recursion relations to complete the introduction to the recently developed methods for tree-level

calculations using MHV type amplitudes. In the following chapter we will use these relations to compare and contrast the collinear limits derived using the MHV-rules approach with those from the BCF relations.

This method arose from the computation of $\mathcal{N} = 4$ one-loop amplitudes. When expanded in terms of scalar box functions, the coefficients are found to be products of tree-level amplitudes. This led to the proposition of the recursion relation given schematically by

$$A_n = \sum_{i=1}^{n-3} \sum_{h=\pm} A_{i+2}^h \frac{1}{P_{n,i}^2} A_{n-i}^{-h} \quad (4.36)$$

where A_n denotes an n -point tree-level gluonic amplitude, and $P_{n,i} = p_n + p_1 + \dots + p_i$, where p_k is the momentum of the k -th gluon. The index h represents the helicity of the particle propagating between the two amplitudes, hence the opposite sign on each of the sub-amplitudes. However in this case, both of the sub-amplitudes remain on-shell, and preserve momentum conservation.

In the following we will use the notation

$$\langle i | \sum_j p_j | k \rangle = \sum_j \langle i j \rangle [j k]. \quad (4.37)$$

To use the recursion relations we must then mark two gluons whose momenta will undergo a complex shift such that the sub-amplitudes in the recursion relations remain on-shell. We choose to label the gluons such that the $(n-1)$ -th gluon has negative helicity and the n -th gluon is positive. These will be the marked gluons which we will denote by hatted momenta. The full recursion relation is then given

by

$$A_n(1, 2, \dots, (n-1)^-, n^+) = \sum_{i=1}^{n-3} \sum_{h=\pm} A_{i+2}(\widehat{n}, 1, 2, \dots, i, -\widehat{P}_{n,i}^h) \frac{1}{P_{n,i}^2} A_{n-i}(+\widehat{P}_{n,i}^{-h}, i+1, \dots, n-2, \widehat{n-1}) \quad (4.38)$$

where

$$\begin{aligned} P_{n,i} &= p_n + p_1 + \dots + p_i, \\ \widehat{P}_{n,i} &= P_{n,i} + \frac{P_{n,i}^2}{\langle n-1|P_{n,i}|n\rangle} \lambda_{n-1} \widetilde{\lambda}_n, \\ \widehat{p}_{n-1} &= p_{n-1} - \frac{P_{n,i}^2}{\langle n-1|P_{n,i}|n\rangle} \lambda_{n-1} \widetilde{\lambda}_n, \\ \widehat{p}_n &= p_n + \frac{P_{n,i}^2}{\langle n-1|P_{n,i}|n\rangle} \lambda_{n-1} \widetilde{\lambda}_n. \end{aligned} \quad (4.39)$$

In practice the following identities are used to compute spinor products involving the marked gluons with any other spinor denoted by \bullet ,

$$\begin{aligned} \langle \bullet \widehat{P}_{n,i} \rangle &= -\langle \bullet | P_{n,i} | n \rangle \times \frac{1}{w}, \\ [\widehat{P}_{n,i} \bullet] &= -\langle n-1 | P_{n,i} | \bullet \rangle \times \frac{1}{\bar{w}}, \\ w\bar{w} &= \langle n-1 | P_{n,i} | n \rangle, \end{aligned} \quad (4.40)$$

where $w = [\widehat{P}_{n,i} n]$ and $\bar{w} = \langle n-1 \widehat{P}_{n,i} \rangle$. These factors only ever appear in the invariant combination $w\bar{w}$ as given above.

4.6.1 An example: $A(1^-, 2^+, 3^+, 4^+, 5^-, 6^-)$.

As an example of the use of the BCF recursion relations we evaluate the six-point amplitude $A(1^-, 2^+, 3^+, 4^+, 5^-, 6^-)$. In section 5.5.1 we shall use this result to test

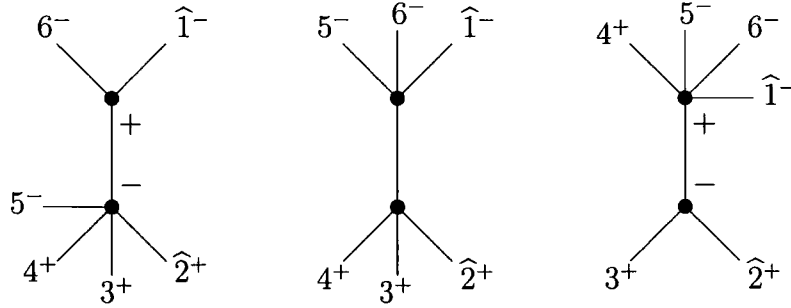


Figure 4.6: The BCF configurations contributing to $A(1^-, 2^+, 3^+, 4^+, 5^-, 6^-)$. Note that the second diagram vanishes for either helicity configuration of the propagator.

the collinear limits we derive via the MHV approach. For this reason we choose the ‘marked’ gluons to be the $\hat{1}^-$ and $\hat{2}^+$ gluons. Note that we have shifted the labels from those used in Eqn. 4.38. The available BCF configurations for this amplitude are shown in Fig. 4.6. The second diagram vanishes for either helicity configuration of the internal line, hence there are only two BCF diagrams which contribute to the full amplitude.

The first diagram in Fig. 4.6 is given by

$$\frac{\langle 61 \rangle^3}{\langle \hat{1} \hat{P} \rangle \langle \hat{P} 6 \rangle} \cdot \frac{1}{s_{2,5}} \cdot \frac{\langle 5 \hat{P} \rangle^3}{\langle \hat{P} \hat{2} \rangle \langle \hat{2} 3 \rangle \langle 3 4 \rangle \langle 4 5 \rangle}. \quad (4.41)$$

This can be simplified using 4.39 and 4.40 to give

$$\frac{\langle 5|6+1|2 \rangle^3}{\langle 3|1+2|6 \rangle \langle 6|1 \rangle \langle 1|2 \rangle \langle 3 4 \rangle \langle 4 5 \rangle s_{3,5}}. \quad (4.42)$$

Note that the pole in the kinematic invariants has changed due to the complex shift of the marked gluons momentum. This will have interesting effects on the use of the BCF results to calculate collinear limits in the following chapter.

The third diagram can be obtained from the first by performing a helicity conjuga-

tion and relabelling the momenta $i \rightarrow 3 - i$. The full amplitude then reads

$$A(1^-, 2^+, 3^+, 4^+, 5^-, 6^-) = \frac{1}{\langle 3|1+2|6\rangle} \left(\frac{\langle 5|6+1|2\rangle^3}{[6\ 1][1\ 2]\langle 3\ 4\rangle\langle 4\ 5\rangle s_{3,5}} + \frac{\langle 1|2+3|4\rangle^3}{[4\ 5][5\ 6]\langle 1\ 2\rangle\langle 2\ 3\rangle s_{1,3}} \right). \quad (4.43)$$

In the following chapter we shall use this result and others from the literature to check collinear limits derived using the MHV rules approach, and to provide a comparison of the structure of results from MHV-rules and BCF recursion relations.

4.7 Summary

In this chapter we have introduced the MHV rules approach of Cachazo, Svrcek and Witten. This approach arose from Witten's observation of a weak-weak coupling duality between $\mathcal{N} = 4$ gauge theory and a string theory in Twistor space. Here we have introduced the recent developments in this theory, and their use in constructing tree-level gauge amplitudes. This construction relies on the use of colour ordered amplitudes which we have introduced in section 4.2, and we have given the colour decomposition of amplitudes involving up to four quarks. We have then introduced the spinor helicity formalism in which the basic MHV amplitudes are expressed. We have then provided the n -gluon MHV amplitudes with up to four quarks. These amplitudes are the vertices used in the MHV rules approach, which we have then outlined with some simple examples to show their use in the construction of amplitudes with arbitrary numbers of positive helicity gluons. An alternative method to the MHV-rules approach are BCF recursion relations, which we have introduced here for completeness. In the next chapter we will make use of the MHV-rules approach to provide a method which enables us to quickly derive multi-parton collinear

limits. We will then use the BCF recursion relations as a basic test of our approach, and at the same time this will provide an interesting examination of the differences between the two methods.

Chapter 5

Collinear limits

In this chapter we will consider the multi-parton collinear limits of QCD at tree-level. We begin with an introduction to collinear limits and define the concept of splitting functions. We then examine the analytic structure of multi-parton collinear limits as expressed in the spinor helicity formalism. This structure enables us to use the MHV-rules method of chapter 4 to derive general results for splitting functions with arbitrary numbers of positive helicity particles and specific numbers of negative helicity particles (or vice versa using $\overline{\text{MHV}}$). The formulas we present are sufficient to describe all collinear limits for up to six gluons, and we complete the set of collinear limits for up to four (massless) partons. These results are published in Refs. [127–129].

5.1 Introduction

The factorisation properties of amplitudes in the infrared play several roles in developing higher order perturbative predictions for observable quantities. First, a detailed knowledge of the structure of unresolved emission enables phase space inte-

grations to be organised such that the infrared singularities due to soft or collinear emission can be analytically subtracted at NLO [130–132] or at NNLO [133]. Second, they enable large logarithmic corrections to be identified and resummed. Third, the collinear limit plays a crucial role in the unitarity-based method for loop calculations [96, 97, 134, 135]. Collinear limits of QCD amplitudes are responsible for parton evolution [136], and as such the n -particle tree-level collinear limits contribute to the Altarelli-Parisi evolution kernels at $N^{n-1}LO$ [137, 138]. These kernels control the scale evolution of parton densities and fragmentation functions, and so are vital for the calculation of multi-jet events at the LHC. Lastly the collinear limits of amplitudes are very useful as consistency checks of the correctness of calculations, though this usually only applies for the two particle collinear limits.

In general, to compute a cross section at N^nLO , one requires detailed knowledge of the infrared factorisation functions describing the unresolved configurations for n -particles at tree-level, $(n-1)$ -particles at one-loop etc. The universal behaviour in the double collinear limit is well known at tree-level (see for example Refs. [139, 140]), one-loop [96, 141–145] and at two-loops [146, 147]. Similarly, the triple collinear limit has been studied at tree-level [148–152] and, in the case of distinct quarks, at one-loop [153]. Finally, the tree-level quadruple gluon collinear limit was derived in Ref. [137]. In a recent paper MHV diagrams have been used to calculate the one-loop gluonic splitting functions in supersymmetric Yang-Mills theories [154].

In this chapter we examine the singularity structure of tree-level QCD amplitudes when n partons (gluons and massless quarks) are simultaneously collinear. Understanding the infrared singular behaviour of multi-parton amplitudes is a prerequisite for computing infrared-finite cross sections at fixed order in perturbation theory. In general, when one or more final state particles are either soft or collinear, the amplitudes factorise. The first factor in this product is a scattering amplitude that

depends only on the remaining hard partons in the process (including any hard partons constructed from an ensemble of unresolved partons). The second factor is the splitting amplitude, which contains all of the singularities due to the unresolved particles. One of the best known examples of this type of factorisation is the limit of tree amplitudes when two particles are collinear. This factorisation is universal (process-independent) and can be generalised to more particles [137, 148–151] and any number of loops [155].

To derive the splitting amplitudes, we will exploit the properties of the MHV-rules introduced in chapter 4. Both the MHV rules and the BCF recursion relations of section 4.6 are remarkably powerful in deriving analytic expressions for massless multi-particle tree-level amplitudes. At the same time, for the specific purpose of deriving general multi-collinear limits, we find the MHV rules approach to be particularly convenient. The major benefits of the MHV-rules approach are that the singularities in the kinematic invariants are explicit, without the spurious singularities of amplitudes that are produced via the BCF recursion relations. At the same time the MHV rules approach enables us to calculate infinite sequences of splitting amplitudes – with fixed numbers of negative helicity partons and arbitrary numbers of positive helicity ones, or vice versa. This enables the derivation of many splitting functions from the same set of MHV skeleton diagrams. Another useful feature of the MHV rules is that it is not required to set reference spinors η_α and $\eta_{\dot{\alpha}}$ to specific values dictated by kinematics or other reasons. In this way, on-shell (gauge-invariant) amplitudes are derived for arbitrary η 's, i.e. without fixing the gauge.

In view of this, we will employ the MHV rules for setting up our formalism and for derivations of general multi-collinear amplitudes. The two-gluon collinear limits of MHV diagrams at tree-level were discussed in the original paper on the MHV-

rules [75]. These two particle limits were found to be in full agreement with the well-known results from Feynman diagram calculations, and as such proved to be a useful check of the validity of the MHV approach. Here we extend this analysis to multiparton singularities. By starting from the appropriate colour ordered amplitude and taking the collinear limit, the full amplitude factorises into an MHV vertex multiplied by a multi-collinear splitting function that depends on the helicities of the collinear gluons. Because the MHV vertex is a single factor, the collinear splitting functions have a similar structure to MHV amplitudes. Furthermore, the gauge or η -dependence of the splitting function drops out.

One of the main points of our approach [127, 128] is that in order to derive all required splitting functions we do not need to know the full amplitude. Out of the complete set of MHV-diagrams contributing to the full amplitude, only a subset will contribute in the multi-collinear limit. This subset includes only those MHV-diagrams where *all* of the internal propagators go on-shell in the multi-collinear limit. In other words, the IR singularities in the MHV approach arise entirely from internal propagators going on-shell. This observation is specific to the MHV rules method and does not apply to the BCF recursive approach. We will see in Section 5.5.1 that in the BCF picture collinear splitting functions generically receive contributions from the full set of allowed BCF diagrams¹. Moreover, the functions multiplying the singular propagators in the splitting amplitude are constrained by the MHV rules to take a purely holomorphic form: they are functions which depend only on the holomorphic spinor products, $\langle i j \rangle$, of the right-handed (undotted) spinors and not on the anti-holomorphic ones $[i j]$. This points towards a simple twistor space picture for the multi-collinear limits.

¹This is because the required IR poles in the BCF approach arise not only from propagators going on-shell, but also from the constituent BCF vertices.

5.2 Collinear limits

To find the splitting functions we work with the colour stripped amplitudes as introduced in section 4.2. For these colour ordered amplitudes, it is known that when the collinear particles are not adjacent there is no collinear divergence [137]. Therefore, without loss of generality, we can take particles $1 \dots n$ collinear.

The multiple collinear limit is approached when the momenta p_1, \dots, p_n become parallel. This implies that all the particle subenergies $s_{ij} = (p_i + p_j)^2$, with $i, j = 1, \dots, n$, are simultaneously small. We thus introduce a pair of light-like momenta P^ν and ξ^ν ($P^2 = 0, \xi^2 = 0$), and we write

$$(p_1 + \dots + p_n)^\nu = P^\nu + \frac{s_{1,n} \xi^\nu}{2 \xi \cdot P}, \quad s_{i,j} = (p_i + \dots + p_j)^2, \quad (5.1)$$

where $s_{1,n}$ is the total invariant mass of the system of collinear partons. In the collinear limit, the vector P^ν denotes the collinear direction, and the individual collinear momenta are $p_i^\nu \rightarrow z_i P^\nu$. Here the longitudinal-momentum fractions z_i are given by

$$z_i = \frac{\xi \cdot p_i}{\xi \cdot P} \quad (5.2)$$

and fulfil the constraint $\sum_{i=1}^m z_i = 1$. To be definite, in the rest of the thesis we work in the time-like region so that ($s_{ij} > 0, 1 > z_i > 0$).

As illustrated in Fig. 5.1, in the multi-collinear limit an N -particle colour ordered tree amplitude factorises and can be written as

$$A_N(1^{\lambda_1}, \dots, N^{\lambda_N}) \rightarrow \text{split}(1^{\lambda_1}, \dots, n^{\lambda_n} \rightarrow P^\lambda) \\ \times A_{N-n+1}((n+1)^{\lambda_{n+1}}, \dots, N^{\lambda_N}, P^\lambda). \quad (5.3)$$

In the splitting amplitude only the terms which are most singular in the collinear

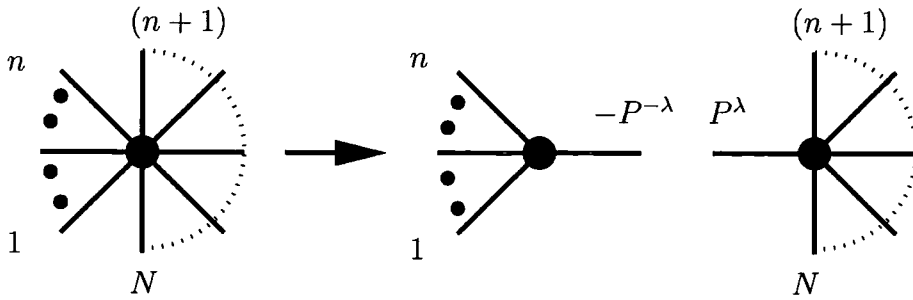


Figure 5.1: Factorisation of an N -point colour ordered amplitude with gluons p_1, \dots, p_n collinear into splitting function for $P \rightarrow 1, \dots, n$ multiplied by an $(N-n+1)$ -point amplitude.

limit are included. This is because upon integration over the small-region of phase space in which the collinear limit is valid, only the most singular terms will give a non-negligible contribution to the cross-section in question [149].

The remnant amplitude after taking the collinear limit has all legs on-shell and so we can refer to this as a ‘hard’ amplitude. The labelling of the splitting amplitude used here, $\text{split}(1^{\lambda_1}, \dots, n^{\lambda_n} \rightarrow P^\lambda)$, differs from the usual definition because we use the momentum and helicity that participates in the resultant amplitude P^λ rather than $-P^{-\lambda}$. With this choice, it is easier to see how the helicity is conserved in the splitting, i.e. helicity $\lambda^1, \dots, \lambda^n$ is replaced by λ , and so the labelling is more intuitive. Since eq. (5.3) applies for all N , we can use it to derive the splitting amplitude by systematically choosing $N = 3 + n$. In this case, we always factorise onto a four-point amplitude with two negative helicity legs, as it is the simplest non-zero amplitude which we can factor onto. We could choose to factor onto amplitudes with larger numbers of external legs, possibly with extra negative helicity particles, but factorising onto the simple four point MHV vertex enables us to easily factor out the vertex and extract the splitting functions from the lowest possible order of MHV diagram.

As such we exploit the universal nature of the splitting function by choosing to start

with an amplitude with $(n+3)$ external legs, i.e. setting $N = n+3$ in Eq. (5.3). For collinear limits where P^λ is a gluon (i.e. the collinear particles in the collinear limit have the properties of a gluon), the helicities of the gluons are adjusted so that the remnant ‘hard’ four point MHV amplitude $A_4(P^\lambda, (n+1)^+, (n+2)^{-\lambda}, (n+3)^-)$ is given by

$$A_4((n+1)^+, (n+2)^{-\lambda}, (n+3)^-, P^\lambda) = \frac{\langle n+3, X \rangle^4}{\langle P, n+1 \rangle \langle n+1, n+2 \rangle \langle n+2, n+3 \rangle \langle n+3, P \rangle} \quad (5.4)$$

with $X = P$ for $\lambda = -$ and $X = n+2$ for $\lambda = +$. This ensures that we always factorise onto the MHV amplitude with two negative and two positive helicity legs. For collinear limits where P^λ is a quark, we factor onto the four-point MHV quark amplitudes in a similar fashion.

To read off the collinear limits from the MHV rules, we use the limiting expressions for the spinor products: $\langle a q \rangle$, $\langle b q \rangle$ and $\langle b a \rangle$. Here a is a particle from the collinear set, b is a particle which is not in the collinear set, and q is the sum of the collinear momenta from $i+1$ to j , associated with the propagators momentum. Hence, using

$$\langle a q \rangle = \sum_{l=i+1}^j \langle a l \rangle [l \eta], \quad \langle b q \rangle = \sum_{l=i+1}^j \langle b l \rangle [l \eta], \quad (5.5)$$

and the expressions for spinors from the collinear set,

$$|l\rangle = \sqrt{z_l} |P\rangle, \quad |l] = \sqrt{z_l} |P], \quad |a\rangle = \sqrt{z_a} |P\rangle, \quad |a] = \sqrt{z_a} |P], \quad (5.6)$$

we have,

$$\langle a q \rangle \rightarrow [P \eta] \sum_{l=i+1}^j \langle a l \rangle \sqrt{z_l} \equiv [P \eta] \Delta_{(1)}(i, j; a) \quad (5.7)$$

$$\langle b q \rangle \rightarrow [P \eta] \langle b P \rangle \sum_{l=i+1}^j z_l \quad (5.8)$$

$$\langle b a \rangle \rightarrow \langle b P \rangle \sqrt{z_a}. \quad (5.9)$$

Here we introduced the definition

$$\Delta_{(1)}(i, j; a) = \sum_{l=i+1}^j \langle a l \rangle \sqrt{z_l}. \quad (5.10)$$

This factor $\Delta_{(1)}$ accounts for the collinear limit of the spinor product of the propagator with a collinear particle.

We also introduce

$$D(i, j, q_{i+1, j}) = q_{i+1, j}^2 \frac{\Delta_{(1)}(i, j; i) \Delta_{(1)}(i, j; i+1) \Delta_{(1)}(i, j; j) \Delta_{(1)}(i, j; j+1)}{\langle i, i+1 \rangle \langle j, j+1 \rangle}, \quad (5.11)$$

which corresponds to the collinear limit of the effective propagator as given in equation 4.33.

Equations (5.7) and (5.8) contain a factor $[P \eta]$ which, however, will always cancel in expressions for relevant splitting functions. As such we can read off the collinear limits of the amplitudes from the MHV-rules expressions by replacing terms on the left hand side of equations (5.7), (5.8) and (5.9) with the expressions on the right hand side of those equations, and further dropping the $[P \eta]$ factors. In essence we can draw the contributing MHV diagrams, and then write down the result for the splitting amplitude by using these collinear terms instead of those used in section 4.5.

Using this method we have a quick and easy way of writing the collinear limits for a process straight from the contributing MHV diagrams, *without the need to evaluate the amplitude first*.

Certain terms in the sums that arise in MHV rules need special attention. These are the boundary terms involving spinor products particles from the collinear set with those not in the collinear set. These terms will include $\langle 01 \rangle$ or $\langle n n + 1 \rangle$, and applying the rules from equations (5.7),(5.8) and (5.9) we have the replacements,

$$\frac{\langle n n + 1 \rangle}{\Delta_{(1)}(i, n; n + 1)} \rightarrow -\frac{\sqrt{z_n}}{\sum_{l=i+1}^n z_l}, \quad (5.12)$$

$$\frac{\langle 01 \rangle}{\Delta_{(1)}(0, j; 0)} \rightarrow \frac{\sqrt{z_1}}{\sum_{l=1}^j z_l}. \quad (5.13)$$

Thus these expressions no longer include terms from outside the collinear set, giving the required splitting amplitudes.

5.3 Analytic structure of splitting amplitudes

We find that there are two different types of collinear limit [75], those that conserve the number of negative helicity gluons between the initial state and the final collinear state, and those that do not. Only the case $-+_n \rightarrow -$ can contribute to the negative helicity conserving case due to the factorisation onto a single particle, and this collinear limit is easy to derive from the simple MHV vertex. All other limits belong to the second class which do not conserve the number of negative helicity gluons, and therefore we classify our results according to the difference between the number of negative helicity gluons before taking the collinear limit, and the number after. We call this difference ΔM .

Splitting amplitudes are calculated using the factorisation formula eq. (5.3). To

facilitate the calculation, it makes sense to factorise onto hard amplitudes with the simplest analytic structure. Hence, in the MHV-rules formalism we will always factorise onto MHV amplitudes which are listed in section 4.4. In this case we find that ΔM of the splitting amplitude satisfies the relation,

$$\Delta M + 2 = N_- \quad (5.14)$$

where 2 is the number of negative helicities in the hard MHV amplitude, and N_- is the total number of negative helicities in the full amplitude. ΔM determines the order of MHV diagram [75] for the full amplitude A_N

$$\begin{aligned}
 \Delta M = 0 & \Rightarrow & 1^+, 2^+, 3^+, \dots, n^+ & \rightarrow P^+ & A_N = \text{MHV} \\
 & & 1^-, 2^+, 3^+, \dots, n^+ & \rightarrow P^- \\
 \\
 \Delta M = 1 & \Rightarrow & 1^-, 2^+, 3^+, \dots, n^+ & \rightarrow P^+ & A_N = \text{NMHV} \\
 & & 1^-, 2^-, 3^+, \dots, n^+ & \rightarrow P^- \\
 \\
 \Delta M = 2 & \Rightarrow & 1^-, 2^-, 3^+, \dots, n^+ & \rightarrow P^+ & A_N = \text{NNMHV} \\
 & & 1^-, 2^-, 3^-, \dots, n^+ & \rightarrow P^-
 \end{aligned} \quad (5.15)$$

and so on for all $\Delta M > 2$ cases.

We can picture this using figures 5.2-5.4. These figures show that for up to four collinear particles, only the NMHV structures are needed to find all collinear limits. This is because we can use the parity transformation to swap $\langle ij \rangle \leftrightarrow -[ij]$ which gives us the limits which we could have calculated via \overline{MHV} . This will provide us

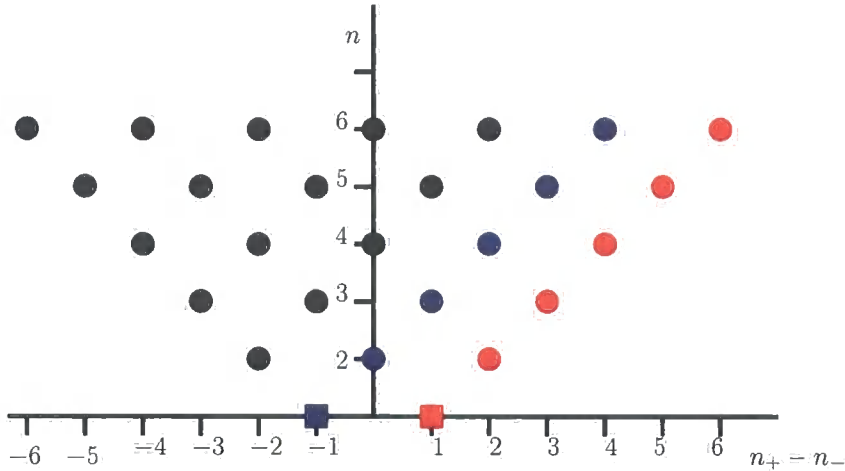


Figure 5.2: Pattern of multi-collinear splitting functions accessible using the MHV amplitudes. The red circles representing any $n_+ = n$ positive helicities, collapse to the red positive helicity square. Similarly, the blue circles representing any $n_+ = n - 1$ positive helicities, collapse to the blue negative helicity square.

with the remaining processes. (This is equivalent to saying that the left hand side of the figure is the parity inverse of the right hand side). Similarly the NNMHV results give us access to all of the splitting functions for up to six collinear particles.

If we choose to use $\overline{\text{MHV}}$ rules, we extract the splitting function by factorising onto $\overline{\text{MHV}}$ amplitudes. Splitting amplitudes are then classified by the difference in the number of positive helicity particles, ΔP , and similar observations apply.

In general, any splitting amplitude can be obtained from either MHV or $\overline{\text{MHV}}$ rules. Examining the general form of MHV diagrams, which consist of MHV vertices and scalar propagators, we can use a simple power counting argument to find

$$\text{split} \propto \frac{1}{[\]^{\Delta M} \langle \ \rangle^{\Delta P}} . \quad (5.16)$$

For an MHV-rules diagram to contribute to $\Delta M \neq 0$ collinear limits, it must contain anti-holomorphic spinor products $[ij]$ of collinear momenta. However, because on-shell MHV vertices are entirely holomorphic, within the MHV rules there are only

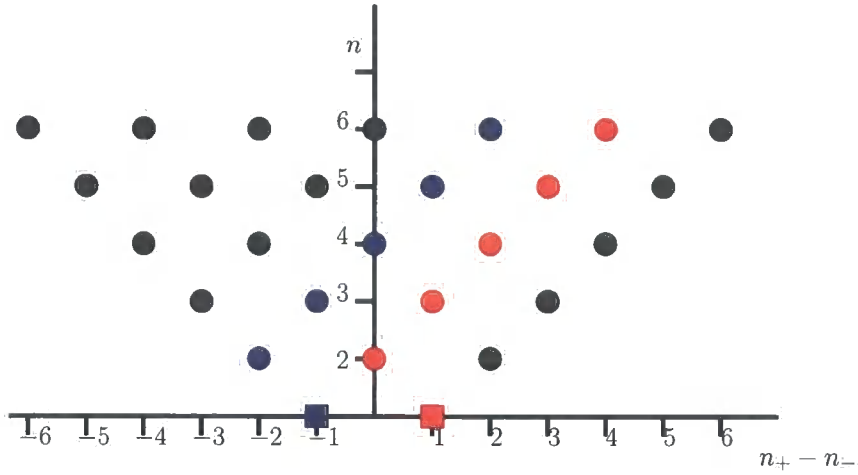


Figure 5.3: Pattern of multi-collinear splitting functions accessible using the NMHV amplitudes. The red circles representing any $n_+ = n - 1$ positive helicities, collapse to the red positive helicity square. Similarly, the blue circles representing any $n_+ = n - 2$ positive helicities, factorise onto the blue negative helicity square.

two potential sources of the anti-holomorphic spinor products. One source is scalar propagators $1/s_{ij} = 1/\langle ij \rangle [ji]$ which connect MHV vertices. The second source is the off-shell continuation of the corresponding connected legs in the MHV vertices. Each off-shell continued leg of momentum P gives rise to a factor $\langle iP \rangle \propto \langle iP | \eta \rangle$ which amounts to anti-holomorphic factors of the form $[j\eta]$. When the reference spinors η_α are kept general, the η -dependence must cancel and therefore the off-shell continuation cannot give rise to an overall factor of $[ij]$.

This implies that within the MHV rules, the anti-holomorphic spinor products in (5.16) arise solely from the internal propagators. Since $\Delta M = v_{MHV} - 1$,² where v_{MHV} is the number of MHV vertices in the diagram, the total number of internal propagators is ΔM , in agreement with (5.16). Similarly, in the $\overline{\text{MHV}}$ approach, the holomorphic products would arise solely from internal propagators whose total

²In principle, $\Delta M = v_{MHV} - v'_{MHV}$ where v'_{MHV} is the number of MHV vertices remaining in the factored amplitude. The splitting function is independent of v'_{MHV} , and because we systematically choose to factor directly onto a single MHV vertex, we set $v'_{MHV} = 1$.

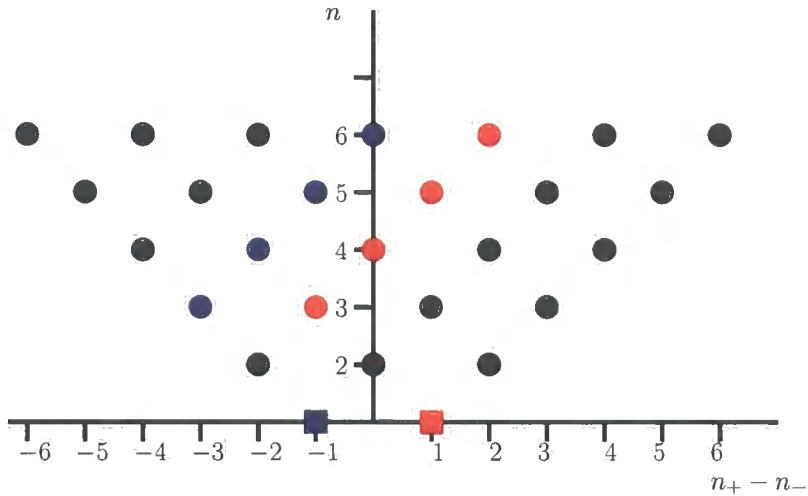


Figure 5.4: Pattern of multi-collinear splitting functions accessible using the NNMHV amplitudes. The red circles representing any $n_+ = n - 2$ positive helicities, collapse to the red positive helicity square. Similarly, the blue circles representing any $n_+ = n - 3$ positive helicities, factorise onto the blue negative helicity square.

number in $\overline{\text{MHV}}$ diagrams is ΔP . This means that the MHV rules for collinear limits are substantially simpler than the rules for the full amplitudes. The collinear splitting functions follow only from a *subset* of the MHV rules diagrams, where only diagrams with all internal propagators on-shell in the multi-collinear limit are included. This is a powerful constraint on the types of the contributing diagrams and it simplifies taking the collinear limit dramatically.

From the above, it follows that all splitting amplitudes can be recast as

$$\text{split} = \sum \frac{1}{\prod_{i,j=1}^{\Delta M} s_{i,j}} f(\langle \rangle) \quad (5.17)$$

$$= \sum \frac{1}{\prod_{i,j=1}^{\Delta P} s_{i,j}} \tilde{f}([\]) \quad (5.18)$$

where the first expression follows from the MHV rules representation, and the second expression – from the $\overline{\text{MHV}}$ formalism. Here the summations are over all inequivalent choices of ΔM (ΔP) products of vanishing kinematic invariants $s_{i,j}$ which

corresponds to different MHV ($\overline{\text{MHV}}$) rules diagrams. The coefficient functions f depend only on holomorphic spinor products, while the $\overline{\text{MHV}}$ coefficients \tilde{f} are purely anti-holomorphic. Moreover, f and \tilde{f} have dimensions,

$$f \propto \frac{1}{\langle \rangle_{\Delta P - \Delta M}}, \quad \tilde{f} \propto \frac{1}{[\]_{\Delta M - \Delta P}}. \quad (5.19)$$

The fact that f (\tilde{f}) is purely (anti)-holomorphic suggests a simple twistor-space interpretation. All splitting functions can be represented as sums over the corresponding poles in s with the coefficients being supported on a single degree-one curve in (anti)-twistor space. This pure (anti)-holomorphic representation of multi-collinear limits is specific to the MHV ($\overline{\text{MHV}}$) formalism and is lost in the usual Feynman-diagram-type approaches as in Ref. [137], or in the BCF recursive approach, as will be shown in section 5.5.1.

As we have already mentioned, each splitting amplitude can be calculated in both the MHV and in the $\overline{\text{MHV}}$ approaches. In practice, eqs. (5.16)-(5.18) imply that the MHV approach is simpler if $\Delta M < \Delta P$, while the $\overline{\text{MHV}}$ approach is more compact in the opposite case, $\Delta P < \Delta M$. This can be seen from figures 5.2-5.4.

In most of what follows we will concentrate on the splitting amplitudes with $\Delta M \leq \Delta P$ and will follow the MHV rules. The remaining amplitudes with $\Delta P < \Delta M$ are obtained from these by complex conjugation.

5.4 General results

In this section we give the results for the multiple collinear limit of quarks and gluons. We categorise the results according to the number of quarks involved in the limit. In each case, we give the general results for collinear limits with $\Delta M = 0, 1$

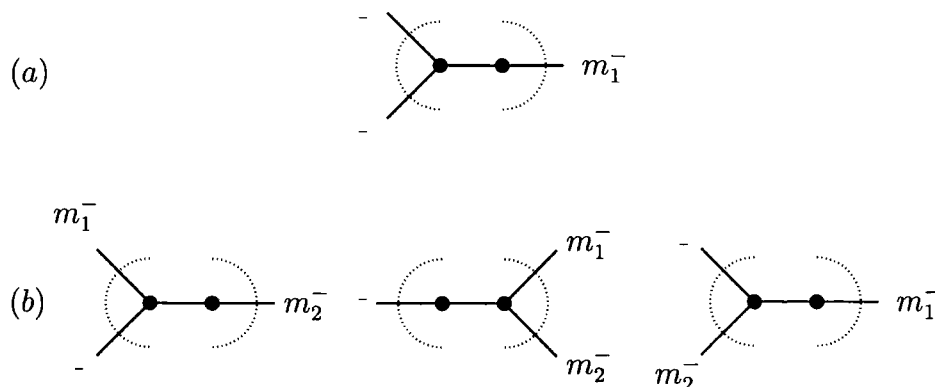


Figure 5.5: MHV topologies contributing to (a) $\text{Split}_+^{(n)}(m_1)$ and (b) $\text{Split}_-^{(n)}(m_1, m_2)$. Negative helicity particles are indicated by solid lines, while arbitrary numbers of positive helicity particles emitted from each vertex are shown as dotted arcs. All particles that are not in the collinear set must be emitted from the left-hand vertex.

and involving an arbitrary number of positive helicity particles.

Limits of the type $\text{split}(1^+, \dots, n^+ \rightarrow P^+)$ and $\text{split}(1^-, 2^+, \dots, n^+ \rightarrow P^-)$ can contribute to the $\Delta M = 0$, and these collinear splitting functions are straightforward to derive directly from the simple MHV vertex.

For the remaining splitting functions, it is useful to introduce the more compact notation

$$\text{split}(1^+, \dots, m_1^-, \dots, m_2^-, \dots, m_r^-, \dots, n^+ \rightarrow P^\pm) = \text{Split}_\pm^{(n)}(m_1, \dots, m_r). \quad (5.20)$$

which denotes the splitting amplitude for n collinear partons, of which r have negative helicity.

For $\Delta M = 1$, there are two possible types of splitting function, $\text{Split}_+^{(n)}(m_1)$ and $\text{Split}_-^{(n)}(m_1, m_2)$. The possible MHV topologies contributing to these splitting functions are illustrated in Fig. 5.5. Only negative helicity particles are shown. In the collinear limit, the propagator goes on-shell. Any MHV diagram with a hard particle emitted from both vertices produces an off-shell propagator. This means that

only particles from the collinear set are allowed to couple to the right-hand vertex. All hard partons couple to the left-hand vertex.

5.4.1 Purely gluonic limits – no quarks in the collinear set:

$$ng \rightarrow g$$

In this section we present the general results for the cases where the number of gluons with negative helicity changes by at most $\Delta M = 2$, and those related by parity where the number of gluons with positive helicity changes at most by the same amount. With the help of parity these general splitting amplitudes are sufficient to obtain the explicit expressions for all helicity combinations of up to six gluons.

$$\Delta M = 0$$

This is the simplest case which is read directly off the single MHV vertex. The denominator of an N -point MHV amplitude is factorised as follows (in the limit of collinear p_1, \dots, p_n):

$$\begin{aligned} \langle N, 1 \rangle \langle 1, 2 \rangle \dots \langle n, n+1 \rangle \dots \langle N-1, N \rangle = \\ \left(\sqrt{z_1 z_n} \prod_{l=1}^{n-1} \langle l, l+1 \rangle \right) \times \left(\langle N, P \rangle \langle P, n+1 \rangle \dots \langle N-1, N \rangle \right) \end{aligned} \quad (5.21)$$

where the first factor contributes to the splitting function, and the second one is the denominator of the remaining hard MHV amplitude. Hence, the splitting function is

$$\text{split}(1^+, \dots, n^+ \rightarrow P^+) = \frac{1}{\sqrt{z_1 z_n} \prod_{l=1}^{n-1} \langle l, l+1 \rangle}, \quad (5.22)$$

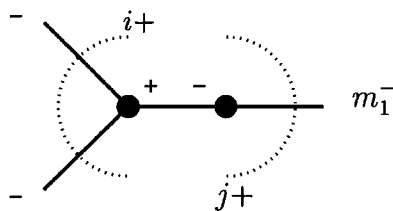


Figure 5.6: MHV diagrams contributing to $\text{Split}_+^{(n)}(m_1)$. Negative helicity gluons are indicated by solid lines, while arbitrary numbers of positive helicity gluons emitted from each vertex are shown as dotted arcs.

and so by parity

$$\text{split}(1^-, \dots, n^- \rightarrow P^-) = \frac{(-1)^{n-1}}{\sqrt{z_1 z_n} \prod_{l=1}^{n-1} [l, l+1]} . \quad (5.23)$$

Similarly,

$$\text{split}(1^+, \dots, m_1^-, \dots, n^+ \rightarrow P^-) = \frac{z_{m_1}^2}{\sqrt{z_1 z_n} \prod_{l=1}^{n-1} \langle l, l+1 \rangle} , \quad (5.24)$$

and

$$\text{split}(1^-, \dots, m_1^+, \dots, n^- \rightarrow P^+) = \frac{(-1)^{n-1} z_{m_1}^2}{\sqrt{z_1 z_n} \prod_{l=1}^{n-1} [l, l+1]} . \quad (5.25)$$

$\Delta M = 1$

This is the next-to-MHV (NMHV) case, and in the collinear limit we need to take into account only a subset of MHV diagrams. In fact, there is only a single MHV diagram (or more precisely a single class of MHV diagrams) which can contribute to $\text{Split}_+^{(n)}(m_1)$. It is shown in Fig. 5.6.³ In the limit where gluons $1, \dots, n$ become collinear. The left vertex in Fig. 5.6 produces a ‘hard’ MHV amplitude while the right vertex generates the splitting function. We need to sum over i and j in Fig. 5.6

³MHV diagrams where hard negative helicity gluons are emitted from more than one vertex do not give rise to on-shell propagators and do not contribute in the singular limit.

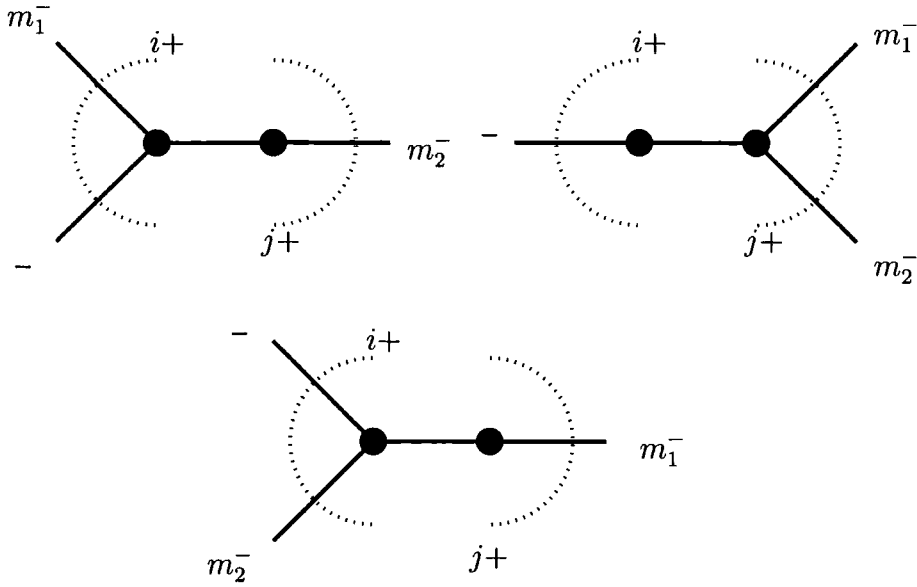


Figure 5.7: MHV diagrams contributing to $\text{Split}_-^{(n)}(m_1, m_2)$.

in such a way that only diagrams with a singular propagator are selected in the collinear limit. This puts a constraint $j \leq n$ where n is the number of collinear gluons. The resulting splitting function reads,

$$\text{Split}_+^{(n)}(m_1) = \frac{1}{\sqrt{z_1 z_n} \prod_{l=1}^{n-1} \langle l, l+1 \rangle} \left(\sum_{i=0}^{m_1-1} \sum_{j=m_1}^n \frac{\Delta_{(1)}(i, j; m_1)^4}{D(i, j, q_{i+1, j})} \right). \quad (5.26)$$

Similarly, there are three (classes of) MHV-diagrams contributing to $\text{Split}_-^{(n)}(m_1, m_2)$.

They are shown in Fig. 5.7 and lead to a splitting function which reads

$$\begin{aligned} \text{Split}_-^{(n)}(m_1, m_2) = & \frac{1}{\sqrt{z_1 z_n} \prod_{l=1}^{n-1} \langle l, l+1 \rangle} \left(\sum_{i=0}^{m_1-1} \sum_{j=m_1}^{m_2-1} \frac{z_{m_2}^2 \Delta_{(1)}(i, j; m_1)^4}{D(i, j, q_{i+1, j})} \right. \\ & + \sum_{i=m_1}^{m_2-1} \sum_{j=m_2}^n \frac{z_{m_1}^2 \Delta_{(1)}(i, j; m_2)^4}{D(i, j, q_{i+1, j})} \\ & \left. + \sum_{i=0}^{m_1-1} \sum_{j=m_2}^n \frac{\langle m_1 m_2 \rangle^4}{D(i, j, q_{i+1, j})} \left(\sum_{l=i+1}^j z_l \right)^4 \right). \quad (5.27) \end{aligned}$$

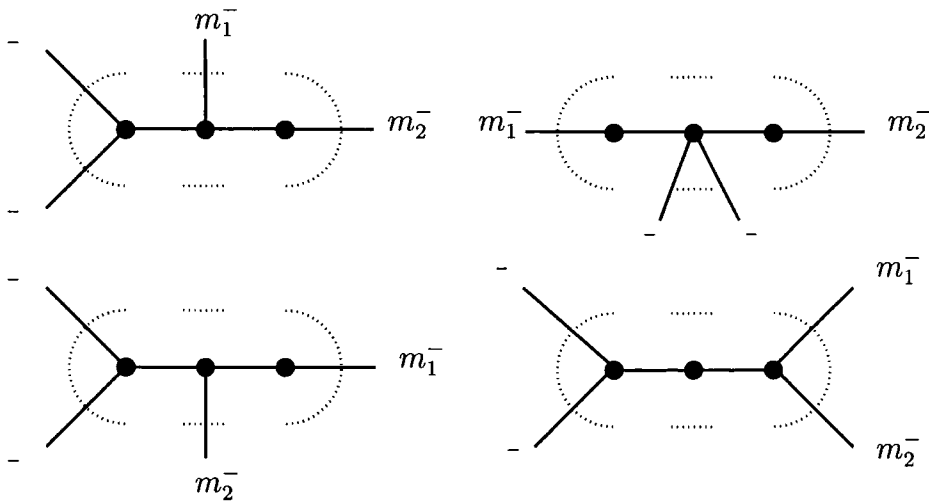


Figure 5.8: MHV diagrams contributing to $\text{Split}_+^{(n)}(m_1, m_2)$.

The remaining splitting amplitudes of the form

$$\text{split}(1^-, \dots, m_1^+, \dots, m_2^+, \dots, m_r^+, \dots, n^- \rightarrow P^\pm) \quad (5.28)$$

are obtained by parity transformation through the usual replacement $\langle l, k \rangle \leftrightarrow -[l, k]$.

$$\Delta M = 2$$

The collinear limits with $\Delta M = 2$ are derived from next-to-next-to-MHV (NNMHV) diagrams. There are four (classes of) MHV-diagrams contributing to $\text{Split}_+^{(n)}(m_1, m_2)$

which are shown in Fig. 5.8. The corresponding splitting function is,

$$\begin{aligned}
\text{Split}_+^{(n)}(m_1, m_2) &= \frac{1}{\sqrt{z_1 z_n} \prod_{l=1}^{n-1} \langle l, l+1 \rangle} \\
&\left(\sum_{i=0}^{m_1-1} \sum_{j=m_2}^n \sum_{k=m_1}^{m_2-1} \sum_{r=m_2}^j \frac{\Delta_{(1)}(i, j; m_1)^4 \Delta_{(1)}(k, r; m_2)^4}{\text{DD}(i, j, q_{i+1, j}; k, r, q_{k+1, r})} \right. \\
&+ \sum_{i=0}^{m_1-1} \sum_{j=m_1}^k \sum_{k=m_1}^{m_2-1} \sum_{r=m_2}^n \frac{\Delta_{(1)}(i, j; m_1)^4 \Delta_{(1)}(k, r; m_2)^4}{\text{DD}(i, j, q_{i+1, j}; k, r, q_{k+1, r})} \\
&+ \sum_{i=0}^k \sum_{j=m_2}^n \sum_{k=0}^{m_1-1} \sum_{r=m_1}^{m_2-1} \frac{\Delta_{(1)}(i, j; m_2)^4 \Delta_{(1)}(k, r; m_1)^4}{\text{DD}(i, j, q_{i+1, j}; k, r, q_{k+1, r})} \\
&\left. + \sum_{i=0}^k \sum_{j=m_2}^n \sum_{k=0}^{m_1-1} \sum_{r=m_2}^j \frac{\langle m_1 m_2 \rangle^4 \Delta_{(2)}(i, j; k, r)^4}{\text{DD}(i, j, q_{i+1, j}; k, r, q_{k+1, r})} \right) \quad (5.29)
\end{aligned}$$

where $\Delta_{(1)}(i, j; k)$ is given in Eq. (5.10) and we introduce

$$\Delta_{(2)}(i, j; k, r) = \sum_{u=i+1}^j \sum_{v=k+1}^r \langle u v \rangle \sqrt{z_u z_v}. \quad (5.30)$$

This function is introduced to account for the collinear limit of the spinor product of two propagators $\langle q_{i, j+1} q_{k, r+1} \rangle$, where both propagators contain only collinear momenta as required in our approach. This spinor product arises when there are more than two vertices, and either both propagators are negative entering the joining vertex, or when they are adjacent. For computational purposes it is useful to know the properties of this function.

$$\Delta_{(2)}(i, j; k, r) = 0 \quad \text{if} \quad \left\{ \begin{array}{l} i = j \\ k = r \\ i = k \text{ and } j = r \\ i = r \text{ and } j = k \end{array} \right. \quad (5.31)$$

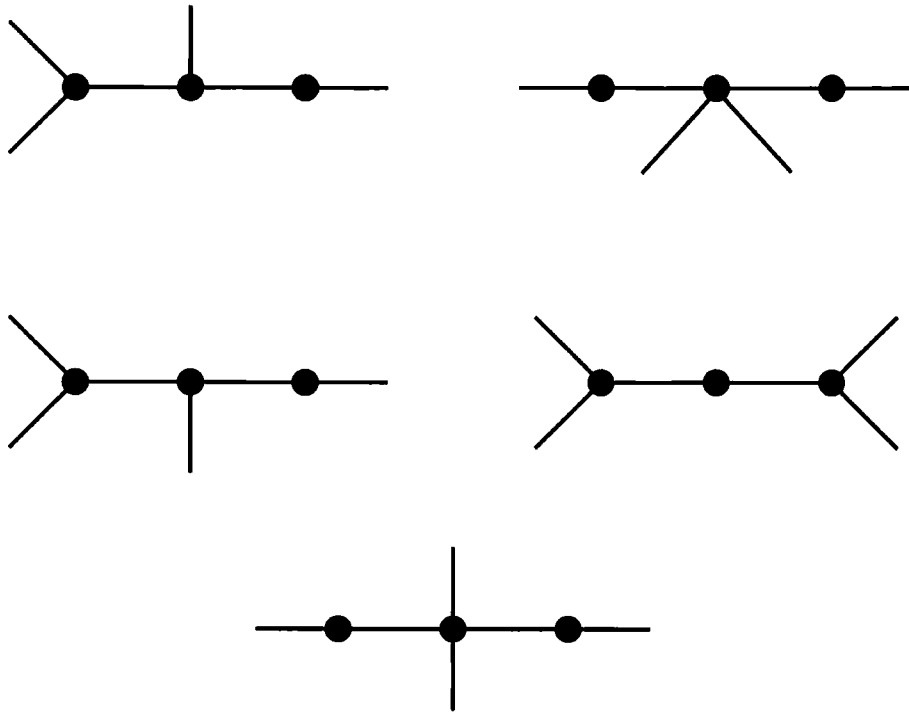


Figure 5.9: MHV topologies contributing to $\text{Split}_-^{(n)}(m_1, m_2, m_3)$. The negative helicity gluons m_1 , m_2 and m_3 are distributed in a cyclic way around each diagram. The remaining leg is the negative helicity gluon that remains after the collinear limit is taken.

The ‘effective propagator’ DD is defined by

$$\text{DD}(i, j, q_1; k, r, q_2) = \chi(i, k, q_1, q_2)\chi(r, j, q_2, q_1)\chi(j, k, q_1, q_2)D(i, j, q_1)D(k, r, q_2) \tag{5.32}$$

in terms of D defined previously in Eq. (5.11), and χ given by

$$\chi(i, k, q_1, q_2) = \begin{cases} 1 & i \neq k \\ \frac{\Delta_{(2)}(q_1, q_2)\langle i, i+1 \rangle}{\Delta_{(1)}(q_1, i+1)\Delta_{(1)}(q_2, i)} & i = k \end{cases} \tag{5.33}$$

This accounts for the spinor products associated with the two propagators, and χ ensures the correct spinors are present when the central vertex has less than four legs.

Finally there are 16 classes of MHV-diagrams contributing to $\text{Split}_-^{(n)}(m_1, m_2, m_3)$, coming from the 5 topologies shown in Fig. 5.9 and their cyclic permutations. The individual contributions are given by

$$\text{Split}_-^{(n)}(m_1, m_2, m_3) = \frac{1}{\sqrt{z_1 z_n} \prod_{l=1}^{n-1} \langle l, l+1 \rangle} \sum_{i=1}^{16} A^{(i)}(m_1, m_2, m_3) \quad (5.34)$$

where

$$\begin{aligned} A^{(1)}(m_1, m_2, m_3) &= \sum_{i=m_1}^{m_2-1} \sum_{j=m_3}^n \sum_{k=m_2}^{m_3-1} \sum_{r=m_3}^j z_{m_1}^2 \frac{\Delta_{(1)}(i, j; m_2)^4 \Delta_{(1)}(k, r; m_3)^4}{\text{DD}(i, j, q_{i+1, j}; k, r, q_{k+1, r})} \\ A^{(2)}(m_1, m_2, m_3) &= \sum_{i=m_1}^k \sum_{j=m_3}^n \sum_{k=m_1}^{m_2-1} \sum_{r=m_2}^{m_3-1} z_{m_1}^2 \frac{\Delta_{(1)}(i, j; m_3)^4 \Delta_{(1)}(k, r; m_2)^4}{\text{DD}(i, j, q_{i+1, j}; k, r, q_{k+1, r})} \\ A^{(3)}(m_1, m_2, m_3) &= \sum_{i=0}^{m_1-1} \sum_{j=m_2}^{m_3-1} \sum_{k=m_1}^{m_2-1} \sum_{r=m_2}^j z_{m_3}^2 \frac{\Delta_{(1)}(i, j; m_1)^4 \Delta_{(1)}(k, r; m_2)^4}{\text{DD}(i, j, q_{i+1, j}; k, r, q_{k+1, r})} \\ A^{(4)}(m_1, m_2, m_3) &= \sum_{i=0}^k \sum_{j=m_2}^{m_3-1} \sum_{k=0}^{m_1-1} \sum_{r=m_1}^{m_2-1} z_{m_3}^2 \frac{\Delta_{(1)}(i, j; m_2)^4 \Delta_{(1)}(k, r; m_1)^4}{\text{DD}(i, j, q_{i+1, j}; k, r, q_{k+1, r})} \\ A^{(5)}(m_1, m_2, m_3) &= \sum_{i=m_1}^k \sum_{j=m_3}^n \sum_{k=m_1}^{m_2-1} \sum_{r=m_3}^j z_{m_1}^2 \frac{\langle m_2 m_3 \rangle^4 \Delta_{(2)}(i, j; k, r)^4}{\text{DD}(i, j, q_{i+1, j}; k, r, q_{k+1, r})} \\ A^{(6)}(m_1, m_2, m_3) &= \sum_{i=0}^k \sum_{j=m_2}^{m_3-1} \sum_{k=0}^{m_1-1} \sum_{r=m_2}^j z_{m_3}^2 \frac{\langle m_1 m_2 \rangle^4 \Delta_{(2)}(i, j; k, r)^4}{\text{DD}(i, j, q_{i+1, j}; k, r, q_{k+1, r})} \\ A^{(7)}(m_1, m_2, m_3) &= \sum_{i=0}^{m_1-1} \sum_{j=m_3}^n \sum_{k=m_2}^{m_3-1} \sum_{r=m_3}^j \left(\sum_{l=i+1}^j z_l \right)^4 \frac{\langle m_1 m_2 \rangle^4 \Delta_{(1)}(k, r; m_3)^4}{\text{DD}(i, j, q_{i+1, j}; k, r, q_{k+1, r})} \\ A^{(8)}(m_1, m_2, m_3) &= \sum_{i=0}^{m_1-1} \sum_{j=m_3}^n \sum_{k=m_1}^{m_2-1} \sum_{r=m_3}^j \left(\sum_{l=i+1}^j z_l \right)^4 \frac{\langle m_2 m_3 \rangle^4 \Delta_{(1)}(k, r; m_1)^4}{\text{DD}(i, j, q_{i+1, j}; k, r, q_{k+1, r})} \\ A^{(9)}(m_1, m_2, m_3) &= \sum_{i=0}^k \sum_{j=m_3}^n \sum_{k=0}^{m_1-1} \sum_{r=m_2}^{m_3-1} \left(\sum_{l=i+1}^j z_l \right)^4 \frac{\langle m_1 m_2 \rangle^4 \Delta_{(1)}(k, r; m_3)^4}{\text{DD}(i, j, q_{i+1, j}; k, r, q_{k+1, r})} \end{aligned}$$

$$\begin{aligned}
A^{(10)}(m_1, m_2, m_3) &= \sum_{i=0}^{m_1-1} \sum_{j=m_3}^n \sum_{k=m_1}^{m_2-1} \sum_{r=m_2}^{m_3-1} \left(\sum_{l=i+1}^j z_l \right)^4 \frac{\langle m_1 m_3 \rangle^4 \Delta_{(1)}(k, r; m_2)^4}{\text{DD}(i, j, q_{i+1, j}; k, r, q_{k+1, r})} \\
A^{(11)}(m_1, m_2, m_3) &= \sum_{i=0}^k \sum_{j=m_3}^n \sum_{k=0}^{m_1-1} \sum_{r=m_1}^{m_2-1} \left(\sum_{l=i+1}^j z_l \right)^4 \frac{\langle m_2 m_3 \rangle^4 \Delta_{(1)}(k, r; m_1)^4}{\text{DD}(i, j, q_{i+1, j}; k, r, q_{k+1, r})} \\
A^{(12)}(m_1, m_2, m_3) &= \sum_{i=m_1}^{m_2-1} \sum_{j=m_3}^n \sum_{k=m_2}^r \sum_{r=m_2}^{m_3-1} z_{m_1}^2 \frac{\Delta_{(1)}(i, k; m_2)^4 \Delta_{(1)}(r, j; m_3)^4}{\text{DD}(i, k, q_{i+1, k}; r, j, q_{r+1, j})} \\
A^{(13)}(m_1, m_2, m_3) &= \sum_{i=0}^{m_1-1} \sum_{j=m_2}^{m_3-1} \sum_{k=m_1}^r \sum_{r=m_1}^{m_2-1} z_{m_3}^2 \frac{\Delta_{(1)}(i, k; m_1)^4 \Delta_{(1)}(r, j; m_2)^4}{\text{DD}(i, k, q_{i+1, k}; r, j, q_{r+1, j})} \\
A^{(14)}(m_1, m_2, m_3) &= \sum_{i=0}^{m_1-1} \sum_{j=m_3}^n \sum_{k=m_2}^r \sum_{r=m_2}^{m_3-1} \left(\sum_{l=i+1}^k z_l \right)^4 \frac{\langle m_1 m_2 \rangle^4 \Delta_{(1)}(r, j; m_3)^4}{\text{DD}(i, k, q_{i+1, k}; r, j, q_{r+1, j})} \\
A^{(15)}(m_1, m_2, m_3) &= \sum_{i=0}^{m_1-1} \sum_{j=m_3}^n \sum_{k=m_1}^r \sum_{r=m_1}^{m_2-1} \left(\sum_{l=r+1}^j z_l \right)^4 \frac{\langle m_2 m_3 \rangle^4 \Delta_{(1)}(i, k; m_1)^4}{\text{DD}(i, k, q_{i+1, k}; r, j, q_{r+1, j})} \\
A^{(16)}(m_1, m_2, m_3) &= \sum_{i=0}^{m_1-1} \sum_{j=m_3}^n \sum_{k=m_1}^{m_2-1} \sum_{r=m_2}^{m_3-1} z_{m_2}^2 \frac{\Delta_{(1)}(i, k; m_1)^4 \Delta_{(1)}(r, j; m_3)^4}{\text{DD}(i, k, q_{i+1, k}; r, j, q_{r+1, j})}.
\end{aligned}$$

5.4.2 One quark in the collinear set: $q(ng) \rightarrow q$

$$\Delta M = 0$$

This is the simplest case which is read directly off the single MHV vertex. For positive helicity quarks, we use the two-quark MHV amplitude of Eq. (4.12) and find,

$$\text{split}(1_q^+, \dots, n^+ \rightarrow P_q^+) = \frac{\sqrt{z_1}}{\sqrt{z_1 z_n} \prod_{l=1}^{n-1} \langle l, l+1 \rangle}. \quad (5.35)$$

For negative helicity quarks,

$$\text{split}(1_q^-, \dots, n^+ \rightarrow P_q^-) = \frac{\sqrt{z_1}^3}{\sqrt{z_1 z_n} \prod_{l=1}^{n-1} \langle l, l+1 \rangle}. \quad (5.36)$$

Note that helicity conservation ensures that the helicity of P is the same as that of q . It is often convenient to combine results for quarks of helicity $\lambda = \pm\frac{1}{2}$ such that,

$$\text{split}(1_q^\lambda, \dots, n^+ \rightarrow P_q^\lambda) = \frac{\sqrt{z_1}^{2-2\lambda}}{\sqrt{z_1 z_n} \prod_{l=1}^{n-1} \langle l, l+1 \rangle}. \quad (5.37)$$

Using parity we find,

$$\text{split}(1_q^+, \dots, n^- \rightarrow P_q^+) = \frac{(-1)^{n-1} \sqrt{z_1}^{-2+2\lambda}}{\sqrt{z_1 z_n} \prod_{l=1}^{n-1} [l, l+1]}. \quad (5.38)$$

The amplitudes where an antiquark is collinear with several gluons are obtained by charge conjugation.

$$\Delta M = 1$$

Because of helicity conservation, $\Delta M = 1$ implies that a single gluon has negative helicity. When the quark has positive helicity, then the MHV diagrams contributing in the collinear limit correspond to topology (a) of Fig. 5.5. There are two types of diagram – one class where the quark is emitted from the right-hand vertex (and the propagating particle is a quark) and one class mediated by gluon exchange where the quark is emitted from the left-hand vertex. We find,

$$\begin{aligned} \text{split}(1_q^+, \dots, m^-, \dots, n^+ \rightarrow P_q^+) &= \frac{1}{\sqrt{z_1 z_n} \prod_{l=1}^{n-1} \langle l, l+1 \rangle} \\ &\times \left[- \sum_{j=m}^n \frac{\Delta_{(1)}^3(0, j; m) \langle 1 m \rangle}{D(0, j, q_{1,j})} \left(\sum_{k=1}^j z_k \right) + \sum_{i=1}^{m-1} \sum_{j=m}^n \frac{\Delta_{(1)}^4(i, j; m)}{D(i, j, q_{i+1,j})} \sqrt{z_1} \right]. \end{aligned} \quad (5.39)$$

In the same manner, for negative helicity quarks, the allowed MHV diagrams correspond to the first and second topologies shown in Fig. 5.5(b),

$$\begin{aligned} \text{split}(1_q^-, \dots, m^-, \dots, n^+ \rightarrow P_q^-) &= \frac{1}{\sqrt{z_1 z_n} \prod_{l=1}^{n-1} \langle l, l+1 \rangle} \\ &\times \left[- \sum_{j=m}^n \frac{\Delta_{(1)}(0, j; m) \langle 1 m \rangle^3}{D(0, j, q_{1,j})} \left(\sum_{k=1}^j z_k \right)^3 + \sum_{i=1}^{m-1} \sum_{j=m}^n \frac{\Delta_{(1)}^4(i, j; m)}{D(i, j, q_{i+1,j})} \sqrt{z_1}^3 \right]. \end{aligned} \quad (5.40)$$

5.4.3 Two quarks in the collinear set: $(ng)\bar{q}q \rightarrow g$

In this collinear limit, the $\bar{q}q$ pair is in the adjoint representation and effectively acts as a gluon.

$$\Delta M = 0$$

This is the simplest case which is read directly off the single MHV vertex. Unlike the previous case, here we start with a two-quark MHV amplitude and factorise onto a gluonic MHV amplitude. Alternatively, we could start with a four-quark amplitude and factorise onto a two-quark amplitude. For quarks with helicity $\lambda = \pm \frac{1}{2}$, we find,

$$\text{split}(1^+, \dots, s_{\bar{q}}^{-\lambda}, (s+1)_q^\lambda, \dots, n^+ \rightarrow P^-) = \frac{\sqrt{z_s}^{-2+2\lambda} \sqrt{z_{s+1}}^{-2-2\lambda}}{\sqrt{z_1 z_n} \prod_{l=1}^{n-1} \langle l, l+1 \rangle}. \quad (5.41)$$

$$\Delta M = 1$$

For amplitudes of the $\text{Split}_+^{(n)}(m_1)$ -type, we find

$$\begin{aligned} \text{split}(1^+, \dots, s_{\bar{q}}^{-\lambda}, (s+1)_q^\lambda, \dots, n^+ \rightarrow P^+) &= \\ &= \frac{1}{\sqrt{z_1 z_n} \prod_{l=1}^{n-1} \langle l, l+1 \rangle} \sum_{i=0}^{s-1} \sum_{j=s+1}^n \frac{\Delta_{(1)}^{2+2\lambda}(i, j; s) \Delta_{(1)}^{2-2\lambda}(i, j; s+1)}{D(i, j, q_{i+1,j})}. \end{aligned} \quad (5.42)$$

There are four diagrams contributing to splitting functions of $\text{Split}_-^{(n)}(m_1, m_2)$ type⁴,

$$\begin{aligned}
\text{split}(1^+, \dots, s_{\bar{q}}^{-\lambda}, (s+1)_q^\lambda, \dots, m^-, \dots, n^+ \rightarrow P^-) &= \frac{1}{\sqrt{z_1 z_n} \prod_{l=1}^{n-1} \langle l, l+1 \rangle} \\
&\times \left[\sum_{i=0}^{s-1} \sum_{j=m}^n \frac{\langle s m \rangle^{2+2\lambda} \langle s+1 m \rangle^{2-2\lambda}}{D(i, j, q_{i+1, j})} \left(\sum_{k=i+1}^j z_k \right)^4 \right. \\
&+ \sum_{i=0}^{s-1} \sum_{j=s+1}^{m-1} \frac{\Delta_{(1)}^{2+2\lambda}(i, j; s) \Delta_{(1)}^{2-2\lambda}(i, j; s+1)}{D(i, j, q_{i+1, j})} z_m^2 \\
&- \sum_{j=m}^n \frac{\Delta_{(1)}^{2+2\lambda}(s, j; m) \langle s+1 m \rangle^{2-2\lambda}}{D(s, j, q_{s+1, j})} \sqrt{z_s}^{2+\lambda} \left(\sum_{k=s+1}^j z_k \right)^{2-2\lambda} \\
&\left. + \sum_{i=s+1}^{m-1} \sum_{j=m}^n \frac{\Delta_{(1)}^4(i, j; m)}{D(i, j, q_{i+1, j})} \sqrt{z_s}^{-2+2\lambda} \sqrt{z_{s+1}}^{2-2\lambda} \right]. \quad (5.43)
\end{aligned}$$

Splitting functions of the type $\text{split}(1^+, \dots, m^-, \dots, s_{\bar{q}}^{-\lambda}, (s+1)_q^\lambda, \dots, n^+ \rightarrow P^-)$ are obtained by line reversal. These results for the two-quark sector are sufficient to calculate all splitting amplitudes for up to four partons.

5.4.4 Two quarks in the collinear set: $q(n_g)\bar{q} \rightarrow \gamma$

In this collinear limit, the $q \dots \bar{q}$ system forms a colour singlet and effectively acts as a photon.

$$\Delta M = 0$$

In this limit the four-quark \tilde{A} MHV amplitudes of eqs. (4.19)–(4.22) factorise directly onto the two-quark+photon amplitudes of (4.13). We find that,

$$\widetilde{\text{split}}(1_q^\lambda, \dots, n_{\bar{q}}^{-\lambda} \rightarrow P_\gamma^-) = \frac{z_1^{\frac{1}{2}-\lambda} z_n^{\frac{1}{2}+\lambda}}{\langle 12 \rangle \dots \langle n-1 n \rangle}. \quad (5.44)$$

⁴Diagrams where both the negative helicity fermion and gluon couple to the right-hand vertex in Fig. 5.5(b) can be mediated by either fermion or gluon exchange.

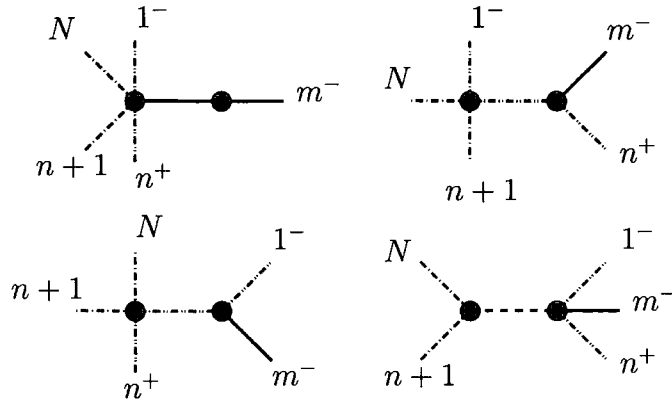


Figure 5.10: MHV topologies contributing to the two quark collinear limit of the type $\widetilde{\text{split}}(1_q^-, \dots, m^-, \dots, n_{\bar{q}}^+ \rightarrow P_\gamma^-)$. Quarks of type Q (q) are shown as green(red)-dotted lines and negative helicity gluons as black solid lines. The negative helicity photon is shown as a blue dashed line.

$$\Delta M = 1$$

For amplitudes of the $\text{Split}_+^{(n)}(m_1)$ type, there is a single MHV diagram and we find

$$\widetilde{\text{split}}(1_q^-, \dots, n_{\bar{q}}^+ \rightarrow P_\gamma^+) = \frac{1}{\sqrt{z_1 z_n} \prod_{l=1}^{n-1} \langle l, l+1 \rangle} \times \frac{\Delta_{(1)}(0, n; 1)^3 \Delta_{(1)}(0, n; n)}{D(0, n; q_{1,n})}. \quad (5.45)$$

As in the previous case, there are four diagrams shown in Fig. 5.10 contributing to splitting functions of $\text{Split}_-^{(n)}(m_1, m_2)$ type such that,

$$\begin{aligned} \widetilde{\text{split}}(1_q^-, \dots, m^-, \dots, n_{\bar{q}}^+ \rightarrow P_\gamma^-) &= \frac{1}{\sqrt{z_1 z_n} \prod_{l=1}^{n-1} \langle l, l+1 \rangle} \\ &\times \left[\sum_{i=1}^{m-1} \sum_{j=m}^{n-1} \frac{\Delta_{(1)}(i, j; m)^4 \sqrt{z_1}^3 \sqrt{z_n}}{D(i, j; q_{i+1,j})} - \sum_{i=1}^{m-1} \frac{\langle n m \rangle \Delta_{(1)}(i, n; m)^3}{D(i, n; q_{i+1,n})} \sqrt{z_1}^3 \left(\sum_{k=i+1}^n z_k \right) \right. \\ &\quad \left. - \sum_{j=m}^{n-1} \frac{\langle 1 m \rangle^3 \Delta_{(1)}(0, j; m)}{D(0, j; q_{1,j})} \sqrt{z_n} \left(\sum_{k=1}^j z_k \right)^3 + \frac{\langle 1 m \rangle^3 \langle n m \rangle}{D(0, n; q_{1,n})} \right]. \quad (5.46) \end{aligned}$$

5.4.5 Three quarks in the collinear set: $q(ng)\bar{Q}Q \rightarrow q$

In this configuration, the \bar{Q} is adjacent with Q and therefore the vertices in the MHV rules include the four-quark amplitudes of eqs. (4.15)–(4.18). The factorised amplitude is a two-quark MHV as given in eq. (4.12). Furthermore, since the helicity of q is conserved and the helicities of Q and \bar{Q} are opposite, there are no $\Delta M = 0$ splitting functions.

$$\Delta M = 1$$

For $\Delta M = 1$, the two diagrams (with quark and gluons exchanged) of $\text{Split}_+^{(n)}(m_1)$ -type yield,

$$\begin{aligned} \text{split}(1_q^+, \dots, s_{\bar{Q}}^-, (s+1)_{\bar{Q}}^+, \dots, n^+ \rightarrow P_q^+) &= \frac{1}{\sqrt{z_1 z_n} \prod_{l=1}^{n-1} \langle l, l+1 \rangle} \\ &\times \left[\sum_{i=1}^{s-1} \sum_{j=s+1}^n \frac{\Delta_{(1)}(i, j; s+1) \Delta_{(1)}^3(i, j; s)}{D(i, j, q_{i+1, j})} \sqrt{z_1} \right. \\ &\left. - \sum_{j=s+1}^n \frac{\langle 1 s \rangle \Delta_{(1)}^2(0, j; s) \Delta_{(1)}(0, j; s+1)}{D(0, j, q_{1, j})} \left(\sum_{k=1}^j z_k \right) \right], \quad (5.47) \end{aligned}$$

$$\begin{aligned} \text{split}(1_q^+, \dots, s_{\bar{Q}}^+, (s+1)_{\bar{Q}}^-, \dots, n^+ \rightarrow P_q^+) &= \frac{1}{\sqrt{z_1 z_n} \prod_{l=1}^{n-1} \langle l, l+1 \rangle} \\ &\times \left[\sum_{i=1}^{s-1} \sum_{j=s+1}^n \frac{\Delta_{(1)}^3(i, j; s+1) \Delta_{(1)}(i, j; s)}{D(i, j, q_{i+1, j})} \sqrt{z_1} \right. \\ &\left. - \sum_{j=s+1}^n \frac{\langle 1 s \rangle \Delta_{(1)}^3(0, j; s+1)}{D(0, j, q_{1, j})} \left(\sum_{k=1}^j z_k \right) \right]. \quad (5.48) \end{aligned}$$

Similarly, the two diagrams of $\text{Split}_-^{(n)}(m_1, m_2)$ -type yield,

$$\begin{aligned} \text{split}(1_q^-, \dots, s_{\bar{Q}}^-, (s+1)_{\bar{Q}}^+, \dots, n^+ \rightarrow P_q^-) &= \frac{1}{\sqrt{z_1 z_n} \prod_{l=1}^{n-1} \langle l, l+1 \rangle} \\ &\times \left[\sum_{i=1}^{s-1} \sum_{j=s+1}^n \frac{\Delta_{(1)}(i, j; s+1) \Delta_{(1)}^3(i, j; s)}{D(i, j, q_{i+1, j})} \sqrt{z_1}^3 \right. \\ &\left. - \sum_{j=s+1}^n \frac{\langle 1 s \rangle^3 \Delta_{(1)}(0, j; s+1)}{D(0, j, q_{1, j})} \left(\sum_{k=1}^j z_k \right)^3 \right], \end{aligned} \quad (5.49)$$

$$\begin{aligned} \text{split}(1_q^-, \dots, s_{\bar{Q}}^+, (s+1)_{\bar{Q}}^-, \dots, n^+ \rightarrow P_q^-) &= \frac{1}{\sqrt{z_1 z_n} \prod_{l=1}^{n-1} \langle l, l+1 \rangle} \\ &\times \left[\sum_{i=1}^{s-1} \sum_{j=s+1}^n \frac{\Delta_{(1)}^3(i, j; s+1) \Delta_{(1)}(i, j; s)}{D(i, j, q_{i+1, j})} \sqrt{z_1}^3 \right. \\ &\left. - \sum_{j=s+1}^n \frac{\langle 1 s \rangle \langle 1 s+1 \rangle^2 \Delta_{(1)}(0, j; s+1)}{D(0, j, q_{1, j})} \left(\sum_{k=1}^j z_k \right)^3 \right]. \end{aligned} \quad (5.50)$$

5.4.6 Three quarks in the collinear set: $q(ng)\bar{q}Q \rightarrow Q$

Here the relevant vertices in the MHV rules include the \tilde{A} four-quark amplitudes of eqs. (4.19)–(4.22) and the factorised amplitude is a two-quark MHV as given in eq. (4.12). As in the previous case, the quark helicities are constrained such that there are no $\Delta M = 0$ splitting functions.

$\Delta M = 1$

There are two diagrams for both $\text{Split}_+^{(n)}(m_1)$ - and $\text{Split}_-^{(n)}(m_1, m_2)$ -types and we find,

$$\begin{aligned}
\widetilde{\text{split}}(1_q^+, \dots, s_{\bar{q}}^-, (s+1)_Q^+, \dots, n^+ \rightarrow P_Q^+) &= \frac{1}{\sqrt{z_1 z_n} \prod_{l=1}^{n-1} \langle l, l+1 \rangle} \\
&\times \left[\frac{\Delta_{(1)}(0, s; 1) \Delta_{(1)}^3(0, s; s)}{D(0, s, q_{1,s})} \sqrt{z_{s+1}} \right. \\
&+ \left. \sum_{j=s+1}^n \frac{\langle s s+1 \rangle \Delta_{(1)}^2(0, j; s) \Delta_{(1)}(0, j; 1)}{D(0, j, q_{1,j})} \left(\sum_{k=1}^j z_k \right) \right], \quad (5.51)
\end{aligned}$$

$$\begin{aligned}
\widetilde{\text{split}}(1_q^-, \dots, s_{\bar{q}}^+, (s+1)_Q^+, \dots, n^+ \rightarrow P_Q^+) &= \frac{1}{\sqrt{z_1 z_n} \prod_{l=1}^{n-1} \langle l, l+1 \rangle} \\
&\times \left[\frac{\Delta_{(1)}^3(0, s; 1) \Delta_{(1)}(0, s; s)}{D(0, s, q_{1,s})} \sqrt{z_{s+1}} \right. \\
&+ \left. \sum_{j=s+1}^n \frac{\langle s s+1 \rangle \Delta_{(1)}^3(0, j; 1)}{D(0, j, q_{1,j})} \left(\sum_{k=1}^j z_k \right) \right], \quad (5.52)
\end{aligned}$$

and,

$$\begin{aligned}
\widetilde{\text{split}}(1_q^+, \dots, s_{\bar{q}}^-, (s+1)_Q^-, \dots, n^+ \rightarrow P_Q^-) &= \frac{1}{\sqrt{z_1 z_n} \prod_{l=1}^{n-1} \langle l, l+1 \rangle} \\
&\times \left[\frac{\Delta_{(1)}^3(0, s; 1) \Delta_{(1)}(0, s; s)}{D(0, s, q_{1,s})} \sqrt{z_{s+1}}^3 \right. \\
&+ \left. \sum_{j=s+1}^n \frac{\langle s s+1 \rangle^3 \Delta_{(1)}(0, j; 1)}{D(0, j, q_{1,j})} \left(\sum_{k=1}^j z_k \right)^3 \right], \quad (5.53)
\end{aligned}$$

$$\begin{aligned}
\widetilde{\text{split}}(1_q^-, \dots, s_{\bar{q}}^+, (s+1)_Q^-, \dots, n^+ \rightarrow P_Q^-) &= \frac{1}{\sqrt{z_1 z_n} \prod_{l=1}^{n-1} \langle l, l+1 \rangle} \\
&\times \left[\frac{\Delta_{(1)}^3(0, s; 1) \Delta_{(1)}(0, s; s)}{D(0, s, q_{1,s})} \sqrt{z_{s+1}}^3 \right. \\
&+ \left. \sum_{j=s+1}^n \frac{\langle s s+1 \rangle \langle 1 s+1 \rangle^2 \Delta_{(1)}(0, j; 1)}{D(0, j, q_{1,j})} \left(\sum_{k=1}^j z_k \right)^3 \right]. \quad (5.54)
\end{aligned}$$

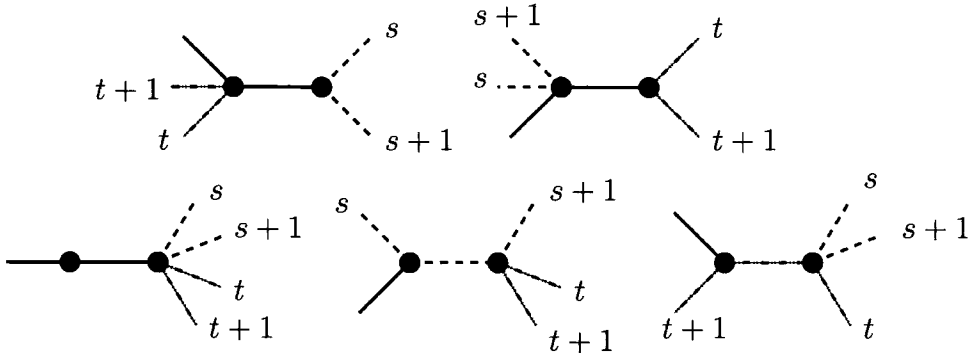


Figure 5.11: MHV topologies contributing to the four quark collinear limit of the type $\text{split}(1^+, \dots, s_Q^\lambda, (s+1)_Q^{-\lambda}, \dots, t_{\bar{q}}^{\lambda'}, (t+1)_{\bar{q}}^{-\lambda'}, \dots, n^+ \rightarrow P^-)$. Quarks of type Q (q) are shown as green (red)-dotted-dashed lines and negative helicity gluons as black solid lines.

5.4.7 Four quarks in the collinear set: $\bar{Q}Q(n_g)\bar{q}q \rightarrow g$

This limit is associated with the four-quark A -type colour ordered amplitude and is obtained by factoring onto a gluonic MHV.

$$\Delta M = 1$$

Because of helicity conservation for the quarks, $\Delta M = 0$ is forbidden. Furthermore, at least two negative helicity quarks participate in the scattering so that $\Delta M = 1$ splittings must be of the $\text{Split}_-^{(n)}(m_1, m_2)$ -type. The five contributing diagrams are shown in Fig. 5.11. Explicit evaluation of the four independent helicity configurations yields,

$$\begin{aligned} \text{split}(1^+, \dots, s_Q^+, (s+1)_Q^-, \dots, t_{\bar{q}}^-, (t+1)_q^+, \dots, n^+ \rightarrow P^-) &= \frac{1}{\sqrt{z_1 z_n} \prod_{l=1}^{n-1} \langle l, l+1 \rangle} \\ &\times \left[\sum_{i=0}^{s-1} \sum_{j=s+1}^{t-1} \frac{\Delta_{(1)}(i, j; s) \Delta_{(1)}^3(i, j; s+1)}{D(i, j, q_{i+1, j})} \sqrt{z_t}^3 \sqrt{z_{t+1}} \right] \end{aligned}$$

$$\begin{aligned}
& + \sum_{i=s+1}^{t-1} \sum_{j=t+1}^n \frac{\Delta_{(1)}^3(i, j; t) \Delta_{(1)}(i, j; t+1)}{D(i, j, q_{i+1, j})} \sqrt{z_s} \sqrt{z_{s+1}}^3 \\
& + \sum_{i=0}^{s-1} \sum_{j=t+1}^n \frac{\langle s+1 t \rangle^3 \langle s t+1 \rangle}{D(i, j, q_{i+1, j})} \left(\sum_{k=i+1}^j z_k \right)^4 \\
& - \sum_{j=t+1}^n \frac{\Delta_{(1)}(s, j; t+1) \langle s+1 t \rangle^3}{D(s, j, q_{s+1, j})} \sqrt{z_s} \left(\sum_{k=s+1}^j z_k \right)^3 \\
& + \sum_{i=0}^{s-1} \frac{\Delta_{(1)}(i, t; s) \langle s+1 t \rangle^3}{D(i, t, q_{i+1, t})} \sqrt{z_{t+1}} \left(\sum_{k=i+1}^t z_k \right)^3 \Big], \quad (5.55)
\end{aligned}$$

$$\begin{aligned}
\text{split}(1^+, \dots, s_{\bar{Q}}^-, (s+1)_{\bar{Q}}^+, \dots, t_{\bar{q}}^-, (t+1)_{\bar{q}}^+, \dots, n^+ \rightarrow P^-) &= \frac{1}{\sqrt{z_1 z_n} \prod_{l=1}^{n-1} \langle l, l+1 \rangle} \\
& \times \left[\sum_{i=0}^{s-1} \sum_{j=s+1}^{t-1} \frac{\Delta_{(1)}^3(i, j; s) \Delta_{(1)}(i, j; s+1)}{D(i, j, q_{i+1, j})} \sqrt{z_t}^3 \sqrt{z_{t+1}} \right. \\
& + \sum_{i=s+1}^{t-1} \sum_{j=t+1}^n \frac{\Delta_{(1)}^3(i, j; t) \Delta_{(1)}(i, j; t+1)}{D(i, j, q_{i+1, j})} \sqrt{z_s}^3 \sqrt{z_{s+1}} \\
& + \sum_{i=0}^{s-1} \sum_{j=t+1}^n \frac{\langle s+1 t \rangle \langle s t+1 \rangle \langle t s \rangle^2}{D(i, j, q_{i+1, j})} \left(\sum_{k=i+1}^j z_k \right)^4 \\
& - \sum_{j=t+1}^n \frac{\Delta_{(1)}(s, j; t+1) \Delta_{(1)}^2(s, j; t) \langle s+1 t \rangle}{D(s, j, q_{s+1, j})} \sqrt{z_s}^3 \left(\sum_{k=s+1}^j z_k \right) \\
& \left. + \sum_{i=0}^{s-1} \frac{\Delta_{(1)}(i, t; s) \langle s+1 t \rangle \langle t s \rangle^2}{D(i, t, q_{i+1, t})} \sqrt{z_{t+1}} \left(\sum_{k=i+1}^t z_k \right)^3 \right], \quad (5.56)
\end{aligned}$$

$$\begin{aligned}
\text{split}(1^+, \dots, s_{\bar{Q}}^+, (s+1)_{\bar{Q}}^-, \dots, t_{\bar{q}}^+, (t+1)_{\bar{q}}^-, \dots, n^+ \rightarrow P^-) &= \frac{1}{\sqrt{z_1 z_n} \prod_{l=1}^{n-1} \langle l, l+1 \rangle} \\
& \times \left[\sum_{i=0}^{s-1} \sum_{j=s+1}^{t-1} \frac{\Delta_{(1)}(i, j; s) \Delta_{(1)}^3(i, j; s+1)}{D(i, j, q_{i+1, j})} \sqrt{z_t} \sqrt{z_{t+1}}^3 \right. \\
& + \sum_{i=s+1}^{t-1} \sum_{j=t+1}^n \frac{\Delta_{(1)}(i, j; t) \Delta_{(1)}^3(i, j; t+1)}{D(i, j, q_{i+1, j})} \sqrt{z_s} \sqrt{z_{s+1}}^3
\end{aligned}$$

$$\begin{aligned}
& + \sum_{i=0}^{s-1} \sum_{j=t+1}^n \frac{\langle s+1t \rangle \langle st+1 \rangle \langle s+1t+1 \rangle^2}{D(i, j, q_{i+1, j})} \left(\sum_{k=i+1}^j z_k \right)^4 \\
& - \sum_{j=t+1}^n \frac{\Delta_{(1)}(s, j; t+1) \langle s+1t \rangle \langle s+1t+1 \rangle^2}{D(s, j, q_{s+1, j})} \sqrt{z_s} \left(\sum_{k=s+1}^j z_k \right)^3 \\
& + \sum_{i=0}^{s-1} \frac{\Delta_{(1)}(i, t; s) \Delta_{(1)}^2(i, t; s+1) \langle s+1t \rangle}{D(i, t, q_{i+1, t})} \sqrt{z_{t+1}}^3 \left(\sum_{k=i+1}^t z_k \right) \Big], \tag{5.57}
\end{aligned}$$

$$\begin{aligned}
\text{split}(1^+, \dots, s_{\bar{Q}}^-, (s+1)_{\bar{Q}}^+, \dots, t_{\bar{q}}^+, (t+1)_{\bar{q}}^-, \dots, n^+ \rightarrow P^-) &= \frac{1}{\sqrt{z_1 z_n} \prod_{l=1}^{n-1} \langle l, l+1 \rangle} \\
& \times \left[\sum_{i=0}^{s-1} \sum_{j=s+1}^{t-1} \frac{\Delta_{(1)}^3(i, j; s) \Delta_{(1)}(i, j; s+1)}{D(i, j, q_{i+1, j})} \sqrt{z_t} \sqrt{z_{t+1}}^3 \right. \\
& + \sum_{i=s+1}^{t-1} \sum_{j=t+1}^n \frac{\Delta_{(1)}(i, j; t) \Delta_{(1)}^3(i, j; t+1)}{D(i, j, q_{i+1, j})} \sqrt{z_s}^3 \sqrt{z_{s+1}} \\
& + \sum_{i=0}^{s-1} \sum_{j=t+1}^n \frac{\langle s+1t \rangle \langle st+1 \rangle^3}{D(i, j, q_{i+1, j})} \left(\sum_{k=i+1}^j z_k \right)^4 \\
& - \sum_{j=t+1}^n \frac{\Delta_{(1)}^3(s, j; t+1) \langle s+1t \rangle}{D(s, j, q_{s+1, j})} \sqrt{z_s}^3 \left(\sum_{k=s+1}^j z_k \right) \\
& \left. + \sum_{i=0}^{s-1} \frac{\Delta_{(1)}^3(i, t; s) \langle s+1t \rangle}{D(i, t, q_{i+1, t})} \sqrt{z_{t+1}}^3 \left(\sum_{k=i+1}^t z_k \right) \right]. \tag{5.58}
\end{aligned}$$

5.4.8 Four quarks in the collinear set: $\bar{Q}q(ng)\bar{q}Q \rightarrow g$

This limit is associated with the four-quark \tilde{A} -type colour ordered amplitude and is obtained by factoring onto a gluonic MHV.

$$\Delta M = 1$$

As in the previous case, helicity conservation for the quarks, ensures that $\Delta M = 0$ is forbidden and that $\text{Split}_+^{(n)}(m_1)$ -type $\Delta M = 1$ splittings are absent. The four

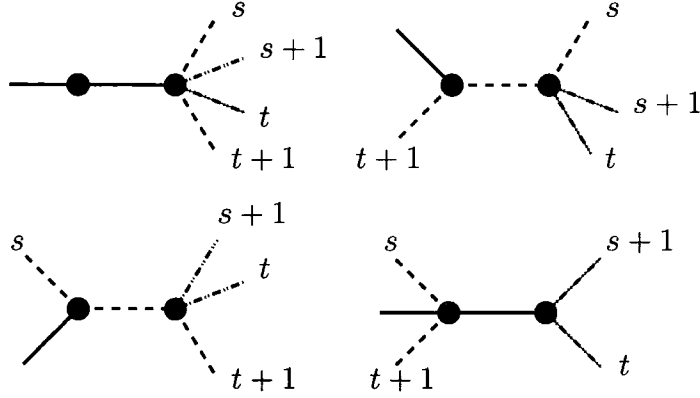


Figure 5.12: MHV topologies contributing to the four quark collinear limit of the type $\widetilde{\text{split}}(1^+, \dots, s_Q^\lambda, (s+1)_q^{-\lambda'}, \dots, t_q^{\lambda'}, (t+1)_Q^{-\lambda}, \dots, n^+ \rightarrow P^-)$. Quarks of type Q (q) are shown as green(red)-dotted-dashed lines and negative helicity gluons as black solid lines.

contributing diagrams of $\text{Split}_-^{(n)}(m_1, m_2)$ -type are shown in Fig. 5.12.

The four independent helicity configurations are given by,

$$\begin{aligned}
 \widetilde{\text{split}}(1^+, \dots, s_Q^+, (s+1)_q^+, \dots, t_q^-, (t+1)_Q^-, \dots, n^+ \rightarrow P^-) &= \frac{1}{\sqrt{z_1 z_n} \prod_{l=1}^{n-1} \langle l, l+1 \rangle} \\
 &\times \left[\sum_{i=0}^{s-1} \sum_{j=t+1}^n \frac{\langle t+1 t \rangle^3 \langle s s+1 \rangle}{D(i, j, q_{i+1, j})} \left(\sum_{k=i+1}^j z_k \right)^4 \right. \\
 &- \sum_{j=t+1}^n \frac{\Delta_{(1)}(s, j; s+1) \langle t+1 t \rangle^3}{D(s, j, q_{s+1, j})} \sqrt{z_s} \left(\sum_{k=s+1}^j z_k \right)^3 \\
 &- \sum_{i=0}^{s-1} \frac{\Delta_{(1)}^3(i, t; t) \langle s s+1 \rangle}{D(i, t, q_{i+1, t})} \sqrt{z_{t+1}}^3 \left(\sum_{k=i+1}^t z_k \right) \\
 &\left. + \frac{\Delta_{(1)}^3(s, t; t) \Delta_{(1)}(s, t; s+1)}{D(s, t, q_{s+1, t})} \sqrt{z_s} \sqrt{z_{t+1}}^3 \right], \quad (5.59)
 \end{aligned}$$

$$\begin{aligned}
 \widetilde{\text{split}}(1^+, \dots, s_Q^+, (s+1)_q^-, \dots, t_q^+, (t+1)_Q^-, \dots, n^+ \rightarrow P^-) &= \frac{1}{\sqrt{z_1 z_n} \prod_{l=1}^{n-1} \langle l, l+1 \rangle} \\
 &\times \left[\sum_{i=0}^{s-1} \sum_{j=t+1}^n \frac{\langle t+1 t \rangle \langle s s+1 \rangle \langle s+1 t+1 \rangle^2}{D(i, j, q_{i+1, j})} \left(\sum_{k=i+1}^j z_k \right)^4 \right.
 \end{aligned}$$

$$\begin{aligned}
& - \sum_{j=t+1}^n \frac{\Delta_{(1)}(s, j; s+1) \langle t+1 t \rangle \langle s+1 t+1 \rangle^2}{D(s, j, q_{s+1, j})} \sqrt{z_s} \left(\sum_{k=s+1}^j z_k \right)^3 \\
& - \sum_{i=0}^{s-1} \frac{\Delta_{(1)}(i, t; t) \Delta_{(1)}^2(i, t; s+1) \langle s s+1 \rangle}{D(i, t, q_{i+1, t})} \sqrt{z_{t+1}}^3 \left(\sum_{k=i+1}^t z_k \right) \\
& + \frac{\Delta_{(1)}(s, t; t) \Delta_{(1)}^3(s, t; s+1)}{D(s, t, q_{s+1, t})} \sqrt{z_s} \sqrt{z_{t+1}}^3, \tag{5.60}
\end{aligned}$$

$$\begin{aligned}
\widetilde{\text{split}}(1^+, \dots, s_{\bar{Q}}^-, (s+1)_q^+, \dots, t_{\bar{q}}^-, (t+1)_Q^+, \dots, n^+ \rightarrow P^-) &= \frac{1}{\sqrt{z_1 z_n} \prod_{l=1}^{n-1} \langle l, l+1 \rangle} \\
& \times \left[\sum_{i=0}^{s-1} \sum_{j=t+1}^n \frac{\langle t+1 t \rangle \langle s s+1 \rangle \langle t s \rangle^2}{D(i, j, q_{i+1, j})} \left(\sum_{k=i+1}^j z_k \right)^4 \right. \\
& - \sum_{j=t+1}^n \frac{\Delta_{(1)}(s, j; s+1) \Delta_{(1)}^2(s, j; t) \langle t+1 t \rangle}{D(s, j, q_{s+1, j})} \sqrt{z_s}^3 \left(\sum_{k=s+1}^j z_k \right) \\
& - \sum_{i=0}^{s-1} \frac{\Delta_{(1)}(i, t; t) \langle s s+1 \rangle \langle t s \rangle^2}{D(i, t, q_{i+1, t})} \sqrt{z_{t+1}} \left(\sum_{k=i+1}^t z_k \right)^3 \\
& \left. + \frac{\Delta_{(1)}^3(s, t; t) \Delta_{(1)}(s, t; s+1)}{D(s, t, q_{s+1, t})} \sqrt{z_s}^3 \sqrt{z_{t+1}} \right], \tag{5.61}
\end{aligned}$$

$$\begin{aligned}
\widetilde{\text{split}}(1^+, \dots, s_{\bar{Q}}^-, (s+1)_q^-, \dots, t_{\bar{q}}^+, (t+1)_Q^+, \dots, n^+ \rightarrow P^-) &= \frac{1}{\sqrt{z_1 z_n} \prod_{l=1}^{n-1} \langle l, l+1 \rangle} \\
& \times \left[\sum_{i=0}^{s-1} \sum_{j=t+1}^n \frac{\langle t+1 t \rangle \langle s s+1 \rangle^3}{D(i, j, q_{i+1, j})} \left(\sum_{k=i+1}^j z_k \right)^4 \right. \\
& - \sum_{j=t+1}^n \frac{\Delta_{(1)}^3(s, j; s+1) \langle t+1 t \rangle}{D(s, j, q_{s+1, j})} \sqrt{z_s}^3 \left(\sum_{k=s+1}^j z_k \right) \\
& - \sum_{i=0}^{s-1} \frac{\Delta_{(1)}(i, t; t) \langle s s+1 \rangle^3}{D(i, t, q_{i+1, t})} \sqrt{z_{t+1}} \left(\sum_{k=i+1}^t z_k \right)^3 \\
& \left. + \frac{\Delta_{(1)}(s, t; t) \Delta_{(1)}^3(s, t; s+1)}{D(s, t, q_{s+1, t})} \sqrt{z_s}^3 \sqrt{z_{t+1}} \right]. \tag{5.62}
\end{aligned}$$

5.5 Specific results

5.5.1 Purely gluonic $n \leq 6$.

In this section we present compact expressions for splitting amplitudes with up to six collinear gluons. These results are obtained directly from the general expressions given in Section 5.4.1.

First we note that splitting amplitudes satisfy reflection symmetry,

$$\text{split}(1^{\lambda_1}, \dots, n^{\lambda_n} \rightarrow P^\pm) = (-1)^{n+1} \text{split}(n^{\lambda_n}, \dots, 1^{\lambda_1} \rightarrow P^\pm) \quad (5.63)$$

and the dual Ward identity, see e.g. [137],

$$\begin{aligned} & \text{split}(1^{\lambda_1}, 2^{\lambda_2}, \dots, n^{\lambda_n} \rightarrow P^\pm) + \text{split}(2^{\lambda_2}, 1^{\lambda_1}, \dots, n^{\lambda_n} \rightarrow P^\pm) + \dots \\ & + \text{split}(2^{\lambda_2}, \dots, 1^{\lambda_1}, n^{\lambda_n} \rightarrow P^\pm) + \text{split}(2^{\lambda_2}, \dots, n^{\lambda_n}, 1^{\lambda_1} \rightarrow P^\pm) = 0. \end{aligned} \quad (5.64)$$

These relations reduce the number of independent splitting amplitudes significantly.

$n = 2$

For two collinear gluons there are two independent splitting amplitudes with $\Delta M = 0$. All others can be obtained by parity and reflection. Setting $z_1 = z$ and $z_2 = (1 - z)$, we find

$$\text{split}(1^+, 2^+ \rightarrow P^+) = \frac{1}{\sqrt{z(1-z)} \langle 12 \rangle}, \quad (5.65)$$

$$\text{split}(1^-, 2^+ \rightarrow P^-) = \frac{z^2}{\sqrt{z(1-z)} \langle 12 \rangle}. \quad (5.66)$$

As expected, the splitting amplitudes have a single pole proportional to $\langle 12 \rangle^{-1}$. Note that in the soft limit $z \rightarrow 0$, we see that helicity conservation ensures that $\text{split}(1^-, 2^+ \rightarrow P^-) \rightarrow 0$.

$n = 3$ result from MHV rules

For three collinear gluons there are three independent splitting amplitudes with $\Delta M = 0$. They all follow directly from a single MHV vertex and are given by

$$\begin{aligned} \text{split}(1^+, 2^+, 3^+ \rightarrow P^+) &= \frac{1}{\sqrt{z_1 z_3} \langle 12 \rangle \langle 23 \rangle}, \\ \text{split}(1^-, 2^+, 3^+ \rightarrow P^-) &= \frac{z_1^2}{\sqrt{z_1 z_3} \langle 12 \rangle \langle 23 \rangle}, \\ \text{split}(1^+, 2^-, 3^+ \rightarrow P^-) &= \frac{z_2^2}{\sqrt{z_1 z_3} \langle 12 \rangle \langle 23 \rangle}. \end{aligned}$$

Parity and the reflection symmetry, $\text{split}(1^+, 2^+, 3^- \rightarrow P^-) = \text{split}(3^-, 2^+, 1^+ \rightarrow P^-)$, give the rest.

When $\Delta M = 1$, there are three amplitudes,

$$\begin{aligned} \text{split}(1^-, 2^+, 3^+ \rightarrow P^+) &= \frac{\langle 12 \rangle z_2^2}{\sqrt{z_1 z_2 z_3} s_{1,2} (z_1 + z_2) (\langle 13 \rangle \sqrt{z_1} + \langle 23 \rangle \sqrt{z_2})} \\ &+ \frac{(\langle 12 \rangle \sqrt{z_2} + \langle 13 \rangle \sqrt{z_3})^3}{s_{1,3} \langle 12 \rangle \langle 23 \rangle (\langle 13 \rangle \sqrt{z_1} + \langle 23 \rangle \sqrt{z_2})}, \end{aligned} \quad (5.67)$$

$$\begin{aligned} \text{split}(1^+, 2^-, 3^+ \rightarrow P^+) &= -\text{split}(2^-, 1^+, 3^+ \rightarrow P^+) - \text{split}(1^+, 3^+, 2^- \rightarrow P^+) \\ &= \frac{\langle 12 \rangle z_1^2}{\sqrt{z_1 z_2 z_3} s_{1,2} (z_1 + z_2) (\langle 13 \rangle \sqrt{z_1} + \langle 23 \rangle \sqrt{z_2})} \\ &+ \frac{(\langle 21 \rangle \sqrt{z_1} + \langle 23 \rangle \sqrt{z_3})^4}{s_{1,3} \langle 12 \rangle \langle 23 \rangle (\langle 13 \rangle \sqrt{z_1} + \langle 23 \rangle \sqrt{z_2}) (\langle 12 \rangle \sqrt{z_2} + \langle 13 \rangle \sqrt{z_3})} \\ &+ \frac{\langle 23 \rangle z_3^2}{\sqrt{z_1 z_2 z_3} s_{2,3} (z_2 + z_3) (\langle 12 \rangle \sqrt{z_2} + \langle 13 \rangle \sqrt{z_3})}, \end{aligned} \quad (5.68)$$

$$\text{split}(1^+, 2^+, 3^- \rightarrow P^+) = \text{split}(3^-, 2^+, 1^+ \rightarrow P^+) . \quad (5.69)$$

In addition to singular terms like $\langle 12 \rangle$, we see that the splitting functions contain mixed terms like $s_{1,3}$. The net singularity is schematically of the form $[] \langle \rangle$.

Note that $\text{split}(1^-, 2^+, 3^+ \rightarrow P^+)$ contains poles in $s_{1,2}$ and the triple invariant $s_{1,3} = s_{123}$ but not in $s_{2,3}$. This is because there is no MHV rule graph with a three-point vertex involving two positive helicity gluons.

Expressions for these splitting functions are given in Eq. (5.52) of Ref. [137]. The results given here are more compact and have a rather different analytic form. After adjusting the normalisation of the colour matrices, the splitting functions of Eqs. (5.67)–(5.68) numerically agree with those of Ref. [137].

$n = 3$ result from the BCF recursion relation

We now want to rederive the above results using the BCF recursion relation of [115]. In doing this we will (a) draw some useful comparisons between the ‘BCF recursion’ and the ‘MHV rules’ formalisms from the perspective of collinear amplitudes; and (b) test our expressions, such as Eq. (5.67) for $\text{split}(1^-, 2^+, 3^+ \rightarrow P^+)$.

We start with the six-point amplitude $A(1^-, 2^+, 3^+, 4^+, 5^-, 6^-)$, which we have calculated in section 4.6. The full amplitude reads

$$A(1^-, 2^+, 3^+, 4^+, 5^-, 6^-) = \frac{1}{\langle 3|1+2|6 \rangle} \left(\frac{\langle 5|6+1|2 \rangle^3}{[61][12]\langle 34 \rangle \langle 45 \rangle s_{3,5}} + \frac{\langle 1|2+3|4 \rangle^3}{[45][56]\langle 12 \rangle \langle 23 \rangle s_{1,3}} \right) , \quad (5.70)$$

where the two terms on the right hand side correspond to the first and third BCF diagrams⁵ of Fig. 4.6. We now note that in this particular collinear limit, only

⁵The second diagram in Fig. 4.6 is zero.

the last of these diagrams contains an on-shell propagator, $1/s_{23}$. Nevertheless, in distinction with the MHV rules approach which we have adopted previously, both non-zero BCF diagrams need to be taken into account in the collinear limit.

In the $1 || 2 || 3 \rightarrow P^+$ collinear limit, the first term in the amplitude becomes

$$\frac{\langle 12 \rangle z_2^2}{\sqrt{z_1 z_2 z_3} s_{1,2} (z_1 + z_2) (\langle 13 \rangle \sqrt{z_1} + \langle 23 \rangle \sqrt{z_2})} \times \frac{\langle 56 \rangle^4}{\langle 56 \rangle \langle 6P \rangle \langle P4 \rangle \langle 45 \rangle}. \quad (5.71)$$

This term factors into a contribution to the splitting amplitudes multiplied by a four-point MHV vertex. In contrast, in the collinear limit the second term factors onto the $\overline{\text{MHV}}$ type diagram, written in terms of the anti-holomorphic spinor products,

$$\frac{(\langle 12 \rangle \sqrt{z_2} + \langle 13 \rangle \sqrt{z_3})^3}{s_{1,3} \langle 12 \rangle \langle 23 \rangle (\langle 13 \rangle \sqrt{z_1} + \langle 23 \rangle \sqrt{z_2})} \times \frac{[P4]^4}{[P4][45][56][6P]}. \quad (5.72)$$

For the special case of four-point amplitudes, the $\overline{\text{MHV}}$ and MHV amplitudes coincide and we find an identical result to Eq. (5.67).

Likewise, to test our expression for $\text{split}(1^+, 2^-, 3^+ \rightarrow P^+)$ we start from Eq. (3.4) in [115];

$$\begin{aligned} A(1^+, 2^-, 3^+, 4^-, 5^+, 6^-) &= \frac{[13]^4 \langle 46 \rangle^4}{[12][23] \langle 45 \rangle \langle 56 \rangle s_{1,3} \langle 6|1+2|3 \rangle \langle 4|2+3|1 \rangle} \\ &+ \frac{\langle 26 \rangle^4 [35]^4}{\langle 61 \rangle \langle 12 \rangle [34][45] s_{3,5} \langle 6|4+5|3 \rangle \langle 2|3+4|5 \rangle} \\ &+ \frac{[15]^4 \langle 24 \rangle^4}{\langle 23 \rangle \langle 34 \rangle [56][61] s_{2,4} \langle 4|2+3|1 \rangle \langle 2|3+4|5 \rangle}. \end{aligned} \quad (5.73)$$

Taking the collinear limit $1 \parallel 2 \parallel 3 \rightarrow P^+$, we find that

$$\begin{aligned} \text{Split}(1^+, 2^-, 3^+ \rightarrow P^+) &= \frac{z_2^2 z_3^2 [1 2]}{\sqrt{z_1 z_2 z_3} s_{1,2} (z_1 + z_2) ([1 3] \sqrt{z_1} + [2 3] \sqrt{z_2})} \\ &+ \frac{[1 3]^4}{s_{1,3} [1 2] [2 3] ([1 3] \sqrt{z_1} + [2 3] \sqrt{z_2}) ([1 2] \sqrt{z_2} + [1 3] \sqrt{z_3})} \\ &+ \frac{z_1^2 z_2^2 [2 3]}{\sqrt{z_1 z_2 z_3} s_{2,3} (z_2 + z_3) ([1 2] \sqrt{z_2} + [1 3] \sqrt{z_3})}. \end{aligned} \quad (5.74)$$

This result has the same kinematic-invariant pole structure as Eq. (5.68), but otherwise is not obviously equivalent to Eq. (5.68). Note that Eq. (5.74) contains terms like $([1 2] \sqrt{z_2} + [1 3] \sqrt{z_3})$ (rather than $(\langle 1 2 \rangle \sqrt{z_2} + \langle 1 3 \rangle \sqrt{z_3})$). Despite appearances, a more careful (e.g. numerical) comparison shows that these two results, Eqs. (5.68) and (5.74), are in fact the same.

$n = 4$

For $n = 4$, there are five collinear limits coming directly from MHV amplitudes where the number of gluons with negative helicity doesn't change, $\Delta M = 0$,

$$\text{split}(1^+, 2^+, 3^+, 4^+ \rightarrow P^+) = \frac{1}{\sqrt{z_1 z_4} \langle 1 2 \rangle \langle 2 3 \rangle \langle 3 4 \rangle}, \quad (5.75)$$

$$\text{split}(1^-, 2^+, 3^+, 4^+ \rightarrow P^-) = \frac{z_1^2}{\sqrt{z_1 z_4} \langle 1 2 \rangle \langle 2 3 \rangle \langle 3 4 \rangle}, \quad (5.76)$$

$$\text{split}(1^+, 2^-, 3^+, 4^+ \rightarrow P^-) = \frac{z_2^2}{\sqrt{z_1 z_4} \langle 1 2 \rangle \langle 2 3 \rangle \langle 3 4 \rangle}. \quad (5.77)$$

The remaining two are obtained by reflection symmetry,

$$\text{split}(1^+, 2^+, 3^-, 4^+ \rightarrow P^-) = -\text{split}(4^+, 3^-, 2^+, 1^+ \rightarrow P^-), \quad (5.78)$$

$$\text{split}(1^+, 2^+, 3^+, 4^- \rightarrow P^-) = -\text{split}(4^-, 3^+, 2^+, 1^+ \rightarrow P^-). \quad (5.79)$$

When $\Delta M = 1$, there are ten splitting amplitudes however only three are independent,

$$\begin{aligned}
\text{split}(1^-, 2^+, 3^+, 4^+ \rightarrow P^+) &= \mathcal{B}_1^+(1, 2, 3, 4) \\
&= -\frac{z_2^{3/2} \langle 12 \rangle}{\sqrt{z_1 z_4} \langle 34 \rangle s_{1,2} (z_1 + z_2) \Delta_{(1)}(0, 2; 3)} \\
&\quad + \frac{\Delta_{(1)}(0, 3; 1)^3}{\sqrt{z_4} \langle 12 \rangle \langle 23 \rangle s_{1,3} (z_1 + z_2 + z_3) \Delta_{(1)}(0, 3; 3) \Delta_{(1)}(0, 3; 4)} \\
&\quad - \frac{\Delta_{(1)}(0, 4; 1)^3}{\langle 12 \rangle \langle 23 \rangle \langle 34 \rangle s_{1,4} \Delta_{(1)}(0, 4; 4)}, \tag{5.80}
\end{aligned}$$

$$\begin{aligned}
\text{split}(1^-, 2^-, 3^+, 4^+ \rightarrow P^-) &= \mathcal{B}_2^-(1, 2, 3, 4) \\
&= -\frac{z_1^{3/2} z_3^{3/2} \langle 23 \rangle}{\sqrt{z_2 z_4} s_{2,3} \Delta_{(1)}(1, 3; 1) \Delta_{(1)}(1, 3; 4)} \\
&\quad - \frac{z_1^{3/2} \Delta_{(1)}(1, 4; 2)^3}{\langle 23 \rangle \langle 34 \rangle s_{2,4} \Delta_{(1)}(1, 4; 1) \Delta_{(1)}(1, 4; 4) (1 - z_1)} \\
&\quad - \frac{\langle 12 \rangle (z_1 + z_2)^3}{\sqrt{z_1 z_2 z_4} \langle 34 \rangle s_{1,2} \Delta_{(1)}(0, 2; 3)} \\
&\quad + \frac{\langle 12 \rangle^3 (1 - z_4)^3}{\sqrt{z_4} \langle 23 \rangle s_{1,3} \Delta_{(1)}(0, 3; 1) \Delta_{(1)}(0, 3; 3) \Delta_{(1)}(0, 3; 4)} \\
&\quad - \frac{\langle 12 \rangle^3}{s_{1,4} \Delta_{(1)}(0, 4; 1) \Delta_{(1)}(0, 4; 4) \langle 23 \rangle \langle 34 \rangle}, \tag{5.81}
\end{aligned}$$

$$\begin{aligned}
\text{split}(1^-, 2^+, 3^-, 4^+ \rightarrow P^-) &= \mathcal{B}_3^-(1, 2, 3, 4) \\
&= -\frac{z_2^{3/2} z_3^2 \langle 12 \rangle}{\sqrt{z_1 z_4} \langle 34 \rangle s_{1,2} (z_1 + z_2) \Delta_{(1)}(0, 2; 3)} \\
&\quad - \frac{z_1^{3/2} z_2^{3/2} \langle 23 \rangle}{\sqrt{z_3 z_4} s_{2,3} \Delta_{(1)}(1, 3; 1) \Delta_{(1)}(1, 3; 4)} \\
&\quad - \frac{z_1^{3/2} \Delta_{(1)}(1, 4; 3)^4}{\langle 23 \rangle \langle 34 \rangle s_{2,4} \Delta_{(1)}(1, 4; 1) \Delta_{(1)}(1, 4; 2) \Delta_{(1)}(1, 4; 4) (1 - z_1)} \\
&\quad - \frac{z_1^{3/2} \Delta_{(1)}(2, 4; 3)^3}{\langle 12 \rangle \langle 34 \rangle s_{3,4} \Delta_{(1)}(2, 4; 2) \Delta_{(1)}(2, 4; 4) (z_3 + z_4)}
\end{aligned}$$

$$\begin{aligned}
& + \frac{\langle 13 \rangle^4 (z_1 + z_2 + z_3)^3}{\sqrt{z_4} \langle 12 \rangle \langle 23 \rangle s_{1,3} \Delta_{(1)}(0, 3; 1) \Delta_{(1)}(0, 3; 3) \Delta_{(1)}(0, 3; 4)} \\
& - \frac{\langle 13 \rangle^4}{\langle 12 \rangle \langle 23 \rangle \langle 34 \rangle s_{1,4} \Delta_{(1)}(0, 4; 4) \Delta_{(1)}(0, 4; 1)}, \tag{5.82}
\end{aligned}$$

where $\Delta_{(1)}(i, j; k)$ is given in Eq. (5.10). The seven remaining $\Delta M = 1$ splitting functions can be obtained by using the dual ward identity,

$$\begin{aligned}
\text{split}(1^+, 2^-, 3^+, 4^+ \rightarrow P^+) &= -\mathcal{B}_1^+(2, 1, 3, 4) - \mathcal{B}_1^+(2, 3, 1, 4) - \mathcal{B}_1^+(2, 3, 4, 1), \\
\text{split}(1^+, 2^+, 3^-, 4^+ \rightarrow P^+) &= \mathcal{B}_1^+(3, 4, 2, 1) + \mathcal{B}_1^+(3, 2, 4, 1) + \mathcal{B}_1^+(3, 2, 1, 4), \\
\text{split}(1^-, 2^+, 3^+, 4^- \rightarrow P^-) &= \mathcal{B}_3^-(4, 3, 1, 2) + \mathcal{B}_2^-(4, 1, 3, 2) + \mathcal{B}_2^-(1, 4, 3, 2), \\
\text{split}(1^+, 2^-, 3^-, 4^+ \rightarrow P^-) &= -\mathcal{B}_3^-(2, 1, 3, 4) - \mathcal{B}_2^-(2, 3, 1, 4) - \mathcal{B}_2^-(2, 3, 4, 1), \tag{5.83}
\end{aligned}$$

or reflection symmetry,

$$\begin{aligned}
\text{split}(1^+, 2^+, 3^+, 4^- \rightarrow P^+) &= -\text{split}(4^-, 3^+, 2^+, 1^+ \rightarrow P^-), \\
\text{split}(1^+, 2^-, 3^+, 4^- \rightarrow P^-) &= -\text{split}(4^-, 3^+, 2^-, 1^+ \rightarrow P^-), \\
\text{split}(1^+, 2^+, 3^-, 4^- \rightarrow P^-) &= -\text{split}(4^-, 3^-, 2^+, 1^+ \rightarrow P^-). \tag{5.84}
\end{aligned}$$

Finally splitting functions with $\Delta M = 2, 3$ are related to those given above by the parity transformation.

Inspection of Eqs. (5.80), (5.81) and (5.82) reveal that each term is inversely proportional to a single invariant, in keeping with its MHV rules origins. For this type of collinear limit, there are potentially six invariants, the double invariants $s_{1,2}, s_{2,3}, s_{3,4}$, the triple invariants $s_{1,3}, s_{2,4}$ and $s_{1,4}$. Some poles are absent because the MHV rules forbid that type of contribution. For example, in $\text{split}(1^-, 2^+, 3^+, 4^+ \rightarrow P^+)$, there are no contributions with poles in $s_{2,3}, s_{3,4}$ or $s_{2,4}$ precisely because these poles

correspond to forbidden MHV diagrams.

Expressions for the four gluon splitting functions are given in Ref. [137]. The results given here are more compact and have a rather different analytic form. After adjusting the normalisation of the colour matrices, the splitting functions of Eqs. (5.80)–(5.82) numerically agree with those of Ref. [137].

$n = 5$

In total there are 64 different splitting amplitudes, but only eleven are independent. The rest can be obtained with the help of parity, reflection and dual ward identities.

The simplest independent collinear limits can be obtained using only MHV rules,

$$\text{split}(1^+, 2^+, 3^+, 4^+, 5^+ \rightarrow P^+) = \frac{1}{\sqrt{z_1 z_5} \langle 1 2 \rangle \langle 2 3 \rangle \langle 3 4 \rangle \langle 4 5 \rangle}$$

$$\text{split}(1^-, 2^+, 3^+, 4^+, 5^+ \rightarrow P^-) = \frac{z_1^2}{\sqrt{z_1 z_5} \langle 1 2 \rangle \langle 2 3 \rangle \langle 3 4 \rangle \langle 4 5 \rangle}$$

$$\text{split}(1^+, 2^-, 3^+, 4^+, 5^+ \rightarrow P^-) = \frac{z_2^2}{\sqrt{z_1 z_5} \langle 1 2 \rangle \langle 2 3 \rangle \langle 3 4 \rangle \langle 4 5 \rangle}$$

$$\text{split}(1^+, 2^+, 3^-, 4^+, 5^+ \rightarrow P^-) = \frac{z_3^2}{\sqrt{z_1 z_5} \langle 1 2 \rangle \langle 2 3 \rangle \langle 3 4 \rangle \langle 4 5 \rangle}$$

$$\text{split}(1^+, 2^+, 3^+, 4^-, 5^+ \rightarrow P^-) = \text{split}(5^+, 4^-, 3^+, 2^+, 1^+ \rightarrow P^-)$$

$$\text{split}(1^+, 2^+, 3^+, 4^+, 5^- \rightarrow P^-) = \text{split}(5^-, 4^+, 3^+, 2^+, 1^+ \rightarrow P^-)$$

$$\begin{aligned}
\text{split}(1^-, 2^+, 3^+, 4^+, 5^+ \rightarrow P^+) &= C_1^+(1, 2, 3, 4, 5) \\
&= \frac{(\Delta_{(1)}(0, 2; 1))^3 \sqrt{z_1}}{\sqrt{z_1 z_5} \langle 12 \rangle \langle 34 \rangle \langle 45 \rangle s_{1,2}(z_1 + z_2) \Delta_{(1)}(0, 2; 2) \Delta_{(1)}(0, 2; 3)} \\
&+ \frac{(\Delta_{(1)}(0, 3; 1))^3 \sqrt{z_1}}{\sqrt{z_1 z_5} \langle 12 \rangle \langle 23 \rangle \langle 45 \rangle s_{1,3}(z_1 + z_2 + z_3) \Delta_{(1)}(0, 3; 3) \Delta_{(1)}(0, 3; 4)} \\
&+ \frac{(\Delta_{(1)}(0, 4; 1))^3 \sqrt{z_1}}{\sqrt{z_1 z_5} \langle 12 \rangle \langle 23 \rangle \langle 34 \rangle s_{1,4}(z_1 + z_2 + z_3 + z_4) \Delta_{(1)}(0, 4; 4) \Delta_{(1)}(0, 4; 5)} \\
&- \frac{(\Delta_{(1)}(0, 5; 1))^3}{\langle 12 \rangle \langle 23 \rangle \langle 34 \rangle \langle 45 \rangle s_{1,5} \Delta_{(1)}(0, 5; 5)} \tag{5.85}
\end{aligned}$$

$$\begin{aligned}
\text{split}(1^+, 2^-, 3^+, 4^+, 5^+ \rightarrow P^+) &= C_2^+(1, 2, 3, 4, 5) \\
&= \frac{(\Delta_{(1)}(0, 2; 2))^3 \sqrt{z_1}}{\sqrt{z_1 z_5} \langle 12 \rangle \langle 34 \rangle \langle 45 \rangle s_{1,2}(z_1 + z_2) \Delta_{(1)}(0, 2; 1) \Delta_{(1)}(0, 2; 3)} \\
&+ \frac{(\Delta_{(1)}(0, 3; 2))^4 \sqrt{z_1}}{\sqrt{z_1 z_5} \langle 12 \rangle \langle 23 \rangle \langle 45 \rangle s_{1,3}(z_1 + z_2 + z_3) \Delta_{(1)}(0, 3; 1) \Delta_{(1)}(0, 3; 3) \Delta_{(1)}(0, 3; 4)} \\
&+ \frac{(\Delta_{(1)}(0, 4; 2))^4 \sqrt{z_1}}{\sqrt{z_1 z_5} \langle 12 \rangle \langle 23 \rangle \langle 34 \rangle s_{1,4}(z_1 + z_2 + z_3 + z_4) \Delta_{(1)}(0, 4; 1) \Delta_{(1)}(0, 4; 4) \Delta_{(1)}(0, 4; 5)} \\
&- \frac{(\Delta_{(1)}(0, 5; 2))^4}{\langle 12 \rangle \langle 34 \rangle \langle 45 \rangle \langle 23 \rangle s_{1,5} \Delta_{(1)}(0, 5; 1) \Delta_{(1)}(0, 5; 5)} \\
&+ \frac{(\Delta_{(1)}(1, 3; 2))^3}{\sqrt{z_1 z_5} \langle 23 \rangle \langle 45 \rangle s_{2,3} \Delta_{(1)}(1, 3; 1) \Delta_{(1)}(1, 3; 3) \Delta_{(1)}(1, 3; 4)} \\
&+ \frac{(\Delta_{(1)}(1, 4; 2))^3}{\sqrt{z_1 z_5} \langle 23 \rangle \langle 34 \rangle s_{2,4} \Delta_{(1)}(1, 4; 1) \Delta_{(1)}(1, 4; 4) \Delta_{(1)}(1, 4; 5)} \\
&- \frac{(\Delta_{(1)}(1, 5; 2))^3 \sqrt{z_5}}{\sqrt{z_1 z_5} \langle 23 \rangle \langle 34 \rangle \langle 45 \rangle s_{2,5} \Delta_{(1)}(1, 5; 1) \Delta_{(1)}(1, 5; 5) (z_2 + z_3 + z_4 + z_5)} \tag{5.86}
\end{aligned}$$

$$\begin{aligned}
\text{split}(1^+, 2^+, 3^-, 4^+, 5^+ \rightarrow P^+) &= -C_1^+(3, 5, 4, 2, 1) - C_1^+(3, 1, 2, 4, 5) \\
&\quad - C_2^+(5, 3, 4, 2, 1) - C_2^+(1, 3, 2, 4, 5)
\end{aligned}$$

$$\text{split}(1^+, 2^+, 3^+, 4^-, 5^+ \rightarrow P^+) = \text{split}(5^+, 4^-, 3^+, 2^+, 1^+ \rightarrow P^+)$$

$$\text{split}(1^+, 2^+, 3^+, 4^+, 5^- \rightarrow P^+) = \text{split}(5^-, 4^+, 3^+, 2^+, 1^+ \rightarrow P^+)$$

$$\begin{aligned} \text{split}(1^-, 2^-, 3^+, 4^+, 5^+ \rightarrow P^-) &= \mathcal{C}_3^-(1, 2, 3, 4, 5) \\ &= \frac{z_1^2 (\Delta_{(1)}(1, 3; 2))^3}{\sqrt{z_1 z_5} \langle 23 \rangle \langle 45 \rangle s_{2,3} \Delta_{(1)}(1, 3; 1) \Delta_{(1)}(1, 3; 3) \Delta_{(1)}(1, 3; 4)} \\ &+ \frac{z_1^2 (\Delta_{(1)}(1, 4; 2))^3}{\sqrt{z_1 z_5} \langle 23 \rangle \langle 34 \rangle s_{2,4} \Delta_{(1)}(1, 4; 1) \Delta_{(1)}(1, 4; 4) \Delta_{(1)}(1, 4; 5)} \\ &- \frac{z_1^2 (\Delta_{(1)}(1, 5; 2))^3 \sqrt{z_5}}{\sqrt{z_1 z_5} \langle 23 \rangle \langle 34 \rangle \langle 45 \rangle s_{2,5} \Delta_{(1)}(1, 5; 1) \Delta_{(1)}(1, 5; 5) (z_2 + z_3 + z_4 + z_5)} \\ &+ \frac{((12))^3 (z_1 + z_2)^3 \sqrt{z_1}}{\sqrt{z_1 z_5} \langle 34 \rangle \langle 45 \rangle s_{1,2} \Delta_{(1)}(0, 2; 1) \Delta_{(1)}(0, 2; 2) \Delta_{(1)}(0, 2; 3)} \\ &+ \frac{((12))^3 (z_1 + z_2 + z_3)^3 \sqrt{z_1}}{\sqrt{z_1 z_5} \langle 23 \rangle \langle 45 \rangle s_{1,3} \Delta_{(1)}(0, 3; 1) \Delta_{(1)}(0, 3; 3) \Delta_{(1)}(0, 3; 4)} \\ &+ \frac{((12))^3 (z_1 + z_2 + z_3 + z_4)^3 \sqrt{z_1}}{\sqrt{z_1 z_5} \langle 23 \rangle \langle 34 \rangle s_{1,4} \Delta_{(1)}(0, 4; 1) \Delta_{(1)}(0, 4; 4) \Delta_{(1)}(0, 4; 5)} \\ &- \frac{((12))^3}{\langle 23 \rangle \langle 34 \rangle \langle 45 \rangle s_{1,5} \Delta_{(1)}(0, 5; 1) \Delta_{(1)}(0, 5; 5)} \end{aligned} \tag{5.87}$$

$$\begin{aligned} \text{split}(1^-, 2^+, 3^-, 4^+, 5^+ \rightarrow P^-) &= \mathcal{C}_4^-(1, 2, 3, 4, 5) \\ &= \frac{z_3^2 (\Delta_{(1)}(0, 2; 1))^3 \sqrt{z_1}}{\sqrt{z_1 z_5} \langle 12 \rangle \langle 34 \rangle \langle 45 \rangle s_{1,2} (z_1 + z_2) \Delta_{(1)}(0, 2; 2) \Delta_{(1)}(0, 2; 3)} \\ &+ \frac{z_1^2 (\Delta_{(1)}(1, 3; 3))^3}{\sqrt{z_1 z_5} \langle 23 \rangle \langle 45 \rangle s_{2,3} \Delta_{(1)}(1, 3; 1) \Delta_{(1)}(1, 3; 2) \Delta_{(1)}(1, 3; 4)} \\ &+ \frac{z_1^2 (\Delta_{(1)}(1, 4; 3))^4}{\sqrt{z_1 z_5} \langle 23 \rangle \langle 34 \rangle s_{2,4} \Delta_{(1)}(1, 4; 1) \Delta_{(1)}(1, 4; 2) \Delta_{(1)}(1, 4; 4) \Delta_{(1)}(1, 4; 5)} \\ &- \frac{z_1^2 (\Delta_{(1)}(1, 5; 3))^4 \sqrt{z_5}}{\sqrt{z_1 z_5} \langle 23 \rangle \langle 34 \rangle \langle 45 \rangle s_{2,5} \Delta_{(1)}(1, 5; 1) \Delta_{(1)}(1, 5; 2) \Delta_{(1)}(1, 5; 5) (z_2 + z_3 + z_4 + z_5)} \\ &+ \frac{z_1^2 (\Delta_{(1)}(2, 4; 3))^3}{\sqrt{z_1 z_5} \langle 12 \rangle \langle 34 \rangle s_{3,4} \Delta_{(1)}(2, 4; 2) \Delta_{(1)}(2, 4; 4) \Delta_{(1)}(2, 4; 5)} \end{aligned}$$

$$\begin{aligned}
& - \frac{z_1^2 (\Delta_{(1)}(2, 5; 3))^3 \sqrt{z_5}}{\sqrt{z_1 z_5} \langle 12 \rangle \langle 34 \rangle \langle 45 \rangle s_{3,5} \Delta_{(1)}(2, 5; 2) \Delta_{(1)}(2, 5; 5) (z_3 + z_4 + z_5)} \\
& + \frac{((13))^4 (z_1 + z_2 + z_3)^3 \sqrt{z_1}}{\sqrt{z_1 z_5} \langle 12 \rangle \langle 23 \rangle \langle 45 \rangle s_{1,3} \Delta_{(1)}(0, 3; 1) \Delta_{(1)}(0, 3; 3) \Delta_{(1)}(0, 3; 4)} \\
& + \frac{((13))^4 (z_1 + z_2 + z_3 + z_4)^3 \sqrt{z_1}}{\sqrt{z_1 z_5} \langle 12 \rangle \langle 23 \rangle \langle 34 \rangle s_{1,4} \Delta_{(1)}(0, 4; 1) \Delta_{(1)}(0, 4; 4) \Delta_{(1)}(0, 4; 5)} \\
& - \frac{((13))^4}{s_{1,5} \Delta_{(1)}(0, 5; 1) \Delta_{(1)}(0, 5; 5) \langle 45 \rangle \langle 12 \rangle \langle 34 \rangle \langle 23 \rangle}
\end{aligned} \tag{5.88}$$

split($1^-, 2^+, 3^+, 4^-, 5^+ \rightarrow P^-$) = $C_5^-(1, 2, 3, 4, 5)$

$$\begin{aligned}
& = \frac{z_4^2 (\Delta_{(1)}(0, 2; 1))^3 \sqrt{z_1}}{\sqrt{z_1 z_5} \langle 12 \rangle \langle 34 \rangle \langle 45 \rangle s_{1,2} (z_1 + z_2) \Delta_{(1)}(0, 2; 2) \Delta_{(1)}(0, 2; 3)} \\
& + \frac{z_4^2 (\Delta_{(1)}(0, 3; 1))^3 \sqrt{z_1}}{\sqrt{z_1 z_5} \langle 12 \rangle \langle 23 \rangle \langle 45 \rangle s_{1,3} (z_1 + z_2 + z_3) \Delta_{(1)}(0, 3; 3) \Delta_{(1)}(0, 3; 4)} \\
& + \frac{z_1^2 (\Delta_{(1)}(1, 4; 4))^3}{\sqrt{z_1 z_5} \langle 23 \rangle \langle 34 \rangle s_{2,4} \Delta_{(1)}(1, 4; 1) \Delta_{(1)}(1, 4; 2) \Delta_{(1)}(1, 4; 5)} \\
& - \frac{z_1^2 (\Delta_{(1)}(1, 5; 4))^4 \sqrt{z_5}}{\sqrt{z_1 z_5} \langle 23 \rangle \langle 34 \rangle \langle 45 \rangle s_{2,5} \Delta_{(1)}(1, 5; 1) \Delta_{(1)}(1, 5; 2) \Delta_{(1)}(1, 5; 5) (z_2 + z_3 + z_4 + z_5)} \\
& + \frac{z_1^2 (\Delta_{(1)}(2, 4; 4))^3}{\sqrt{z_1 z_5} \langle 12 \rangle \langle 34 \rangle s_{3,4} \Delta_{(1)}(2, 4; 2) \Delta_{(1)}(2, 4; 3) \Delta_{(1)}(2, 4; 5)} \\
& - \frac{z_1^2 (\Delta_{(1)}(2, 5; 4))^4 \sqrt{z_5}}{\sqrt{z_1 z_5} \langle 12 \rangle \langle 34 \rangle \langle 45 \rangle s_{3,5} \Delta_{(1)}(2, 5; 2) \Delta_{(1)}(2, 5; 3) \Delta_{(1)}(2, 5; 5) (z_3 + z_4 + z_5)} \\
& - \frac{z_1^2 (\Delta_{(1)}(3, 5; 4))^3 \sqrt{z_5}}{\sqrt{z_1 z_5} \langle 12 \rangle \langle 23 \rangle \langle 45 \rangle s_{4,5} \Delta_{(1)}(3, 5; 3) \Delta_{(1)}(3, 5; 5) (z_4 + z_5)} \\
& + \frac{((14))^4 (z_1 + z_2 + z_3 + z_4)^3 \sqrt{z_1}}{\sqrt{z_1 z_5} \langle 12 \rangle \langle 23 \rangle \langle 34 \rangle s_{1,4} \Delta_{(1)}(0, 4; 1) \Delta_{(1)}(0, 4; 4) \Delta_{(1)}(0, 4; 5)} \\
& - \frac{((14))^4}{s_{1,5} \Delta_{(1)}(0, 5; 1) \Delta_{(1)}(0, 5; 5) \langle 12 \rangle \langle 23 \rangle \langle 34 \rangle \langle 45 \rangle}
\end{aligned} \tag{5.89}$$

$$\text{split}(1^-, 2^+, 3^+, 4^+, 5^- \rightarrow P^-) = -\mathcal{C}_3^-(1, 5, 2, 3, 4) - \mathcal{C}_3^-(5, 1, 2, 3, 4)$$

$$-\mathcal{C}_4^-(1, 2, 5, 3, 4) - \mathcal{C}_5^-(1, 2, 3, 5, 4)$$

$$\text{split}(1^+, 2^-, 3^-, 4^+, 5^+ \rightarrow P^-) = -\mathcal{C}_3^-(2, 3, 1, 4, 5) - \mathcal{C}_3^-(2, 3, 4, 1, 5)$$

$$-\mathcal{C}_3^-(2, 3, 4, 5, 1) - \mathcal{C}_4^-(2, 1, 3, 4, 5)$$

$$\text{split}(1^+, 2^-, 3^+, 4^-, 5^+ \rightarrow P^-) = -\mathcal{C}_4^-(2, 3, 4, 1, 5) - \mathcal{C}_4^-(2, 3, 4, 5, 1)$$

$$-\mathcal{C}_5^-(2, 1, 3, 4, 5) - \mathcal{C}_5^-(2, 3, 1, 4, 5)$$

$$\text{split}(1^+, 2^-, 3^+, 4^+, 5^- \rightarrow P^-) = \text{split}(5^-, 4^+, 3^+, 2^-, 1^+ \rightarrow P^-)$$

$$\text{split}(1^+, 2^+, 3^-, 4^-, 5^+ \rightarrow P^-) = \text{split}(5^+, 4^-, 3^-, 2^+, 1^+ \rightarrow P^-)$$

$$\text{split}(1^+, 2^+, 3^-, 4^+, 5^- \rightarrow P^-) = \text{split}(5^-, 4^+, 3^-, 2^+, 1^+ \rightarrow P^-)$$

$$\text{split}(1^+, 2^+, 3^+, 4^-, 5^- \rightarrow P^-) = \text{split}(5^-, 4^-, 3^+, 2^+, 1^+ \rightarrow P^-)$$

$$\text{split}(1^-, 2^-, 3^+, 4^+, 5^+ \rightarrow P^+) = \mathcal{C}_3^+(1, 2, 3, 4, 5)$$

$$\begin{aligned} &= -\frac{(\Delta_{(1)}(0, 3; 1))^3 (\Delta_{(1)}(1, 3; 2))^3 \sqrt{z_1}}{\sqrt{z_1 z_5} \langle 23 \rangle \langle 45 \rangle \Delta_{(2)}(0, 3; 1, 3) s_{1,3} (z_1 + z_2 + z_3) \Delta_{(1)}(0, 3; 4) s_{2,3} \Delta_{(1)}(1, 3; 1) \Delta_{(1)}(1, 3; 3)} \\ &+ \frac{(\Delta_{(1)}(0, 4; 1))^3 (\Delta_{(1)}(1, 3; 2))^3 \sqrt{z_1}}{\sqrt{z_1 z_5} \langle 23 \rangle s_{1,4} (1 - z_5) \Delta_{(1)}(0, 4; 4) \Delta_{(1)}(0, 4; 5) s_{2,3} \Delta_{(1)}(1, 3; 1) \Delta_{(1)}(1, 3; 3) \Delta_{(1)}(1, 3; 4)} \\ &- \frac{(\Delta_{(1)}(0, 4; 1))^3 (\Delta_{(1)}(1, 4; 2))^3 \sqrt{z_1}}{\sqrt{z_1 z_5} \langle 23 \rangle \langle 34 \rangle \Delta_{(2)}(0, 4; 1, 4) s_{1,4} (1 - z_5) \Delta_{(1)}(0, 4; 5) s_{2,4} \Delta_{(1)}(1, 4; 1) \Delta_{(1)}(1, 4; 4)} \\ &- \frac{(\Delta_{(1)}(0, 5; 1))^3 (\Delta_{(1)}(1, 3; 2))^3}{\langle 23 \rangle \langle 45 \rangle s_{1,5} \Delta_{(1)}(0, 5; 5) s_{2,3} \Delta_{(1)}(1, 3; 1) \Delta_{(1)}(1, 3; 3) \Delta_{(1)}(1, 3; 4)} \\ &- \frac{(\Delta_{(1)}(0, 5; 1))^3 (\Delta_{(1)}(1, 4; 2))^3}{\langle 23 \rangle \langle 34 \rangle s_{1,5} \Delta_{(1)}(0, 5; 5) s_{2,4} \Delta_{(1)}(1, 4; 1) \Delta_{(1)}(1, 4; 4) \Delta_{(1)}(1, 4; 5)} \\ &+ \frac{(\Delta_{(1)}(0, 5; 1))^3 (\Delta_{(1)}(1, 5; 2))^3}{\langle 23 \rangle \langle 34 \rangle \langle 45 \rangle s_{1,5} \Delta_{(1)}(1, 5; 1) \Delta_{(1)}(1, 5; 5) \Delta_{(2)}(0, 5; 1, 5) s_{2,5}} \\ &- \frac{(\langle 12 \rangle)^3 (\Delta_{(2)}(0, 5; 0, 4))^3}{\langle 23 \rangle \langle 34 \rangle s_{1,5} \Delta_{(1)}(0, 5; 5) s_{1,4} \Delta_{(1)}(0, 4; 1) \Delta_{(1)}(0, 4; 4) \Delta_{(1)}(0, 4; 5)} \end{aligned}$$

$$\begin{aligned}
& + \frac{(\langle 12 \rangle)^3 (\Delta_{(2)}(0, 3; 0, 2))^3 \sqrt{z_1}}{\sqrt{z_1 z_5} \langle 45 \rangle s_{1,3} (z_1 + z_2 + z_3) \Delta_{(1)}(0, 3; 3) \Delta_{(1)}(0, 3; 4) s_{1,2} \Delta_{(1)}(0, 2; 1) \Delta_{(1)}(0, 2; 2) \Delta_{(1)}(0, 2; 3)} \\
& + \frac{(\langle 12 \rangle)^3 (\Delta_{(2)}(0, 4; 0, 2))^3 \sqrt{z_1}}{\sqrt{z_1 z_5} \langle 34 \rangle s_{1,4} (1 - z_5) \Delta_{(1)}(0, 4; 4) \Delta_{(1)}(0, 4; 5) s_{1,2} \Delta_{(1)}(0, 2; 1) \Delta_{(1)}(0, 2; 2) \Delta_{(1)}(0, 2; 3)} \\
& + \frac{(\langle 12 \rangle)^3 (\Delta_{(2)}(0, 4; 0, 3))^3 \sqrt{z_1}}{\sqrt{z_1 z_5} \langle 23 \rangle s_{1,4} (1 - z_5) \Delta_{(1)}(0, 4; 4) \Delta_{(1)}(0, 4; 5) s_{1,3} \Delta_{(1)}(0, 3; 1) \Delta_{(1)}(0, 3; 3) \Delta_{(1)}(0, 3; 4)} \\
& - \frac{(\langle 12 \rangle)^3 (\Delta_{(2)}(0, 5; 0, 2))^3}{\langle 34 \rangle \langle 45 \rangle s_{1,5} \Delta_{(1)}(0, 5; 5) s_{1,2} \Delta_{(1)}(0, 2; 1) \Delta_{(1)}(0, 2; 2) \Delta_{(1)}(0, 2; 3)} \\
& - \frac{(\langle 12 \rangle)^3 (\Delta_{(2)}(0, 5; 0, 3))^3}{\langle 23 \rangle \langle 45 \rangle s_{1,5} \Delta_{(1)}(0, 5; 5) \Delta_{(1)}(0, 3; 3) s_{1,3} \Delta_{(1)}(0, 3; 4) \Delta_{(1)}(0, 3; 1)} \tag{5.90}
\end{aligned}$$

$$\text{split}(1^-, 2^+, 3^-, 4^+, 5^+ \rightarrow P^+) = \mathcal{C}_4^+(1, 2, 3, 4, 5)$$

$$\begin{aligned}
& = \frac{(\langle 13 \rangle)^4 (\Delta_{(2)}(0, 4; 0, 3))^3 \sqrt{z_1}}{\sqrt{z_1 z_5} \langle 12 \rangle \langle 23 \rangle s_{1,4} (1 - z_5) \Delta_{(1)}(0, 4; 4) \Delta_{(1)}(0, 4; 5) s_{1,3} \Delta_{(1)}(0, 3; 1) \Delta_{(1)}(0, 3; 3) \Delta_{(1)}(0, 3; 4)} \\
& - \frac{(\Delta_{(2)}(0, 5; 0, 4))^3 (\langle 13 \rangle)^4}{\langle 12 \rangle \langle 23 \rangle \langle 34 \rangle s_{1,4} \Delta_{(1)}(0, 4; 4) s_{1,5} \Delta_{(1)}(0, 5; 5) \Delta_{(1)}(0, 4; 1) \Delta_{(1)}(0, 4; 5)} \\
& - \frac{(\Delta_{(1)}(0, 3; 1))^3 (\Delta_{(1)}(1, 3; 3))^3 \sqrt{z_1}}{\sqrt{z_1 z_5} \langle 23 \rangle \langle 45 \rangle \Delta_{(2)}(0, 3; 1, 3) s_{1,3} (z_1 + z_2 + z_3) \Delta_{(1)}(0, 3; 4) s_{2,3} \Delta_{(1)}(1, 3; 1) \Delta_{(1)}(1, 3; 2)} \\
& - \frac{(\Delta_{(2)}(0, 5; 0, 3))^3 (\langle 13 \rangle)^4}{\langle 12 \rangle \langle 23 \rangle \langle 45 \rangle s_{1,5} \Delta_{(1)}(0, 5; 5) s_{1,3} \Delta_{(1)}(0, 3; 1) \Delta_{(1)}(0, 3; 3) \Delta_{(1)}(0, 3; 4)} \\
& + \frac{(\Delta_{(1)}(0, 4; 3))^4 (\Delta_{(1)}(0, 2; 1))^3 \sqrt{z_1}}{\sqrt{z_1 z_5} \langle 12 \rangle \langle 34 \rangle \Delta_{(2)}(0, 4; 0, 2) s_{1,4} (1 - z_5) \Delta_{(1)}(0, 4; 4) \Delta_{(1)}(0, 4; 5) s_{1,2} \Delta_{(1)}(0, 2; 2) \Delta_{(1)}(0, 2; 3)} \\
& + \frac{(\Delta_{(1)}(0, 3; 3))^3 (\Delta_{(1)}(0, 2; 1))^3 \sqrt{z_1}}{\sqrt{z_1 z_5} \langle 12 \rangle \langle 45 \rangle \Delta_{(2)}(0, 3; 0, 2) s_{1,3} (z_1 + z_2 + z_3) \Delta_{(1)}(0, 3; 4) s_{1,2} \Delta_{(1)}(0, 2; 2) \Delta_{(1)}(0, 2; 3)} \\
& - \frac{(\Delta_{(1)}(0, 5; 3))^4 (\Delta_{(1)}(0, 2; 1))^3}{\langle 12 \rangle \langle 34 \rangle \langle 45 \rangle \Delta_{(2)}(0, 5; 0, 2) s_{1,5} \Delta_{(1)}(0, 5; 5) s_{1,2} \Delta_{(1)}(0, 2; 2) \Delta_{(1)}(0, 2; 3)} \\
& - \frac{(\Delta_{(1)}(0, 2; 1))^3 (\Delta_{(1)}(2, 5; 3))^3}{\langle 12 \rangle \langle 34 \rangle \langle 45 \rangle s_{1,2} \Delta_{(1)}(0, 2; 2) \Delta_{(2)}(0, 2; 2, 5) (z_1 + z_2) s_{3,5} \Delta_{(1)}(2, 5; 5) (z_3 + z_4 + z_5)} \\
& - \frac{(\Delta_{(1)}(0, 5; 1))^3 (\Delta_{(1)}(1, 4; 3))^4}{\langle 23 \rangle \langle 34 \rangle s_{2,4} \Delta_{(1)}(1, 4; 1) \Delta_{(1)}(1, 4; 2) \Delta_{(1)}(1, 4; 4) \Delta_{(1)}(1, 4; 5) s_{1,5} \Delta_{(1)}(0, 5; 5)} \\
& + \frac{(\Delta_{(1)}(0, 2; 1))^3 (\Delta_{(1)}(2, 4; 3))^3 \sqrt{z_1}}{\sqrt{z_1 z_5} \langle 12 \rangle \langle 34 \rangle \Delta_{(2)}(0, 2; 2, 4) s_{1,2} (z_1 + z_2) \Delta_{(1)}(0, 2; 2) s_{3,4} \Delta_{(1)}(2, 4; 4) \Delta_{(1)}(2, 4; 5)} \\
& - \frac{(\Delta_{(1)}(0, 5; 1))^3 (\Delta_{(1)}(1, 3; 3))^3}{\langle 23 \rangle \langle 45 \rangle s_{2,3} \Delta_{(1)}(1, 3; 1) \Delta_{(1)}(1, 3; 2) s_{1,5} \Delta_{(1)}(0, 5; 5) \Delta_{(1)}(1, 3; 4)}
\end{aligned}$$

$$\begin{aligned}
& - \frac{(\Delta_{(1)}(0, 4; 1))^3 (\Delta_{(1)}(2, 4; 3))^3 \sqrt{z_1}}{\sqrt{z_1 z_5} \langle 12 \rangle \langle 34 \rangle \Delta_{(2)}(0, 4; 2, 4) s_{1,4} (1 - z_5) \Delta_{(1)}(0, 4; 5) s_{3,4} \Delta_{(1)}(2, 4; 2) \Delta_{(1)}(2, 4; 4)} \\
& - \frac{(\Delta_{(1)}(0, 4; 1))^3 (\Delta_{(1)}(1, 4; 3))^4 \sqrt{z_1}}{\sqrt{z_1 z_5} \langle 23 \rangle \langle 34 \rangle \Delta_{(2)}(0, 4; 1, 4) s_{1,4} (1 - z_5) \Delta_{(1)}(0, 4; 5) s_{2,4} \Delta_{(1)}(1, 4; 1) \Delta_{(1)}(1, 4; 2) \Delta_{(1)}(1, 4; 4)} \\
& - \frac{(\Delta_{(1)}(0, 5; 1))^3 (\Delta_{(1)}(2, 4; 3))^3}{\langle 12 \rangle \langle 34 \rangle \Delta_{(1)}(2, 4; 2) s_{1,5} \Delta_{(1)}(0, 5; 5) s_{3,4} \Delta_{(1)}(2, 4; 4) \Delta_{(1)}(2, 4; 5)} \\
& + \frac{(\Delta_{(1)}(0, 5; 1))^3 (\Delta_{(1)}(1, 5; 3))^4}{\langle 23 \rangle \langle 34 \rangle \langle 45 \rangle s_{1,5} \Delta_{(2)}(0, 5; 1, 5) s_{2,5} \Delta_{(1)}(1, 5; 1) \Delta_{(1)}(1, 5; 2) \Delta_{(1)}(1, 5; 5)} \\
& + \frac{(\Delta_{(1)}(0, 5; 1))^3 (\Delta_{(1)}(2, 5; 3))^3}{\langle 12 \rangle \langle 34 \rangle \langle 45 \rangle s_{1,5} \Delta_{(2)}(0, 5; 2, 5) \Delta_{(1)}(2, 5; 2) s_{3,5} \Delta_{(1)}(2, 5; 5)} \\
& + \frac{(\Delta_{(1)}(0, 4; 1))^3 (\Delta_{(1)}(1, 3; 3))^3 \sqrt{z_1}}{\sqrt{z_1 z_5} \langle 23 \rangle s_{1,4} (1 - z_5) \Delta_{(1)}(0, 4; 4) \Delta_{(1)}(0, 4; 5) s_{2,3} \Delta_{(1)}(1, 3; 1) \Delta_{(1)}(1, 3; 2) \Delta_{(1)}(1, 3; 4)}
\end{aligned} \tag{5.91}$$

$$\begin{aligned}
& \text{split}(1^-, 2^+, 3^+, 4^-, 5^+ \rightarrow P^+) = C_5^+(1, 2, 3, 4, 5) \\
& = - \frac{((14))^4 (\Delta_{(2)}(0, 5; 0, 4))^3}{\langle 12 \rangle \langle 23 \rangle \langle 34 \rangle s_{1,5} \Delta_{(1)}(0, 5; 5) s_{1,4} \Delta_{(1)}(0, 4; 1) \Delta_{(1)}(0, 4; 4) \Delta_{(1)}(0, 4; 5)} \\
& - \frac{(\Delta_{(1)}(0, 4; 1))^3 (\Delta_{(1)}(1, 4; 4))^3 \sqrt{z_1}}{\sqrt{z_1 z_5} \langle 23 \rangle \langle 34 \rangle \Delta_{(2)}(0, 4; 1, 4) s_{1,4} (1 - z_5) \Delta_{(1)}(0, 4; 5) s_{2,4} \Delta_{(1)}(1, 4; 1) \Delta_{(1)}(1, 4; 2)} \\
& - \frac{(\Delta_{(1)}(0, 5; 1))^3 (\Delta_{(1)}(1, 4; 4))^3}{\langle 23 \rangle \langle 34 \rangle \Delta_{(1)}(1, 4; 5) s_{1,5} \Delta_{(1)}(0, 5; 5) s_{2,4} \Delta_{(1)}(1, 4; 1) \Delta_{(1)}(1, 4; 2)} \\
& + \frac{(\Delta_{(1)}(0, 5; 1))^3 (\Delta_{(1)}(1, 5; 4))^4}{\langle 23 \rangle \langle 34 \rangle \langle 45 \rangle \Delta_{(2)}(0, 5; 1, 5) s_{2,5} \Delta_{(1)}(1, 5; 1) \Delta_{(1)}(1, 5; 2) \Delta_{(1)}(1, 5; 5) s_{1,5}} \\
& - \frac{(\Delta_{(1)}(0, 4; 1))^3 (\Delta_{(1)}(2, 4; 4))^3 \sqrt{z_1}}{\sqrt{z_1 z_5} \langle 12 \rangle \langle 34 \rangle \Delta_{(2)}(0, 4; 2, 4) s_{1,4} (1 - z_5) \Delta_{(1)}(0, 4; 5) s_{3,4} \Delta_{(1)}(2, 4; 2) \Delta_{(1)}(2, 4; 3)} \\
& - \frac{(\Delta_{(1)}(0, 5; 1))^3 (\Delta_{(1)}(2, 4; 4))^3}{\langle 12 \rangle \langle 34 \rangle s_{1,5} \Delta_{(1)}(0, 5; 5) \Delta_{(1)}(2, 4; 5) s_{3,4} \Delta_{(1)}(2, 4; 2) \Delta_{(1)}(2, 4; 3)} \\
& + \frac{(\Delta_{(1)}(0, 5; 1))^3 (\Delta_{(1)}(2, 5; 4))^4}{\langle 12 \rangle \langle 34 \rangle \langle 45 \rangle \Delta_{(2)}(0, 5; 2, 5) s_{3,5} \Delta_{(1)}(2, 5; 2) \Delta_{(1)}(2, 5; 3) \Delta_{(1)}(2, 5; 5) s_{1,5}} \\
& + \frac{(\Delta_{(1)}(0, 5; 1))^3 (\Delta_{(1)}(3, 5; 4))^3}{\langle 12 \rangle \langle 23 \rangle \langle 45 \rangle \Delta_{(2)}(0, 5; 3, 5) s_{4,5} \Delta_{(1)}(3, 5; 3) \Delta_{(1)}(3, 5; 5) s_{1,5}} \\
& + \frac{(\Delta_{(1)}(0, 2; 1))^3 (\Delta_{(1)}(2, 4; 4))^3 \sqrt{z_1}}{\sqrt{z_1 z_5} \langle 12 \rangle \langle 34 \rangle \Delta_{(2)}(0, 2; 2, 4) s_{1,2} (z_1 + z_2) \Delta_{(1)}(0, 2; 2) s_{3,4} \Delta_{(1)}(2, 4; 3) \Delta_{(1)}(2, 4; 5)}
\end{aligned}$$

$$\begin{aligned}
& - \frac{(\Delta_{(1)}(2, 5; 4))^4 (\Delta_{(1)}(0, 2; 1))^3}{\langle 12 \rangle \langle 34 \rangle \langle 45 \rangle s_{3,5} \Delta_{(1)}(2, 5; 3) \Delta_{(1)}(2, 5; 5) s_{1,2} (z_1 + z_2) \Delta_{(1)}(0, 2; 2) \Delta_{(2)}(0, 2; 2, 5) (z_3 + z_4 + z_5)} \\
& - \frac{(\Delta_{(1)}(3, 5; 4))^3 (\Delta_{(1)}(0, 2; 1))^3}{\langle 12 \rangle \langle 45 \rangle s_{4,5} \Delta_{(1)}(3, 5; 3) \Delta_{(1)}(3, 5; 5) \Delta_{(1)}(0, 2; 3) (z_4 + z_5) s_{1,2} (z_1 + z_2) \Delta_{(1)}(0, 2; 2)} \\
& - \frac{(\Delta_{(1)}(3, 5; 4))^3 (\Delta_{(1)}(0, 3; 1))^3}{\langle 12 \rangle \langle 23 \rangle \langle 45 \rangle s_{4,5} \Delta_{(1)}(3, 5; 5) (z_4 + z_5) \Delta_{(2)}(0, 3; 3, 5) s_{1,3} (z_1 + z_2 + z_3) \Delta_{(1)}(0, 3; 3)} \\
& + \frac{(\Delta_{(1)}(0, 4; 4))^3 (\Delta_{(1)}(0, 2; 1))^3 \sqrt{z_1}}{\sqrt{z_1 z_5} \langle 12 \rangle \langle 34 \rangle \Delta_{(2)}(0, 4; 0, 2) s_{1,4} (1 - z_5) \Delta_{(1)}(0, 4; 5) s_{1,2} \Delta_{(1)}(0, 2; 2) \Delta_{(1)}(0, 2; 3)} \\
& - \frac{(\Delta_{(1)}(0, 2; 1))^3 (\Delta_{(1)}(0, 5; 4))^4}{\langle 12 \rangle \langle 34 \rangle \langle 45 \rangle s_{1,5} \Delta_{(1)}(0, 5; 5) \Delta_{(1)}(0, 2; 3) s_{1,2} \Delta_{(1)}(0, 2; 2) \Delta_{(2)}(0, 5; 0, 2)} \\
& + \frac{(\Delta_{(1)}(0, 4; 4))^3 (\Delta_{(1)}(0, 3; 1))^3 \sqrt{z_1}}{\sqrt{z_1 z_5} \langle 12 \rangle \langle 23 \rangle \Delta_{(2)}(0, 4; 0, 3) s_{1,4} (1 - z_5) \Delta_{(1)}(0, 4; 5) s_{1,3} \Delta_{(1)}(0, 3; 3) \Delta_{(1)}(0, 3; 4)} \\
& - \frac{(\Delta_{(1)}(0, 3; 1))^3 (\Delta_{(1)}(0, 5; 4))^4}{\langle 12 \rangle \langle 23 \rangle \langle 45 \rangle s_{1,5} \Delta_{(1)}(0, 5; 5) s_{1,3} \Delta_{(1)}(0, 3; 3) \Delta_{(1)}(0, 3; 4) \Delta_{(2)}(0, 5; 0, 3)} \tag{5.92}
\end{aligned}$$

$$\text{split}(1^-, 2^+, 3^+, 4^+, 5^- \rightarrow P^+) = -C_3^+(1, 5, 2, 3, 4) - C_3^+(5, 1, 2, 3, 4)$$

$$-C_4^+(1, 2, 5, 3, 4) - C_5^+(1, 2, 3, 5, 4)$$

$$\text{split}(1^+, 2^-, 3^-, 4^+, 5^+ \rightarrow P^+) = -C_3^+(2, 3, 1, 4, 5) - C_3^+(2, 3, 4, 1, 5)$$

$$-C_3^+(2, 3, 4, 5, 1) - C_4^+(2, 1, 3, 4, 5)$$

$$\text{split}(1^+, 2^-, 3^+, 4^-, 5^+ \rightarrow P^+) = -C_4^+(2, 3, 4, 1, 5) - C_4^+(2, 3, 4, 5, 1)$$

$$-C_5^+(2, 1, 3, 4, 5) - C_5^+(2, 3, 1, 4, 5)$$

$$\text{split}(1^+, 2^-, 3^+, 4^+, 5^- \rightarrow P^+) = \text{split}(5^-, 4^+, 3^+, 2^-, 1^+ \rightarrow P^+)$$

$$\text{split}(1^+, 2^+, 3^-, 4^-, 5^+ \rightarrow P^+) = \text{split}(5^+, 4^-, 3^-, 2^+, 1^+ \rightarrow P^+)$$

$$\text{split}(1^+, 2^+, 3^-, 4^+, 5^- \rightarrow P^+) = \text{split}(5^-, 4^+, 3^-, 2^+, 1^+ \rightarrow P^+)$$

$$\text{split}(1^+, 2^+, 3^+, 4^-, 5^- \rightarrow P^+) = \text{split}(5^-, 4^-, 3^+, 2^+, 1^+ \rightarrow P^+)$$

$n = 6$

Finally, for six collinear gluons there are $2^7 = 128$ different splitting amplitudes, which can be expressed by 23 independent ones. To find all independent amplitudes we have to use Eq. (5.34) for the first time. Due to the length of the results we give here only two examples obtained with the help of Eqs. (5.26) and (5.27),

$$\begin{aligned}
& \text{split}(1^-, 2^+, 3^+, 4^+, 5^+, 6^+ \rightarrow P^+) = \\
& \frac{(\Delta_{(1)}(0, 2; 1))^3 \sqrt{z_1}}{\sqrt{z_1 z_6} \langle 12 \rangle \langle 34 \rangle \langle 45 \rangle \langle 56 \rangle s_{1,2} (z_1 + z_2) \Delta_{(1)}(0, 2; 2) \Delta_{(1)}(0, 2; 3)} \\
& + \frac{(\Delta_{(1)}(0, 3; 1))^3 \sqrt{z_1}}{\sqrt{z_1 z_6} \langle 12 \rangle \langle 23 \rangle \langle 45 \rangle \langle 56 \rangle s_{1,3} (z_1 + z_2 + z_3) \Delta_{(1)}(0, 3; 3) \Delta_{(1)}(0, 3; 4)} \\
& + \frac{(\Delta_{(1)}(0, 4; 1))^3 \sqrt{z_1}}{\sqrt{z_1 z_6} \langle 12 \rangle \langle 23 \rangle \langle 34 \rangle \langle 56 \rangle s_{1,4} (z_1 + z_2 + z_3 + z_4) \Delta_{(1)}(0, 4; 4) \Delta_{(1)}(0, 4; 5)} \\
& + \frac{(\Delta_{(1)}(0, 5; 1))^3 \sqrt{z_1}}{\sqrt{z_1 z_6} \langle 12 \rangle \langle 23 \rangle \langle 34 \rangle \langle 45 \rangle s_{1,5} (z_1 + z_2 + z_3 + z_4 + z_5) \Delta_{(1)}(0, 5; 5) \Delta_{(1)}(0, 5; 6)} \\
& - \frac{(\Delta_{(1)}(0, 6; 1))^3}{\langle 12 \rangle \langle 23 \rangle \langle 34 \rangle \langle 45 \rangle \langle 56 \rangle s_{1,6} \Delta_{(1)}(0, 6; 6)}, \tag{5.93}
\end{aligned}$$

$$\begin{aligned}
& \text{split}(1^-, 2^-, 3^+, 4^+, 5^+, 6^+ \rightarrow P^-) = \tag{5.94} \\
& \frac{z_1^2 (\Delta_{(1)}(1, 3; 2))^3}{\sqrt{z_1 z_6} \langle 23 \rangle \langle 45 \rangle \langle 56 \rangle s_{2,3} \Delta_{(1)}(1, 3; 1) \Delta_{(1)}(1, 3; 3) \Delta_{(1)}(1, 3; 4)} \\
& + \frac{z_1^2 (\Delta_{(1)}(1, 4; 2))^3}{\sqrt{z_1 z_6} \langle 23 \rangle \langle 34 \rangle \langle 56 \rangle s_{2,4} \Delta_{(1)}(1, 4; 1) \Delta_{(1)}(1, 4; 4) \Delta_{(1)}(1, 4; 5)} \\
& + \frac{z_1^2 (\Delta_{(1)}(1, 5; 2))^3}{\sqrt{z_1 z_6} \langle 23 \rangle \langle 34 \rangle \langle 45 \rangle s_{2,5} \Delta_{(1)}(1, 5; 1) \Delta_{(1)}(1, 5; 5) \Delta_{(1)}(1, 5; 6)} \\
& - \frac{z_1^2 (\Delta_{(1)}(1, 6; 2))^3 \sqrt{z_6}}{\sqrt{z_1 z_6} \langle 23 \rangle \langle 34 \rangle \langle 45 \rangle \langle 56 \rangle s_{2,6} \Delta_{(1)}(1, 6; 1) \Delta_{(1)}(1, 6; 6) (1 - z_1)} \\
& + \frac{(\langle 12 \rangle)^3 (z_1 + z_2)^3 \sqrt{z_1}}{\sqrt{z_1 z_6} \langle 34 \rangle \langle 45 \rangle \langle 56 \rangle s_{1,2} \Delta_{(1)}(0, 2; 1) \Delta_{(1)}(0, 2; 2) \Delta_{(1)}(0, 2; 3)}
\end{aligned}$$

$$\begin{aligned}
& + \frac{(\langle 12 \rangle)^3 (z_1 + z_2 + z_3)^3 \sqrt{z_1}}{\sqrt{z_1 z_6} \langle 23 \rangle \langle 45 \rangle \langle 56 \rangle s_{1,3} \Delta_{(1)}(0, 3; 1) \Delta_{(1)}(0, 3; 3) \Delta_{(1)}(0, 3; 4)} \\
& + \frac{(\langle 12 \rangle)^3 (z_1 + z_2 + z_3 + z_4)^3 \sqrt{z_1}}{\sqrt{z_1 z_6} \langle 23 \rangle \langle 34 \rangle \langle 56 \rangle s_{1,4} \Delta_{(1)}(0, 4; 1) \Delta_{(1)}(0, 4; 4) \Delta_{(1)}(0, 4; 5)} \\
& + \frac{(\langle 12 \rangle)^3 (1 - z_6)^3 \sqrt{z_1}}{\sqrt{z_1 z_6} \langle 23 \rangle \langle 34 \rangle \langle 45 \rangle s_{1,5} \Delta_{(1)}(0, 5; 1) \Delta_{(1)}(0, 5; 5) \Delta_{(1)}(0, 5; 6)} \\
& - \frac{(\langle 12 \rangle)^3}{\langle 23 \rangle \langle 34 \rangle \langle 45 \rangle \langle 56 \rangle s_{1,6} \Delta_{(1)}(0, 6; 1) \Delta_{(1)}(0, 6; 6)}. \tag{5.95}
\end{aligned}$$

5.5.2 Selected specific results for triple collinear limits involving quarks

To illustrate our general results for multi-collinear limits, in this section we list some of the triple-collinear splitting functions. The $\Delta M = 0$ splitting amplitudes are obtained directly from MHV amplitudes and we do not list them here. Explicit results are given in Section 5.4. For the $\Delta M = 1$ (and therefore $\Delta P = 1$) amplitudes, there are two types of splitting function corresponding to $\text{Split}_+^{(n)}(m_1)$ and $\text{Split}_-^{(n)}(m_1, m_2)$. In the specific case of three collinear particles, these are related by parity thereby reducing the number of independent amplitudes to at most two for each splitting. Here, we list only the most compact form of the amplitudes.

$qgg \rightarrow q$

There are only two independent $\Delta M = 1$ splitting amplitudes, which can be obtained by setting $m = n = 3$ in Eqs. (5.39) and (5.40). Explicitly we find,

$$\text{split}(1_q^+, 2^+, 3^- \rightarrow P_q^+) = \frac{\langle 23 \rangle z_2^{3/2}}{\sqrt{z_3} s_{2,3} (\langle 21 \rangle \sqrt{z_2} + \langle 31 \rangle \sqrt{z_3}) (z_2 + z_3)} \frac{\langle 13 \rangle (\langle 13 \rangle \sqrt{z_1} + \langle 23 \rangle \sqrt{z_2})^2}{\langle 12 \rangle \langle 23 \rangle s_{1,3} (\langle 21 \rangle \sqrt{z_2} + \langle 31 \rangle \sqrt{z_3})}, \quad (5.96)$$

$$\text{split}(1_q^-, 2^+, 3^- \rightarrow P_q^-) = \frac{z_1 \langle 23 \rangle z_2^{3/2}}{\sqrt{z_3} s_{2,3} (\langle 21 \rangle \sqrt{z_2} + \langle 31 \rangle \sqrt{z_3}) (z_2 + z_3)} \frac{\langle 13 \rangle^3}{\langle 12 \rangle \langle 23 \rangle s_{1,3} (\langle 21 \rangle \sqrt{z_2} + \langle 31 \rangle \sqrt{z_3})}. \quad (5.97)$$

All others can be obtained by parity and charge conjugation. These expressions numerically agree with the splitting functions given in [137]⁶,

$$\begin{aligned} \text{split}(1_q^+, 2^+, 3^- \rightarrow P_q^+) &= -\frac{1}{s_{1,2} s_{2,3}} \\ &\times \left[\frac{[12] (\langle 13 \rangle \sqrt{z_1} + \langle 23 \rangle \sqrt{z_2})^2 ([12] \sqrt{z_1} + [32] \sqrt{z_3})}{s_{1,3}} \right. \\ &+ \frac{\sqrt{z_2} (z_1 + z_2) [12] (\langle 13 \rangle \sqrt{z_1} + \langle 23 \rangle \sqrt{z_2})}{\sqrt{z_3}} \\ &\left. + \frac{\sqrt{z_1} z_2 s_{1,2}}{(z_2 + z_3)} \right], \quad (5.98) \end{aligned}$$

$$\begin{aligned} \text{split}(1_q^-, 2^+, 3^- \rightarrow P_q^-) &= -\frac{1}{s_{1,2} s_{2,3}} \\ &\times \left[\frac{[13] (\langle 12 \rangle \sqrt{z_1} + \langle 32 \rangle \sqrt{z_3})^2 ([13] \sqrt{z_1} + [23] \sqrt{z_2})}{s_{1,3}} \right. \\ &+ \frac{\sqrt{z_2} (z_1 + z_2) [13] (\langle 12 \rangle \sqrt{z_1} + \langle 32 \rangle \sqrt{z_3})}{\sqrt{z_3}} \\ &\left. + \frac{\sqrt{z_1} z_2 s_{1,2}}{(z_2 + z_3)} + \sqrt{z_2} \langle 23 \rangle [13] \right]. \quad (5.99) \end{aligned}$$

⁶Note that there is a small typographical error in Eq. (5.56) of Ref. [137]. s_{23} should be replaced by s_{12} in the last term of the equation for $\text{split}_-^{q \rightarrow qgg}(k_1^+, k_2^+, k_3^-)$

We see that the two sets of results have the same types of singularity structure as $z_3 \rightarrow 0$ and $z_1 \rightarrow 1$ corresponding to the soft and double soft gluon limits.

$\bar{q}qg \rightarrow g$

There are again only two independent $\Delta M = 1$ amplitudes, both of which can be obtained from Eq. (5.42) by setting $s = 2$ and $\lambda = \pm\frac{1}{2}$. We find,

$$\begin{aligned} \text{split}(1^+, 2_{\bar{q}}^+, 3_q^- \rightarrow P^+) &= -\frac{(\langle 12 \rangle \sqrt{z_1} + \langle 32 \rangle \sqrt{z_3}) (\langle 13 \rangle \sqrt{z_1} + \langle 23 \rangle \sqrt{z_2})^2}{\langle 12 \rangle \langle 23 \rangle s_{1,3} (\langle 21 \rangle \sqrt{z_2} + \langle 31 \rangle \sqrt{z_3})} \\ &\quad + \frac{z_2 \langle 23 \rangle}{\sqrt{z_1} s_{2,3} (\langle 21 \rangle \sqrt{z_2} + \langle 31 \rangle \sqrt{z_3}) (z_2 + z_3)}, \end{aligned} \quad (5.100)$$

$$\begin{aligned} \text{split}(1^+, 2_{\bar{q}}^-, 3_q^+ \rightarrow P^+) &= -\frac{(\langle 12 \rangle \sqrt{z_1} + \langle 32 \rangle \sqrt{z_3})^3}{\langle 12 \rangle \langle 23 \rangle s_{1,3} (\langle 21 \rangle \sqrt{z_2} + \langle 31 \rangle \sqrt{z_3})} \\ &\quad + \frac{z_3 \langle 23 \rangle}{\sqrt{z_1} s_{2,3} (\langle 21 \rangle \sqrt{z_2} + \langle 31 \rangle \sqrt{z_3}) (z_2 + z_3)}. \end{aligned} \quad (5.101)$$

All others can be obtained via parity and charge conjugation. Eq. (5.100) numerically agrees with the analogous expression given in Ref. [137]. Eq. (5.101) numerically agrees with the splitting functions given in Ref. [137] after correcting a small typographical error in Ref. [137], Eq. (5.54). The factor of $[13]z_3$ in the denominator of the second term for $\text{split}_-^{g \rightarrow g\bar{q}q}(k_1^+, k_2^-, k_3^+)$ should be replaced by $[13]$.

$q\bar{Q}Q \rightarrow q$ and $q\bar{q}Q \rightarrow Q$

In this special case both colour structures lead to the same splitting amplitude. There is only one independent $\Delta M = 1$ helicity configuration, the specific splitting

$1_q^-, 2_{\bar{Q}}^+, 3_{\bar{Q}}^- \rightarrow P_q^-$. Our MHV rules approach yields,

$$\begin{aligned} \text{split}(1_q^+, 2_{\bar{Q}}^+, 3_{\bar{Q}}^- \rightarrow P_q^+) &= -\frac{\langle 23 \rangle z_2}{s_{2,3} (\langle 12 \rangle \sqrt{z_2} + \langle 13 \rangle \sqrt{z_3}) (z_2 + z_3)} \\ &+ \frac{(\langle 13 \rangle \sqrt{z_1} + \langle 23 \rangle \sqrt{z_2})^2}{s_{1,3} (\langle 12 \rangle \sqrt{z_2} + \langle 13 \rangle \sqrt{z_3}) \langle 23 \rangle}, \end{aligned} \quad (5.102)$$

As expected, the s_{12} pole is absent because there is no $q\bar{Q}$ collinear limit.

We can use this splitting amplitude to analyse the singularity structure of collinear limits derived from different methods. When $\Delta M = \Delta P$ both MHV and $\overline{\text{MHV}}$ rules are expected to yield results of similar complexity. Here we have $\Delta M = \Delta P = 1$. In full generality, the MHV ($\overline{\text{MHV}}$) rules approach should generate a maximum of three terms corresponding to simple poles in $s_{1,2}$, $s_{2,3}$ and $s_{1,3} \equiv (p_1 + p_2 + p_3)^2$. We can see from equation (5.102) that this is indeed the case here.

The $\overline{\text{MHV}}$ rules approach finds this splitting amplitude to have the form,

$$\begin{aligned} \text{split}(1_q^+, 2_{\bar{Q}}^+, 3_{\bar{Q}}^- \rightarrow P_q^+) &= \frac{z_1 z_3 [23]}{s_{2,3} ([12] \sqrt{z_2} + [13] \sqrt{z_3}) (z_2 + z_3)} \\ &- \frac{[12]^2}{s_{1,3} ([12] \sqrt{z_2} + [13] \sqrt{z_3}) [23]}. \end{aligned} \quad (5.103)$$

Again, the s_{12} pole is absent.

By taking the limit of a Feynman diagram calculation, Ref. [137] finds,

$$\text{split}(1_q^+, 2_{\bar{Q}}^+, 3_{\bar{Q}}^- \rightarrow P_q^+) = \frac{\sqrt{z_1 z_2 z_3}}{s_{2,3} (z_2 + z_3)} + \frac{[12] (\langle 13 \rangle \sqrt{z_1} + \langle 23 \rangle \sqrt{z_2})}{s_{1,3} s_{2,3}} \quad (5.104)$$

Results (5.102), (5.103) and (5.104) are for the same amplitude and all three expressions agree numerically. But the analytic form of these specific representations is different. In agreement with eqs. (5.17)-(5.18), the functions accompanying the $1/s$ poles, are holomorphic in the MHV result (5.102), are anti-holomorphic in the $\overline{\text{MHV}}$

expression (5.103), while the Feynman diagram result (5.104) contains a mixture of holomorphic and anti-holomorphic terms. (In this case, it happens to give a more compact result.) In general, the limit of an amplitude computed using the BCF recursion relations will also provide a mixed holomorphic/anti-holomorphic splitting function as we have seen in section 5.5.1. In this specific case, taking the collinear limit of the compact expression for the appropriate six-parton amplitude given in Ref. [119] exactly reproduces the MHV result of eq. (5.103).

5.6 Summary

In this chapter we have considered the collinear limit of multi-parton QCD amplitudes at tree level. We have begun by introducing collinear limits and the concept of splitting functions, before examining their singular structure in the spinor formalism. We have found that in the collinear limit, only a subset of the MHV rules diagrams contribute – those where every propagator invariant s goes on-shell in the multi-collinear limit. This is a strong restriction on the number of contributing diagrams, and enables us to find collinear limits without the use of full amplitudes. We have then used this fact and the MHV rules to find general expressions for collinear limits with arbitrary numbers of positive helicity gluons, and up to three negative gluons, or four (massless) quarks. These general results are enough to provide **all** the splitting functions for up to 6 gluons, and up to four partons. We explicitly give results for up to 5 gluons and three quarks.

Chapter 6

Conclusion

In this thesis we have explored various aspects of perturbative field theory contributing to cross-sections beyond the leading order in QCD. To test the Standard Model (SM) we need theoretical predictions with the same or better accuracy than the results obtained from state of the art experiments, such as the forthcoming Large Hadron Collider (LHC). To increase the accuracy of our theoretical predictions for cross-sections, we need to evaluate them beyond the leading order in the perturbative expansion in the coupling constant. When we proceed to higher orders, we need to be able to evaluate the loop-integrals which occur and the singularities which they possess. Correspondingly, to cancel these singularities, the limits of tree-level processes when two or more particles become collinear must also be known. These two subjects form the basis of the studies carried out in this thesis.

To enable us to study the higher order corrections to physical processes, in Chapter 1 we have introduced the fundamental underlying field theories in the SM. From the Lagrangian the Feynman rules for the theory can be derived, which give us the mathematical structure of Feynman diagrams. Beyond the leading order, we see that two types of singularities occur. The Ultra-Violet (UV) singularities are associ-

ated with high loop-momenta, and these divergences can be removed order by order through the redefinition of fields and parameters, a process known as renormalisation. Infra-Red (IR) divergences occur through specific values of low loop-momenta causing divergences of loop integrals. These divergences are cancelled when we consider tree-level processes with extra final state particles. The phase-space integral will be divergent in the limits when these extra particles become soft or collinear, and these divergences will cancel against those arising from the loop integrals. To deal with the singularities which arise in a mathematically consistent way we have introduced the concept of regularisation, in particular Dimensional Regularisation, in which the space-time dimension of the theory is analytically continued away from $d = 4$ to $d = 4 - 2\epsilon$. The singularities then manifest themselves as poles in the continuation parameter ϵ .

We have proceeded to outline some of the available methods with which to solve loop integrals, in particular massless integrals, beginning with the basic one loop integral in Minkowski space, which we have solved using the method of Feynman Parameters and Wick-rotation. In Chapter 2 this has allowed us to derive the one-loop scalar bubble with arbitrary powers of propagators. Using this result we can solve many simple multi-loop integrals through the method of bubble insertions, for example we have derived the two-loop sunset integral, and through factorisation we have found the two-loop Glasses integral. When examining multi-loop processes, the number of integrals which need to be evaluated grows unmanageable, and so we look for an automated method for their solution. The linear identities obeyed by loop integrals, the IBP and LI identities, allow us to express all of the required integrals in terms of a small subset of so-called Master Integrals. This reduction process has been automated via the Laporta reduction algorithm which we have outlined here. The remaining Master Integrals which are not already known can

then be solved through the method of Differential Equations. This method, as outlined in section 2.6, relies on the use of the IBP and LI identities to express the differential equations in external invariants in terms of previously known integrals. These differential equations can then be solved order by order in ϵ using repeated integration. The boundary conditions required to fix the solutions are obtained either from corresponding integrals with fewer off-shell legs, or from the integral itself. The Harmonic Polylogarithms described here form a natural basis set of functions in which to express the solutions to these differential equations. This is due to their definition by repeated integration, which matches the method of solution for the differential equations.

In Chapter 3 we use the method of differential equations to provide series expansions in ϵ for all two-loop Master Integrals with three external off-shell legs and all internal lines being massless. The results are presented in terms of an extended basis of 2-dimensional harmonic polylogarithms. The novel feature here is that this basis set includes quadratic forms. These are introduced as a natural set of functions which match on to the allowed phase space boundary for the $1 \rightarrow 2$ decay. For each Master Integral, we have given sufficient terms in the ϵ -expansion to describe two-loop vertex corrections for physical processes. The MI presented here are ingredients for a variety of interesting two-loop processes such as the QCD corrections to $H \rightarrow V^*V^*$ decay in the heavy top quark limit and the QCD corrections to the fully off-shell triple gluon (and quark-gluon) vertices. These MI also form a staging post for the study of massless two-loop $2 \rightarrow 2$ scattering amplitudes with two off-shell legs. These processes include the NNLO QCD corrections to $q\bar{q} \rightarrow V^*V^*$ (where $V = W, Z$) and the NLO corrections to $gg \rightarrow V^*V^*$. Altogether there are 11 planar box and 3 non-planar box master topologies for the massless two-loop $2 \rightarrow 2$ scattering amplitudes with two off-shell legs, which depend on the Master Integrals evaluated

here. Their evaluation remains a future application of the Master integrals and methods described in this thesis.

In Chapter 4 we have introduced the MHV construction. This is a recent development which enables tree-level helicity amplitudes to be evaluated giving compact results. To use this method we have introduced colour ordered amplitudes. These greatly reduce the number of tree-level diagrams which need to be calculated by factoring out the colour factors from the purely kinematic amplitudes. When expressed in the spinor helicity formalism the helicity amplitudes have a simple form which is not apparent from their Feynman rule construction. The MHV rules of Cachazo, Svrcek and Witten use the Maximal Helicity Violating amplitudes as vertices, which are combined via scalar propagators and summed over all possible configurations to reproduce the tree-level helicity amplitudes. A second method for the calculation of tree-level helicity amplitudes has recently been developed, the BCF recursion relations, which we have introduced here for the sake of completeness, and which we have used as a check of the methods developed in chapter 5.

We have considered the collinear limit of multi-parton QCD amplitudes at tree level in Chapter 5. Collinear limits are required in higher order calculations to cancel against the IR singularities of loop-integrals. In general, to compute a cross section at N^n LO, one requires detailed knowledge of the infrared factorisation functions describing the unresolved configurations for n -particles at tree-level, $(n-1)$ -particles at one-loop etc. The factorisation properties of amplitudes in the infrared play several roles in developing higher order perturbative predictions for observable quantities. A detailed knowledge of the structure of unresolved emission enables phase space integrations to be organised such that the infrared singularities due to soft or collinear emission can be analytically subtracted at NLO. Collinear limits enable large logarithmic corrections to be identified and resummed, and they play a crucial role in the

unitarity-based method for loop calculations. Collinear limits of QCD amplitudes are responsible for parton evolution and as such the n -particle tree-level collinear limits contribute to the Altarelli-Parisi evolution kernels at $N^{n-1}LO$. These kernels control the scale evolution of parton densities and fragmentation functions, and so are vital for the calculation of multi-jet events at the LHC. Lastly the collinear limits of amplitudes are very useful as consistency checks of the correctness of calculations.

We have used the new MHV rules for constructing colour ordered amplitudes from MHV vertices together with the general collinear factorisation formula to derive timelike splitting functions that are valid for specific numbers of negative helicity gluons with an arbitrary number of positive helicity gluons (or vice versa). In this limit, the full amplitude factorises into an MHV vertex multiplied by a multi-collinear splitting function that depends on the helicities of the collinear gluons. These splitting functions are derived directly using collinear limits of MHV rules. A key point of our approach is that in the collinear limit only a subset of MHV rules diagrams contribute - those where every propagator invariant s goes on-shell in the multi-collinear limit. We observe that the splitting functions have a simple structure, and can be written as sums over the corresponding poles in s multiplied by a coefficient that is either entirely composed of holomorphic spinor products $\langle ij \rangle$ or entirely composed of anti-holomorphic spinor products $[ij]$. This implies that the coefficients are supported on a single degree-one curve in (anti)-twistor space.

We find that the splitting functions can be characterised by ΔM , the difference between the number of negative helicity partons before taking the collinear limit, and the number after. $\Delta M + 1$ also coincides with the number of MHV vertices involved in the splitting functions. Our main results are splitting functions for arbitrary numbers of gluons where $\Delta M = 0, 1, 2$. Splitting functions where the difference in the number of positive helicity gluons $\Delta P = 0, 1, 2$ are obtained by the

parity transformation. These general results are sufficient to describe *all* collinear limits with up to six gluons. We have given explicit results for up to four collinear gluons for all independent helicity combinations, which numerically agree with the results of Ref. [137], together with new results for five and six collinear gluons. This method could be applied to higher numbers of negative helicity gluons.

We have also considered the collinear limit of multi-parton QCD amplitudes at tree level. Our main results are general formulae for timelike splitting functions involving up to two negative helicity partons and an arbitrary number of positive helicity partons. This completes the set of all possible partonic splitting functions for up to 4 partons. Again the method here is applicable to collinear limits with higher numbers of negative helicity partons. We anticipate that the expressions presented here will be useful in developing higher order perturbative predictions for observable quantities, such as jet cross sections at the LHC or in examining the high energy limit of QCD.

The combined results of this thesis are a small contribution to the wide-ranging efforts of the theoretical community in preparation for the next generation of particle colliders. Our results will aid in the evaluation of physical processes at NNLO and beyond, helping elucidate the QCD backgrounds to searches for new processes, and testing the standard model to the highest levels of precision in the search for evidence of new physics.

Appendix A

Properties of extended HPL's

In this appendix, we detail the connection between the harmonic polylogarithms produced by a linear basis and those introduced by the quadratic basis of Eqs. (3.8)–(3.11).

The integrals in the quadratic basis depend on λ (as defined in Eq. (3.3)) and are of the form,

$$I_1 = \int \frac{1}{\lambda} f(x) dx, \quad I_2 = \int \frac{1}{\lambda^2} f(x) dx. \quad (\text{A.1})$$

With the help of one of the Euler Transformations

$$\lambda = 2t + x \quad \Rightarrow \quad x = -\frac{(t-a)(t+a)}{(t-b)} \quad (\text{A.2})$$

with

$$a = -\frac{1-y}{2}, \quad b = -\frac{1+y}{2} \quad (\text{A.3})$$

the integrals in (A.1) can be transformed into the linear basis,

$$I_1 = -\int \frac{1}{t-b} f(t) dt, \quad I_2 = -\int \frac{1}{(t-a_1)(t-a_2)} f(t) dt \quad (\text{A.4})$$

where a_1, a_2 are the roots of the polynomial,

$$\mathcal{P} = \frac{1}{4}(1 + 4t + 4t^2 - 2y + 4ty + y^2) \quad (\text{A.5})$$

yielding

$$a_1 = -\frac{1}{2}(1 + \sqrt{y})^2, \quad a_2 = -\frac{1}{2}(1 - \sqrt{y})^2. \quad (\text{A.6})$$

In the following we will present relation between the function in the x and in the t basis. We will give transformations for the basis function in combination with the measure and the relation between the integrated functions. Let the functions in the set involving the roots be denoted by f and H and the functions in the linear basis by g and G ,

$$f(0)dx \rightarrow g(a)dt + g(-a)dt - g(b)dt$$

$$H(0, x) = G(a, t) + G(-a, t) - G(b, t)$$

$$f(\lambda)dx \rightarrow -g(b)dt$$

$$H(\lambda, x) = -G(b, t)$$

$$f(x\lambda)dx \rightarrow \frac{1}{y-1}g(a)dt + \frac{1}{y-1}g(-a)dt$$

$$H(x\lambda) \rightarrow \frac{1}{y-1}G(a) + \frac{1}{y-1}G(-a)dt$$

$$f(x_{0,1})dx \rightarrow g(b)dt - 2g(a_{2,1})dt$$

$$H(x_{0,1}, x) = G(b, t) - 2G(a_{2,1}, t),$$

where

$$g(\pm A; t) = \frac{1}{t \mp A}$$

with $A \in \{a, b, a_1, a_2\}$.

From the boundary conditions, we need limits of our extended HPLs when one of the scales is zero. In this limit the HPL's will only depend on one scale and so we can express them in terms of the 1-d HPL's of section 2.7. With explicit (x, y) dependence, we have at weight one,

$$\begin{aligned}
 G(\lambda; 0, y) &= \frac{1}{2}H(0; y), \\
 G(x_1; 0, y) &= 2H(1; y) + H(0; x_0) + 2 \ln 2 + \frac{1}{2}H(0; y), \\
 \Delta G(0; 0, y) &= -2H(1; y) - H(0; x_0) - \frac{1}{2}H(0; y).
 \end{aligned}
 \tag{A.7}$$

$G(x_0; 0, y)$ is singular. At weight 2 we have for example,

$$\begin{aligned}
 G(\lambda, 0; 0, y) &= \frac{\pi^2}{6} - H(0, 1; y) - \frac{1}{2}H(0; x_0)H(0; y), \\
 G(\lambda, \lambda; 0, y) &= \frac{1}{4}H(0, 0; y), \\
 G(\lambda, x\lambda; 0, y) &= \frac{1}{y-1} \left(-\frac{\pi^2}{6} - H(0, 1; y) - \frac{1}{4}H(0, 0; y) + 2H(0, 1; \sqrt{y}) \right), \\
 G(\lambda, x_1; 0, y) &= -\frac{\pi^2}{6} + \ln 2H(0; y) - \frac{1}{4}H(0, 0; y) - 2H(0, 1; -\frac{1}{\sqrt{y}}), \\
 G(x_1, \lambda; 0, y) &= \frac{\pi^2}{6} + H(0; y)H(1; y) + \frac{1}{2}H(0; y)H(0; x_0) \\
 &\quad + \frac{3}{4}H(0, 0; y) + 2H(0, 1; -\frac{1}{\sqrt{y}}), \\
 \Delta G(0, \lambda; 0, y) &= -2H(0, 1; \frac{1}{y}) - \frac{7}{4}H(0, 0; y) + 2H(0, 1; \frac{1}{\sqrt{y}}) + H(0; y)H(0; y-1).
 \end{aligned}$$

The first of these results is necessary to show that F_3 is finite. Higher weight results can be found using the linear basis, properties of 1-d HPL's and relations between dilogarithms.

Appendix B

F_4 at $\mathcal{O}(\epsilon)$

$$\begin{aligned}
 f_4^1(x, y) = & + 112 \zeta_3 G(\lambda, \lambda; x, y) + 8 (y - 1) \zeta_3 G(\lambda, x\lambda; x, y) \\
 & + 8 (y - 1) \zeta_3 G(x\lambda, \lambda; x, y) + 32 (y - 1)^2 \zeta_3 G(x\lambda, x\lambda; x, y) \\
 & + \frac{4\pi^2}{3} G(\lambda, 0, \lambda; x, y) + \frac{4\pi^2 (y - 1)}{3} G(\lambda, 0, x\lambda; x, y) \\
 & + \frac{4\pi^2}{3} G(\lambda, \lambda, 0; x, y) + \frac{8\pi^2}{3} G(\lambda, x_0, \lambda; x, y) + \frac{4\pi^2 (y - 1)}{3} G(\lambda, x_0, x\lambda; x, y) \\
 & + \frac{8\pi^2}{3} G(\lambda, x_1, \lambda; x, y) + \frac{4\pi^2 (y - 1)}{3} G(\lambda, x_1, x\lambda; x, y) \\
 & + \frac{4\pi^2 (y - 1)}{3} G(\lambda, x\lambda, 0; x, y) - \frac{8\pi^2}{3} G(x_0, \lambda, \lambda; x, y) \\
 & - \frac{4\pi^2 (y - 1)}{3} G(x_0, \lambda, x\lambda; x, y) - \frac{4\pi^2 (y - 1)}{3} G(x_0, x\lambda, \lambda; x, y) \\
 & - \frac{8\pi^2}{3} G(x_1, \lambda, \lambda; x, y) - \frac{4\pi^2 (y - 1)}{3} G(x_1, \lambda, x\lambda; x, y) \\
 & - \frac{4\pi^2 (y - 1)}{3} G(x_1, x\lambda, \lambda; x, y) + \frac{8\pi^2 (y - 1)}{3} G(x\lambda, 0, \lambda; x, y) \\
 & + \frac{4\pi^2 (y - 1)}{3} G(x\lambda, \lambda, 0; x, y) + \frac{4\pi^2 (y - 1)}{3} G(x\lambda, x_0, \lambda; x, y) \\
 & + \frac{4\pi^2 (y - 1)}{3} G(x\lambda, x_1, \lambda; x, y) - \frac{4\pi^2 (y - 1)^2}{3} G(x\lambda, x\lambda, 0; x, y) \\
 & + 16 G(\lambda, 0, 0, \lambda, 0; x, y) + 24 G(\lambda, 0, \lambda, 0, 0; x, y) + 8 G(\lambda, 0, x_0, \lambda, 0; x, y) \\
 & + 8 G(\lambda, 0, x_1, \lambda, 0; x, y) + 48 G(\lambda, \lambda, 0, 0, 0; x, y) - 72 G(\lambda, \lambda, \lambda, \lambda, 0; x, y) \\
 & + 8 G(\lambda, x_0, 0, \lambda, 0; x, y) + 16 G(\lambda, x_0, \lambda, 0, 0; x, y) + 8 G(\lambda, x_1, 0, \lambda, 0; x, y) +
 \end{aligned}$$

$$\begin{aligned}
& + 16 G(\lambda, x_1, \lambda, 0, 0; x, y) + 24 (y - 1)^2 G(\lambda, x\lambda, x\lambda, \lambda, 0; x, y) \\
& - 8 G(x_0, \lambda, 0, \lambda, 0; x, y) - 16 G(x_0, \lambda, \lambda, 0, 0; x, y) - 8 G(x_1, \lambda, 0, \lambda, 0; x, y) \\
& - 16 G(x_1, \lambda, \lambda, 0, 0; x, y) + 24 (y - 1)^2 G(x\lambda, \lambda, x\lambda, \lambda, 0; x, y) \\
& + 24 (y - 1)^2 G(x\lambda, x\lambda, \lambda, \lambda, 0; x, y) + \frac{-2\pi^2}{3} \Delta G(0; 0, x_0) G(\lambda, \lambda; x, y) \\
& + \frac{2\pi^2 (y - 1)^2}{3} \Delta G(0; 0, x_0) G(x\lambda, x\lambda; x, y) \\
& + \frac{-4\pi^2 (y - 1)}{3} \Delta G(0; 0, y) G(\lambda, x\lambda; x, y) \\
& + \frac{-4\pi^2 (y - 1)}{3} \Delta G(0; 0, y) G(x\lambda, \lambda; x, y) - 12 \Delta G(0, \lambda, 0; 0, x_0) G(\lambda, \lambda; x, y) \\
& + 12 (y - 1)^2 \Delta G(0, \lambda, 0; 0, x_0) G(x\lambda, x\lambda; x, y) \\
& - 16 (y - 1) \Delta G(0, \lambda, 0; 0, y) G(\lambda, x\lambda; x, y) \\
& - 16 (y - 1) \Delta G(0, \lambda, 0; 0, y) G(x\lambda, \lambda; x, y) + \frac{-2\pi^2}{3} G(\lambda; 0, x_0) G(\lambda, \lambda; x, y) \\
& + \frac{2\pi^2 (y - 1)^2}{3} G(\lambda; 0, x_0) G(x\lambda, x\lambda; x, y) \\
& + \frac{8\pi^2}{3} G(\lambda; 0, y) G(\lambda, \lambda; x, y) \\
& - 8 G(\lambda, 0; 0, x_0) G(\lambda, 0, \lambda; x, y) - 8 G(\lambda, 0; 0, x_0) G(\lambda, \lambda, 0; x, y) \\
& - 16 G(\lambda, 0; 0, x_0) G(\lambda, x_0, \lambda; x, y) - 16 G(\lambda, 0; 0, x_0) G(\lambda, x_1, \lambda; x, y) \\
& + 16 G(\lambda, 0; 0, x_0) G(x_0, \lambda, \lambda; x, y) + 16 G(\lambda, 0; 0, x_0) G(x_1, \lambda, \lambda; x, y) \\
& + 8 (y - 1)^2 G(\lambda, 0; 0, x_0) G(x\lambda, x\lambda, 0; x, y) + (8 - 8y) G(\lambda, 0; 0, y) G(\lambda, 0, x\lambda; x, y) \\
& + (8 - 8y) G(\lambda, 0; 0, y) G(\lambda, x_0, x\lambda; x, y) + (8 - 8y) G(\lambda, 0; 0, y) G(\lambda, x_1, x\lambda; x, y) \\
& + (8 - 8y) G(\lambda, 0; 0, y) G(\lambda, x\lambda, 0; x, y) + 8 (y - 1) G(\lambda, 0; 0, y) G(x_0, \lambda, x\lambda; x, y) \\
& + 8 (y - 1) G(\lambda, 0; 0, y) G(x_0, x\lambda, \lambda; x, y) + 8 (y - 1) G(\lambda, 0; 0, y) G(x_1, \lambda, x\lambda; x, y) \\
& + 8 (y - 1) G(\lambda, 0; 0, y) G(x_1, x\lambda, \lambda; x, y) - 16 (y - 1) G(\lambda, 0; 0, y) G(x\lambda, 0, \lambda; x, y) \\
& + (8 - 8y) G(\lambda, 0; 0, y) G(x\lambda, \lambda, 0; x, y) + (8 - 8y) G(\lambda, 0; 0, y) G(x\lambda, x_0, \lambda; x, y) \\
& + (8 - 8y) G(\lambda, 0; 0, y) G(x\lambda, x_1, \lambda; x, y) - 16 G(\lambda, \lambda; x, y) G(\lambda, 0, 0; 0, x_0) \\
& - 16 G(\lambda, \lambda; x, y) G(\lambda, 0, \lambda; 0, y) - 12 G(\lambda, \lambda; x, y) G(\lambda, \lambda, 0; 0, x_0) \\
& + 16 G(\lambda, \lambda; x, y) G(\lambda, \lambda, 0; 0, y) - 8 G(\lambda, \lambda; x, y) G(x_0, \lambda, 0; 0, x_0) +
\end{aligned}$$

$$\begin{aligned}
& -8G(\lambda, \lambda; x, y)G(x_1, \lambda, 0; 0, x_0) + \frac{4\pi^2}{3}G(\lambda, \lambda; x, y)H(0; x_0) \\
& + \frac{-8\pi^2}{3}G(\lambda, \lambda; x, y)H(0; y) + \frac{-4\pi^2}{3}G(\lambda, \lambda; x, y)H(1; x_0) \\
& + 48G(\lambda, \lambda; x, y)H(0, 0, 0; x_0) + 12G(\lambda, \lambda; x, y)H(0, 0, 0; y) \\
& + 8G(\lambda, \lambda; x, y)H(0, 1, 0; x_0) - 16G(\lambda, \lambda; x, y)H(0, 1, 0; y) \\
& + 8G(\lambda, \lambda; x, y)H(1, 0, 0; x_0) + 16G(\lambda, \lambda; x, y)H(1, 0, 0; y) \\
& - 8G(\lambda, \lambda; x, y)H(1, 1, 0; x_0) - 16(y-1)G(\lambda, x\lambda; x, y)G(\lambda, 0, 0; 0, y) \\
& + 8(y-1)^2G(\lambda, x\lambda; x, y)G(\lambda, 0, x\lambda; 0, y) + 8(y-1)^2G(\lambda, x\lambda; x, y)G(\lambda, x\lambda, 0; 0, y) \\
& - 16(y-1)G(\lambda, x\lambda; x, y)G(x_0, \lambda, 0; 0, y) - 16(y-1)G(\lambda, x\lambda; x, y)G(x_1, \lambda, 0; 0, y) \\
& + \frac{4\pi^2(y-1)}{3}G(\lambda, x\lambda; x, y)H(0; y) + \frac{-8\pi^2(y-1)}{3}G(\lambda, x\lambda; x, y)H(1; y) \\
& + 12(y-1)G(\lambda, x\lambda; x, y)H(0, 0, 0; y) + 8(y-1)G(\lambda, x\lambda; x, y)H(0, 1, 0; y) \\
& + 24(y-1)G(\lambda, x\lambda; x, y)H(1, 0, 0; y) - 16(y-1)G(\lambda, x\lambda; x, y)H(1, 1, 0; y) \\
& - 16(y-1)G(x\lambda, \lambda; x, y)G(\lambda, 0, 0; 0, y) + 8(y-1)^2G(x\lambda, \lambda; x, y)G(\lambda, 0, x\lambda; 0, y) \\
& + 8(y-1)^2G(x\lambda, \lambda; x, y)G(\lambda, x\lambda, 0; 0, y) - 16(y-1)G(x\lambda, \lambda; x, y)G(x_0, \lambda, 0; 0, y) \\
& - 16(y-1)G(x\lambda, \lambda; x, y)G(x_1, \lambda, 0; 0, y) + \frac{4\pi^2(y-1)}{3}G(x\lambda, \lambda; x, y)H(0; y) \\
& + \frac{-8\pi^2(y-1)}{3}G(x\lambda, \lambda; x, y)H(1; y) + 12(y-1)G(x\lambda, \lambda; x, y)H(0, 0, 0; y) \\
& + 8(y-1)G(x\lambda, \lambda; x, y)H(0, 1, 0; y) + 24(y-1)G(x\lambda, \lambda; x, y)H(1, 0, 0; y) \\
& - 16(y-1)G(x\lambda, \lambda; x, y)H(1, 1, 0; y) + 16(y-1)^2G(x\lambda, x\lambda; x, y)G(\lambda, 0, 0; 0, x_0) \\
& + 12(y-1)^2G(x\lambda, x\lambda; x, y)G(\lambda, \lambda, 0; 0, x_0) + 8(y-1)^2G(x\lambda, x\lambda; x, y)G(x_0, \lambda, 0; 0, x_0) \\
& + 8(y-1)^2G(x\lambda, x\lambda; x, y)G(x_1, \lambda, 0; 0, x_0) + \frac{-4\pi^2(y-1)^2}{3}G(x\lambda, x\lambda; x, y)H(0; x_0) \\
& + \frac{4\pi^2(y-1)^2}{3}G(x\lambda, x\lambda; x, y)H(1; x_0) + 12(y-1)^2G(x\lambda, x\lambda; x, y)H(0, 0, 0; y) \\
& - 8(y-1)^2G(x\lambda, x\lambda; x, y)H(0, 1, 0; x_0) - 8(y-1)^2G(x\lambda, x\lambda; x, y)H(1, 0, 0; x_0) \\
& + 8(y-1)^2G(x\lambda, x\lambda; x, y)H(1, 1, 0; x_0) + 24G(\lambda, 0, \lambda; x, y)H(0, 0; x_0) \\
& - 4G(\lambda, 0, \lambda; x, y)H(0, 0; y) + 8G(\lambda, 0, \lambda; x, y)H(1, 0; x_0) \\
& + (4-4y)G(\lambda, 0, x\lambda; x, y)H(0, 0; y) + 8(y-1)G(\lambda, 0, x\lambda; x, y)H(1, 0; y) \\
& + 48G(\lambda, \lambda, 0; x, y)H(0, 0; x_0) - 20G(\lambda, \lambda, 0; x, y)H(0, 0; y) +
\end{aligned}$$

$$\begin{aligned}
& + 8G(\lambda, \lambda, 0; x, y) H(1, 0; x_0) + 16G(\lambda, x_0, \lambda; x, y) H(0, 0; x_0) \\
& + 4G(\lambda, x_0, \lambda; x, y) H(0, 0; y) + 16G(\lambda, x_0, \lambda; x, y) H(1, 0; x_0) \\
& + 4(y-1)G(\lambda, x_0, x\lambda; x, y) H(0, 0; y) + 8(y-1)G(\lambda, x_0, x\lambda; x, y) H(1, 0; y) \\
& + 16G(\lambda, x_1, \lambda; x, y) H(0, 0; x_0) + 4G(\lambda, x_1, \lambda; x, y) H(0, 0; y) \\
& + 16G(\lambda, x_1, \lambda; x, y) H(1, 0; x_0) + 4(y-1)G(\lambda, x_1, x\lambda; x, y) H(0, 0; y) \\
& + 8(y-1)G(\lambda, x_1, x\lambda; x, y) H(1, 0; y) + (8-8y)G(\lambda, x\lambda, 0; x, y) H(0, 0; y) \\
& + 8(y-1)G(\lambda, x\lambda, 0; x, y) H(1, 0; y) - 16G(x_0, \lambda, \lambda; x, y) H(0, 0; x_0) \\
& - 4G(x_0, \lambda, \lambda; x, y) H(0, 0; y) - 16G(x_0, \lambda, \lambda; x, y) H(1, 0; x_0) \\
& + (4-4y)G(x_0, \lambda, x\lambda; x, y) H(0, 0; y) + (8-8y)G(x_0, \lambda, x\lambda; x, y) H(1, 0; y) \\
& + (4-4y)G(x_0, x\lambda, \lambda; x, y) H(0, 0; y) + (8-8y)G(x_0, x\lambda, \lambda; x, y) H(1, 0; y) \\
& - 4(y-1)^2G(x_0, x\lambda, x\lambda; x, y) H(0, 0; y) - 16G(x_1, \lambda, \lambda; x, y) H(0, 0; x_0) \\
& - 4G(x_1, \lambda, \lambda; x, y) H(0, 0; y) - 16G(x_1, \lambda, \lambda; x, y) H(1, 0; x_0) \\
& + (4-4y)G(x_1, \lambda, x\lambda; x, y) H(0, 0; y) + (8-8y)G(x_1, \lambda, x\lambda; x, y) H(1, 0; y) \\
& + (4-4y)G(x_1, x\lambda, \lambda; x, y) H(0, 0; y) + (8-8y)G(x_1, x\lambda, \lambda; x, y) H(1, 0; y) \\
& - 4(y-1)^2G(x_1, x\lambda, x\lambda; x, y) H(0, 0; y) + 8(y-1)G(x\lambda, 0, \lambda; x, y) H(0, 0; y) \\
& + 16(y-1)G(x\lambda, 0, \lambda; x, y) H(1, 0; y) + 8(y-1)^2G(x\lambda, 0, x\lambda; x, y) H(0, 0; y) \\
& + (8-8y)G(x\lambda, \lambda, 0; x, y) H(0, 0; y) + 8(y-1)G(x\lambda, \lambda, 0; x, y) H(1, 0; y) \\
& + 4(y-1)G(x\lambda, x_0, \lambda; x, y) H(0, 0; y) + 8(y-1)G(x\lambda, x_0, \lambda; x, y) H(1, 0; y) \\
& + 4(y-1)^2G(x\lambda, x_0, x\lambda; x, y) H(0, 0; y) + 4(y-1)G(x\lambda, x_1, \lambda; x, y) H(0, 0; y) \\
& + 8(y-1)G(x\lambda, x_1, \lambda; x, y) H(1, 0; y) + 4(y-1)^2G(x\lambda, x_1, x\lambda; x, y) H(0, 0; y) \\
& + 4(y-1)^2G(x\lambda, x\lambda, 0; x, y) H(0, 0; y) - 8(y-1)^2G(x\lambda, x\lambda, 0; x, y) H(1, 0; x_0) \\
& + 16G(\lambda, 0, 0, \lambda; x, y) H(0; x_0) - 8G(\lambda, 0, 0, \lambda; x, y) H(0; y) \\
& + (8-8y)G(\lambda, 0, 0, x\lambda; x, y) H(0; y) + 24G(\lambda, 0, \lambda, 0; x, y) H(0; x_0) \\
& - 4G(\lambda, 0, \lambda, 0; x, y) H(0; y) + 8G(\lambda, 0, x_0, \lambda; x, y) H(0; x_0) \\
& - 4G(\lambda, 0, x_0, \lambda; x, y) H(0; y) + (4-4y)G(\lambda, 0, x_0, x\lambda; x, y) H(0; y) +
\end{aligned}$$

$$\begin{aligned}
& + 8G(\lambda, 0, x_1, \lambda; x, y) H(0; x_0) - 4G(\lambda, 0, x_1, \lambda; x, y) H(0; y) \\
& + (4 - 4y) G(\lambda, 0, x_1, x\lambda; x, y) H(0; y) + (4 - 4y) G(\lambda, 0, x\lambda, 0; x, y) H(0; y) \\
& + 48G(\lambda, \lambda, 0, 0; x, y) H(0; x_0) - 8G(\lambda, \lambda, 0, 0; x, y) H(0; y) \\
& - 72G(\lambda, \lambda, \lambda, \lambda; x, y) H(0; x_0) + 36G(\lambda, \lambda, \lambda, \lambda; x, y) H(0; y) \\
& + 36(y - 1) G(\lambda, \lambda, \lambda, x\lambda; x, y) H(0; y) + 8G(\lambda, x_0, 0, \lambda; x, y) H(0; x_0) \\
& - 4G(\lambda, x_0, 0, \lambda; x, y) H(0; y) + (4 - 4y) G(\lambda, x_0, 0, x\lambda; x, y) H(0; y) \\
& + 16G(\lambda, x_0, \lambda, 0; x, y) H(0; x_0) - 8G(\lambda, x_0, \lambda, 0; x, y) H(0; y) \\
& + (4 - 4y) G(\lambda, x_0, x\lambda, 0; x, y) H(0; y) + 8G(\lambda, x_1, 0, \lambda; x, y) H(0; x_0) \\
& - 4G(\lambda, x_1, 0, \lambda; x, y) H(0; y) + (4 - 4y) G(\lambda, x_1, 0, x\lambda; x, y) H(0; y) \\
& + 16G(\lambda, x_1, \lambda, 0; x, y) H(0; x_0) - 8G(\lambda, x_1, \lambda, 0; x, y) H(0; y) \\
& + (4 - 4y) G(\lambda, x_1, x\lambda, 0; x, y) H(0; y) + 24(y - 1)^2 G(\lambda, x\lambda, x\lambda, \lambda; x, y) H(0; x_0) \\
& - 12(y - 1)^2 G(\lambda, x\lambda, x\lambda, \lambda; x, y) H(0; y) - 12(y - 1)^3 G(\lambda, x\lambda, x\lambda, x\lambda; x, y) H(0; y) \\
& - 8G(x_0, \lambda, 0, \lambda; x, y) H(0; x_0) + 4G(x_0, \lambda, 0, \lambda; x, y) H(0; y) \\
& + 4(y - 1) G(x_0, \lambda, 0, x\lambda; x, y) H(0; y) - 16G(x_0, \lambda, \lambda, 0; x, y) H(0; x_0) \\
& + 8G(x_0, \lambda, \lambda, 0; x, y) H(0; y) + 4(y - 1) G(x_0, \lambda, x\lambda, 0; x, y) H(0; y) \\
& + 4(y - 1) G(x_0, x\lambda, \lambda, 0; x, y) H(0; y) - 8G(x_1, \lambda, 0, \lambda; x, y) H(0; x_0) \\
& + 4G(x_1, \lambda, 0, \lambda; x, y) H(0; y) + 4(y - 1) G(x_1, \lambda, 0, x\lambda; x, y) H(0; y) \\
& - 16G(x_1, \lambda, \lambda, 0; x, y) H(0; x_0) + 8G(x_1, \lambda, \lambda, 0; x, y) H(0; y) \\
& + 4(y - 1) G(x_1, \lambda, x\lambda, 0; x, y) H(0; y) + 4(y - 1) G(x_1, x\lambda, \lambda, 0; x, y) H(0; y) \\
& + (8 - 8y) G(x\lambda, 0, \lambda, 0; x, y) H(0; y) + 24(y - 1)^2 G(x\lambda, \lambda, x\lambda, \lambda; x, y) H(0; x_0) \\
& - 12(y - 1)^2 G(x\lambda, \lambda, x\lambda, \lambda; x, y) H(0; y) - 12(y - 1)^3 G(x\lambda, \lambda, x\lambda, x\lambda; x, y) H(0; y) \\
& + (4 - 4y) G(x\lambda, x_0, \lambda, 0; x, y) H(0; y) + (4 - 4y) G(x\lambda, x_1, \lambda, 0; x, y) H(0; y) \\
& + 24(y - 1)^2 G(x\lambda, x\lambda, \lambda, \lambda; x, y) H(0; x_0) - 12(y - 1)^2 G(x\lambda, x\lambda, \lambda, \lambda; x, y) H(0; y) \\
& - 12(y - 1)^3 G(x\lambda, x\lambda, \lambda, x\lambda; x, y) H(0; y) + 4\Delta G(0; 0, x_0) G(\lambda, 0; 0, x_0) G(\lambda, \lambda; x, y) \\
& - 4(y - 1)^2 \Delta G(0; 0, x_0) G(\lambda, 0; 0, x_0) G(x\lambda, x\lambda; x, y) + 4\Delta G(0; 0, x_0) G(\lambda, \lambda; x, y) H(0, 0; x_0) +
\end{aligned}$$

$$\begin{aligned}
& - 4 \Delta G(0; 0, x_0) G(\lambda, \lambda; x, y) H(1, 0; x_0) - 4 (y - 1)^2 \Delta G(0; 0, x_0) G(x\lambda, x\lambda; x, y) H(0, 0; x_0) \\
& + 4 (y - 1)^2 \Delta G(0; 0, x_0) G(x\lambda, x\lambda; x, y) H(1, 0; x_0) + 4 \Delta G(0; 0, x_0) G(\lambda, 0, \lambda; x, y) H(0; x_0) \\
& + 4 \Delta G(0; 0, x_0) G(\lambda, \lambda, 0; x, y) H(0; x_0) + 8 \Delta G(0; 0, x_0) G(\lambda, x_0, \lambda; x, y) H(0; x_0) \\
& + 8 \Delta G(0; 0, x_0) G(\lambda, x_1, \lambda; x, y) H(0; x_0) - 8 \Delta G(0; 0, x_0) G(x_0, \lambda, \lambda; x, y) H(0; x_0) \\
& - 8 \Delta G(0; 0, x_0) G(x_1, \lambda, \lambda; x, y) H(0; x_0) - 4 (y - 1)^2 \Delta G(0; 0, x_0) G(x\lambda, x\lambda, 0; x, y) H(0; x_0) \\
& + 8 \Delta G(0; 0, y) G(\lambda, \lambda; x, y) H(0, 0; y) + 12 (y - 1) \Delta G(0; 0, y) G(\lambda, x\lambda; x, y) H(0, 0; y) \\
& + (8 - 8y) \Delta G(0; 0, y) G(\lambda, x\lambda; x, y) H(1, 0; y) + 12 (y - 1) \Delta G(0; 0, y) G(x\lambda, \lambda; x, y) H(0, 0; y) \\
& + (8 - 8y) \Delta G(0; 0, y) G(x\lambda, \lambda; x, y) H(1, 0; y) + 4 (y - 1) \Delta G(0; 0, y) G(\lambda, 0, x\lambda; x, y) H(0; y) \\
& + 4 (y - 1) \Delta G(0; 0, y) G(\lambda, x_0, x\lambda; x, y) H(0; y) + 4 (y - 1) \Delta G(0; 0, y) G(\lambda, x_1, x\lambda; x, y) H(0; y) \\
& + 4 (y - 1) \Delta G(0; 0, y) G(\lambda, x\lambda, 0; x, y) H(0; y) + (4 - 4y) \Delta G(0; 0, y) G(x_0, \lambda, x\lambda; x, y) H(0; y) \\
& + (4 - 4y) \Delta G(0; 0, y) G(x_0, x\lambda, \lambda; x, y) H(0; y) + (4 - 4y) \Delta G(0; 0, y) G(x_1, \lambda, x\lambda; x, y) H(0; y) \\
& + (4 - 4y) \Delta G(0; 0, y) G(x_1, x\lambda, \lambda; x, y) H(0; y) + 8 (y - 1) \Delta G(0; 0, y) G(x\lambda, 0, \lambda; x, y) H(0; y) \\
& + 4 (y - 1) \Delta G(0; 0, y) G(x\lambda, \lambda, 0; x, y) H(0; y) + 4 (y - 1) \Delta G(0; 0, y) G(x\lambda, x_0, \lambda; x, y) H(0; y) \\
& + 4 (y - 1) \Delta G(0; 0, y) G(x\lambda, x_1, \lambda; x, y) H(0; y) + 2 \Delta G(0, 0; 0, x_0) G(\lambda, \lambda; x, y) H(0; x_0) \\
& - 2 (y - 1)^2 \Delta G(0, 0; 0, x_0) G(x\lambda, x\lambda; x, y) H(0; x_0) + (4 - 4y) \Delta G(0, 0; 0, y) G(\lambda, x\lambda; x, y) H(0; y) \\
& + (4 - 4y) \Delta G(0, 0; 0, y) G(x\lambda, \lambda; x, y) H(0; y) + 6 \Delta G(0, \lambda; 0, x_0) G(\lambda, \lambda; x, y) H(0; x_0) \\
& - 12 \Delta G(0, \lambda; 0, x_0) G(\lambda, \lambda; x, y) H(0; y) - 6 (y - 1)^2 \Delta G(0, \lambda; 0, x_0) G(x\lambda, x\lambda; x, y) H(0; x_0) \\
& + 12 (y - 1)^2 \Delta G(0, \lambda; 0, x_0) G(x\lambda, x\lambda; x, y) H(0; y) + 8 \Delta G(0, \lambda; 0, y) G(\lambda, \lambda; x, y) H(0; y) \\
& - 16 (y - 1) \Delta G(0, \lambda; 0, y) G(\lambda, x\lambda; x, y) H(0; x_0) + 8 (y - 1) \Delta G(0, \lambda; 0, y) G(\lambda, x\lambda; x, y) H(0; y) \\
& - 16 (y - 1) \Delta G(0, \lambda; 0, y) G(x\lambda, \lambda; x, y) H(0; x_0) + 8 (y - 1) \Delta G(0, \lambda; 0, y) G(x\lambda, \lambda; x, y) H(0; y) \\
& + 6 (-2\sqrt{y} + y) \Delta G(0, x\lambda; 0, x_0) G(\lambda, \lambda; x, y) H(0; x_0) \\
& - 6 (-2 + \sqrt{y}) (y - 1)^2 \sqrt{y} \Delta G(0, x\lambda; 0, x_0) G(x\lambda, x\lambda; x, y) H(0; x_0) \\
& + 4 (y - 1)^2 \Delta G(0, x\lambda; 0, y) G(\lambda, x\lambda; x, y) H(0; y) + 4 (y - 1)^2 \Delta G(0, x\lambda; 0, y) G(x\lambda, \lambda; x, y) H(0; y) \\
& + 4 G(\lambda; 0, x_0) G(\lambda, 0; 0, x_0) G(\lambda, \lambda; x, y) - 4 (y - 1)^2 G(\lambda; 0, x_0) G(\lambda, 0; 0, x_0) G(x\lambda, x\lambda; x, y) \\
& + 4 G(\lambda; 0, x_0) G(\lambda, \lambda; x, y) H(0, 0; x_0) - 16 G(\lambda; 0, x_0) G(\lambda, \lambda; x, y) H(0, 0; y) \\
& - 4 G(\lambda; 0, x_0) G(\lambda, \lambda; x, y) H(1, 0; x_0) - 4 (y - 1)^2 G(\lambda; 0, x_0) G(x\lambda, x\lambda; x, y) H(0, 0; x_0) +
\end{aligned}$$

$$\begin{aligned}
& + 16 (y - 1)^2 G(\lambda; 0, x_0) G(x\lambda, x\lambda; x, y) H(0, 0; y) + 4 (y - 1)^2 G(\lambda; 0, x_0) G(x\lambda, x\lambda; x, y) H(1, 0; x_0) \\
& + 4 G(\lambda; 0, x_0) G(\lambda, 0, \lambda; x, y) H(0; x_0) - 8 G(\lambda; 0, x_0) G(\lambda, 0, \lambda; x, y) H(0; y) \\
& + 4 G(\lambda; 0, x_0) G(\lambda, \lambda, 0; x, y) H(0; x_0) - 8 G(\lambda; 0, x_0) G(\lambda, \lambda, 0; x, y) H(0; y) \\
& + 8 G(\lambda; 0, x_0) G(\lambda, x_0, \lambda; x, y) H(0; x_0) - 16 G(\lambda; 0, x_0) G(\lambda, x_0, \lambda; x, y) H(0; y) \\
& + 8 G(\lambda; 0, x_0) G(\lambda, x_1, \lambda; x, y) H(0; x_0) - 16 G(\lambda; 0, x_0) G(\lambda, x_1, \lambda; x, y) H(0; y) \\
& - 8 G(\lambda; 0, x_0) G(x_0, \lambda, \lambda; x, y) H(0; x_0) + 16 G(\lambda; 0, x_0) G(x_0, \lambda, \lambda; x, y) H(0; y) \\
& - 8 G(\lambda; 0, x_0) G(x_1, \lambda, \lambda; x, y) H(0; x_0) + 16 G(\lambda; 0, x_0) G(x_1, \lambda, \lambda; x, y) H(0; y) \\
& - 4 (y - 1)^2 G(\lambda; 0, x_0) G(x\lambda, x\lambda, 0; x, y) H(0; x_0) + 8 (y - 1)^2 G(\lambda; 0, x_0) G(x\lambda, x\lambda, 0; x, y) H(0; y) \\
& + 8 G(\lambda; 0, y) G(\lambda, \lambda; x, y) H(0, 0; y) + 16 G(\lambda; 0, y) G(\lambda, \lambda; x, y) H(1, 0; y) \\
& - 32 (y - 1) G(\lambda; 0, y) G(\lambda, x\lambda; x, y) H(0, 0; x_0) + 12 (y - 1) G(\lambda; 0, y) G(\lambda, x\lambda; x, y) H(0, 0; y) \\
& - 32 (y - 1) G(\lambda; 0, y) G(x\lambda, \lambda; x, y) H(0, 0; x_0) + 12 (y - 1) G(\lambda; 0, y) G(x\lambda, \lambda; x, y) H(0, 0; y) \\
& + (8 - 8y) G(\lambda; 0, y) G(\lambda, 0, x\lambda; x, y) H(0; x_0) + 4 (y - 1) G(\lambda; 0, y) G(\lambda, 0, x\lambda; x, y) H(0; y) \\
& + (8 - 8y) G(\lambda; 0, y) G(\lambda, x_0, x\lambda; x, y) H(0; x_0) + 4 (y - 1) G(\lambda; 0, y) G(\lambda, x_0, x\lambda; x, y) H(0; y) \\
& + (8 - 8y) G(\lambda; 0, y) G(\lambda, x_1, x\lambda; x, y) H(0; x_0) + 4 (y - 1) G(\lambda; 0, y) G(\lambda, x_1, x\lambda; x, y) H(0; y) \\
& + (8 - 8y) G(\lambda; 0, y) G(\lambda, x\lambda, 0; x, y) H(0; x_0) + 4 (y - 1) G(\lambda; 0, y) G(\lambda, x\lambda, 0; x, y) H(0; y) \\
& + 8 (y - 1) G(\lambda; 0, y) G(x_0, \lambda, x\lambda; x, y) H(0; x_0) + (4 - 4y) G(\lambda; 0, y) G(x_0, \lambda, x\lambda; x, y) H(0; y) \\
& + 8 (y - 1) G(\lambda; 0, y) G(x_0, x\lambda, \lambda; x, y) H(0; x_0) + (4 - 4y) G(\lambda; 0, y) G(x_0, x\lambda, \lambda; x, y) H(0; y) \\
& + 8 (y - 1) G(\lambda; 0, y) G(x_1, \lambda, x\lambda; x, y) H(0; x_0) + (4 - 4y) G(\lambda; 0, y) G(x_1, \lambda, x\lambda; x, y) H(0; y) \\
& + 8 (y - 1) G(\lambda; 0, y) G(x_1, x\lambda, \lambda; x, y) H(0; x_0) + (4 - 4y) G(\lambda; 0, y) G(x_1, x\lambda, \lambda; x, y) H(0; y) \\
& - 16 (y - 1) G(\lambda; 0, y) G(x\lambda, 0, \lambda; x, y) H(0; x_0) + 8 (y - 1) G(\lambda; 0, y) G(x\lambda, 0, \lambda; x, y) H(0; y) \\
& + (8 - 8y) G(\lambda; 0, y) G(x\lambda, \lambda, 0; x, y) H(0; x_0) + 4 (y - 1) G(\lambda; 0, y) G(x\lambda, \lambda, 0; x, y) H(0; y) \\
& + (8 - 8y) G(\lambda; 0, y) G(x\lambda, x_0, \lambda; x, y) H(0; x_0) + 4 (y - 1) G(\lambda; 0, y) G(x\lambda, x_0, \lambda; x, y) H(0; y) \\
& + (8 - 8y) G(\lambda; 0, y) G(x\lambda, x_1, \lambda; x, y) H(0; x_0) + 4 (y - 1) G(\lambda; 0, y) G(x\lambda, x_1, \lambda; x, y) H(0; y) \\
& + 2 G(\lambda, 0; 0, x_0) G(\lambda, \lambda; x, y) H(0; x_0) - 16 G(\lambda, 0; 0, x_0) G(\lambda, \lambda; x, y) H(0; y) \\
& - 2 (y - 1)^2 G(\lambda, 0; 0, x_0) G(x\lambda, x\lambda; x, y) H(0; x_0) + 16 (y - 1)^2 G(\lambda, 0; 0, x_0) G(x\lambda, x\lambda; x, y) H(0; y) \\
& - 24 (y - 1) G(\lambda, 0; 0, y) G(\lambda, x\lambda; x, y) H(0; x_0) + (4 - 4y) G(\lambda, 0; 0, y) G(\lambda, x\lambda; x, y) H(0; y) +
\end{aligned}$$

$$\begin{aligned}
& - 24 (y - 1) G(\lambda, 0; 0, y) G(x\lambda, \lambda; x, y) H(0; x_0) + (4 - 4y) G(\lambda, 0; 0, y) G(x\lambda, \lambda; x, y) H(0; y) \\
& + 6 G(\lambda, \lambda; 0, x_0) G(\lambda, \lambda; x, y) H(0; x_0) - 12 G(\lambda, \lambda; 0, x_0) G(\lambda, \lambda; x, y) H(0; y) \\
& - 6 (y - 1)^2 G(\lambda, \lambda; 0, x_0) G(x\lambda, x\lambda; x, y) H(0; x_0) \\
& + 12 (y - 1)^2 G(\lambda, \lambda; 0, x_0) G(x\lambda, x\lambda; x, y) H(0; y) \\
& + 16 G(\lambda, \lambda; 0, y) G(\lambda, \lambda; x, y) H(0; x_0) - 8 G(\lambda, \lambda; 0, y) G(\lambda, \lambda; x, y) H(0; y) \\
& + 6 (-2\sqrt{y} + y) G(\lambda, \lambda; x, y) G(\lambda, x\lambda; 0, x_0) H(0; x_0) \\
& - 16 (y - 1) G(\lambda, \lambda; x, y) G(\lambda, x\lambda; 0, y) H(0; y) \\
& + 4 G(\lambda, \lambda; x, y) G(x_0, \lambda; 0, x_0) H(0; x_0) - 8 G(\lambda, \lambda; x, y) G(x_0, \lambda; 0, x_0) H(0; y) \\
& + 4 (-2\sqrt{y} + y) G(\lambda, \lambda; x, y) G(x_0, x\lambda; 0, x_0) H(0; x_0) \\
& + 4 G(\lambda, \lambda; x, y) G(x_1, \lambda; 0, x_0) H(0; x_0) - 8 G(\lambda, \lambda; x, y) G(x_1, \lambda; 0, x_0) H(0; y) \\
& + 4 (-2\sqrt{y} + y) G(\lambda, \lambda; x, y) G(x_1, x\lambda; 0, x_0) H(0; x_0) \\
& - 4 G(\lambda, \lambda; x, y) H(0; x_0) H(0, 0; y) - 4 G(\lambda, \lambda; x, y) H(0; y) H(0, 0; x_0) \\
& - 6 (-2 + \sqrt{y}) (y - 1)^2 \sqrt{y} G(\lambda, x\lambda; 0, x_0) G(x\lambda, x\lambda; x, y) H(0; x_0) \\
& + 8 (y - 1)^2 G(\lambda, x\lambda; 0, y) G(\lambda, x\lambda; x, y) H(0; x_0) - 4 (y - 1)^2 G(\lambda, x\lambda; 0, y) G(\lambda, x\lambda; x, y) H(0; y) \\
& + 8 (y - 1)^2 G(\lambda, x\lambda; 0, y) G(x\lambda, \lambda; x, y) H(0; x_0) - 4 (y - 1)^2 G(\lambda, x\lambda; 0, y) G(x\lambda, \lambda; x, y) H(0; y) \\
& - 16 (y - 1) G(\lambda, x\lambda; x, y) G(x_0, \lambda; 0, y) H(0; x_0) + 8 (y - 1) G(\lambda, x\lambda; x, y) G(x_0, \lambda; 0, y) H(0; y) \\
& + 8 (y - 1)^2 G(\lambda, x\lambda; x, y) G(x_0, x\lambda; 0, y) H(0; y) - 16 (y - 1) G(\lambda, x\lambda; x, y) G(x_1, \lambda; 0, y) H(0; x_0) \\
& + 8 (y - 1) G(\lambda, x\lambda; x, y) G(x_1, \lambda; 0, y) H(0; y) + 8 (y - 1)^2 G(\lambda, x\lambda; x, y) G(x_1, x\lambda; 0, y) H(0; y) \\
& + 4 (y - 1) G(\lambda, x\lambda; x, y) H(0; x_0) H(0, 0; y) + 4 (y - 1) G(\lambda, x\lambda; x, y) H(0; y) H(0, 0; x_0) \\
& - 4 (y - 1)^2 G(x_0, \lambda; 0, x_0) G(x\lambda, x\lambda; x, y) H(0; x_0) \\
& + 8 (y - 1)^2 G(x_0, \lambda; 0, x_0) G(x\lambda, x\lambda; x, y) H(0; y) \\
& - 16 (y - 1) G(x_0, \lambda; 0, y) G(x\lambda, \lambda; x, y) H(0; x_0) + 8 (y - 1) G(x_0, \lambda; 0, y) G(x\lambda, \lambda; x, y) H(0; y) \\
& - 4 (-2 + \sqrt{y}) (y - 1)^2 \sqrt{y} G(x_0, x\lambda; 0, x_0) G(x\lambda, x\lambda; x, y) H(0; x_0) \\
& + 8 (y - 1)^2 G(x_0, x\lambda; 0, y) G(x\lambda, \lambda; x, y) H(0; y) \\
& - 4 (y - 1)^2 G(x_1, \lambda; 0, x_0) G(x\lambda, x\lambda; x, y) H(0; x_0) +
\end{aligned}$$

$$\begin{aligned}
& + 8 (y - 1)^2 G(x_1, \lambda; 0, x_0) G(x\lambda, x\lambda; x, y) H(0; y) \\
& - 16 (y - 1) G(x_1, \lambda; 0, y) G(x\lambda, \lambda; x, y) H(0; x_0) \\
& + 8 (y - 1) G(x_1, \lambda; 0, y) G(x\lambda, \lambda; x, y) H(0; y) \\
& - 4 (-2 + \sqrt{y}) (y - 1)^2 \sqrt{y} G(x_1, x\lambda; 0, x_0) G(x\lambda, x\lambda; x, y) H(0; x_0) \\
& + 8 (y - 1)^2 G(x_1, x\lambda; 0, y) G(x\lambda, \lambda; x, y) H(0; y) + 4 (y - 1) G(x\lambda, \lambda; x, y) H(0; x_0) H(0, 0; y) \\
& + 4 (y - 1) G(x\lambda, \lambda; x, y) H(0; y) H(0, 0; x_0) - 4 (y - 1)^2 G(x\lambda, x\lambda; x, y) H(0; x_0) H(0, 0; y) \\
& - 4 (y - 1)^2 G(x\lambda, x\lambda; x, y) H(0; y) H(0, 0; x_0) - 4 G(\lambda, \lambda, 0; x, y) H(0; x_0) H(0; y) \\
& + 4 (y - 1) G(\lambda, x\lambda, 0; x, y) H(0; x_0) H(0; y) + 4 (y - 1) G(x\lambda, \lambda, 0; x, y) H(0; x_0) H(0; y) \\
& - 4 (y - 1)^2 G(x\lambda, x\lambda, 0; x, y) H(0; x_0) H(0; y)
\end{aligned}$$

Appendix C

Spinor product identities

The spinor products obey the following identities, with $i \equiv p_i$,

$$\begin{aligned}\langle i j \rangle &= -\langle j i \rangle, \\ [i j] &= -[j i], \\ \langle i j \rangle &= \text{sign}(p_i^0 p_j^0) [j i], \\ 2p_i \cdot p_j &= \langle i j \rangle [j i], \\ \langle i^- | j | k^- \rangle &= \langle i j \rangle [j k],\end{aligned}$$

and the Schouten identity,

$$\begin{aligned}\langle i j \rangle \langle k l \rangle &= \langle i k \rangle \langle j l \rangle + \langle i l \rangle \langle k j \rangle, \\ [i j][k l] &= [i k][j l] + [i l][k j].\end{aligned}$$

If $\sum_{i=1}^n p_i = 0$, we have that

$$\sum_{i=1}^n \langle j i \rangle [i k] = 0. \tag{C.1}$$

Bibliography

- [1] M. Gell-Mann, *A Schematic Model Of Baryons And Mesons*, Phys. Lett. **8**, 214 (1964).
- [2] M. Y. Han and Y. Nambu, *Three-Triplet Model With Double $SU(3)$ Symmetry*, Phys. Rev. **139**, B1006 (1965).
- [3] H. Fritzsch and M. Gell-Mann, *Current Algebra: Quarks And What Else?*, arXiv:hep-ph/0208010.
- [4] H. Fritzsch, M. Gell-Mann and H. Leutwyler, *Advantages Of The Color Octet Gluon Picture*, Phys. Lett. B **47**, 365 (1973).
- [5] S. R. Coleman and D. J. Gross, *Price Of Asymptotic Freedom*, Phys. Rev. Lett. **31**, 851 (1973).
- [6] M. E. Peskin and D. V. Schroeder, *An Introduction to Quantum Field Theory*, Westview Press (1995) 842p.
- [7] T. Muta, *Foundations of Quantum Chromodynamics*, World Scientific (2000) 409p.
- [8] F. Halzen and A. D. Martin, *Quarks and Leptons*, Wiley (1984) 396p.
- [9] R. K. Ellis, W. J. Stirling and B. R. Webber, *QCD and Collider Physics*, Cambridge University Press (1996) 435p.
- [10] D. Bailin and A. Love, *Introduction to Gauge Field Theory*, Institute of Physics Publishing, (1993) 364p.
- [11] I.J.R. Aitchison, A.J.G. Hey, *Gauge theories in particle physics : a practical introduction*, Institute of Physics Publishing, (1989) 550p.
- [12] A. Salam, *Elementary particle theory: Relativistic Groups and Analyticity*, 8th Nobel Symposium, Stockholm publishing, (1968).
- [13] S. L. Glashow, *Partial Symmetries Of Weak Interactions*, Nucl. Phys. **22**, 579 (1961).

- [14] S. Weinberg, *A Model Of Leptons*, Phys. Rev. Lett. **19**, 1264 (1967).
- [15] M. Kramer and F.J.P. Soler (Editors), *Large Hadron Collider Phenomenology*, Institute of Physics Publishing, (2004) 473p.
- [16] C. Becchi, A. Rouet and R. Stora, *Renormalization of Gauge Theories*, Annals Phys. **98** (1976) 287;
M.Z. Iofa and I.V. Tyutin, Theor. Math. Phys. **27** (1976) 316.
- [17] T. Kinoshita, *Mass singularities of Feynman amplitudes*, J. Math. Phys. **3** (1962) p650.
- [18] T.D. Lee and M. Nauenberg, Phys.Rev **133** B1549 (1964).
- [19] J. B. Tausk, *Non-planar massless two-loop feynman diagrams with four on-shell legs*, Phys. Lett. **B469** (1999) 225, [arXiv:hep-ph/9909506].
- [20] C. Anastasiou, T. Gehrmann, C. Oleari, E. Remiddi, and J. B. Tausk, *The tensor reduction and master integrals of the two-loop massless crossed box with light-like legs*, Nucl. Phys. **B580** (2000) 577, [arXiv:hep-ph/0003261].
- [21] T. Gehrmann and E. Remiddi, *Differential equations for two-loop four-point functions*, Nucl. Phys. **B580** (2000) 485, [arXiv:hep-ph/9912329].
- [22] C. Anastasiou and A. Lazopoulos, *Automatic integral reduction for higher order perturbative calculations*, arXiv:hep-ph/0404258.
- [23] S. Laporta, *High-precision calculation of multi-loop feynman integrals by difference equations*, Int. J. Mod. Phys. **A15** (2000) 5087, [arXiv:hep-ph/0102033].
- [24] A. V. Kotikov, *Differential Equations Method: New Technique For Massive Feynman Diagrams Calculation*, Phys. Lett. B **254** (1991) 158;
A. V. Kotikov, *Differential Equations Method: The Calculation Of Vertex Type Feynman Diagrams*, Phys. Lett. B **259** (1991) 314;
A. V. Kotikov, *Differential Equation Method: The Calculation Of N Point Feynman Diagrams*, Phys. Lett. B **267** (1991) 123;
Z. Bern, L. J. Dixon and D. A. Kosower, *Dimensionally regulated pentagon integrals*, Nucl. Phys. B **412** (1994) 751, [arXiv:hep-ph/9306240];
E. Remiddi, *Differential equations for Feynman graph amplitudes*, Nuovo Cim. A **110** (1997) 1435, [arXiv:hep-th/9711188].
- [25] T. Gehrmann and E. Remiddi, *Differential equations for two-loop four-point functions*, Nucl. Phys. B **580** (2000) 485 [arXiv:hep-ph/9912329].
- [26] T. Gehrmann and E. Remiddi, *Two-loop master integrals for $\gamma^* \rightarrow 3\text{jets}$: The planar topologies*, Nucl. Phys. B **601** (2001) 248, [arXiv:hep-ph/0008287].

- [27] T. Gehrmann and E. Remiddi, *Two-loop master integrals for $\gamma^* \rightarrow 3\text{jets}$: The non-planar topologies*, Nucl. Phys. B **601** (2001) 287, [arXiv:hep-ph/0101124].
- [28] M. Czakon, J. Gluza and T. Riemann, *A complete set of scalar master integrals for massive 2-loop Bhabha scattering: Where we are*, arXiv:hep-ph/0406203.
- [29] R. Bonciani, P. Mastrolia and E. Remiddi, Nucl. Phys. B **661**, 289 (2003) [arXiv:hep-ph/0301170].
- [30] U. Aglietti and R. Bonciani, *Master integrals with one massive propagator for the two-loop electroweak form factor*, Nucl. Phys. B **668**, 3 (2003) [arXiv:hep-ph/0304028].
- [31] R. Bonciani, P. Mastrolia and E. Remiddi, *Master integrals for the 2-loop QCD virtual corrections to the forward-backward asymmetry*, Nucl. Phys. B **690**, 138 (2004) [arXiv:hep-ph/0311145].
- [32] U. Aglietti and R. Bonciani, *Master integrals with 2 and 3 massive propagators for the 2-loop electroweak form factor: Planar case*, arXiv:hep-ph/0401193.
- [33] J. A. M. Vermaseren, *New features of FORM*, arXiv:math-ph/0010025.
- [34] E. Remiddi and J. A. M. Vermaseren, *Harmonic polylogarithms*, Int. J. Mod. Phys. A **15** (2000) 725, [arXiv:hep-ph/9905237].
- [35] T. Gehrmann and E. Remiddi, *Numerical evaluation of harmonic polylogarithms*, Comput. Phys. Commun. **141** (2001) 296, [arXiv:hep-ph/0107173];
Numerical evaluation of two-dimensional harmonic polylogarithms, Comput. Phys. Commun. **144** (2002) 200, [arXiv:hep-ph/0111255].
- [36] T. G. Birthwright, E. W. N. Glover and P. Marquard, *Master integrals for massless two-loop vertex diagrams with three offshell legs*, JHEP **0409**, 042 (2004) [arXiv:hep-ph/0407343].
- [37] A. I. Davydychev and P. Osland, *On-shell two-loop three-gluon vertex*, Phys. Rev. D **59** (1999) 014006 [arXiv:hep-ph/9806522].
- [38] K. S. Kolbig, J. A. Mignaco, and E. Remiddi, *On Nielsen's generalised polylogarithms and their numerical calculation*, B.I.T. **10** (1970) 38.
- [39] K. G. Chetyrkin, A. L. Kataev, and F. V. Tkachov, *New approach to evaluation of multiloop feynman integrals: The gegenbauer polynomial x space technique*, Nucl. Phys. **B174** (1980) 345.
- [40] K. G. Chetyrkin and F. V. Tkachov, *Integration by parts: The algorithm to calculate beta functions in 4 loops*, Nucl. Phys. **B192** (1981) 159.

- [41] E. E. Boos and A. I. Davydychev, *A Method Of Evaluating Massive Feynman Integrals*, Theor. Math. Phys. **89** (1991) 1052, [Teor. Mat. Fiz. **89** (1991) 56].
- [42] V. A. Smirnov, *Analytical result for dimensionally regularized massless on-shell double box*, Phys. Lett. **B460** (1999) 397, [arXiv:hep-ph/9905323].
- [43] V. A. Smirnov and O. L. Veretin, *Analytical results for dimensionally regularized massless on-shell double boxes with arbitrary indices and numerators*, Nucl. Phys. **B566** (2000) 469, [arXiv:hep-ph/9907385].
- [44] C. Anastasiou, J. B. Tausk, and M. E. Tejeda-Yeomans, *The on-shell massless planar double box diagram with an irreducible numerator*, Nucl. Phys. Proc. Suppl. **89** (2000) 262, [arXiv:hep-ph/0005328].
- [45] T. Binoth and G. Heinrich, *An automatized algorithm to compute infrared divergent multi-loop integrals*, Nucl. Phys. B **585** (2000) 741, [arXiv:hep-ph/0004013];
Numerical evaluation of multi-loop integrals by sector decomposition, Nucl. Phys. B **680** (2004) 375, [arXiv:hep-ph/0305234].
- [46] Z. Bern, L. J. Dixon, and D. A. Kosower, *A two-loop four-gluon helicity amplitude in QCD*, JHEP **01** (2000) 027, [arXiv:hep-ph/0001001].
- [47] Z. Bern, A. De Freitas, and L. Dixon, *Two-loop helicity amplitudes for gluon gluon scattering in QCD and supersymmetric Yang-Mills theory*, JHEP **03** (2002) 018, [arXiv:hep-ph/0201161].
- [48] Z. Bern, A. De Freitas, and L. Dixon, *Two-loop helicity amplitudes for quark-gluon scattering in QCD and gluino-gluon scattering in supersymmetric yang-mills theory*, JHEP **0306** (2003) 028, [arXiv:hep-ph/0304168].
- [49] E. W. N. Glover and M. E. Tejeda-Yeomans, *Two-loop QCD helicity amplitudes for massless quark massless gauge boson scattering*, JHEP **06** (2003) 033, [arXiv:hep-ph/0304169].
- [50] E. W. N. Glover, *Two-loop QCD helicity amplitudes for massless quark quark scattering*, JHEP **0404** (2004) 021, [arXiv:hep-ph/0401119].
- [51] C. Anastasiou, E. W. N. Glover, C. Oleari, and M. E. Tejeda-Yeomans, *Two-loop QCD corrections to q anti- q to q' anti- q'* , Nucl. Phys. **B601** (2001) 318, [arXiv:hep-ph/0010212].
- [52] C. Anastasiou, E. W. N. Glover, C. Oleari, and M. E. Tejeda-Yeomans, *Two-loop QCD corrections to q anti- q to q anti- q* , Nucl. Phys. **B601** (2001) 341, [arXiv:hep-ph/0011094].
- [53] C. Anastasiou, E. W. N. Glover, C. Oleari, and M. E. Tejeda-Yeomans, *Two-loop QCD corrections to massless quark gluon scattering*, Nucl. Phys. **B605** (2001) 486, [arXiv:hep-ph/0101304].

- [54] E. W. N. Glover, C. Oleari, and M. E. Tejeda-Yeomans, *Two-loop QCD corrections to gluon gluon scattering*, Nucl. Phys. **B605** (2001) 467, [arXiv:hep-ph/0102201].
- [55] Z. Bern, A. De Freitas, and L. J. Dixon, *Two-loop amplitudes for gluon fusion into two photons*, JHEP **09** (2001) 037, [arXiv:hep-ph/0109078].
- [56] C. Anastasiou, E. W. N. Glover, and M. E. Tejeda-Yeomans, *Two-loop QED and QCD corrections to massless fermion boson scattering*, Nucl. Phys. **B629** (2002) 255, [arXiv:hep-ph/0201274].
- [57] Z. Bern, A. De Freitas, L. J. Dixon, A. Ghinculov, and H. L. Wong, *QCD and QED corrections to light-by-light scattering*, JHEP **11** (2001) 031, [arXiv:hep-ph/0109079].
- [58] T. Binoth, E. W. N. Glover, P. Marquard, and J. J. van der Bij, *Two-loop corrections to light-by-light scattering in supersymmetric QED*, JHEP **05** (2002) 060, [arXiv:hep-ph/0202266].
- [59] Z. Bern, L. J. Dixon, and A. Ghinculov, *Two-loop correction to bhabha scattering*, Phys. Rev. **D63** (2001) 053007, [arXiv:hep-ph/0010075].
- [60] L. W. Garland, T. Gehrmann, E. W. N. Glover, A. Koukoutsakis, and E. Remiddi, *Two-loop QCD matrix element for $e^+e^- \rightarrow 3$ jets*, Nucl. Phys. **B627** (2002) 107, [arXiv:hep-ph/0112081].
- [61] L. W. Garland, T. Gehrmann, E. W. N. Glover, A. Koukoutsakis, and E. Remiddi, *Two-loop QCD helicity amplitudes for $e^+e^- \rightarrow 3$ jets*, Nucl. Phys. **B642** (2002) 227, [arXiv:hep-ph/0206067].
- [62] S. Moch, P. Uwer and S. Weinzierl, *Two-loop amplitudes with nested sums: Fermionic contributions to $e^+e^- \rightarrow q$ anti- q g* , arXiv:hep-ph/0207043.
- [63] V. A. Smirnov, *Analytical result for dimensionally regularized massive on-shell planar double box*, Phys. Lett. B **524** (2002) 129 [arXiv:hep-ph/0111160].
- [64] V. A. Smirnov, *Evaluating multiloop Feynman integrals by Mellin-Barnes representation*, arXiv:hep-ph/0406052;
G. Heinrich and V. A. Smirnov, *Analytical evaluation of dimensionally regularized massive on-shell double boxes*, arXiv:hep-ph/0406053.
- [65] R. Bonciani, A. Ferroglia, P. Mastrolia, E. Remiddi and J. J. van der Bij, *Planar box diagram for the $(N(F) = 1)$ 2-loop QED virtual corrections to Bhabha scattering*, Nucl. Phys. B **681**, 261 (2004) [arXiv:hep-ph/0310333].
- [66] R. Bonciani, P. Mastrolia and E. Remiddi, *QED vertex form factors at two loops*, Nucl. Phys. B **676**, 399 (2004) [arXiv:hep-ph/0307295].

- [67] W. Bernreuther, R. Bonciani, T. Gehrmann, R. Heinesch, T. Leineweber, P. Mastrolia and E. Remiddi, *Two-loop QCD corrections to the heavy quark form factors: The vector contributions*, arXiv:hep-ph/0406046.
- [68] A. I. Davydychev, *Recursive algorithm of evaluating vertex type Feynman integrals*, J. Phys. A **25** (1992) 5587.
- [69] A. I. Davydychev, *General Results For Massive N Point Feynman Diagrams With Different Masses*, J. Math. Phys. **33** (1992) 358;
A. I. Davydychev, *Some Exact Results For N Point Massive Feynman Integrals*, J. Math. Phys. **32** (1991) 1052.
- [70] C. Anastasiou, E. W. N. Glover and C. Oleari, *Scalar one-loop integrals using the negative-dimension approach*, Nucl. Phys. B **572** (2000) 307 [arXiv:hep-ph/9907494].
- [71] A. I. Davydychev, *Explicit results for all orders of the epsilon-expansion of certain massive and massless diagrams*, Phys. Rev. D **61** (2000) 087701 [arXiv:hep-ph/9910224].
- [72] L. Lewin, *Polylogarithms and associated functions*, Elsevier North Holland (1981) 359p.
- [73] A. I. Davydychev and M. Y. Kalmykov, *New results for the epsilon-expansion of certain one-, two- and three-loop Feynman diagrams*, Nucl. Phys. B **605** (2001) 266 [arXiv:hep-th/0012189];
A. I. Davydychev and M. Y. Kalmykov, *Some remarks on the epsilon-expansion of dimensionally regulated Feynman diagrams*, Nucl. Phys. Proc. Suppl. **89** (2000) 283 [arXiv:hep-th/0005287].
- [74] N. I. Usyukina and A. I. Davydychev, *New results for two loop off-shell three point diagrams*, Phys. Lett. B **332** (1994) 159 [arXiv:hep-ph/9402223].
- [75] F. Cachazo, P. Svrček and E. Witten, *MHV vertices and tree amplitudes in gauge theory*, JHEP **09** (2004) 006 [arXiv:hep-th/0403047].
- [76] E. Witten, *Perturbative gauge theory as a string theory in twistor space*, Commun. Math. Phys. **252** (2004) 189 [arXiv:hep-th/0312171].
- [77] B. DeWitt, *Quantum Theory Of Gravity, III: Applications Of The Covariant Theory*, Phys. Rev. **162** (1967) 1239
- [78] S.J. Parke and T.R. Taylor, *An amplitude for n-gluon scattering*, Phys. Rev. Lett. **56**, 2459 (1986).
- [79] F. A. Berends and W. T. Giele, *Recursive Calculations For Processes With N Gluons*, Nucl. Phys. **B306** (1988) 759.

- [80] F.A. Berends, R. Kleiss, P. De Causmaecker, R. Gastmans and T.T. Wu, *Single Bremsstrahlung processes in gauge theories*, Phys. Lett. B **103** (1981) 124;
P. De Causmaecker, R. Gastmans, W. Troost and T.T. Wu, *Multiple Bremsstrahlung in gauge theories at high energies. 1. General formalism for quantum electrodynamics*, Nucl. Phys. B **206** (1982) 53;
Z. Xu, D.-H. Zhang, L. Chang, Tsinghua University preprint TUTP-84/3 (1984), unpublished;
R. Kleiss and W.J. Stirling, *Spinor techniques for calculating $p\bar{p} \rightarrow W^\pm Z^0 + \text{jets}$* , Nucl. Phys. B **262** (1985) 235;
J.F. Gunion and Z. Kunszt, *Improved analytic techniques for tree graph calculations and the $ggq\bar{q}\ell\ell$ subprocess*, Phys. Lett. B **161** (1985) 333;
Z. Xu, D.-H. Zhang and L. Chang, *Helicity amplitudes for multiple Bremsstrahlung in massless nonabelian gauge theories*, Nucl. Phys. B **291**, 392 (1987);
M.L. Mangano and S.J. Parke, *Multiparton amplitudes in gauge theories*, Phys. Rept. **200**, 301 (1991).
- [81] F. Cachazo and P. Svrcek, *Lectures on twistor strings and perturbative Yang-Mills theory*, arXiv:hep-th/0504194.
- [82] R. Penrose, *Twistor Algebra*, J. Math. Phys **8** (1967) 345.
- [83] K. Risager, *A direct proof of the CSW rules*, arXiv:hep-th/0508206.
- [84] G. Georgiou and V.V. Khoze, *Tree amplitudes in gauge theory as scalar MHV diagrams*, JHEP **05** (2004) 070 hep-th/0404072.
- [85] C.-J. Zhu, *The googly amplitudes in gauge theory*, JHEP **04** (2004) 032 [arXiv:hep-th/0403115].
- [86] D.A. Kosower, *Next-to-maximal helicity violating amplitudes in gauge theory*, Phys. Rev. **D71** (2005) 045007 [arXiv:hep-th/0406175].
- [87] I. Bena, Z. Bern and D.A. Kosower, *Twistor-space recursive formulation of gauge theory amplitudes*, Phys. Rev. **D71** (2005) 045008 hep-th/0406133.
- [88] G. Georgiou, E.W.N. Glover and V.V. Khoze, *Non-MHV tree amplitudes in gauge theory*, JHEP **07** (2004) 048 hep-th/0407027.
- [89] J.-B. Wu and C.-J. Zhu, *MHV vertices and scattering amplitudes in gauge theory*, JHEP **07** (2004) 032 [arXiv:hep-th/0406085].
- [90] J.-B. Wu and C.-J. Zhu, *MHV vertices and fermionic scattering amplitudes in gauge theory with quarks and gluinos*, JHEP **09** (2004) 063 hep-th/0406146.
- [91] L.J. Dixon, E.W.N. Glover and V.V. Khoze, *MHV rules for Higgs plus multi-gluon amplitudes*, JHEP **12** (2004) 015 hep-th/0411092.

- [92] S.D. Badger, E.W.N. Glover and V.V. Khoze, *MHV rules for Higgs plus multi-parton amplitudes*, hep-th/0412275.
- [93] Z. Bern, D. Forde, D.A. Kosower and P. Mastrolia, *Twistor-inspired construction of electroweak vector boson currents*, hep-ph/0412167.
- [94] K. J. Ozeren and W. J. Stirling, *MHV techniques for QED processes*, *JHEP* **11** (2005) 016 arXiv:hep-th/0509063.
- [95] A. Brandhuber, B. Spence and G. Travaglini, *One-loop gauge theory amplitudes in $N = 4$ super yang-mills from MHV vertices*, *Nucl. Phys.* **B706** (2005) 150 hep-th/0407214.
- [96] Z. Bern, L.J. Dixon, D.C. Dunbar and D.A. Kosower, *One loop n point gauge theory amplitudes, unitarity and collinear limits*, *Nucl. Phys.* **B425** (1994) 217–260 hep-ph/9403226.
- [97] Z. Bern, L.J. Dixon, D.C. Dunbar and D.A. Kosower, *Fusing gauge theory tree amplitudes into loop amplitudes*, *Nucl. Phys.* **B435** (1995) 59–101 hep-ph/9409265.
- [98] F. Cachazo, P. Svrcek and E. Witten, *Twistor space structure of one-loop amplitudes in gauge theory*, *JHEP* **10** (2004) 074 hep-th/0406177.
- [99] F. Cachazo, P. Svrcek and E. Witten, *Gauge theory amplitudes in twistor space and holomorphic anomaly*, *JHEP* **10** (2004) 077 [arXiv:hep-th/0409245].
- [100] I. Bena, Z. Bern, D. A. Kosower and R. Roiban, *Loops in twistor space*, arXiv:hep-th/0410054.
- [101] F. Cachazo, *Holomorphic anomaly of unitarity cuts and one-loop gauge theory amplitudes*, hep-th/0410077.
- [102] R. Britto, F. Cachazo and B. Feng, *Computing one-loop amplitudes from the holomorphic anomaly of unitarity cuts*, *Phys. Rev.* **D71** (2005) 025012 hep-th/0410179.
- [103] Z. Bern, V. Del Duca, L.J. Dixon and D.A. Kosower, *All non-maximally-helicity-violating one-loop seven-gluon amplitudes in $N = 4$ super-yang-mills theory*, *Phys. Rev.* **D71** (2005) 045006 hep-th/0410224.
- [104] R. Britto, F. Cachazo and B. Feng, *Coplanarity in twistor space of $N = 4$ next-to-MHV one-loop amplitude coefficients*, arXiv:hep-th/0411107.
- [105] R. Britto, F. Cachazo and B. Feng, *Generalized unitarity and one-loop amplitudes in $N = 4$ super-yang-mills*, hep-th/0412103.

- [106] Z. Bern, L.J. Dixon and D.A. Kosower, *All next-to-maximally-helicity-violating one-loop gluon amplitudes in $N=4$ super-yang-mills theory*, hep-th/0412210.
- [107] C. Quigley and M. Rozali, *One-loop MHV amplitudes in supersymmetric gauge theories*, *JHEP* **01** (2005) 053 hep-th/0410278.
- [108] S.J. Bidder, N.E.J. Bjerrum-Bohr, L.J. Dixon and D.C. Dunbar, *$N = 1$ supersymmetric one-loop amplitudes and the holomorphic anomaly of unitarity cuts*, *Phys. Lett.* **B606** (2005) 189 hep-th/0410296.
- [109] J. Bedford, A. Brandhuber, B. Spence and G. Travaglini, *A twistor approach to one-loop amplitudes in $N = 1$ supersymmetric yang-mills theory*, hep-th/0410280.
- [110] S.J. Bidder, N.E.J. Bjerrum-Bohr, D.C. Dunbar and W.B. Perkins, *Twistor space structure of the box coefficients of $N = 1$ one-loop amplitudes*, hep-th/0412023.
- [111] R. Britto, E. Buchbinder, F. Cachazo and B. Feng, *One-loop amplitudes of gluons in SQCD*, arXiv:hep-ph/0503132.
- [112] J. Bedford, A. Brandhuber, B. Spence and G. Travaglini, *Non-supersymmetric loop amplitudes and MHV vertices*, *Nucl. Phys.* **B706** (2005) 100 hep-th/0412108.
- [113] S.J. Bidder, N.E.J. Bjerrum-Bohr, D.C. Dunbar and W.B. Perkins, *One-loop gluon scattering amplitudes in theories with $N < 4$ supersymmetries*, arXiv:hep-th/0502028.
- [114] A. Brandhuber, S. McNamara, B. Spence and G. Travaglini, *Loop Amplitudes in Pure Yang-Mills from Generalised Unitarity*, arXiv:hep-th/0506068.
- [115] R. Britto, F. Cachazo and B. Feng, *New recursion relations for tree amplitudes of gluons*, hep-th/0412308.
- [116] R. Britto, F. Cachazo, B. Feng and E. Witten, *Direct proof of tree-level recursion relation in Yang-Mills theory*, hep-th/0501052.
- [117] R. Roiban, M. Spradlin and A. Volovich, *Dissolving $N = 4$ loop amplitudes into QCD tree amplitudes*, hep-th/0412265.
- [118] M.X. Luo and C.K. Wen, *Recursion relations for tree amplitudes in super gauge theories*, hep-th/0501121.
- [119] M.X. Luo and C.K. Wen, *Compact formulas for all tree amplitudes of six partons*, hep-th/0502009.

- [120] R. Britto, F. Cachazo, B. Feng and E. Witten, *Direct proof of tree-level recursion relation in Yang-Mills theory*, Phys. Rev. Lett. **94**, 181602 (2005) [arXiv:hep-th/0501052].
- [121] Z. Bern, L.J. Dixon and D.A. Kosower, *On-shell recurrence relations for one-loop QCD amplitudes*, hep-th/0501240.
- [122] Z. Bern, L.J. Dixon and D.A. Kosower, *The last of the finite loop amplitudes in QCD*, hep-ph/0505055.
- [123] S.D. Badger, E.W.N. Glover, V.V. Khoze and P. Svrcek, *Recursion relations for gauge theory amplitudes with massive particles*, hep-th/0504159.
- [124] C. Quigley and M. Rozali, *Recursion relations, helicity amplitudes and dimensional regularization*, arXiv:hep-ph/0510148.
- [125] J. Bedford, A. Brandhuber, B. J. Spence and G. Travaglini, *A recursion relation for gravity amplitudes*, Nucl. Phys. B **721**, 98 (2005) [arXiv:hep-th/0502146].
- [126] F. Cachazo and P. Svrcek, *Tree level recursion relations in general relativity*, arXiv:hep-th/0502160.
- [127] T.G. Birthwright, E.W.N. Glover, V.V. Khoze and P. Marquard, *Multi-gluon collinear limits from MHV diagrams*, JHEP **05** (2005) 013 [arXiv:hep-ph/0503063].
- [128] T. G. Birthwright, E. W. N. Glover, V. V. Khoze and P. Marquard, *Collinear limits in QCD from MHV rules*, arXiv:hep-ph/0505219.
- [129] P. Marquard and T. G. Birthwright, *Multi-gluon collinear limits from MHV amplitudes*, arXiv:hep-ph/0505264.
- [130] W. T. Giele and E.W.N. Glover, *Higher order corrections to jet cross-sections in e^+e^- annihilation*, Phys. Rev. **D46** (1992) 1980–2010.
- [131] S. Frixione, Z. Kunszt, and A. Signer, *Three-jet cross sections to next-to-leading order*, Nucl. Phys. **B467** (1996) 399–442, hep-ph/9512328.
- [132] S. Catani and M.H. Seymour, *A general algorithm for calculating jet cross sections in NLO QCD*, Nucl. Phys. **B485** (1997) 291–419, [hep-ph/9605323].
- [133] A. Gehrmann-De Ridder, T. Gehrmann and E.W.N. Glover, *Antenna Subtraction at NNLO*, arXiv:hep-ph/0505111.
- [134] Z. Bern and A. G. Morgan, *Massive loop amplitudes from unitarity*, Nucl. Phys. **B467** (1996) 479–509, hep-ph/9511336.

- [135] Z. Bern, L.J. Dixon, and D.A. Kosower, *Progress in one-loop QCD computations*, *Ann. Rev. Nucl. Part. Sci.* **46** (1996) 109 hep-ph/9602280.
- [136] L.J. Dixon, *Calculating scattering amplitudes efficiently*, hep-ph/9601359.
- [137] V. Del Duca, A. Frizzo and F. Maltoni, *Factorization of tree QCD amplitudes in the high-energy limit and in the collinear limit*, *Nucl. Phys.* **B568**, 211 (2000) hep-ph/9909464.
- [138] G. Rodrigo, S. Catani, D. de Florian and W. Vogelsang, *Collinear splitting, parton evolution and the strange-quark asymmetry of the nucleon in NNLO QCD*, *Nucl. Phys. Proc. Suppl.* **135**, 188 (2004) [arXiv:hep-ph/0406338].
- [139] G. Altarelli and G. Parisi, *Asymptotic freedom in parton language*, *Nucl. Phys.* **B126** (1977) 298.
- [140] A. Bassetto, M. Ciafaloni, and G. Marchesini, *Jet structure and infrared sensitive quantities in perturbative QCD*, *Phys. Rept.* **100** (1983) 201
- [141] Z. Bern and G. Chalmers, *Factorization in one loop gauge theory*, *Nucl. Phys.* **B447** (1995) 465 hep-ph/9503236.
- [142] Z. Bern, V. Del Duca, and C.R. Schmidt, *The infrared behavior of one-loop gluon amplitudes at next-to-next-to-leading order*, *Phys. Lett.* **B445** (1998) 168 hep-ph/9810409.
- [143] D.A. Kosower and P. Uwer, *One-loop splitting amplitudes in gauge theory*, *Nucl. Phys.* **B563** (1999) 477 hep-ph/9903515.
- [144] Z. Bern, V. Del Duca, W.B. Kilgore, and C.R. Schmidt, *The infrared behavior of one-loop QCD amplitudes at next-to-next-to-leading order*, *Phys. Rev.* **D60** (1999) 116001, hep-ph/9903516.
- [145] S. Catani and M. Grazzini, *The soft-gluon current at one-loop order*, *Nucl. Phys.* **B591** (2000) 435 hep-ph/0007142.
- [146] S.D. Badger and E.W.N. Glover, *Two-loop splitting functions in QCD*, *JHEP* **07** (2004) 040 hep-ph/0405236.
- [147] Z. Bern, L.J. Dixon, and D.A. Kosower, *Two-loop $g \rightarrow gg$ splitting amplitudes in QCD*, *JHEP* **08** (2004) 012 hep-ph/0404293.
- [148] A. Gehrmann-De Ridder and E.W.N. Glover, *A complete $\mathcal{O}(\alpha_s)$ calculation of the photon + 1jet rate in e^+e^- annihilation*, *Nucl. Phys.* **B517** (1998) 269 hep-ph/9707224.
- [149] J.M. Campbell and E.W.N. Glover, *Double unresolved approximations to multiparton scattering amplitudes*, *Nucl. Phys.* **B527** (1998) 264 hep-ph/9710255.

- [150] S. Catani and M. Grazzini, *Collinear factorization and splitting functions for next-to-next-to-leading order QCD calculations*, *Phys. Lett.* **B446** (1999) 143 hep-ph/9810389.
- [151] S. Catani and M. Grazzini, *Infrared factorization of tree level QCD amplitudes at the next-to-next-to-leading order and beyond*, *Nucl. Phys.* **B570** (2000) 287 hep-ph/9908523.
- [152] D.A. Kosower, *Multiple singular emission in gauge theories*, *Phys. Rev.* **D67** (2003) 116003 hep-ph/0212097.
- [153] S. Catani, D. de Florian and G. Rodrigo, *The triple collinear limit of one-loop amplitudes*, *Phys. Lett.* **B586** (2004) 323 hep-ph/0312067.
- [154] A. Brandhuber, B. Spence and G. Travaglini, *From trees to loops and back*, arXiv:hep-th/0510253.
- [155] D.A. Kosower, *All-order collinear behavior in gauge theories*, *Nucl. Phys.* **B552** (1999) 319 hep-ph/9901201.

